UNIVERSIDAD AUTONOMA DE MADRID

Departamento de Biología Molecular

IDENTIFICACION Y ESTUDIO DE NUEVOS MECANISMOS MOLECULARES IMPLICADOS EN LA MORFOGENESIS EPITELIAL: MECANOTRANSDUCCION, ORIENTACION DEL HUSO MITOTICO Y ENDOCITOSIS

Alejo E. Rodríguez Fraticelli

Madrid, 2014

FACULTAD DE CIENCIAS

Departamento de Biología Molecular

FACULTAD DE CIENCIAS

UNIVERSIDAD AUTONOMA DE MADRID

IDENTIFICACION Y ESTUDIO DE NUEVOS MECANISMOS MOLECULARES IMPLICADOS EN LA MORFOGENESIS EPITELIAL: MECANOTRANSDUCCION, ORIENTACION DEL HUSO MITOTICO Y ENDOCITOSIS

D. Alejo E. Rodríguez Fraticelli
Licenciado en Bioquímica

Presenta esta memoria para optar al grado de Doctor en Bioquímica, Biología Molecular, Biomedicina y Biotecnología

DIRECTORES
Dr. Fernando Martín Belmonte
Dr. Miguel Ángel Alonso Lebrero

Tesis Doctoral realizada en el
CENTRO DE BIOLOGIA MOLECULAR
“SEVERO OCHOA”
MADRID, 2014

Esta tesis ha sido realizada en el Centro de Biología Molecular "Severo Ochoa" (CSIC-UAM) bajo la tutela del Dr. Fernando Martín Belmonte, Investigador del CSIC y el Dr. Miguel Ángel Alonso Lebrero, Profesor de Investigación del CSIC.

Esta tesis ha sido posible gracias a una beca JAE-Predoctoral concedida a D. Alejo Ezequiel Rodríguez Fraticelli por el Consejo Superior de Investigaciones Científicas.

A mis abuelos, Adolfo y Emilio,
mis mejores amigos,
y la inspiración de mi vida.

Esta tesis para mí es mucho más que la redacción trámite de un compendio de trabajos, realizados entre 2009 y este año 2014. Esta tesis para mí representa la culminación de un largo largo viaje a España, a Europa, a mis raíces, un viaje de 11 años, más de un tercio de mi vida. Quizás por esta razón los agradecimientos de esta tesis sean la parte más complicada de escribir. Especialmente para mi, no hay forma de ordenar la importancia relativa que han tenido todos aquellos y aquellas acompañantes que he tenido en mi vida. Yo solo soy una constelación de todas esas estrellas que han estado ahí dándome su calor y su luz. Es por eso que en acto de asumida rebeldía me dispongo a desordenar sistemáticamente la lista de personas, y sus motivos, que me han llevado hasta aquí, ahora. Ah, y perdónenme el "argeñol".

Vamos a empezar por decir que esta tesis no es mía. O sea, sí, tiene mi nombre, pero en realidad no es sino el logro de toda una gran familia argentoitaloespañola. Empezando por mi mamá y mi papá sin los cuales jamás habría llegado a poder imaginar todo esto. Papá, Mamá. Gracias por hacer realidad mis sueños, y por no parar hasta verme sonreir. Después, siguiendo por mi hermano, el ying de mi yang, aquello que le ha dado balance y cabalidad a todo lo que hago. Agus, empecé esta vida siendo tu maestro y estoy seguro de que terminaré siendo tu aprendiz. Cerrando por mis abuelos y abuelas, por haberme enseñado el valor de la lucha, del coraje, del esfuerzo, del no dejarse jamás. Y terminando el núcleo duro con mis primos y tíos, y todo el resto, por su infinita paciencia con la oveja negra de la familia. Una mención especial merece mi tío Edy, por fascinarme con la química desde que tenía 5 años, el primero de una larga lista de, digamos, "responsables" de que yo haya terminado siendo científico. Algo me dice que al terminar de pincelar estas hojas, habrá más de unos cuantos de estos, e incluso algunos más.

Pero si tengo que hablar de influencias, nadie ni nada me ha influenciado más que mis maestros y profesores. A ver. Si venís como yo de una familia donde nadie se ha dedicado a la academia, y de repente va y te sale un hijo PhD: está claro, echale la culpa al profe. Jajaja. No, pero ahora en serio. A los profes, gracias por dedicar sus vidas a intentar enderezar la mía; por ser los precarios directores de esta disfonía de sociedad en la que vivimos. Los primeros que me empujaron fueron el profe de matemáticas y la profe de ciencias naturales de sexto de primaria. Pero si hay algo que no se me va a borrar nunca de la cabeza es el momento en que entré por primera vez en los salones del Colegio Nacional de Buenos Aires. Pocos profesores, pocas cátedras y pocos amigos te hacen sentir así, como que no los estás aprovechando todo lo que podrías, aun cuando estas atendiendo y dando todo lo que podés de vos. Aunque si algún profesor tiene el mérito de esta tésis, esos son los profesores de la Universidad Autónoma de Madrid. Con esa mezcla extraña de cercanía, camaradería, dedicación y sabiduría, que quizás solo sea entrópicamente posible en un lugar como Castilla, les debo a los profesores de la UAM todos y cada uno de los pasos que voy dando, y en especial este.

Con buenos profes y todo, aun así yo no habría llegado a absolutamente nada de todo esto si no fuera por mi creatividad. Y eso que ni siquiera fue mia. Bueno. La tomé prestada (más bien robada), como no, de todos mis amigos de la infancia: Manu, Hernan, Luco, Morenio, Hernan, Juan Martin, Franco, Lucas, Pablo. Esas horas interminables que le dedicamos a nuestra imaginación terminaron siendo la semilla de todo lo que me he atrevido a intentar construir. En cierta medida sigo midiéndome cada día con la vara de nuestra amistad, intentando convertirme en aquello que ustedes una vez creyeron que me podría convertir.

La locura de todo este viaje arrancó cuando todavía no sabía pronunciar ni la cé, acababa de llegar a tierras hispanas y sin embargo, ya era amigo de la mejor cuadrilla de estudiantes de biología que nadie hubiera tenido jamás. Nunca había vivido algo similar: un grupo de 30 o más, que sé yo cuántas personas. En fin, que biología me enseñó lecciones de compañerismo que nunca se me van a olvidar. Lecciones sobre compartir, sobre dar sin pensar en recibir, sobre cantar y llorar a partes iguales, sobre dormir con el cielo estrellado por techo. Marneus, Jose, Ivan, David, David, David, María, Sandra, Almu, Silvia, Jorge, Angel, Ana, Edu… Mi corazón es de color ladrillo y azul. Vine a España en busca de mis raíces… pero no fue hasta que los conocí a ustedes, que entendí en busca de qué había venido en realidad. Y fue ahí en biología, que me terminé por cruzar con la gente más increíble, de la forma más inesperada. Unos compañeros de clase, Tony, Ana y Jose me presentaron a Juan, Irene, Salva y Kike, y el flechazo fue total: ya no hubo vuelta atrás. Los Marmotianos fuimos inseparables casi 10 años. De ellos aprendí que los valores como la honestidad y el coraje, no se nace con ellos, sino que nos los tenemos que ganar cada día de nuestros compañeros.

Biología me enseñó como ser mejor persona, y cuando me fui, sentí que me había dejado un pedacito de mi corazón en esa facultad. Pero al llegar a bioquímica, hubo un grupo de gente que me hizo darme cuenta de aquello que yo había empezado a vivir no era sino el comienzo de una gran aventura. Dicen que los 20 son los mejores. No te quepa la menor duda. Mis compañeros de la carrera de bioquímica están hechos de otra madera. Nunca estuve rodeado de tanto cerebrito y aún así me sentí parte de algo que era mucho más grande que mi mismo. De toda aquella gente que conocí, me quedé con los mejores sin duda: Bea, Irene, Elisa, Alex, Jara, Lara, Carlos, David, Alfonso, Jaime, Miguel y Lucía. Los debates científicos, los exámenes, las birras y las fiestas. Sois las personas más inteligentes, capaces y entregadas que conozco. Que sí, que sí. En serio, chicos, gracias por hacerme un hueco entre vosotros cuando más lo necesité.

Hay unas personitas en ese grupo que sin embargo merecen una mención especial para mí, por la cantidad de lata que les he dado durante todos estos años. Inés, gracias por apoyarme a muerte casi desde que pisé suelo madrileño. Nunca pensé que podía encontrar una amiga tan incondicional, y aunque a veces dejemos pasar mil años, siempre encuentro refugio en tus palabras. Cris, gracias por creer en mí antes que yo mismo, y por conseguir arrancarme sonrisas con esa facilidad prodigiosa.

Y lo lindo de la vida es esto: que justo cuando crees que ya lo tenés todo, la vida te da más. El máster me trajo al primer amor de mi vida, Pilar. El viaje que hicimos, es y será nuestro para siempre, y de nadie más. Gracias por tener infinita paciencia y ánimos para mí. Todos, todos mis primeros logros te los debo a vos.
Pero no solo eso, el máster también me trajo a los dos amigos más alocados e inseparables que tengo a este lado del atlántico. Chicos, sois la clase de persona por la que sería capaz de saltar de un avión, meterme en el fondo de un océano, o sencillamente pasarme millones de horas haciendo nada, juntos. Gracias por estar ahí, para mí, siempre. Y a los cracks que me encontré en el máster, Jaime, Marta y Jesus. Gracias por redescubrirme que la mejor forma de ser alternativo, es ser uno mismo.

Y ahora llega el momento del laboratorio… Llevo tanto tiempo meditando esto que la tarea me parece titánica. Y sin embargo, extrañamente, las palabras fluyen con más facilidad. Es como hablar de tu propia familia.

Cuando entré por primera vez al lab 322 … jamás pensé que conocería a personas tan maravillosas en este mundo. No lo digo yo, lo dicen todos. Este labo tiene un no se qué especial. Vamos, como si pudiéramos montar un bar, o un colegio, en lugar de un lab, y nos iría fenomenal igualmente. Los primeros que conocí ya se fueron hace mucho, Juanfra, Alicia, Maica, Ricardo, Olga y Laura… Fueron los primeros que me llevaron de la mano, sin miedo pero sin prisa, con una paciencia eterna. Pero quizás los principales responsables de que me haya enamorado de la biología celular. Maica me enseñó todo lo que sé de inmunofluorescencias… esa atención al detalle. Esa forma de alcanzar la paz haciendo lo que más te gusta, la aprendí de vos. Ricardo, con vos perdí la virginidad (científica, che!)… Nadie me enseñó como vos a apreciar ese miniuniverso estético que hay oculto dentro de los microscopios. Juanfra y Alicia me enseñaron que no había que conceder, y que se podía hacer ciencia y ser auténtico a partes iguales, y que con el tiempo, la gente eso lo sabe apreciar. Yo por lo menos, esa lección la aprendí y bien aprendida. Olga y Laura fueron mis primeras hermanas mayores. Me llevaron de la mano, y me enseñaron con una pizca de melancolía y otra pizca de sorna, propia de unas doctorandas ya encaminadas, como funcionaba este mundo, con sus lecciones llenas de tesón y carcajadas. Con Alberto aprendí los cacharros, pero sobre todo aprendí a hacer las cosas con el corazón, porque en esto como todo, si no le ponés corazón, mejor no lo hagas.

Poco después vinieron Nati y Lean… Que se yo. Se me ahogan las palabras en el teclado. Son las dos mejores personas que he visto pasar por este mundillo, sin lugar a dudas. Dos niños grandes, cargados de ilusión hasta en los momentos más de bajón, de esos que te hacen dar ganas de haberlos conocido con 5 años, porque sabés que habrían sido amigos tuyos para toda la vida.

Y qué decir de las nuevas incorporaciones del 322, con Miguel, Javi y Jaime, la pandilla está de vuelta y se rumorea que el labo por fin vuelve a tener aires del 98. Miguel es un líder nato, de esos que te enseñan cosas sin tener que decir nada. Javi es una de las personas más inteligentes que conocí. Y Jaime tiene un hambre de gol tremendo. Chicos, como me gustaría ser parte de este nuevo dream team.

El lab 324 merece especial atención. Cuando entré Ana era un cuadro vivo de todo lo que quería ser yo como estudiante, y cuando se fue, fue una de las primeras veces que me di cuenta de que había vacíos que la gente te deja que ya no se pueden llenar. Bea me enseñó que la ciencia había que tomársela con la seriedad justa, y que el descubrimiento más lindo, como el amor, es el inesperado. Diego, que la decisión más justa es la que tomas por vos mismo. Diana, que aunque trabajes mil horas al día, nunca tenes que olvidarte de vos mismo. Laura, que el glam-science es una forma de vida, y Laura, que la frente más alta es la del que menos dice y más hace. Y remato agradeciendo a Isabel, Jaime y Carlos. Los pilares del 324. Cansados, abatidos, con sus agendas de infarto múltiple, pero siempre capaces de sacar las fuerzas y el tiempo de donde se pueda, de donde haiga, para venir y dejarse los cuernos y los huesos en la ciencia. Podría llenar libros con las lecciones que me habéis soltado en solo estos pocos años. Lo vuestro es un ejemplo constante de esfuerzo y de sabiduría.

Cuando llega el momento de agradecer a mis directores de tesis, se me quedan cortas todas las palabras. Que decirte, Fernando. Ya casi ni me acuerdo de cómo terminé embarcándome en esta aventura que fue empezar con vos este labo desde cero. Pero ¡por tutatis!, qué divertido ha sido. Que me hayas elegido como tu primer estudiante ha sido un honor que sobrepasa todos los honores que me esperan en este largo camino. Con tu equilibrio perfecto de genialidad y sencillez, siempre serás el modelo de científico que aspire a intentar alcanzar.

A mi codirector, Miguel Ángel. Si no hubiera sido por Miguel, yo habría terminado de cualquier otra cosa, cocinero, músico callejero, banquero. Allá por 2005 se te ocurrió hacerle caso a JAL, y decidiste meterme en tu labo. En cierta medida siento que siempre seré parte de él. Gracias por enseñarme qué era y qué es la ciencia, y mucho más importante, gracias por enseñarme lo hermoso que podía ser dedicarle tu vida a algo que valiera la pena.

Honestamente, para agradecerle a Manu, necesitaría dos páginas solo para él. A lo largo de todo este viaje, si alguna vez me medí con alguien de tu a tu, fue con vos. Esos combates científicos, esas discusiones acaloradas de ciencia, tête a tête, intentando ganarle a este mundo que todavía nos era ajeno. Pibe, te veo al otro lado del charco.

A mis dos minisemillitas, Mariam y Minerva. Haberlas visto crecer hasta donde habéis llegado, científica y personalmente, es una de las cosas más maravillosas que me llevo de toda esta experiencia de haber pasado por un laboratorio. Son puro amor. En una época de mi vida en la que me había dejado estar muchísimo, ustedes me dieron las alegrías más lindas. Si alguna duda me quedaba de que yo me quería dedicar a esto, ustedes dos fueron las responsables, con sus sonrisas, con sus buenos gestos, con esa paciencia. Sí, ustedes, las responsables de darme el último empujoncito que me lleva a querer ir a por todas. Cuídense mucho. Nosotros ya nos vamos. Ahora ustedes llevan la antorcha. Sí, sí, ayúdense, que pesa.

Aunque por mucho que mi "U" sea como mi segundo hogar, no me puedo dejar afuera a los seniors del lab: Silvia, Ilenia e Inma. A ver… siendo absolutamente honestos, el jefe ya estaba un poquin oxidado para cuando arranqué la tesis. Así que a Silvia, Inma e Ilenia les debo casi todo lo que aprendí del hardcore bench (no los cacharros, sino los experimentos más copados). Por eso, y por tantisimas risas, siempre les estaré eternamente agradecido. Y para cerrar, no me puedo dejar afuera a la rubia, Arantxa, que es como un Atlas en femenino, encogido de hombros, que sujeta nuestro minimundo. Quiero que sepas que de todo este tiempo que pasé con vos en este lab, vos, y sobre todo vos, marcaste totalmente la diferencia.

No me quiero dejar afuera a aquellos que han venido más tarde y aquellos que se fueron demasiado temprano como para poder conocerlos bien: Belén, Sara, Lorena, Rocío, Tamara, Helena, Edu, María, Antonio y algunos más, que no fueron pocos. Aunque no se hayan percatado, todos ustedes dejaron cosas maravillosas en mí, y me hubiera encantado haberme podido quedar un poquito más con ustedes para disfrutarlas juntos.

Quizás una de las cosas más lindas de la tesis fue la oportunidad de viajar por el mundo y conocer algunos de esos clones espirituales, que tienes, sin saberlo, al otro lado del mundo. Además de las incontables anécdotas de laboratorio que tuvimos, Jennifer y Kathryn, me tratasteis como si fuera un hermano, y me hicisteis darme cuenta de que el

verdadero buenrollismo americano no estaba en California, sino en vuestros corazones. No lo voy a olvidar nunca, así como tampoco a Chris, Batich, Pham, Adam, Ashley, Lindsey, Sean, Sami, Mark…
En Michel y Michel, más que dos colaboradores, encontré dos mentores. Y aunque hayan pasado 30 años entre que uno y el otro pasaron por los labos del EMBL, siento que siempre van a tener esa chapa de vieja casta, de oxido en los guantes, y quemaduras en las batas. Ojalá pueda algún día medirme con ustedes, y echarle un cable a un pibe como hicieron ustedes conmigo. Y cierro con Joanne, Muriel, y la troupe de CYTOO, por haberme abierto los ojos al mundo real, pero siempre con ojos cargados de ilusión.

Y por ultimo quiero agradecerle a toda la gente que trabaja en el Centro de Biología Molecular. Porque sin ellos no somos nada. Sin ellos no hay ciencia. Son el motor que mantiene la nave a flote, sujetando desde los remos hasta los amarres. Tuve el privilegio de veros levantar y montar con vuestras manos este edificio cuando yo no era más que un bebé de pecho. Quizás sea algún día consciente de todo lo que me llevo de ustedes cuando cierre esas puertas grises por última vez.

I.
PRESENTACION/SUMMARY

PRESENTACIÓN

Las células epiteliales constituyen la piedra angular de la evolución de los metazoos. La polaridad epitelial es evidente en la organización de distintos dominios de membrana plasmática que llevan a cabo funciones esenciales en el animal, como la nutrición y la excreción. Los tejidos epiteliales presentan frecuentemente involuciones y ramificaciones dentro del cuerpo animal, en forma de tubos, que ayudan a proteger dichas funciones fisiológicas de posibles daños provenientes del entorno, y contribuyen a regular y aumentar la superficie de intercambio de sustancias con el entorno. La morfogénesis epitelial es el proceso mediante el cual las células epiteliales proliferan y organizan la arquitectura tridimensional del órgano definitivo, generando y manteniendo el fenotipo polarizado. Utilizando el modelo *in vitro* de células MDCK cultivadas en tres dimensiones (3D), y el modelo *in vivo* de la morfogénesis del intestino del pez cebra, nos hemos propuesto estudiar los mecanismos implicados en la morfogénesis epitelial de los vertebrados. Primero, mediante el uso de microsuperficies adhesivas (micropatterns), hemos caracterizado que el confinamiento espacial de la adhesión celular proporciona señales mecanofísicas fundamentales para la adquisición de la polaridad epitelial. Segundo, mediante el estudio de la regulación de la GTPasa monomérica Cdc42, esencial para el generación de la polaridad celular, hemos contribuido a establecer el papel de la orientación del huso mitótico durante la formación del lumen de los órganos epiteliales en 3D. Por último, hemos caracterizado la función de un grupo de genes inducidos específicamente durante la morfogénesis epitelial en 3D *in vitro* e *in vivo*, en el modelo del pez cebra. De este modo hemos determinado que el proceso de endocitosis controla la polaridad y la proliferación celular y se encuentra finamente regulado en el tiempo y en el espacio para dar lugar a la formación de órganos epiteliales especializados. En resumen, nuestro trabajo ha ayudado a comprender el papel fundamental de tres mecanismos celulares relacionados con el proceso de morfogénesis epitelial en vertebrados. Además, algunos de estos mecanismos son comunes a más de un tipo de órgano epitelial, y por lo tanto proporcionan un conocimiento esencial sobre cómo se regulan la polaridad y la proliferación durante el desarrollo, y podrían proporcionar nuevas vías de estudio para entender los procesos de pérdida de polaridad y displasia durante la aparición de carcinomas.

SUMMARY

Epithelial cells represent the founding stone at the dawn of metazoan evolution. Epithelial cell polarity is apparent in the organization of different membrane domains, which carry out essential functions in the animal, such as nutrient uptake and excretion. Epithelial tissues are frequently convoluted and wrapped inside the animal body, in the form of tubes, providing protection from the environment and augmenting the exchange surface for different physiological functions. Epithelial organ morphogenesis is the process by which epithelial cells proliferate and organize the three-dimensional architecture of the final organ while generating and maintaining the polarized phenotype. Using the 3D-MDCK cell culture system and zebrafish gut morphogenesis as *in vitro* and *in vivo* models of epithelial morphogenesis we have investigated three mechanisms that regulate epithelial morphogenesis in vertebrates. Firstly, through use of adhesive micropatterns, we have characterized that spatial confinement of cell adhesion provides essential mechanophysical cues for the acquisition of 3D epithelial polarity. Second, through the analysis of the small GTPase Cdc42, a master regulator of cell polarity, we have found that mitotic spindle formation and orientation are required for the maintenance of planar symmetric cell divisions, which is necessary for single lumen formation. Finally, we characterized a specific gene set induced *in vivo* and *in vitro* during epithelial morphogenesis, and we contributed to elucidate that one of these genes is responsible for the fine regulation of endocytosis during development to control the process of epithelial morphogenesis and differentiation. In conclusion, we have analyzed three mechanisms involved in the process of epithelial morphogenesis in vertebrates. Furthermore, these mechanisms are common to most epithelial glands, and therefore provide essential knowledge on how polarity and proliferation are controlled during development, and point to new approaches to unravel the process of polarity loss and dysplasia at the origin of carcinomagenesis.

INDEX

II.
GLOSSARY

2D: two-dimensional
3D: three-dimensional
AJ: Adherens Junctions
aPKC: atypical Protein Kinase C
ARE: Apical Recycling Endosome
avl: avalanche protein (*Drosophila* homolog of Stx7/Stx12)
Cdc42: Cell division control 42 protein
CRB (Crb3a): Crumbs protein
Dap160: Dynamin associated protein 160 kDa
Dlg: Discs large protein
dpf: days post-fertilization
ECM: Extracellular Matrix
EpsR: EpsinR
F-actin: Filamentous (polymeric) actin
G-actin: Globular (monomeric) actin
GAP: GTPase Activating Protein
GDP: Guanine nucleotide bisphosphate
GEF: Guanine nucleotide Exchange Factor
GFP: Green Fluorescent Protein
gp135: glycoprotein of 135 kDa; Podocalyxin-like (PODXL, PCX, Pdxl)
GPI: glycosylphosphatidylinositol
GTP: Guanine nucleotide trisphosphate
GTPases: Guanine nucleotide trisphosphatase
HA: Hemagglutinin protein from influenza virus
hpf: Hours post-fertilization
ILK: Integrin-Linked Kinase
ITSN1/2: Intersectin 1/2
JAM: Junction Adhesion Molecule protein
KD: Knock-Down
LAMP2: Lysosomal-Associated Membrane Protein 2
LE: Late Endosomes
Lgl: Lethal giants larvae protein
LGN: Pins/AGS3 protein with N-terminal Leucine-Glycine-Asparragine repeats
LKB1: Liver Kinase B1 protein
Lys: Lysosome
MAL: Myelin And Lymphocyte protein
MARVEL: MAL and Related proteins for VEsicle trafficking and membrane Link
MDCK: Madin-Darby Canine Kidney cells
MT: Microtubules
MyoII: Myosin-II protein complex
NHERF: Sodium (Na+) and Proton (H+) Exchange Regulatory Factor protein
NICD: Notch Intracellular Domain
NuMA: Nuclear Mitotic Apparatus protein
NWASP: Neuronal-Wiskott Aldrich Syndrome Protein
PAR-1/3/4/5/6: Partitioning defective proteins 1/3/4/5/6
PCP: Planar cell polarity
PCX/Pdxl: Podocalyxin, podocalyxin-like, gp135
Pdx1: Pancreatic and duodenal homeobox 1
PDZ: post synaptic density protein (PSD95), *Drosophila* disc large tumor suppressor (Dlg1), and zonula occludens-1 protein (zo-1)

PI3K: Phosphatidylinositol-3-kinase
pIgR: polymeric Immunoglobulin receptor
Pins: Partner of inscuteable, LGN, AGS3
PLLP: Plasmolipin
PtdIns(3,4,5)p3: Phosphatidylinositol-3,4,5-trisphosphate, PIP3
PtdIns(4,5)p2: Phosphatidylinositol-4,5-bisphosphate, PIP2
PtdIns(3,5)p2: Phosphatidylinositol-3,5-bisphosphate
PtdIns(3)p: Phosphatidylinositol-3-monophosphate
PTEN: Phosphatase and tensin homolog
RE: Recycling Endosomes
ROCK: Rho-associated Protein Kinase
SH3: Src-Homology type 3 domain
SNARE: Soluble N-ethylmaleimide sensitive factor attachment protein receptor
SRF: Serum Response Factor
Stx3: Syntaxin-3
Stx7: Syntaxin-7
TGN: Trans Golgi Network
TJ: Tight Junctions
VAC: Vacuolar Apical Compartment
VAMP: Vesicle Associated Membrane Protein
YAP: Yes-associated protein
ZO-1/2/3: Zonula occludens-1/2/3

III.
INTRODUCTION

The synapomorphic metazoan body plan fundamentally consists of a sheet of tightly connected cells, termed epithelial cells, enclosing an underlying mesenchyme or stroma. This organization of cells into epithelial sheets is reused in a diversity of animal organs, which carry out a large number of complex functions. The lungs, the gastrointestinal tract and its glands such as the liver or the pancreas, the skin and its glands, the excretory system, and the central nervous system are all made of wrapped sheets of epithelial cells. The phenotype of epithelial cells is characterized by a stereotypic organization of cell polarity, that is, a differential localization of the cellular components along the axes of the cell. Epithelial cell polarity is defined by the existence of an apicobasal axis, which is apparent in several cellular organelles. For instance, the plasma membrane of epithelial cells is organized into an apical domain, which faces the exterior milieu, and a basolateral domain, which faces the underlying stroma. The majority of functions of epithelial organs are related to the establishment of barriers for the regulated exchange of substances between these comparments, along the apicobasal axis. Thus, the exchange function of epithelia depends on the differential localization of specific protein activities to each of these plasma membrane domains, which is controlled by a complex set of highly conserved mechanisms, known as the epithelial polarity program.

1. The epithelial polarity program

The genetic program that controls epithelial polarization is highly conserved throughout the animal kingdom, and may possibly predate eumetazoans (Dickinson et al., 2011; Rodriguez-Boulan and Macara, 2014). Multiple cellular processes are required for establishing apicobasal polarity, including polarized vesicular transport, polarization of the cytoskeleton and the proper establishment and maintenance of cell adhesion and cell junction complexes (**Figure 1**). Perhaps the most obvious feature of epithelial cells is that they posses a plasma membrane divided into three highly distinct surfaces: the apical, basal and lateral plasma membranes. The apical membrane is the free surface that contacts the exterior milieu; it contains small actin-based protrusions, termed microvilli, and a sensory organelle, the primary cilium. The basal membrane is in contact with a specialized extracellular matrix (ECM), the basal lamina, which provides cell support and establishes a secondary filtration barrier for epithelial transport. The lateral membrane connects neighboring cells through a set of specialized cellular

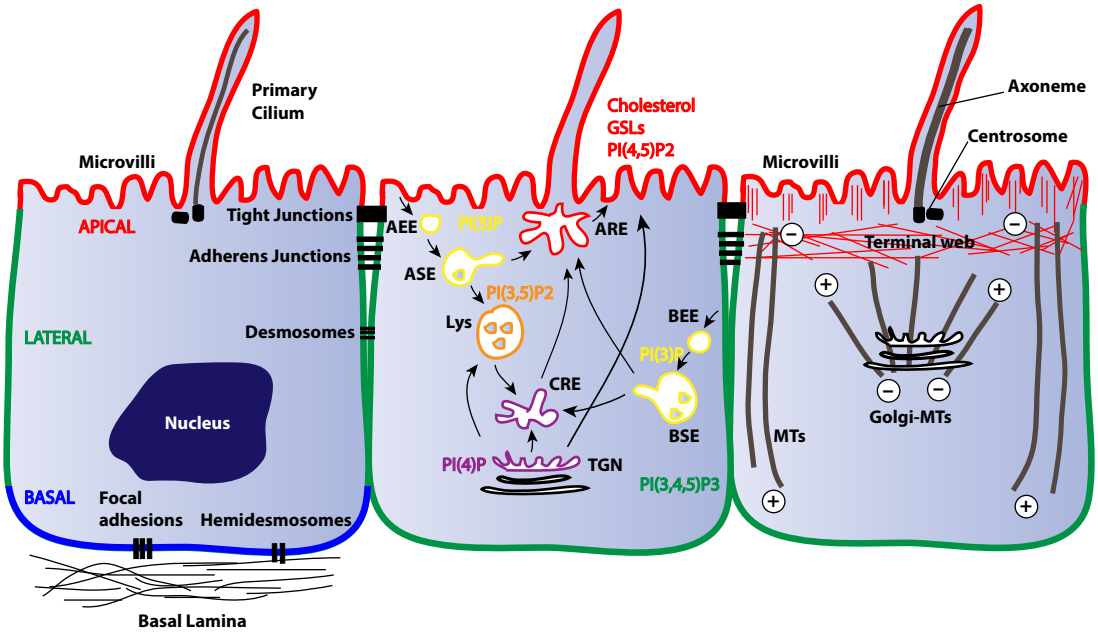

Figure 1. The epithelial polarity phenotype. Epithelial cells present polarized apical, lateral and basal membrane domain. Specific junctions bind to other cells and to a specialized ECM, the basal lamina. Membrane lipid and protein transport is also polarized, and different phosphoinositide species provide membrane identity. The polarized cytoskeleton of epithelial cells consists of microvillar actin-bundles, an apical actin network (terminal web) and apicobasally oriented microtubules.

junctions that anchor cells to one another. These cellular junctions provide a structural integrity in the epithelium and perform a paracellular transport barrier function. In addition, the cellular junctions preserve the different composition of the membranes by restricting the lateral movement of proteins and outer-leaflet lipids (Mostov et al., 2003). The apical membrane is often covered by abundant microvilli, and appears to be the more specialized domain, since it contains most of the proteins required for organ-specific functions, such as terminal digestion and nutrient absorption or resorption. Generally, the apical plasma membrane is enriched in *PtdIns(4,5)p2*, glycosphingolipids, cholesterol and glycosylphosphatidylinositol(GPI)-anchored proteins. By contrast, the basolateral membrane is enriched in *PtdIns(3,4,5)p3* and carries most of the constitutive functions of the cells (for example cholesterol and transferrin uptake, growth-factor receptor signaling, etc).

To maintain cell polarity, and play their specific functions, epithelial cells have to ensure proper delivery of apical and basolateral cargo to their respective target location. Polarized protein delivery is regulated by sorting signals contained within the proteins themselves, which are recognized by specific sorting machineries (Folsch, 2008; Mostov et al., 2003; Rodriguez-Boulan et al., 2005). The different trafficking routes and sorting mechanism in epithelial cells include: biosynthetic, endocytic,

recycling and transcytotic pathways. The biosynthetic route provides newly synthesized proteins to the apical and basolateral membranes. After the synthesis of the proteins, they are transported along the secretory pathway: endoplasmic reticulum, Golgi and trans-Golgi network (TGN) and sorted into carriers to different membrane domains at either the TGN or the endosomes. Once at the plasma membrane, proteins can also be endocytosed and delivered to the early endosomes where they follow the endocytic route until degradation (lysosomes) or, after passing through the recycling endosomes, they can be sorted back to the cell surface of origin (recycling), or transported across the cell to the opposite plasma membrane domain (transcytosis). The importance of these pathways varies with the type of epithelial cell, but they must be finely regulated in order to induce and maintain the steady-state polarity of the cells. The transport of the proteins along these trafficking routes is regulated by sorting signals present in the proteins themselves and recognized by specific sorting machineries.

2. Protein sorting signals encode polarized protein trafficking and delivery

The basolateral sorting information is composed of small peptide sequences included in the cytoplasmic tails of the basolateral targeted transmembrane proteins (**Figure 2a**). Basolateral sorting signals, first described for the polymeric IgA receptor (pIgR) (Casanova et al., 1991; Mostov et al., 1986), are typically tyrosine-based (YXXØ) or leucine-based (mono- or di- leucine) peptide motifs (Rodriguez-Boulan et al., 2005). They are usually dominant over apical sorting signals, which explains the fact that when they are removed, certain basolateral proteins are missorted to the apical surface (Folsch, 2008). These peptidic sorting signals are recognized by cytosolic adaptor proteins, which in general form heterotetramers and interact with the vesicle coating protein clathrin, also required for basolateral distribution (Deborde et al., 2008). There are mainly four types of adaptin protein complexes, AP-1, AP-2, AP-3 and AP-4, each consisting of two large subunits (α,γ,ε,δ, and β, 1-4), a medium subunit (μ, 1-4), and a small subunit (σ, 1-4). The interaction of the adaptor proteins with the cargo and the clathrin coats induces the clustering of the basolateral proteins into clathrin-coated pits, which are subsequently budded into the cytoplasm for basolateral distribution. The two AP1 adaptor complexes, AP1A and AP1B (which diverge in a single specific isoform of μ adaptin, μ1A or μ1B), are essential to sort basolateral proteins at the TGN and recycling endosomes respectively, and interestingly AP1B seems to be specific of

certain but not all epithelial tissues (Deborde et al., 2008; Gonzalez and Rodriguez-Boulan, 2009; Gravotta et al., 2012; Gravotta et al., 2007; Perez Bay et al., 2013). In turn, the AP2 adaptor is fundamental for removal of incorrectly sorted basolateral proteins at the apical plasma membrane (Folsch et al., 1999; Gan et al., 2002).

It was initially proposed that whereas the basolateral sorting was dependent on cytoplasmic signals, the apical sorting was a "default" pathway. This hypothesis originated in experiments in which the mutation of the basolateral signals induced the missorting of the proteins to the apical domain (Matter and Mellman, 1994). However, further work has proved the existence of apical sorting information that typically consists of ectodomain, membrane or cytoplasmic signals (**Figure 2a**). The first apical signal characterized was the glycosylphosphatidylinositol (GPI) anchor present in certain proteins (GPI-anchored proteins) (Brown et al., 1989; Lisanti et al., 1989; Lisanti et al., 1988). A second group of apical sorting signals includes N-linked or O-linked glycans, present in the exoplasmic region of many glycoproteins. A third group of apical sorting signals is encoded by the protein sequences themselves (Rodriguez-Boulan et al., 2005; Tall et al., 2003). Finally, it has been recently described that apical sorting information can also be encoded by cytoplasmic and exoplasmic protein domains present in the apical proteins (Marzolo et al., 2003; Takeda et al., 2003)

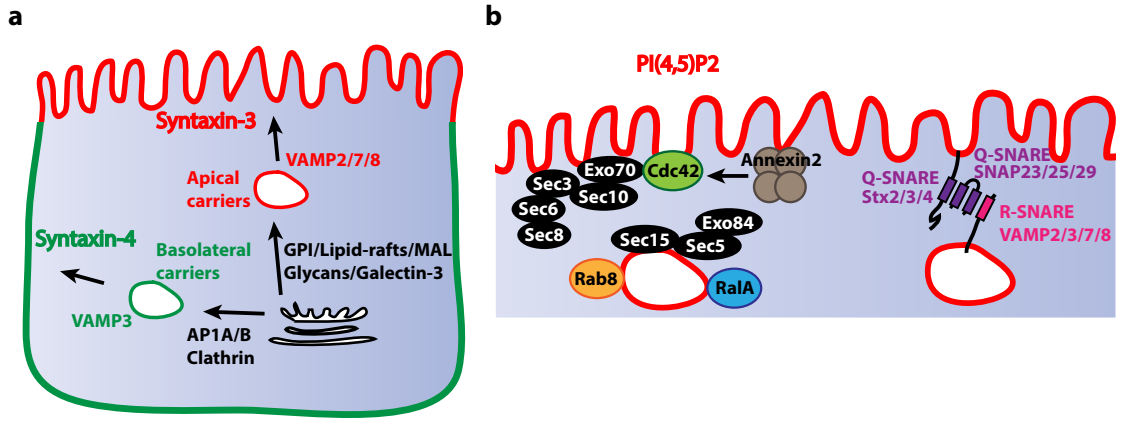

Figure 2. Polarized protein trafficking and fusion. a) Apical and basolateral proteins are synthesized in a common biosynthetic route, and have to be sorted into specific vesicular carriers both at the Golgi and at endosomal compartments. Basolateral sorting depends on clathrin and Syntaxin-4, whereas apical sorting depends on glycans, lipid-rafts and Syntaxin-3. **b)** The membrane fusion process is controlled by Annexin-2 and Cdc42 activation and assembly of the Exocyst complex by Rab8/RalA. The fundamental membrane fusion machine depends on pairing of v/t-SNAREs.

A common requirement for apical sorting seems to be a clustering of the apical proteins into specific membrane domains, perhaps with the help of lectins that recognize N- or O-linked glycans, for direct delivery from the TGN to the apical membrane (Delacour et al., 2005; Fiedler and Simons, 1995) or, due to the ability of some apical directed

proteins such as GPI-anchored proteins, to oligomerize during their passage through the Golgi complex (Paladino et al., 2004). Additionally, lipid raft domains could mediate this clustering. The lipid-raft hypothesis (van Meer and Simons, 1988) postulates that apical targeted proteins are clustered and incorporated in transport vesicles due to their affinity for microdomains enriched in glycosphingolipids and cholesterol (Lingwood and Simons, 2010). Different proteins have been postulated to promote the clustering of lipid rafts, including MAL (Alonso and Millan, 2001; Li et al., 1996; Puertollano et al., 1997). The association of the MAL family of proteins with lipid rafts and their biological function seems to be related to its MARVEL domain, which is also present in physin, gyrin and occludin families (Sanchez-Pulido et al., 2002). The function of the MARVEL domain could be related to cholesterol-rich membrane apposition events in a variety of cellular processes, such as biogenesis of vesicular transport carriers or tight junction regulation. The role of MAL and other members of the MAL family in raft-associated vesicle transport has been extensively addressed in epithelial cells (Cheong et al., 1999; de Marco et al., 2002; Martin-Belmonte et al., 2001; Martin-Belmonte et al., 2003; Martin-Belmonte et al., 2000; Puertollano et al., 1999).

3. The membrane fusion machinery consists of SNARE proteins and the exocyst

The tethering (or docking) and fusion of transport vesicles with the apical or the basolateral domains are essential during exocytosis, and for the acquisition of cell polarity and membrane identity (Wu et al., 2008) (**Figure 2b**). The exocyst protein complex function has been reported to be involved in the tethering, docking and fusion of post-Golgi vesicles with the plasma membrane in polarized cells. Studies from several model systems have demonstrated that the activity of the exocyst complex, which is composed of eight subunits (Sec3, Sec5, Sec6, Sec8, Sec10, Sec15, Exo70 and Exo84) is conserved from yeast to mammals and is regulated by the activity of small monomeric GTPases from the Rab, Ral and Rho families (Wu et al., 2008). Small GTPases cycle between a GTP (active) and a GDP-bound (inactive) state, and constitute molecular switches in cell physiology. GTP-bound Rab11/Rab8 and RalA regulate the initial vesicle-docking event, perhaps by promoting exocyst assembly (Moskalenko et al., 2002; Moskalenko et al., 2003). Assembly is followed by local activation of the exocyst complex by a Rho GTPase, Cdc42. Exocyst activation results in a stimulation of downstream fusion activity, although the molecular effectors are still unknown. In

epithelial cells, the exocyst is localized in the Golgi apparatus, the trans-Golgi network (TGN), recycling endosomes, and the junctional complexes, and is proposed to promote the targeting and fusion of biosynthetic and endocytic recycling cargo carriers with the basolateral plasma membrane domain, possibly at sites near the tight junction (Folsch et al., 2003; Grindstaff et al., 1998; Yeaman et al., 2004; Yeaman et al., 2001). However recent results have shown that the exocyst could function in several endocytic pathways as well, including basolateral recycling, apical recycling, and basolateral-to-apical transcytosis (Oztan et al., 2007).

The current information about the machinery for vesicle fusion at the apical membrane is limited (Weisz and Rodriguez-Boulan, 2009). The annexin family of proteins, which associate with the plasma membrane in a Ca^{2+} and negative phospholipid-dependent manner (Rescher and Gerke, 2004), are enriched at the apical domain through its association with *PtdIns(4,5)p2* (Martin-Belmonte et al., 2007; Rescher et al., 2004). Apical protein trafficking in MDCK cells requires annexin A2 (Jacob et al., 2004). Furthermore, recent results have shown that annexin A2 is required for the activation of Cdc42 at the apical plasma membrane (Martin-Belmonte et al., 2007).

The last step of fusion of vesicles with a target membrane is mediated by the soluble N-ethylmaleimide sensitive factor attachment protein receptor (SNARE) complexes. These complexes are formed by the regulated assembly of a 4-helix bundle of 3 Q-SNARE motifs and one R-SNARE motif present in the SNAREs of adjacent fusing membranes. Q-SNARE proteins are usually found on the target membranes and receive the name of t-SNAREs, and those that present a transmembrane domain belong to the family of Syntaxins. In contrast, R-SNARE proteins usually localize to vesicles and endosomes, and receive the name of v-SNAREs. In polarized epithelial cells, apical and basolateral vesicles contain different v-SNAREs (such as VAMP7 for apical, VAMP8/endobrevin and VAMP3/cellubrevin for basolateral transport). Certain t-SNAREs are segregated to the apical (syntaxin-3) and basolateral (syntaxin-4) plasma membrane domains. Loss-of-function or mislocalization of syntaxin-3 or -4 leads to a concomitant disruption of plasma membrane delivery of the apical or basolateral vesicle population, suggesting a role for polarized syntaxin localization in apicobasal polarity (ter Beest et al., 2005). The role of other SNAREs in vesicle trafficking and cell polarity is still unclear.

4. Cell-cell junctions assemble and regulate the activity of polarity complexes

Epithelial polarity in multicellular organisms is also regulated by the formation of cell-cell junctions between cells as well as by the presence of polarity protein complexes, which are well conserved throughout evolution (**Figure 3**). The polarity program is partially executed in epithelial cells by the competition and sequestration of these polarity complexes in different subcellular domains.

All along the lateral membrane that connects neighboring cells, junctional complexes delimit the apicobasal axis. In vertebrates, these complexes include apical tight junctions (TJs), laterally localized adherens junctions (AJs), desmosomes, focal-adhesions and hemi-desmosomes (**Figure 1**). Analogous structures exist in the *Drosophila* epithelium with some small differences. The *Drosophila* equivalents of the TJ, known as the septate junction, are localized basal, rather than apical to the AJ, although their cellular functions appear similar. TJs serve not only to establish an apical-basal barrier that inhibits the diffusion of solutes across the epithelial layer (gate function), but they also restrict the movement of proteins and outer-leaflet lipids between the apical and the basolateral membranes (fence function) (Matter and Balda, 2003). The TJs are composed primarily of membrane-bound junctional adhesion molecules (JAMs), claudins and occludins, which are connected to the cytoskeleton through the PDZ containing proteins zonula occludens 1-3 (ZO-1, ZO-2 and ZO-3) (Kohler and Zahraoui, 2005).

Adherens junctions perform multiple functions including initiation and stabilization of cell–cell adhesion, regulation of the actin cytoskeleton, intracellular signaling and transcriptional regulation. The central regulation of the AJs depends on interactions among transmembrane glycoproteins of the classical cadherin superfamily, such as E-cadherin, and the catenin family members including p120-catenin, β-catenin, and α-catenin. Together, these proteins control the formation, maintenance and function of AJs (Hartsock and Nelson, 2008). E-cadherin is the major transmembrane protein of the epithelial AJs, and initiates intercellular contacts through trans-pairing between cadherins on opposing cells (Gumbiner, 2005). Classical cadherins also bind directly and indirectly to many cytoplasmic proteins, particularly members of the catenin family, which locally regulate the organization of the actin cytoskeleton, cadherin stability and

intracellular signaling pathways that control gene transcription (Perez-Moreno and Fuchs, 2006).

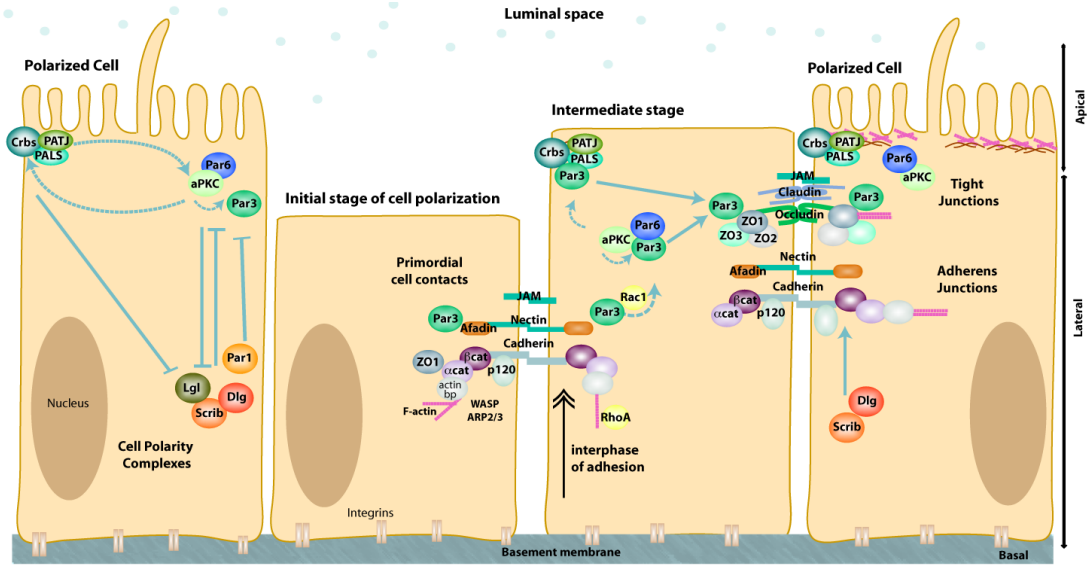

Figure 3. Polarity protein complexes. Polarized cells present polarized apical Crb and Par/aPKC complexes and basolateral Scribble and Par1 complexes, which act through phosphorylation and mutual apical vs. basolateral exclusion. During polarization, Nectin and Cadherin-based cell junction formation recruits ZO1 and Par3, which are later stabilized by Crb and Par/aPKC complex-mediated phosphorylation, and stabilization of claudins and occludin.

Throughout evolution and the development of highly complex multicellular organisms, the master regulator mechanisms of polarity generation and maintenance have been fundamentally conserved. Originally discovered in *C. elegans* and then in *Drosophila*, the PARtitioning defective genes (PARs) are involved in regulating cell polarity across all the animal kingdom. Other genes well known to regulate cell polarity have been found to interact directly or indirectly with the PAR proteins, constituting a complex polarity network that consists of several protein complexes.

Apical-basolateral polarization is essentially mediated by three interacting protein complexes: (1) the Par3/Par6/aPKC complex, consisting of Par3 (Bazooka in *Drosophila*), Par6, and atypical protein kinase C (aPKC); (2) the Crumbs complex, consisting of Crumbs, Stardust, PATJ and several other interacting proteins, such as Yurt, Coracle and Expanded (Laprise et al., 2006; Massey-Harroche et al., 2007); and (3) the Scribble complex, consisting of Scribble, Discs large (Dlg), and Lethal giant larvae (Lgl) (Goldstein and Macara, 2007; Wang and Margolis, 2007). The Par3/Par6/aPKC complex is involved in polarity and spatial organization in almost all metazoan cells, whereas the Crumbs complex is more specific to epithelial cells. Even though the molecular nature of these relationships is mostly unknown, these three complexes interact by a system of mutual exclusion to define the apical and basolateral

surfaces of epithelial cells in *Drosophila* (Bilder et al., 2003; Tanentzapf and Tepass, 2003), and they could function similarly in mammalian cells (Fig. 3). The Par/aPKC complex is a master regulator of polarity (Munro, 2006). Mammalian Par3 is localized to tight junctions through the interaction with JAM at the apical/lateral boundary (Izumi et al., 1998), and functions in their assembly (Chen and Macara, 2005), whereas Par6/ aPKC maintains the integrity of the apical domain (Martin-Belmonte et al., 2007). Par6 acts as a targeting subunit for aPKC, and it recruits both Crumbs complex (Hurd et al., 2003b; Lemmers et al., 2004) and Lgl (Scribble complex) as substrates (Betschinger et al., 2005). Crumbs controls the extension of the apical membrane (Macara, 2004), whereas the Par3-mediated phosphorilation of Lgl restricts the localization of Lgl to the basolateral domain. On the other hand, the Scribble complex suppresses apical membrane identity in the basolateral domain by inhibiting the Par3 complex (Tanentzapf and Tepass, 2003). How these opposing activities lead to the coalescence of AJs into the mature zonula adherens is not known, although it could involve regulation of the polarized transport of membrane proteins and polarized cytoskeletal regulation (Gangar et al., 2005).

Apart from the Scribble complex, one of the PAR proteins, Par1 is involved in basolateral specification through Par3 phosphorylation and exclusion (Benton and St Johnston, 2003). In contrast, Par3/Par6/aPKC phosphorylates Par1, eliminating it from the basolateral membrane. Par5 has been identified to function as a 14-3-3 protein with a role in sequestering S/T phosphorylated substrates of Par6/aPKC or Par1. In addition, Par1 determines the organization of microtubules in mammalian cells, which in turn establishes the position of the luminal surface (Cohen et al., 2004; Cohen et al., 2007).

Another PAR protein, Par4, also called LKB1 in mammals, is the most frequent genetic mutation found in Peutz-Jeghers syndrome, causing a predisposition to benign and malignant epithelial tumors (Morton et al., 2010; Shackelford and Shaw, 2009). Activation of LKB1 in mammalian intestinal epithelial cells in culture has demonstrated an essential role in cell polarity (Baas et al., 2004). Interestingly, LKB1 is phosphorylated by Par1, and LKB1 is required for polarity functions of Par1, suggesting that LKB1 mediates basolateral identity specification (Martin and St Johnston, 2003).

5. Epithelial organs are made of tubes with an interconnected lumen

Since exchange through an epithelium is proportional with its surface size, due to scaling laws, larger animals benefited from strategies to increase the surface of their epithelial organs (Lubarsky and Krasnow, 2003). In order to increase the exchange surface and transport efficiencies of the epithelial sheets, the majority of epithelial organs have evolved their shapes into wrapped or tubular architectures. Arguably, most epithelial organs are constructed by modular repetition of a single structure, the epithelial tube. These tubes consist of a monolayer of epithelial cells with a single interconnected extracellular space, the lumen (from latin, light), which communicates with the external environment. The formation of epithelial tubes during development has been extensively observed in most animal models. However, the mechanisms implicated in polarity maintenance are well understood when compared to our knowledge on the mechanisms that control tube formation. Upon careful examination, the developmental mechanisms leading to the formation of a single lumen are more diverse than initially expected. Tubular organs can be formed either from a previously established epithelial sheet, for instance during the process of invagination (Myat and Andrew, 2002), or from a group of precursors with mesenchymal phenotype which have to acquire epithelial cell polarity *de novo* (Bagnat et al., 2007). In some cases, epithelial cells can undergo a partial conversion into a mesenchymal phenotype, and then re-acquire epithelial polarity to form a new lumen, such as during the process of branching tube morphogenesis (Ochoa-Espinosa and Affolter, 2012).

In the past years many different cell models have been used to analyze the molecular and cellular events required to organize individual cells into 3D epithelial organs. Several *in vitro* systems consisting on cultured epithelial cell lines grown in a layer of (or embedded in) extracellular matrix (ECM) have been developed to study the molecular and cellular events required to organize individual cells into epithelial organs. Madin-Darby Canine Kidney (MDCK) epithelial cell system is perhaps the best and most widely used *in vitro* model to investigate cell polarity during epithelial morphogenesis (Lubarsky and Krasnow, 2003; Martin-Belmonte and Mostov, 2008; Zegers et al., 2003). MDCK cells, which have properties of the kidney distal tubule and collecting duct, have been used for decades as a 2D model to study epithelial polarity and protein trafficking. However, since the culture support provides an overriding extrinsic cue to orient cell polarity, they represent a less appropriate model to analyze

morphogenesis. By contrast, MDCK cells embedded in ECM form cysts, spherical monolayers enclosing a central fluid-filled lumen (Montesano et al., 1991), which have proven to be a very informative model system (**Figure 4a**). Especially, MDCK cells cultured in laminin-rich ECM extracts, such as Matrigel, rapidly form clonal polarized structures with an enclosed lumen between two cells after just 24h. From then on, the cysts continue to grow by cell division and lumen expansion. This rapid polarized growth allows fast genetic analysis of lumen formation mechanisms, perhaps the main advantage of this system.

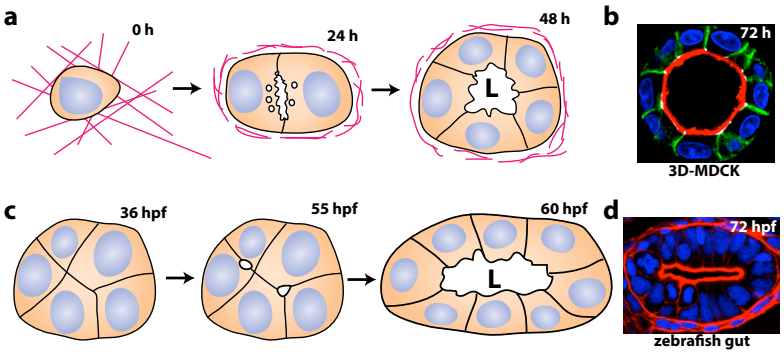

Figure 4. *De novo* lumen formation. a) *in vitro* MDCK cells cultured on laminin ECM extracts organize a 3D architecture and form a spherical monolayer enclosing a central single fluid-filled lumen. **b)** Immunofluorescence of MDCK cysts showing apical membrane (red), basolateral membrane (green), TJ (white) and DNA (blue) **c)** *in vivo* the zebrafish gut forms multiple small lumens that coalesce to form a single lumen continuous from the mouth to the cloaca. **d)** Immunofluorescence of a tranverse section of a zebrafish gut, showing apical actin (red) and DNA (blue).

The most studied *in vivo* model systems for tubulogenesis include the *Drosophila* trachea and salivary gland, the zebrafish gut and vasculature. Because of its powerful genetics, the *Drosophila* trachea and salivary gland are widely studied model systems for branched and unbranched tubes, respectively. Both organs begin as polarized epithelial placodes, which through coordinated cell shape changes, cell rearrangement, and cell migration form elongated tubes (Kerman et al., 2006). In addition to common, shared machineries with vertebrate epithelial morphogenesis, certain mechanisms appear to be specific of fly development. In particular, in the morphogenesis of the *Drosophila* trachea, the control of cell invagination, migration, competition, and rearrangement is accompanied by the sequential secretion and resorption of chitinal matrix proteins into and from the apical luminal space, a vital step in the elaboration of the trachea's complex tubular networks (Affolter and Caussinus, 2008).

Although great advances have been made in *Drosophila*, the study of tube morphogenesis using vertebrates represents a closer approach to understanding human development and disease. For instance, genetic analysis using the zebrafish model has led to identification of mutations in molecules that are required for gut morphogenesis (Pack et al., 1996). In the zebrafish gut, lumen formation occurs by de novo apical

polarization, and its individual steps have been recently characterized (**Figure 4b**) (Alvers et al., 2014; Bagnat et al., 2007; Ng et al., 2005; Wallace et al., 2005). Endoderm-derived intestinal progenitors converge in the medial line forming a rod-like structure consisting of about 1000 cells at 36 hours post-fertilization (hpf), which already present intercelular junctions. After a single division cycle, tight junctions become apparent at multiple sites in the rod. These sites accumulate apical polarity markers and later expand into small microlumens which rapidly become fluid filled at about 55-60 hpf. Then, at about 72 hpf lumens start progresively coalescing with anterior-to-posterior directionality through a mechanism that requires removal of interluminal junctions. Interestingly, the genetic program required for lumen coalescence is dependent on Hedgehog signaling, and its crosstalk with the underlying smooth muscle is essential for gut integrity (Alvers et al., 2014; Seiler et al., 2012). Thus, studies of morphogenesis in zebrafish could be critical for elucidating the molecular basis of uncharacterized congenital gut defects and potentially provide novel insight into intestinal oncogenic processes (Rubin, 2007; Zhong, 2005).

6. Lumen positioning is oriented by extracellular matrix cues that are transduced into cytoskeletal changes

Despite the diversity in the way cells assemble into tubes, there are many conserved morphogenetic processes. These include, at least, the orientation of the axis of polarity, and then the symmetry breaking process at the level of the plasma membrane by the formation of the apical domain and the central lumen.

In a simple tube, all of the epithelial cells are oriented so that their apical surfaces face the central lumen (O'Brien et al., 2002). To build a 3D tissue, the polarity of each cell must be coordinated. The orientation of epithelial polarity depends ultimately on the interaction of the cells with the surrounding ECM (**Figure 5**) (Kass et al., 2007). The association of basement membrane components and lumen formation was first described in studies in the 1980s using anti-laminin antibodies on mammary gland cells, hepatocytes, endothelial cells and developmental studies on the mouse neural tube (Spenle et al., 2013). Studies from the Brugge and Mostov labs later identified that laminin binding was required for lumen for polarity orientation, during which laminin binding by β1 integrin and activity of the small GTPase Rac1 were

required to form a polarized structure (Debnath et al., 2002; Muschler et al., 1999; O'Brien et al., 2001).

Although the requirement for laminin in epithelial morphogenesis is well established, cells can also sense physical properties of the environment, which impacts on their ability to communicate signals from the ECM that modify their behaviour (DuFort et al., 2011). To analyze the role of mechanical matrix properties in epithelial differentiation initial studies attempted to use different ECM mimics of varying stiffness. In such experiments, increasing matrix rigidity was shown to block cell polarity and lumen formation, and to promote a cancer-like invasive behavior (Alcaraz et al., 2008; Leight et al., 2012; Paszek et al., 2005). Another way of assessing mechanotransduction is through the use of micropatterns, which allow precise physical regulation of adhesion and have served to study the role of mechanotransduction in different processes, and could potentially be adapted for understanding lumen initiation mechanisms (Thery, 2010).

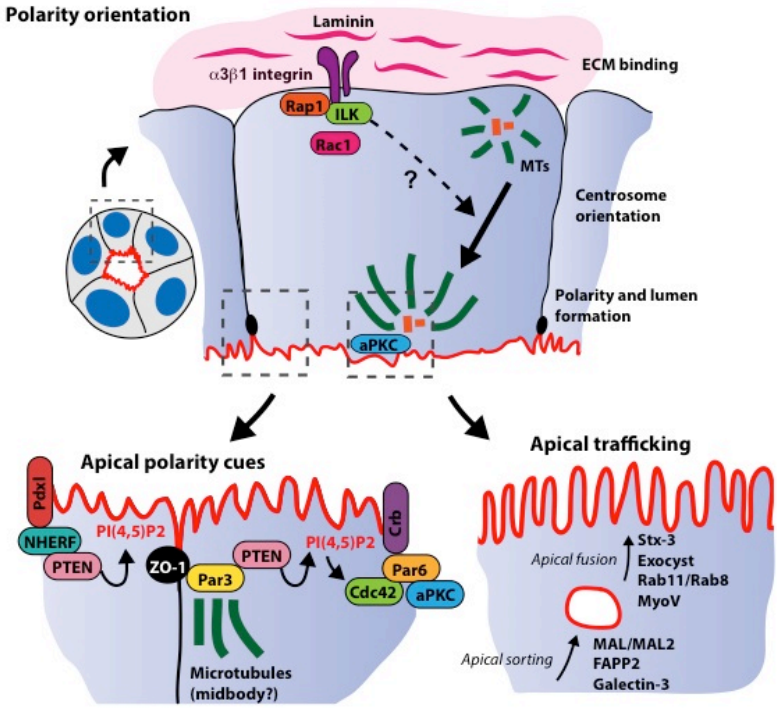

Figure 5. Polarity orientation and lumen initiation. Orientation of epithelial polarity depends on integrin-sensing of laminin cues in the ECM. Integrin activates ILK, which orients the microtubule cytoskeleton to polarize aPKC at the apical membrane. Apical polarity cues are maintained through Par3 and NHERF by recruitment of PTEN and enrichment of PtdIns(4,5)p2. Apical trafficking to form the lumen depends on specific sorting and fusion machineries.

Interestingly, both integrins and cadherins relay their signals to similar pathways that integrate the polarizing cues during the acquisition and maintenance of epithelial polarity. Previous work *in vitro* and *in vivo* has demonstrated important roles for small GTPsases in the establishment of the cadherin- and integrin-mediated adhesion. These include the Rho subfamily, mainly through Rac1 (O'Brien et al., 2001; Van Aelst and Symons, 2002; Yu et al., 2005), Arf GTPases and Rap1, a Ras-subfamily member (Fujita et al., 2006; Price et al., 2004; Rangarajan et al.,

2003). In addition, integrins and cadherins have the ability to induce, through the PI3K, the generation of *PtdIns(3,4,5)p3* (Kovacs et al., 2002; Velling et al., 2008) a phosphoinositide that controls the formation and identity of the basolateral plasma membrane (Gassama-Diagne et al., 2006). Since GTPases and phosphoinositides regulate the cytoskeleton in different cell types and processes (Fukata et al., 2003), they relay the engagement of cadherins and integrins into cytoskeletal changes that are essential for establishing epithelial polarity.

Ultimately the orientation of epithelial polarity depends on the localization of the centrosome and the orientation of microtubules. On the cytoplasmic side, β1 integrin binds and assembles a multiprotein complex named the IPP complex, which consists of Parvin, PINCH and Integrin-linked kinase (ILK) (Wickstrom et al., 2010). This complex has been shown to negatively regulate actin contractility through control of RhoA activity, although the molecular mechanism is incompletely understood. Perhaps as a consequence to its actin regulatory function ILK also regulates the polarity of the microtubule cytoskeleton. For instance, ILK is required for the organization of microtubules during polarized planar orientation of cell division and is required to control microtubule orientation during the initial steps of lumen formation in mammary gland acini (Akhtar and Streuli, 2012; Lange et al., 2009).

7. Lumen formation requires de novo fusion of apical membrane-loaded vesicles into the initiating luminal surface

Once the epithelial cells have established the orientation of apical-basolateral polarity and formed junctional complexes, the next step is to form the central lumen. How epithelial cells form this lumen is a key question in morphogenesis (Lubarsky and Krasnow, 2003).

Emerging data from different models have concluded that, probably in all systems, epithelial cells create lumens by sorting and secretion of apical-precursor containing vesicles (Lubarsky and Krasnow, 2003; O'Brien et al., 2002) (**Figure 5**). Apical targeted proteins might be delivered to the nascent luminal surface by exocytosis of a specialized organelle, the vacuolar apical compartment (VAC). The existence of these VACs was characterized *in vivo* in the developing blood vessels of fish embryos (Kamei et al., 2006), although it could follow different morphogenesis programs (Blum et al., 2008). In epithelial cells, VACs seems to appear only in non physiological

situations (Vega-Salas et al., 1987). In fact, the accumulation of apparent VACs was observed when Cdc42 was depleted in the 3D MDCK model, indicating a role for Cdc42 in exocytosis during lumen formation (Martin-Belmonte et al., 2007). In addition, disruption of other elements of the apical sorting machinery such as MAL, MAL2, INF2, annexin A2, annexin A13, Galectin-3, syntaxin 3 and FAPP2, have been found to regulate lumen formation (Madrid et al., 2010; Martin-Belmonte et al., 2007; Torkko et al., 2008; Vieira et al., 2005).

Small GTPases of the Rab family of proteins control different aspects of vesicle transport and fusion, both in endocytosis, recycling and exocytosis. At least two members, Rab11 and Rab8, regulate exocytosis of apical proteins *in vitro* and *in vivo* to form the lumen (Bryant et al., 2010; Li et al., 2007; Sato et al., 2007). Rab11 and Rab8 label apically targeted vesicles derived from the apical recycling endosome (ARE) and the TGN. In their active GTP-bound state, Rab11 and Rab8 bind to its effector, Myosin V, which is a plus-end directed actin motor (Roland et al., 2011; Roland et al., 2007). By virtue of the highly polarized apical actin cytoskeleton in epithelial cells, Myosin V tethers Rab11 and Rab8 vesicles to the apical plasma membrane. Finally, the exocyst is also an effector of Rab11 and Rab8 in trafficking during lumen formation (Beronja et al., 2005; Sang and Ready, 2002).

8. Phosphatidylinositides are required for establishing plasma membrane identity through regulation of polarity complexes

Phosphoinositides and other lipids are implicated in the generation of cell polarity (Carracedo and Pandolfi, 2008; Di Paolo and De Camilli, 2006). Diverse phosphoinositides are enriched in specific subcellular compartments, concentrated at the cytosolic surface of cellular membranes. In mammalian epithelial cells *PtdIns(4,5)p2* is a key determinant of the apical surface, whereas *PtdIns(3,4,5)p3* is a determinant of the basolateral surface (Gassama-Diagne et al., 2006; Martin-Belmonte and Mostov, 2007). The lipid phosphatase, PTEN (*phosphatase and tensin homolog deleted on chromosome 10*), which converts *PtdIns(3,4,5)p3* to *PtdIns(4,5)p2*, becomes localized early to the apical domain, and its activity is required both for segregation of the two lipids, and for normal morphogenesis in different epithelia (Leslie et al., 2008). However, our understanding of how phosphoinositides are connected to cell polarity is still very limited. A possible explanation may involve the small GTPase Cdc42, which is a center

molecule in different polarity process in unicellular and multicellular organism (Etienne-Manneville, 2004). *PtdIns(4,5)p2* to the cell membrane leads to the recruitment and activation of Cdc42 in 3D-MDCK (**Figure 5**) (Martin-Belmonte et al., 2007). Although the role of *PtdIns(4,5)p2* in regulating apical Cdc42 is established, the molecular mechanism immediately upstream of Cdc42 has not been identified.

Downstream of *PtdIns(4,5)p2,* Cdc42 also binds to Par6 and is necessary for correct localization of Par6/aPKC, as well as for normal apico-basal polarization of *Drosophila* neuroblasts and epithelial cells (both in 3D MDCK and in *Drosophila*) (Atwood et al., 2007; Hutterer et al., 2004; Martin-Belmonte et al., 2007). Recent results in *Drosophila* neuroblasts have shown that Cdc42 localizes Par6/aPKC at the apical cortex in a Par3-dependent manner, indicating that Par3 is upstream of Cdc42 in these cells (Atwood et al., 2007), and upstream of Par6/aPKC in embryonic epithelial cells (Harris and Peifer, 2005).

Par3 contains multiple PDZ domains, which interact with tight-junction proteins such as ZO-1, with NHERF (Na+/H+ exchanger regulatory factor) adaptor proteins, which bind to apical receptors and channels, and with PTEN, thus directing *PtdIns(3,4,5)p3* depletion at the tight junctions (Martin-Belmonte et al., 2007; Morales et al., 2007; von Stein et al., 2005; Wu et al., 2007). Par3 malfunction has proved to induce defects in central lumen formation *in vitro* in the 3D-MDCK model system (Hurd et al., 2003a), and also *in vivo* in cardiac cyst development in mice (Hirose et al., 2006). However, the mechanism that first targets Par3 to the preapical zone is still unclear. Interestingly, Par3 binds microtubules and becomes highly enriched after division and then in the midbody remnants of dividing cells (Feldman and Priess, 2012; Pollarolo et al., 2011). Thus, it has been proposed that the positioning of the midbody could establish an initial landmark for assembly of the cell polarity machinery, analogous to the budding yeast scar formation (Johnson et al., 2011).

9. The orientation of cell divisions is controlled in epithelial tissues and depends on the polarity program

Epithelial cells divide in a stereotypical fashion, with the plane of division always aligned perpendicular to the apicobasal axis (**Figure 6**). The midbody, an inter-cellular structure derived from central spindle microtubules, is asymmetrically localized near the apical surface during cytokinesis. Interestingly, the midbody colocalizes with apical

determinants such as Par3, aPKC and Crumbs3a (Crb3a) and trafficking of Crbs3a in Rab11 vesicles to the midbody is necessary for early lumen formation (Schluter et al., 2009). Since the orientation of the spindle determines the position of the midbody in mitosis and therefore the lumen initiation site, these experiments suggest that spindle misorientation may induce multiple dysfunctional lumens arising from multiple mislocalized midbodies in the epithelial estructure. Thus, the control of the positioning of the mitotic spindle and the midbody requires a tightly regulated mechanism.

Spindle orientation is regulated through astral microtubule capture at the plasma membrane by a protein complex formed by the small G-protein Gαi, Pins (LGN) and NuMA (Siller and Doe, 2009). Originally discovered in *Drosophila*, the mechanism was characterized in the regulation of asymmetric cell division during neuroblast differentiation (Cai et al., 2003; Du et al., 2001; Schaefer et al., 2000; Yu et al., 2000). In particular a role for Pins in epithelial morphogenesis has been established (Rodriguez-Fraticelli et al., 2010; Zheng et al., 2010). When these cells divide, the mitotic spindle is initially formed with an apicobasal orientation, and rapidly rotates 90 degrees aligning itself parallel to the epithelial monolayer. Pins localization to the lateral membrane helps astral microtubule anchoring in this region, and prevents the spindle from realigning in the apicobasal axis (Blumer et al., 2006; Morin et al., 2007; Peyre et al., 2011; Zheng et al., 2010). Disruption or mislocalization of Pins inhibits normal lumen formation and causes spindle misorientation. Pins segregation appears to be regulated by aPKC-mediated phosphorylation at the apical membrane, which causes it to be sequestered in the cytoplasm by 14-3-3ζ (Hao et al., 2010). Disruption of either of the components of the Par6-Par3-aPKC complex causes multiple lumen formation, abnormal spindle orientation, and loss of polarized localization of Pins (Fig. 3) (Hao et al., 2010; Munson et al., 2008).

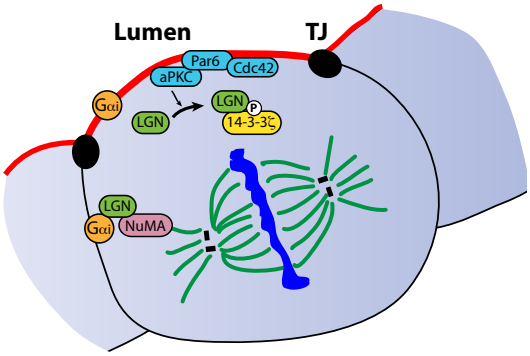

Figure 6. Spindle orientation in epithelial cells. Spindle orientation depends on apical exclusion, similar to Par-protein exclusion mechanisms. During symmetric planar division, aPKC phosphorylates and excludes LGN/Pins, which anchors astral microtubules to the basolateral membrane.

10. Endocytic control of epithelial morphogenesis

Membrane traffic does not simply reinforce polarity, but is critical for the generation of cortical epithelial cell asymmetry. Endosomes act as polarized sorting centers and are instrumental in the establishment, maintenance and plasticity of epithelial polarity and separated membrane domains (Golachowska et al., 2010).

Endocytosis of receptors is a common strategy for regulating the activity of many types of cell-signaling pathways. Similarly, cell polarity requires controlled plasma membrane levels of certain transmembrane proteins that act as 'master regulators' of apico-basal polarity (Shivas et al., 2010). Endocytosis could function to restrict surface levels of these proteins by mediating their transport to lysosomes for degradation or recycling (**Figure 7**).

Crumbs (Crb) was first identified as an apical determinant in *Drosophila melanogaster* embryonic epithelia, where it is required for the maintenance of apicobasal polarity (Grawe et al., 1996; Tepass, 1996; Tepass and Knust, 1993; Tepass et al., 1990; Wodarz et al., 1993). Accumulated evidence suggests that membrane Crb is

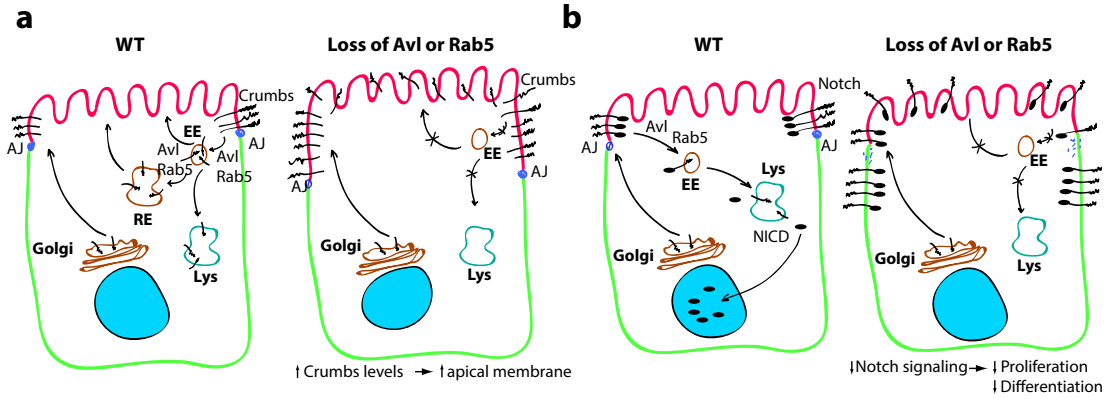

Figure 7. Endocytic regulation of epithelial morphogenesis in *Drosophila melanogaster*. a) Disruption of the early-endosome formation machinery, by Avl or Rab5 mutation, leads to apical accumulation of Crb, which results in the expansion of the apical membrane domain. **b)** Loss of Avl/Rab5 also results in defective Notch endocytosis and cleavage, leading to defects in epithelial differentiation. Adapted from Eaton and Martin-Belmonte, 2014.

constantly internalized to maintain the level of surface expression that allows appropriate overall apicobasal polarity. In order to maintain the proper levels of Crb in the apical domain, the endocytic uptake of Crb at this domain must be finely regulated (Fletcher et al., 2012). A mosaic genetic screen described that a mutant of a protein required for apical internalization of Crb, *avalanche* (*avl*), caused a defect in apico-basal polarity in follicle cells (Lu and Bilder, 2005). Interestingly, *avl* encodes an endosomal syntaxin required for endosomal fusion (homologous to human Syntaxin 7

and 12), and colocalizes with early (Rab5-positive) and recycling (Rab11-positive) endosomes. *Rab5* null deletion mutant showed multilayered, overproliferative phenotypes very similar to *avl,* which suggest that apical Crb is internalized, via Avl and Rab5, to maintain the level of surface expression that allows appropriate overall apico-basal polarity.

The Notch pathway is another archetypal pathway required for epithelial morphogenesis that relies on endocytosis for its activity and regulation (Fortini and Bilder, 2009; Windler and Bilder, 2010). Notch receptors were initially characterized to be required for wing development and neurogenesis in *Drosophila,* and have since been implicated in most asymmetric fate decision mechanisms in most animal models (Guruharsha et al., 2012). Upon ligand binding, Notch receptors are cleaved by an intracellular protease, γ-secretase, which releases its intracellular domain (NICD) to the cytoplasm, where it may enter the nucleus and act as a context dependent transcriptional regulator. Notch receptor internalization appears to be required for Notch signaling and both *avl* and *rab5* mutants present defects in Notch activity (Vaccari et al., 2008). Since defective apical endocytosis directly regulates Crb levels, and Notch signaling, this suggests that endocytosis could be finely tuned during development to regulate apico-basal polarity and epithelial morphogenesis. At least one study has shown that apical endocytosis increases as epithelial polarity is acquired in the *Drosophila* embryo (Fabrowski et al., 2013), raising the question of whether endocytic regulation might be a widespread mechanism used for epithelial morphogenesis also in vertebrates.

11. Developmental regulation of epithelial morphogenesis

The epithelial polarity program constitutes a series of modules, which are reused by different epithelial cells and organs to build the complexity of shapes and functions observed in the adult. Morphogenesis is a genetically controlled developmental process that is governed by a sequential cascade of master patterning genes and morphogenesis genes that interact and regulate these universal polarity modules (St Johnston and Sanson, 2011). Studies in the *Drosophila* trachea and the mouse pancreas have elucidated the existence of master tubulogenesis regulators, such as Trachealess and Pdx1 (Ghabrial et al., 2011; Svensson et al., 2007). Studies using genetic ablation of these master genes have established a relative gene set list size of about 100-300 genes that lie downstream of these master regulators. Unbiased genome wide genetic

screenings have estimated a similar size of gene sets that are required to organize an epithelial organ. Similar unbiased genome-wide strategies could provide useful information on novel machinery that controls different epithelial organ models, both *in vivo* and *in vitro*, in order to elucidate common or specific machineries.

IV.
MATERIALS AND METHODS AND RESULTS

CELL CONFINEMENT CONTROLS CENTROSOME POSITIONING AND LUMEN INITIATION DURING EPITHELIAL MORPHOGENESIS

***Alejo E. Rodríguez-Fraticelli**, Muriel Auzan, Miguel A. Alonso, Michel Bornens, Fernando Martín-Belmonte.*

Publicado en septiembre de 2012 en The Journal of Cell Biology *198; págs* 1011-23.

PRESENTACION

La morfogénesis epitelial depende de la correcta orientación del eje apicobasal de todas las células epiteliales que componen el órgano. Esta orientación depende de señales de la matriz extracelular (ECM), como lamininas y colágenos. Sin embargo, las células también son sensibles a estímulos mecánicos, como la tensión de la matriz, y el confinamiento celular. Las propiedades mecánicas de la ECM se encuentran frecuentemente alteradas en procesos patológicos como la tumorogénesis, pero los efectos de la mecanotransducción en la orientación de la polaridad y la formación del lumen se encuentran poco detallados.

Las superficies adhesivas microimprimidas ("micropatterns") constituyen una forma altamente estandarizada del control de la superficie de adhesión celular, permitiendo estudiar el efecto del confinamiento celular. Usando micropatterns, otros grupos han descrito que las células epiteliales responden a estímulos de confinamiento, y que estos regulan la proliferación y la diferenciación celular. De este modo, nos propusimos estudiar si el confinamiento celular podría estar regulando la capacidad de las células epiteliales de formar un único lumen central cuando son cultivadas en 3D. Para ello, empleamos células MDCK cultivadas en 3D, aprovechando que el lumen primordial se genera inmediatamente entre las dos células hijas producto de la primera división celular. Desarrollamos un método de cultivo tridimensional de MDCK en micropatterns, en colaboración con la empresa francesa CYTOO, y lo utilizamos para estudiar el papel del confinamiento celular.

Cuando las células se cultivaban en micropatterns recubiertos de colágeno tipo-I, éstas se adherían fuertemente al sustrato, y se estiraban hasta casi recubrir la superficie entera, prerrequisito para estudiar el papel del confinamiento. Al reducir la superficie de adhesión, las células perdían progresivamente la formación de fibras de estrés de actina, al igual que la formación de grandes adhesiones focales. Luego de la primera división, las células en alto confinamiento formaban rápidamente un lumen entre las dos células hijas, mientras que las células en confinamiento reducido eran incapaces de formar el

lumen inicial luego de la primera división, y requerían muchas divisiones más hasta ser capaces de orientar la polaridad, e incluso la polaridad final del organoide estaba mal organizada. Cuando las células se cultivaban, en lugar de colágeno, en extractos de laminina purificada de lamina basal, todos los efectos del confinamiento eran irrelevantes, dado que la laminina inhibía la adhesión celular independientemente del tamaño de la superficie.

Aprovechando los cultivos en colágeno, describimos qué mecanismos estaban siendo regulados por el confinamiento celular y que eran necesarios para la orientación de la polaridad. Así, dilucidamos que una ruta dependiente de la quinasa basolateral Par4/LKB1 controlaba la actividad de la GTPasa monomérica RhoA, y sus efectores ROCK y Myosin-II, e inhibía la orientación de la polaridad luego de la división celular. Así, la inhibición de LKB1, ROCK o Myosin-II rescataba el fenotipo de formación del lumen en condiciones de bajo confinamiento, mientras que la activación de RhoA o Myosin-II en condiciones de alto confinamiento prevenía la orientación de la polaridad apicobasal. Además demostramos que estos efectos se encuentran por encima de la ruta de activación de Par6/aPKC, fundamental para la iniciación del proceso de formación del lumen, ya que los inhibidores químicos de aPKC bloqueaban la orientación de la polaridad y la formación del lumen incluso en condiciones de inhibición de Myosin-II.

Estos estudios nos permitieron esclarecer que además de la ruta de orientación celular dependiente de Rac1 y fosfoinosítidos, el proceso de formación del lumen también está regulado por un proceso de mecanotransducción. Además, nuestros estudios esclarecieron que esta ruta de mecanotransducción es dependiente de LKB1/RhoA/ROCK/Myosin-II, y que la presencia de laminina inhibe esta ruta independientemente del estado de confinamiento celular.

Published September 10, 2012

Cell confinement controls centrosome positioning and lumen initiation during epithelial morphogenesis

Alejo E. Rodríguez-Fraticelli,[1] Muriel Auzan,[2] Miguel A. Alonso,[1] Michel Bornens,[3] and Fernando Martín-Belmonte[1]

[1]Centro de Biología Molecular Severo Ochoa, Consejo Superior de Investigaciones Científicas-Universidad Autónoma de Madrid, 28049 Madrid, Spain
[2]CYTOO SA, Commissariat à l'Energie Atomique et aux Energies Alternatives Grenoble, 38054 Grenoble, Cedex 09, France
[3]Unité Mixte de Recherche 144, Centre National de la Recherche Scientifique, Institut Curie, 75006 Paris, Cedex 05, France

Epithelial organ morphogenesis involves sequential acquisition of apicobasal polarity by epithelial cells and development of a functional lumen. In vivo, cells perceive signals from components of the extracellular matrix (ECM), such as laminin and collagens, as well as sense physical conditions, such as matrix stiffness and cell confinement. Alteration of the mechanical properties of the ECM has been shown to promote cell migration and invasion in cancer cells, but the effects on epithelial morphogenesis have not been characterized. We analyzed the effects of cell confinement on lumen morphogenesis using a novel, micropatterned, three-dimensional (3D) Madin-Darby canine kidney cell culture method. We show that cell confinement, by controlling cell spreading, limits peripheral actin contractility and promotes centrosome positioning and lumen initiation after the first cell division. In addition, peripheral actin contractility is mediated by master kinase Par-4/LKB1 via the RhoA–Rho kinase–myosin II pathway, and inhibition of this pathway restores lumen initiation in minimally confined cells. We conclude that cell confinement controls nuclear–centrosomal orientation and lumen initiation during 3D epithelial morphogenesis.

Introduction

Epithelial organs are essentially formed by a monolayer of epithelial cells surrounding a central lumen. Lumen formation is a sequential process during which individually polarized cells differentiate and acquire collective apicobasal polarity. The ECM provides the initial cue that orients the apicobasal polarity axis, which is regulated by the activities of β1 integrin, Rac1 GTPase, and laminin, a component of the basal epithelial ECM (O'Brien et al., 2001; Yu et al., 2005). Once oriented, the apicobasal axis directs apical vesicle trafficking toward cell–cell junctions to initiate the process of lumen formation (Bryant and Mostov, 2008). In addition, the physiological extracellular environment of epithelial cells, comprising a wide array of physical stimuli, including tissue stiffness, water tension, and cell confinement, is perceived by cells through a process termed mechanotransduction, which is essential for cell shape, development, and tissue homeostasis (DuFort et al., 2011). Recent advances have established the importance of mechanotransduction in the regulation of tumor progression and cancer cell migration (Butcher et al., 2009). However, analysis of individual properties of the extracellular physical environment has remained a challenge for many years. Micropatterned adhesive surfaces have proved a key tool for the analysis of the interactions between ECM and cell morphogenesis in a wide variety of models (Théry, 2010). For example, cell confinement on micropatterns has been shown to regulate the assembly and orientation of the primary cilium in single epithelial cells (Pitaval et al., 2010). Despite these advances, however, no studies have yet addressed the role of cell confinement in the acquisition of 3D cell polarity and lumen formation, which are essential physiological processes in epithelial organs.

To analyze the effect of cell confinement on lumen formation, we devised a method to control the adhesive microenvironment (i.e., the components and size of the adhesive matrix) using micropatterned surfaces coated with either collagen or laminin to induce 3D lumen formation from single MDCK cells. Using this

Correspondence to Fernando Martín-Belmonte: fmartin@cbm.uam.es

Abbreviations used in this paper: aPKC, atypical PKC; BB, blebbistatin; dox, doxycycline; GEF, guanine nucleotide exchange factor; KD, knockdown; ROCK, Rho kinase; PS, pseudosubstrate; shRNA, small hairpin RNA.

Supplemental Material can be found at:
http://jcb.rupress.org/content/suppl/2012/09/07/jcb.201203075.DC1.html
http://jcb.rupress.org/content/suppl/2012/09/17/jcb.201203075.DC2.html
Original image data can be found at:
http://jcb-dataviewer.rupress.org/jcb/browse/5420

The Rockefeller University Press $30.00
J. Cell Biol. Vol. 198 No. 6 1011–1023
www.jcb.org/cgi/doi/10.1083/jcb.201203075

Published September 10, 2012

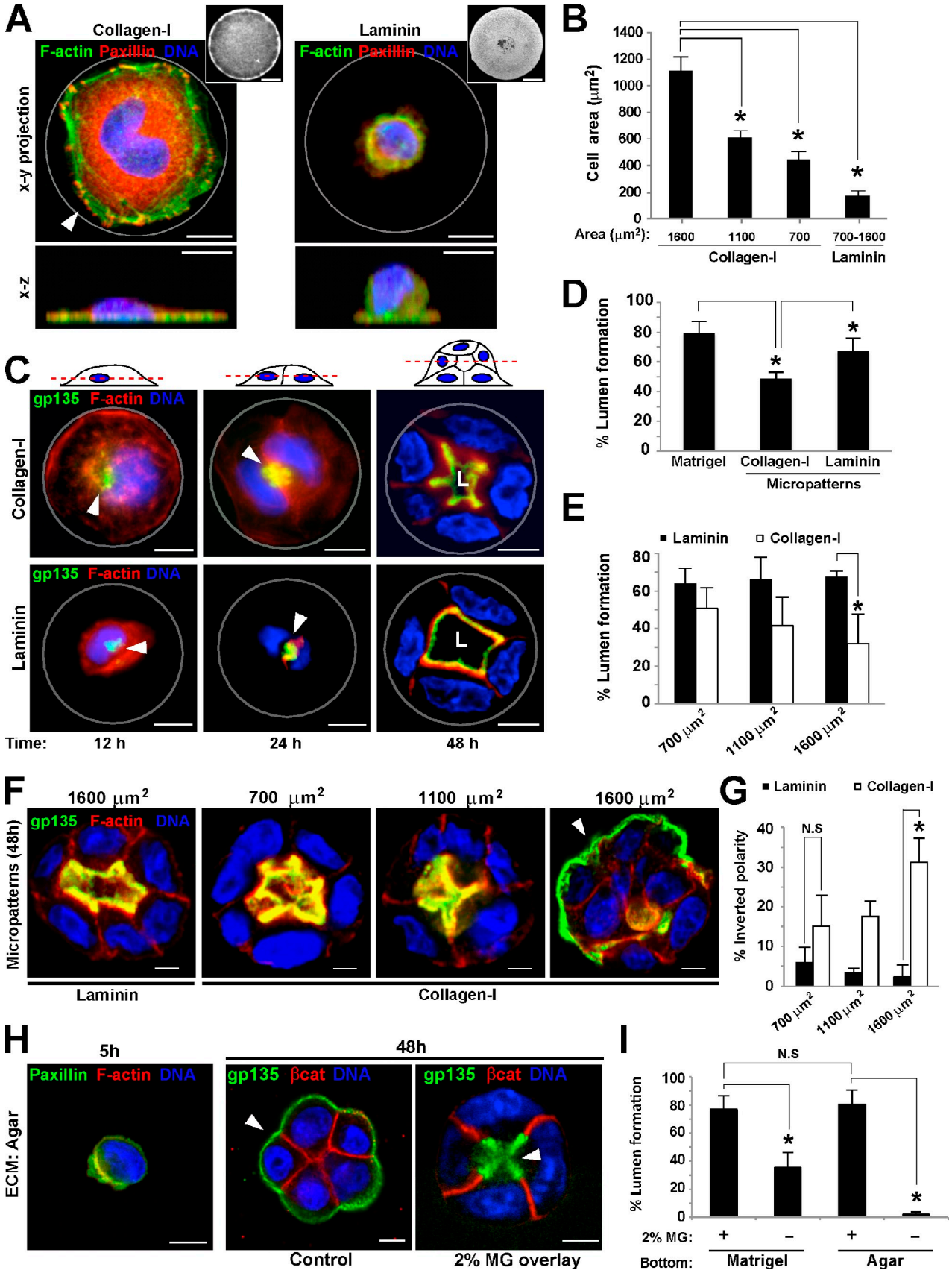

Figure 1. **Cell confinement in micropatterned surfaces regulates lumen formation.** (A) MDCK cells spreading on collagen I or laminin micropatterns. MDCK cells were seeded on 1,100-μm²-diam disk-shaped micropatterns using CYTOOchips. Cells were fixed 5 h after seeding. Cells were stained to detect F-actin, paxillin, and DNA and analyzed with confocal microscopy (maximum z projection). Micropattern collagen I or laminin staining is shown in the

Published September 10, 2012

method, we show that cell confinement regulates lumen initiation by modulating actin-mediated contractility from early cell aggregates to fully polarized epithelial tissues.

Results

Cell confinement regulates apicobasal polarity orientation and lumen formation

Confluent MDCK cells are typically grown in a 2D support and develop into a polarized columnar epithelium, in which the apical membrane forms by default at the only membrane domain in contact with the free medium. Upon reaching confluence, addition of ECM components generates a 3D cue that induces the formation of multicellular tubules in which cells develop a central lumen, separated from the surrounding medium (Ojakian et al., 1997). Lumen formation and apical membrane positioning have been traditionally studied in cells cultured at high confluence or using soft matrices, which prevent cell spreading and induce conditions similar to high cell confinement. As such, the contribution of cell confinement and cell spreading during the acquisition of epithelial cell polarity and lumen formation remains unknown. To address this issue, we first analyzed the effect of cell confinement on cell spreading using single epithelial cells seeded in disk-shaped micropatterns coated with different ECM substrates. Cells plated on collagen spread flat to cover the entire surface of the micropattern and formed extensive focal adhesions (visualized by paxillin staining), whereas those plated on laminin were taller and failed to spread or form focal adhesions, regardless of micropattern size (Fig. 1 A). Furthermore, in contrast to collagen-plated cells, in which cell spreading and focal adhesion formation depended on the surface area of the micropattern, cell spreading of laminin-plated cells was dramatically reduced regardless of micropattern size (Fig. 1 B and Fig. S1, A and B).

To investigate the effect of cell spreading on epithelial lumen formation, we seeded MDCK cells on disk-shaped micropatterns with Matrigel-supplemented medium to form 3D cysts and stained for the apical marker gp135/podocalyxin and F-actin to determine apical membrane localization. Interestingly, cells on collagen-coated micropatterns developed normal cysts with single central lumens (Fig. 1 C, top; Fig. S1, E and F; and Video 1), although less efficiently than cells cultured on laminin-coated micropatterns, in which lumen formation efficiency resembled that observed in normal 3D culture conditions (Fig. 1, C [bottom] and D). The observed improvement in normal lumen yield on laminin-coated micropatterns is consistent with previous studies, which found that laminin is required to orient apical–basal polarity in collagen gels (O'Brien et al., 2001; Yu et al., 2005). More importantly, our results suggested that physical confinement promotes 3D epithelial polarization and central lumen formation.

To test this hypothesis, we analyzed the role of cell confinement in lumen formation by plating MDCK cells on collagen I–coated micropatterns of different sizes. When cells were cultured on large micropatterns (low confinement conditions; 1,600 μm^2), we observed a significant increase in inverted polarity phenotypes and a reduction in lumen formation (Fig. 1, E–G). In contrast, culture of cells on smaller surfaces (high confinement conditions; 700 μm^2) resulted in a significant increase in the efficiency of lumen formation (Fig. 1, E–G). Cysts grown on laminin-coated micropatterns exhibited high lumen formation efficiencies independent of micropattern size (Fig. 1 E). To rule out a collagen I–specific effect, we cultured MDCK cells on micropatterns lacking any ECM substrate and observed similar results to those seen for collagen I–treated cells, although cell spreading was diminished, and the efficiency of lumen formation was slightly increased (Fig. S1, E and F). Collectively, these results indicate that high cell confinement promotes lumen formation under conditions that induce cell spreading, such as collagen I, and suggests that laminin signaling, which plays a key role in the orientation of cell polarity, also contributes to epithelial polarity by inhibiting cell spreading. Alternatively, laminin could diffuse into the basal side of the cell aggregates more easily in small micropatterns to promote cell polarization. We found, however, that laminin was exclusively deposited on the dorsal side of the cell aggregates, independent of cell confinement (Fig. S1 G). Thus, laminin diffusion does not alter lumen initiation in different cell confinement conditions.

To confirm the effect of cell confinement on lumen formation, we developed a novel method of cyst culture on agar, which prevents cell spreading (Discher et al., 2005). MDCK cells plated on agar mimicked the behavior of laminin-plated cells 5 h after

small top right insets. Arrowhead shows stress fibers. (B) Quantification of MDCK cell spreading in micropatterns of varying surface area (1,600, 1,100, and 700 μm^2) coated with collagen I or laminin. $n \geq 10$ cells/experiment. (C) Lumen formation in micropatterned MDCK cysts. MDCK cells were seeded on disk-shaped micropatterns (1,100 μm^2) coated with collagen I or laminin and grown to form cysts. Cysts were fixed at 12, 24, and 48 h. Samples were stained for gp135, F-actin, and DNA and analyzed with confocal microscopy. A scheme indicates the z plane shown in each image. Arrowheads indicate position of the apical membranes. L indicates the lumen. (D) Quantification of lumen formation in micropatterned MDCK cysts. MDCK cells were cultured to form cysts on collagen I– or laminin-coated micropatterns or cultured to form cysts on Matrigel (control). Cysts were fixed at 72 h, and normal lumen formation was quantified. $n \geq 30$ cysts/experiment. (E) Quantification of lumen formation efficiency in MDCK cysts formed on collagen- or laminin-coated micropatterns of different sizes (1,600, 1,100, and 700 μm^2). Cysts were fixed at 60 h, and normal lumen formation efficiency was quantified. $n \geq 30$ cysts/experiment. (F) Lumen formation in MDCK cysts using micropatterns of different sizes. MDCK cells were seeded on collagen I– or laminin-coated micropatterns of different sizes (1,600, 1,100, and 700 μm^2) and grown to form cysts. Cysts were fixed after 60 h and stained to detect gp135, F-actin, and DNA. Cysts were analyzed by confocal microscopy (central z slice is shown). Arrowhead indicates inverted apical polarity. (G) Quantification of cysts with inverted polarity in micropatterns of different sizes. MDCK cells were cultured to form micropatterned cysts, and the percentage of inverted apical polarity phenotypes was quantified. $n \geq 30$ cysts/experiment. (H) Cell spreading and lumen formation in MDCK cysts on soft agar. MDCK cells were seeded on agar-coated coverslips, fixed after 5 h, and stained to detect paxillin, F-actin, and DNA. Otherwise, MDCK cells were overlaid with 2% Matrigel-supplemented complete medium or nonsupplemented control medium. Cysts were cultured for 72 h and then fixed and stained to detect gp135, β-catenin, and DNA. Cysts were analyzed by confocal microscopy (central z slice is shown). Arrowheads indicate apical membrane localization. (I) Quantification of lumen formation on Matrigel or on soft agar, with or without 2% Matrigel (MG) overlay. $n \geq 50$ cysts/experiment. Values are means ± SD from three independent experiments. *, $P < 0.005$. Gray circles indicate micropattern shape. Bars, 5 µm.

Published September 10, 2012

System	Support	Medium	Bottom ECM	Cell spreading	Lumen formation	Scheme
Matrigel (3D-MDCK)	Matrigel	Matrigel	Matrigel	No	High	
2D-monolayers	Glass	MEM	None	Cell confluence-dependent	No lumens	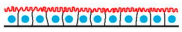
3D-monolayers	Glass	Matrigel-supplemented MEM	Laminin Collagen-I	Low High	High Very low	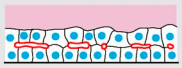
2D-micropatterns	Micropatterns	MEM	Laminin Collagen-I	Low Cell confinement-dependent	No	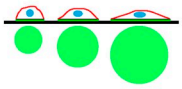
3D-micropatterns	Micropatterns	Matrigel-supplemented MEM	Laminin Collagen-I	Low Cell confinement-dependent	High Cell confinement-dependent	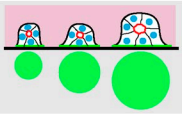
Agar	Agar gel	Matrigel-supplemented MEM	Agar	No	Yes	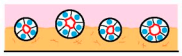

Apical membranes Nuclei Micropatterns Agar Matrigel Matrigel-supplemented medium

Figure 2. **Culture systems to analyze lumen formation using MDCK cells.** Description of MDCK cell culture systems. The table summarizes cell support, bottom ECM coating, and culture medium and provides information on cell spreading behavior and lumen formation in each condition. The right column shows a scheme of an x-z section of each culture system, indicating position of cells and apical membranes in different ECM supports. Additionally, in micropattern culture systems, an x-y view of micropatterns and their different sizes is also shown.

seeding (Fig. 1 H, left). When cells were grown for 72 h on agar in 2% Matrigel-supplemented medium, we observed significant cyst formation, with correct positioning of the apical membrane and comparable efficiency to MDCK cells plated in normal 3D cyst culture conditions (Fig. 1 H). Lumen formation on agar was highly dependent on Matrigel supplementation of the culture medium (Fig. 1 I). Collectively, these findings indicate that cell confinement suffices to promote lumen formation regardless of the substrate to which the cells are attached.

Of the many different culture techniques used, the 3D micropatterned MDCK method on collagen was the only one that afforded precise control of cell spreading and cell confinement (Fig. 2). Thus, to characterize the mechanism that regulates lumen formation, we performed all subsequent analyses using collagen I–coated micropatterns of different sizes.

Peripheral actin contractility induced by cell spreading impairs nuclear-centrosomal positioning and lumen initiation

The actin cytoskeleton is a mechanical biosensor that detects modifications in the surrounding environment and modifies cell behavior and shape to control cellular processes, such as migration and polarity (Li and Gundersen, 2008). To analyze in detail the effect of cell confinement on lumen formation and the actin cytoskeleton, we tracked actin dynamics by live-cell microscopy using a fluorescent F-actin probe (GFP-Life-actin) in MDCK cells on collagen I–coated micropatterns of different sizes. At the time of seeding, F-actin was concentrated in stress fibers and other peripheral structures, such as lamellipodia (Fig. 3 A, left; and Videos 2 and 3). After the first cell division, F-actin was progressively enriched at cell–cell contacts. Interestingly, actin localization was polarized almost exclusively to cell–cell contacts in high cell confinement conditions (700 μm^2). The lumen was visible after 10 h and fully opened at 24 h (Fig. 3 A, top, arrowheads). In contrast, cells in low confinement conditions exhibited more peripheral actin structures after the first cell division. Moreover, lumen formation in low confinement was substantially delayed, and cell morphology in the aggregates differed significantly from cell to cell (Fig. 3, A [bottom, arrows] and B [quantification]). Quantitative analysis revealed that lumens formed faster and more efficiently in high versus low confinement conditions (Fig. 3 C and Fig. S2 A). However, the final number of cells was similar in high and low confinement, indicating that cell proliferation was not significantly affected (Fig. 3 A, right). Collectively, these results suggest that peripheral actin contractility is increased in cells in low confinement conditions, which delays early apicobasal cell polarization and lumen initiation after the first cell division. Moreover, these findings indicate that regulation of apical membrane positioning is defined immediately after the first cell division. In subsequent experiments, we thus assessed the contribution of cell confinement to cell polarity and lumen initiation using two-cell early aggregates (24 h) grown on collagen I–coated micropatterns of different sizes.

In animal cells, the centrosome, the main microtubule-organizing center, is a key organelle for cell polarity (Bornens, 2012). In division, the centrosomes organize the mitotic spindle, which should be properly oriented for normal lumen formation (Jaffe et al., 2008). One possible explanation to our findings is that the orientation of cell division might change in different confinement conditions and thereby differentially affects the formation of the lumen. However, we observed that the orientation of the first cell

Published September 10, 2012

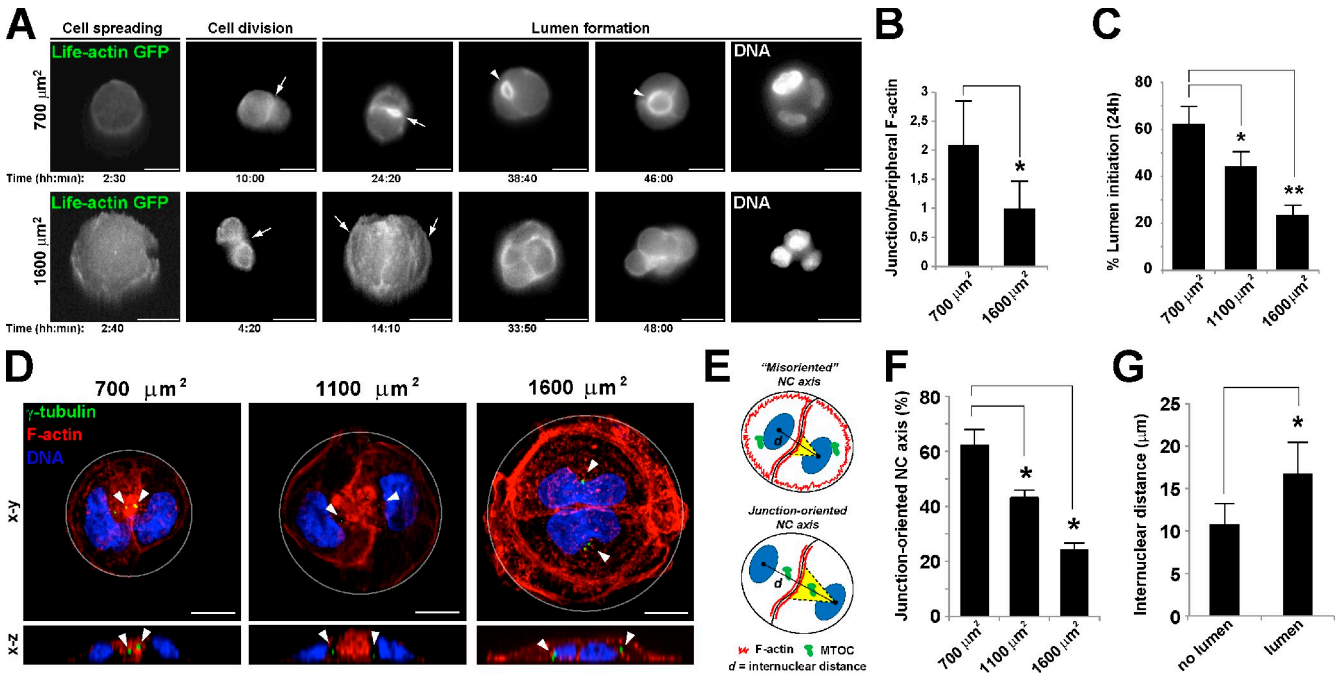

Figure 3. **Cell confinement regulates nuclear–centrosomal axis orientation after the first cell division.** (A) Life-actin-GFP localization during cyst formation in different confinement conditions. Life-actin-GFP MDCK cells were seeded on collagen I micropatterns of different sizes (700 and 1,600 μm²) to grow cysts and analyzed by video microscopy for 48 h (one frame = 10 min). After 48 h, DNA was stained with cell-permeable Hoechst to show nuclei. Cysts contained an aggregate of approximately four cells, of which three nuclei are visible in the same plane. Still images were selected at different time points, and in some cases, intensity was enhanced to facilitate visualization of cell structures. Arrows indicate accumulation of actin at the cell–cell junctions or peripheral actin fibers. Arrowheads indicate lumen. Bars, 20 μm. (B) Quantification of polarization of actin during micropatterned cyst formation in collagen. Life-actin-GFP signal was analyzed after first cell division using live-cell imaging. The ratio between Life-actin fluorescent signal at junctions and periphery was quantified ($n = 6$; *, $P < 0.05$). (C) Quantification of lumen initiation in collagen I micropatterned cysts at 24 h. $n \geq 50$ cysts/experiment; *, $P < 0.005$; **, $P < 0.001$. (D) Centrosome orientation in micropatterned MDCK cells. MDCK cells were seeded to grow cysts on collagen I–coated micropatterns of different sizes and fixed after 20 h. Cells were stained for F-actin, γ-tubulin, and nuclei. Cells were analyzed by confocal microscopy (z-stack projections and x-z cross sections are shown). Gray circles indicate micropattern shape. Arrowheads indicate position of the centrosome. Bars, 10 μm. (E) Scheme of procedures for quantification of centrosome and nuclear positioning in cell doublets. Distances between nuclei are quantified (*d*). The orientation of the nucleus–centrosome (NC) axis is considered incorrect (misoriented) when the centrosome is facing the periphery and correct (junction oriented) when the centrosome is within the 90° quadrant formed between the nucleus and the cell–cell junctions. MTOC, microtubule-organizing center. (F) Quantification of centrosome positioning in different confinement conditions. $n \geq 30$ cysts/experiment; *, $P < 0.005$. (G) Quantification of internuclear distance. $n \geq 30$ cysts/experiment; *, $P < 0.005$. Values are means ± SD from three independent experiments.

division is not significantly changed using micropatterns of different sizes (Fig. S2, B–D). On the other hand, the components of the vesicular trafficking pathway that regulates lumen formation are repositioned together with the centrosome, which orients toward the apical pole as epithelial cells differentiate (Datta et al., 2011). It remains unclear though whether centrosome positioning is essential for lumen formation (Rodríguez-Fraticelli et al., 2011). To determine the effect of cell confinement on centrosome localization, we analyzed the position of centrosomes in MDCK cells cultured on collagen-coated micropatterns of different sizes. After cell division in high confinement conditions, most centrosomes were oriented toward the lumen initiation site at the center of the micropattern, whereas the centrosomes of cells in low confinement conditions were predominantly oriented toward the periphery (Fig. 3, D–F; and Fig. S2, E and F). In addition, Golgi apparatus was polarized toward the junctions in high confinement, thus essentially mimicking centrosome positioning behavior in different confinement conditions (Fig. S3 A, top). Cell polarity is also defined by the relative position of the nucleus with respect to the centrosome (Luxton and Gundersen, 2011), and in migrating cells, actin contractility regulates nuclear movements and orients the nuclear–centrosomal axis (Gomes et al., 2005). We quantified the distance between the centers of nuclei in micropatterned MDCK cells as a measure of relative nuclear positioning (Fig. 3 E). In different confinement conditions, lumen-initiating cells consistently exhibited larger internuclear distances (Fig. 3 G). These findings indicate that cell confinement controls the orientation of the nuclear–centrosomal axis and suggest that centrosomal positioning, by repositioning the vesicular trafficking machinery toward the cell junctions, is required for lumen initiation.

Myosin II inhibition suppresses peripheral actin contractility and induces centrosomal orientation and lumen initiation

Alterations in actin contractility, regulated by myosin II, constitute the main cellular response to changes in cell confinement and consequent cell spreading. Increased cell spreading (low confinement) results in augmented ventral actin polymerization and filament bundling (Pitaval et al., 2010). Accordingly, highly confined MDCK cells on collagen I micropatterns exhibited fewer stress fibers and decreased paxillin staining as compared with cells in low confinement conditions (Fig. 1 A and Fig. S1, A and B). On the other hand, it is well established that cortical actomyosin contractility controls the position of the centrosome

Published September 10, 2012

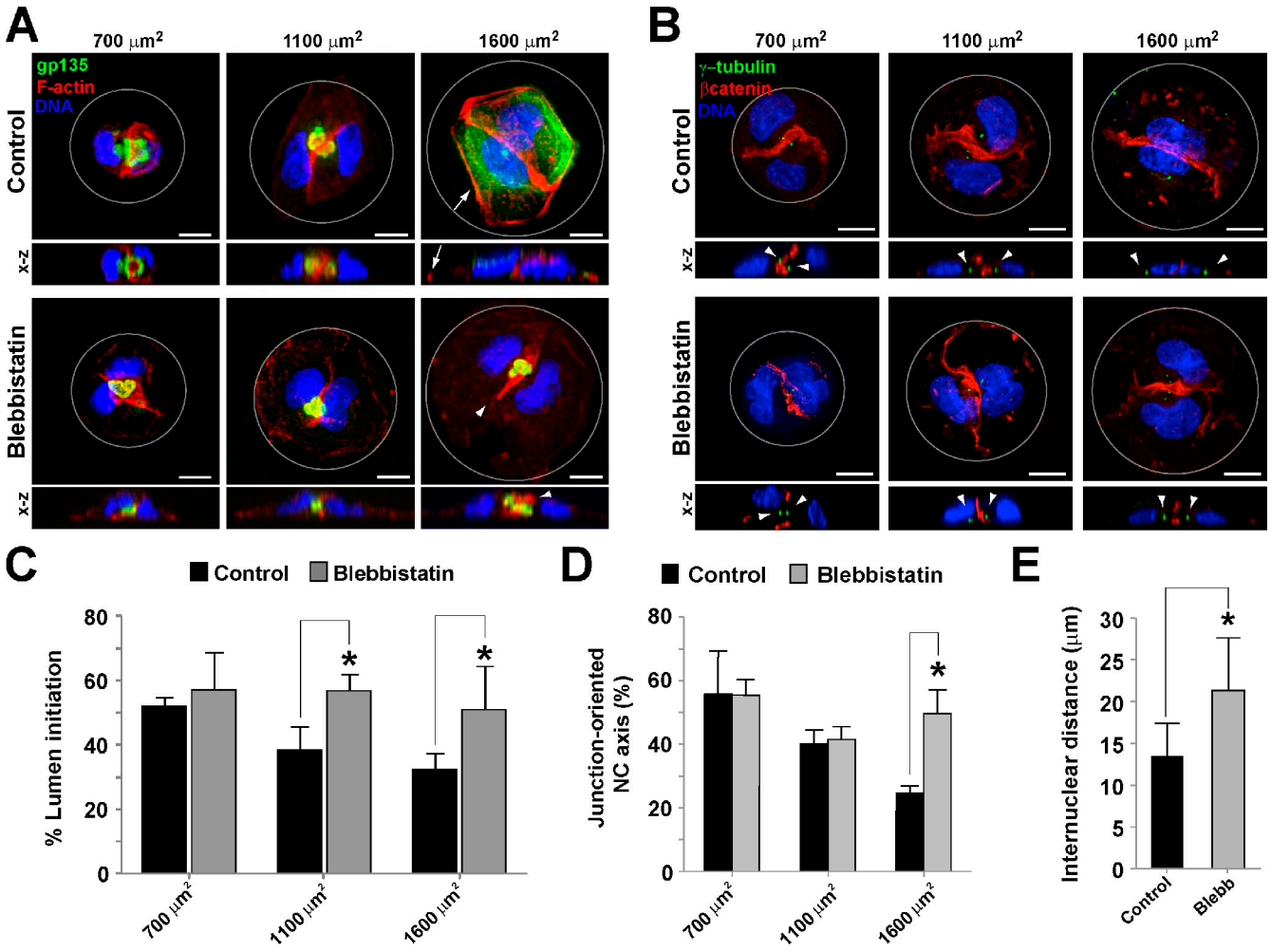

Figure 4. **Effect of myosin II inhibition on actin polarization, centrosome positioning, and lumen initiation.** (A) Effect of BB on lumen initiation. MDCK cells were seeded to grow cysts on collagen I–coated micropatterns of different sizes for 24 h. Cell cultures were treated with 50 µM BB for 30 min and then fixed and stained for F-actin, gp135, and nuclei. Cells were analyzed by confocal microscopy (z-stack projections are shown). Gray circles indicate pattern shape. An x-z view is shown for each image. Arrows indicate peripheral actin fibers. Arrowheads indicate junctional actin polarization and normal apical membrane formation. (B) Effect of BB on centrosome positioning. MDCK cells were seeded on micropatterns of different sizes, and cysts were grown for 24 h. Cell cultures were treated with 50 µM BB for 30 min and then fixed and stained for DNA, γ-tubulin, and β-catenin (red). Cells were analyzed by confocal microscopy (z-stack projections are shown). Gray circles indicate pattern shape. An x-z cross section is shown for each image. Arrowheads indicate centrosome localization. (C) Quantification of BB effect on lumen initiation. (D) Quantification of BB effect on centrosome positioning. NC, nucleus–centrosome. (E) Quantification of BB effect on internuclear distance in 1,600-µm² micropatterns. Values are means ± SD from three independent experiments ($n \geq 30$ cysts/experiment; *, $P < 0.005$). Bars, 10 µm.

in different animal species during both interphase and cell division (Bornens et al., 1989; Burakov et al., 2003; Gomes et al., 2005; Théry et al., 2005; Paluch et al., 2006; Fink et al., 2011). We thus investigated whether inhibition of actin contractility affected lumen initiation on micropatterns. Treatment of 3D micropatterned MDCK cells with the myosin II inhibitor blebbistatin (BB) suppressed actin contractility. Indeed, BB-treated cells exhibited a significant reduction in peripheral actin fibers, indicating that these structures are myosin II dependent (actomyosin II), but had no effect on junctional actin (Fig. 4 A, arrows and arrowheads). BB treatment of cells in low confinement conditions significantly rescued lumen initiation (Fig. 4 A). This result indicates that peripheral actomyosin II contractility in low confinement conditions prevents lumen initiation. To analyze the effect of BB on centrosome positioning, we stained cells for the centrosome marker γ-tubulin (Fig. 4 B). BB treatment of cells in low confinement conditions rectified centrosome orientation toward the cell junctions (Fig. 4, C and D), normal Golgi localization (Fig. S3 A, bottom), and nuclear positioning (Fig. 4, A, B, and E). These results suggest that low confinement conditions promote cell spreading and peripheral actomyosin II contractility, which may prevent the nuclear–centrosomal orientation required for lumen initiation. Inhibition of myosin II could be sufficient to correctly position the centrosome and initiate lumen formation.

Alternatively, increased cellular confinement may favor the formation or maintenance of cell–cell junctions that would then trigger centrosome repositioning and lumen initiation toward this compartment. To address this possibility, we analyzed the adherens junction markers β-catenin and E-cadherin and the focal adhesion marker vinculin in control and BB-treated cells attached to different-sized micropatterns (Fig. S3). Interestingly, we observed

Published September 10, 2012

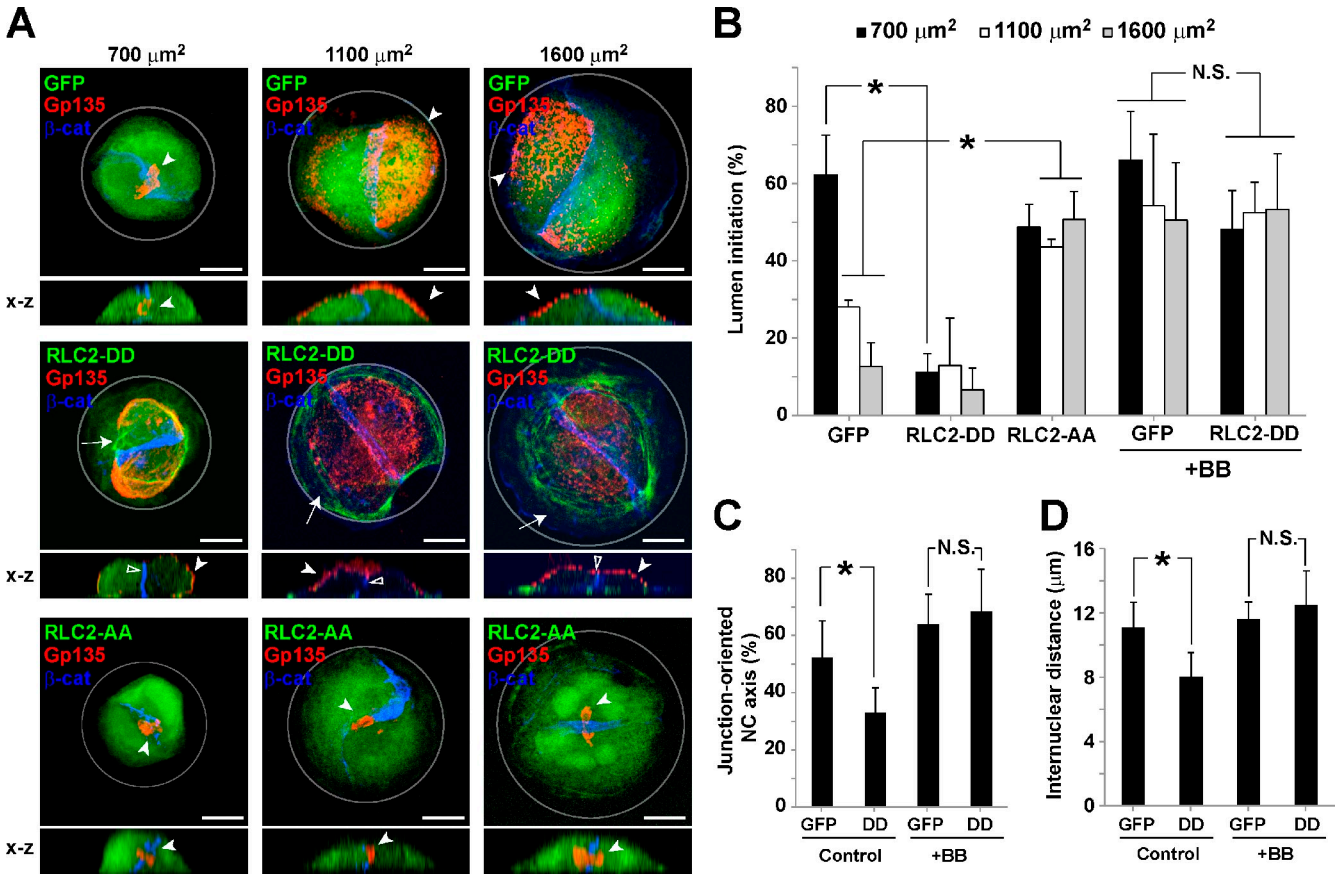

Figure 5. **Effect of myosin activation on lumen initiation.** (A) Effect of myosin RLC2 mutants (RLC2-DD and RLC2-AA) on lumen initiation. MDCK cells transfected with GFP-RLC2-DD, GFP-RLC2-AA, or GFP (control) were seeded on micropatterns of different sizes, and cysts were grown for 24 h. Cell cultures were fixed and stained for gp135 and β-catenin (β-cat). Cells were analyzed by confocal microscopy (z-stack projections are shown). Gray circles indicate pattern shape. An x-z view is shown for each image. Arrows indicate localization of RLC2-DD in peripheral contractile bundles. Filled arrowheads indicate apical membrane localization. Empty arrowheads indicate cell–cell junction position. Bars: (main images) 10 µm; (cross sections) 5 µm. (B) Quantification of RLC2-DD and RLC2-AA effects on lumen initiation. $n \geq 30$ cysts/experiment. (C) Quantification of RLC2-DD effect on centrosome positioning in high confinement (700 µm²). $n \geq 30$ cysts/experiment. NC, nucleus–centrosome. (D) Quantification of RLC2-DD effect on internuclear distance in high confinement (700 µm²). $n \geq 15$ cysts. Values are means ± SD from three independent experiments. *, $P < 0.05$.

similar distributions of β-catenin (Fig. S3, B and C, quantification) and E-cadherin (not depicted) in control and BB-treated cells in different confinement conditions. In contrast, vinculin was almost absent from cell–cell junctions and was mostly localized to peripheral focal adhesions, suggesting that these are the main tensile actin structures in micropatterned MDCK cells (Fig. S3 B, arrowheads). In fact, BB treatment disrupted peripheral vinculin staining, confirming the loss of peripheral contractility signaling (Fig. S3 B, bottom) but had no effect on vinculin levels at cellular junctions. Collectively, these results indicate that, in our experimental conditions, cell confinement does not significantly affect cell junction formation or maintenance, thus favoring the first possibility, in which nuclear–centrosomal orientation is modulated by peripheral actomyosin II contractility.

Constitutively active myosin II induces peripheral contractility and inhibits lumen initiation in conditions of high cell confinement

Myosin II activity is regulated by the myosin II regulatory light chain (RLC2), a subunit of the myosin II complex. The RLC2 subunit is phosphorylated by distinct protein kinases in two adjacent serine/threonine residues. Because the diphosphorylation of RLC2 activates the myosin II complex, expression of a double phosphomimetic RLC2 mutant, Thr-18-Asp/Ser-19-Asp (RLC2-DD), induces the formation of stable actin bundles and stress fibers in migrating cells (Vicente-Manzanares et al., 2008) and highly contractile structures in epithelial cells (Watanabe et al., 2007). RLC2-DD localized to peripheral bundles and stress fibers independently of cell confinement (Fig. 5 A, middle, arrows). Remarkably, cells expressing RLC2-DD formed significantly fewer lumens (Fig. 5, A [middle, arrowheads] and B [quantification]), and centrosome orientation was reduced in conditions of high confinement (Fig. 5 C). RLC2-DD expression also reduced internuclear distance (Fig. 5 D) but did not disrupt adherens junction formation (Fig. 5 A, middle, empty arrowheads). To confirm that cell confinement regulates lumen initiation specifically via myosin II activity, we treated RLC2-DD–transfected cells with BB, which significantly rescued lumen initiation (Fig. 5, B–D; and Fig. S3 D), and corrected centrosome orientation and nuclear positioning (Fig. 5, C and D). In contrast, overexpression of a nonphosphorylatable RLC2 mutant, Thr-18-Ala/Ser-19-Ala (RLC2-AA), produced similar effects to BB treatment in lumen initiation (Fig. 5 A, bottom;

Published September 10, 2012

and Fig. 4 B). Together, these findings indicate that low confinement increases cell spreading and peripheral contractility and inhibits lumen initiation and that inhibition of actomyosin II contractility is sufficient to restore centrosome positioning and initiate lumen morphogenesis.

An LKB1–RhoA pathway controls peripheral actin contractility in low confinement conditions

The Rho family GTPases are central regulators of cytoskeletal polarity and contractility (Heasman and Ridley, 2008). Different Rho-GTPases have been reported to activate myosin II via specific effectors, such as Rho kinase (ROCK) and myotonic dystrophy kinase–related Cdc42-binding kinase, which phosphorylate RLC2 (Wilkinson et al., 2005). In addition, Rho family GTPases control several steps associated with lumen formation (Martin-Belmonte et al., 2007; Ferrari et al., 2008; Yu et al., 2008; Strilić et al., 2009; Rodriguez-Fraticelli et al., 2010).

To analyze the contribution of the Rho–ROCK pathway to actomyosin II contractility during epithelial morphogenesis, we studied the effect of ROCK disruption on nuclear–centrosome positioning and lumen initiation in micropatterned MDCK cells. Treatment of cells with the ROCK inhibitor Y27632 resulted in a reduction in cortical stress fibers and significantly rescued normal lumen initiation and nuclear–centrosomal orientation in low confinement conditions (Fig. S4, A–C), thus mimicking the effects of BB treatment. These results indicate that peripheral actomyosin contractility is controlled by Rho–ROCK and that ROCK inhibition is sufficient to initiate lumen formation in conditions of low cell confinement.

Actin contractility is regulated by the master kinase Par-4/LKB1 both in culture (Williams and Brenman, 2008; Zagórska et al., 2010; Mirouse and Billaud, 2011) and in vivo (Chartier et al., 2011). Recent experiments have shown that LKB1 directly regulates RhoA–ROCK activation in epithelial cells (Xu et al., 2010) and centrosome positioning in neuronal cells (Asada et al., 2007). We thus analyzed the role of LKB1 in actin contractility and lumen formation in micropatterned cells. LKB1 localized to actin-rich intercellular junctions and peripheral actin structures in MDCK cells in both micropatterns and 3D cysts (Fig. S5, A and C), suggesting a role in actin contractility, consistent with a previous study (Sebbagh et al., 2009).

To analyze LKB1 function, we used a doxycycline (dox)-inducible MDCK cell line expressing small hairpin RNA (shRNA) for specific LKB1 silencing (Boehlke et al., 2010), which efficiently silenced LKB1 in dox-treated cells (Fig. S5 B). Interestingly, LKB1-silenced cells on micropatterns exhibited a significant decrease in peripheral F-actin staining in low cell confinement conditions (Fig. 6, A and B), which was sufficient to restore correct centrosome orientation (Fig. 6, C and E), lumen initiation, and nuclear positioning (Fig. 6, A–F). However, LKB1 function was required at later stages for normal cyst development (Fig. S5, D and E), consistent with previous studies that have characterized a role for LKB1 in apical junction formation (Hezel et al., 2008; Amin et al., 2009). To determine whether the effect of LKB1 on early lumen initiation was Rho dependent, we analyzed RhoA activity by pull-down assay, which revealed a 60% decrease in GTP-bound RhoA levels in LKB1-silenced cells in low confinement conditions (Fig. 6 G). Furthermore, in LKB1-silenced cells, expression of constitutively active RhoA (RhoA-V14) inhibited lumen initiation, whereas treatment with ROCK inhibitor had no further effect on lumen initiation (Fig. 6, H and I), confirming that RhoA lies downstream of LKB1 in this pathway. Collectively, these results indicate that in low confinement conditions, LKB1 activity regulates RhoA–ROCK-mediated actomyosin contractility, which in turn impairs normal centrosome positioning and lumen initiation.

Disruption of aPKC impairs centrosome positioning and lumen initiation independent of cell confinement or contractility

Our data indicate that cell confinement modulates centrosome position, which localize near the cell junctions to form the lumen in permissive conditions. These observations could be compatible with the existence of specific machinery to maintain the positioning of centrosome at the cell junction, independent of cell confinement or actin contractility. In that case, the disruption of this machinery should inhibit lumen initiation independent of cell confinement or actin contractility. To test this hypothesis, we targeted the Par6–atypical PKC (aPKC) complex, which is an important regulator of centrosome orientation and is required for lumen formation (Etienne-Manneville and Hall, 2003; Etienne-Manneville et al., 2005; Manneville and Etienne-Manneville, 2006; Martin-Belmonte et al., 2007). We found that in low confinement conditions, active aPKC (phosphorylated aPKC) was localized at cell–cell junctions in both normal and BB-treated cells (Fig. 7 A). Inhibition of aPKC activity using a myristoylated pseudosubstrate (PS) aPKC inhibitor (aPKC-PS) reduced lumen initiation and disrupted centrosome positioning both in conditions of high or low confinement (Fig. 7, B–D). BB treatment was not sufficient to rescue centrosome positioning or lumen formation in aPKC-PS–treated cells in either low or high confinement conditions (Fig. 7, B–D), implying that positioning of the centrosome at the cell junctions depends on aPKC activity independent of actin contractility. Thus, our data indicate that aPKC activity is required to properly position the centrosome at the cell junction during lumen initiation and suggest that centrosome positioning is required for lumen initiation. Interestingly, internuclear distance was significantly increased in cells treated with BB and aPKC-PS, indicating that nuclear positioning is regulated by actomyosin II, but not by aPKC, and suggesting that nuclear positioning and centrosome positioning might be regulated differently during lumen initiation in 3D MDCK cells (Fig. 7, E and F). In summary, our data indicate that aPKC activity is required to keep the centrosome in proper position during lumen initiation.

Discussion

In the present study, we characterized the role of cell confinement in lumen formation using a new methodology to analyze 3D epithelial morphogenesis in micropatterns. We found that

Published September 10, 2012

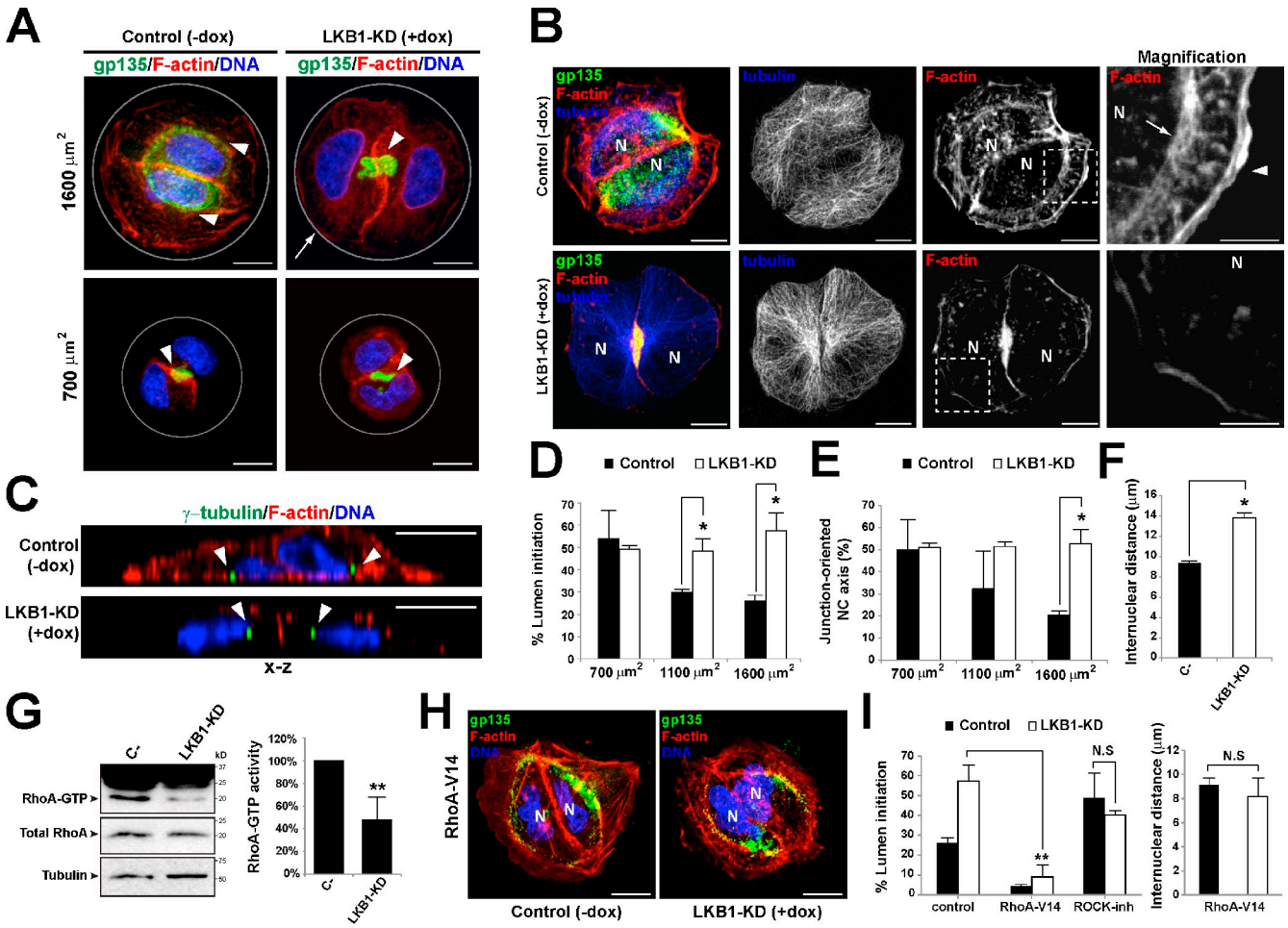

Figure 6. **LKB1 controls peripheral actin contractility through RhoA activation.** (A) Effect of LKB1 silencing in lumen initiation in micropatterned cysts. Control cells (−dox) or LKB1-KD (+dox) cells were seeded on micropatterns of different sizes and grown to form cysts. Micropatterned cells were fixed at 24 h and stained for gp135, F-actin, and nuclei. Gray circles indicate pattern shape. Arrowheads show apical membrane. Arrow shows reduced peripheral actin staining. (B) Effect of LKB1-KD in actin and microtubule cytoskeleton. Control cells (−dox) or LKB1-KD (+dox) cells on collagen-coated 1,600-μm² micropatterns were stained for gp135, F-actin, and tubulin. N, nuclei. Arrow indicates subcortical actin stress fibers. Arrowheads indicate cortical actin fibers. (C) Effect of LKB1-KD in centrosome positioning. Control cells (−dox) or LKB1-KD (+dox) cells grown to form cysts on collagen-coated 1,600-μm² micropatterns were fixed after 24 h. Cells were stained for γ-tubulin, F-actin, and DNA. An x-z cross section of cell doublets is shown. Arrowheads indicate centrosome position. (D) Quantification of correct lumen initiation in LKB1-KD cells. Control cells (−dox) or LKB1-KD (+dox) cysts fixed at 24 h were stained for gp135, F-actin, and nuclei. $n \geq 50$ cysts/experiment. (E) Quantification of centrosome position in LKB1-KD cells. $n \geq 50$ cysts/experiment. (F) Quantification of internuclear distance in LKB1-KD cells. $n \geq 50$ cysts/experiment. (G) RhoA-GTP levels in LKB1-KD cells. Control (C−) or LKB1-KD cells cultured at low density on collagen I–treated dishes were lysed, and RhoA-GTP levels were analyzed by pull-down assay using GST-tagged Rhotekin Rho-binding domain. Band intensity was quantified from three different experiments. Values are mean percentages of control ± SD (**, $P < 0.001$). (H) Effect of RhoA-V14 expression in LKB1-KD cells. Control or LKB1-KD cells transfected with RhoA-V14 were seeded on circular 1,600-μm² micropatterns to grow cysts and fixed after 24 h. Cysts were stained for gp135, F-actin, and tubulin. N, nuclei. (I) Quantification of lumen initiation and internuclear distances in RhoA-V14–expressing and ROCK-inhibited (inh) LKB1-KD cells. $n \geq 30$ cysts/experiment; **, $P < 0.005$. Values are means ± SD from three independent experiments. *, $P < 0.005$. Bars, 10 μm.

cell confinement, which modifies the actomyosin II–mediated contractility, is able to regulate epithelial polarity and lumen formation and the positioning of the centrosome and the nucleus. In conditions of low confinement, cell spreading increases peripheral actin contractility, which in turn impairs the initiation of lumen formation. Peripheral actomyosin contractility maintains centrosome positioning at the center of the cell perimeter and forces nuclear positioning toward the cell–cell junctions (Fig. 8). In contrast, in highly confined cells, peripheral actomyosin contractility is suppressed, allowing centrosome positioning toward the junctional membrane compartment and lumen initiation between adjacent cells (Fig. 8). Interestingly, laminin-rich ECMs inhibited cell spreading, recreating high confinement conditions and improving lumen formation outcomes. Supporting this hypothesis, myosin II inhibition induced lumen initiation on lowly confined cells, whereas expression of constitutively diphosphorylated RLC2 (RLC2-DD), an active form of myosin II, suppressed lumen initiation on high confinement. On the other hand, we observed that the activity of the aPKC signaling pathway at cellular junctions mediates centrosome relocation independent of cell confinement, consistent with previous studies (Georgiou et al., 2008; Desai et al., 2009; Wallace et al., 2010). In summary, these data suggest that the balance between the pathways controlling peripheral and junctional actin-stabilized compartments regulates centrosome positioning and initiation of epithelial morphogenesis (Fig. 8).

Published September 10, 2012

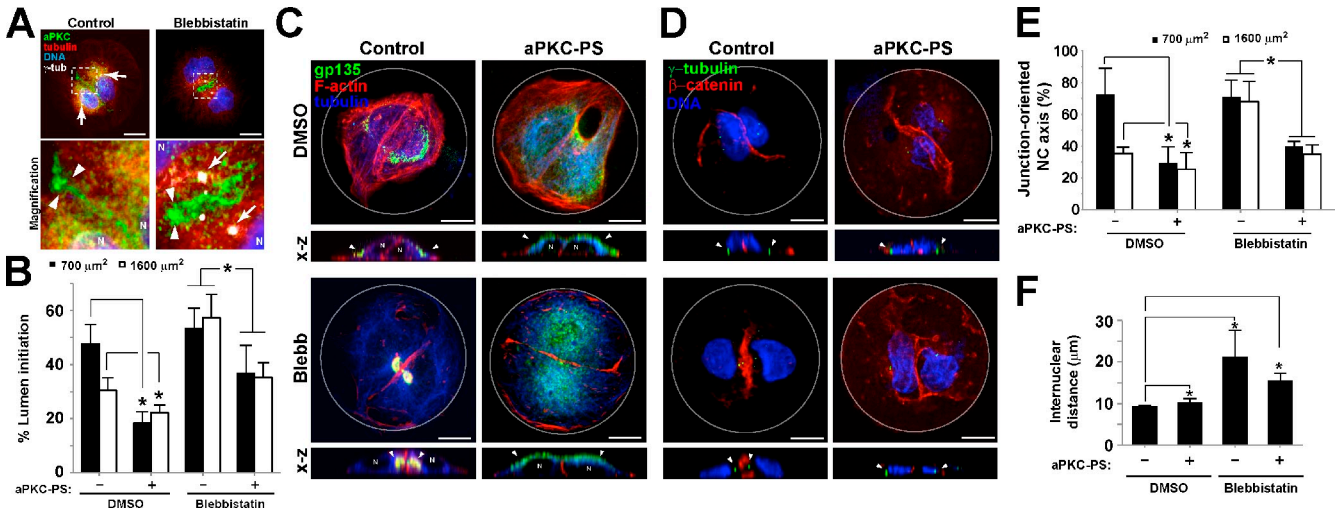

Figure 7. **Nuclear–centrosomal orientation during lumen initiation requires aPKC.** (A) Localization of aPKC in control or BB-treated MDCK cells. MDCK cells were seeded on micropatterns and treated with BB. Cells were fixed and stained to detect aPKC, tubulin, nuclei (blue), and γ-tubulin (γ-tub; gray). Arrowheads indicate aPKC localization at lateral plasma membrane. Arrows indicate centrosome localization. Dotted boxes show areas of magnification. (B) Quantification of lumen initiation in aPKC-PS inhibitor-treated cells. $n \geq 50$ cysts/experiment. (C) Effect of aPKC inhibition in BB (Bleb)-induced lumen morphogenesis on low confinement. MDCK cells were seeded on 1,600-μm² collagen I micropatterns and treated with 40 μg/ml aPKC-PS overnight. After 24 h, cells were treated with BB for 45 min and then were fixed and stained to detect gp135, F-actin, and tubulin. Cells were analyzed by confocal microscopy (z-stack projections and x-z cross sections are shown). Arrowheads show apical membrane. (D) Effect of aPKC inhibition on centrosome positioning. Cells grown as in C were fixed and stained to detect γ-tubulin, β-catenin, and DNA. Cells were analyzed by confocal microscopy (z-stack projections and x-z cross sections are shown). Gray circles indicate pattern shape. Arrowheads show centrosome position. (E) Quantification of centrosome positioning in aPKC inhibitor–treated cells. $n \geq 30$ cysts/experiment. NC, nucleus–centrosome. (F) Quantification of internuclear distance in aPKC inhibitor–treated cells. $n \geq 30$ cysts/experiment. Values are means ± SD from three independent experiments. *, $P < 0.05$. N, nuclei. Bars, 10 μm.

Centrosome positioning to specific regions close to the plasma membrane is considered essential for protein trafficking processes, such as the delivery of secretory granules to the immunological synapse in cytotoxic T lymphocytes, and for axon formation during the development of neuronal polarity (de Anda et al., 2005; Stinchcombe et al., 2006). Similarly, proper centrosome positioning could be critical to position the vesicular trafficking machinery for normal lumen formation. However, the role of centrosome positioning in epithelial lumen formation has not been clearly established. Our findings reveal that aPKC is required for centrosome positioning and lumen initiation independent of actin contractility, suggesting that centrosome positioning is required to initiate the lumen, but further studies will be required to clearly demonstrate this mechanism. Lumen initiation requires the activation of small GTPases, such as Cdc42, Rab8, Rab11, and the exocyst (Martin-Belmonte et al., 2007; Sfakianos et al., 2007; Schlüter et al., 2009; Bryant et al., 2010). Notably, Cdc42 guanine nucleotide exchange factors (GEFs; ITSN2) and Rab8 GEFs (Rabin8) localize at the centrosome in MDCK cells (Bryant et al., 2010; Rodriguez-Fraticelli et al., 2010). This suggests that centrosome positioning could potentially define Rab8 and Cdc42 activation in target plasma membrane compartments during lumen formation.

In accordance with previous studies in migrating cells, actomyosin II contractility also affected the position of the nuclei (Gomes et al., 2005; Luxton and Gundersen, 2011). Peripheral contractility actively localizes nuclei to the center of the cell aggregate, precluding nuclear–centrosomal axis orientation to form the lumen. When peripheral actin contractility is reduced, nuclear positioning appears to facilitate polarity reorientation and lumen initiation. In this respect, cells in low confinement conditions mimic the behavior of cells in wound closure assays, which produce contractile actin at the wound edge that repels the nuclei from the wound to orient the nuclear–centrosomal axis (Gomes et al., 2005). However, it remains unclear whether nuclear positioning in epithelial cells is controlled directly by nuclear membrane actin-binding proteins (Luxton et al., 2010).

Our results also demonstrate that the tumor suppressor kinase LKB1 and the RhoA signaling pathway regulate peripheral actomyosin II–mediated contractility. LKB1 control of myosin II activity through RLC2 phosphorylation has been previously described, although there is some controversy as to how this effect is directly mediated downstream of LKB1 (Mirouse et al., 2007; Zagórska et al., 2010; Chartier et al., 2011). Furthermore, LKB1 overexpression has been shown to control RhoA activity through the activation of a RhoGEF (Xu et al., 2010), which may result in ROCK activation. Our results suggest that LKB1 pathways activate RhoA–ROCK-mediated contractility in the basal compartment, preventing lumen initiation when the conditions of confinement are inappropriate. However, epithelial cells also require LKB1 and Rho–ROCK activity to stabilize the cell–cell junctions and maintain epithelial polarity (Mirouse et al., 2007). Consistent with this, disruption of the LKB1–Rho–ROCK–myosin pathway for longer periods after lumen initiation abolishes lumen expansion and normal epithelial morphogenesis (Fig. S5; Ferrari et al., 2008). Epithelial cells therefore need to finely control the mechanisms that regulate contractility and confinement to preserve the polarized phenotype. In fact, aggressive epithelial cancer cells, which frequently harbor mutations in LKB1 or Rho-GTPase signaling

Published September 10, 2012

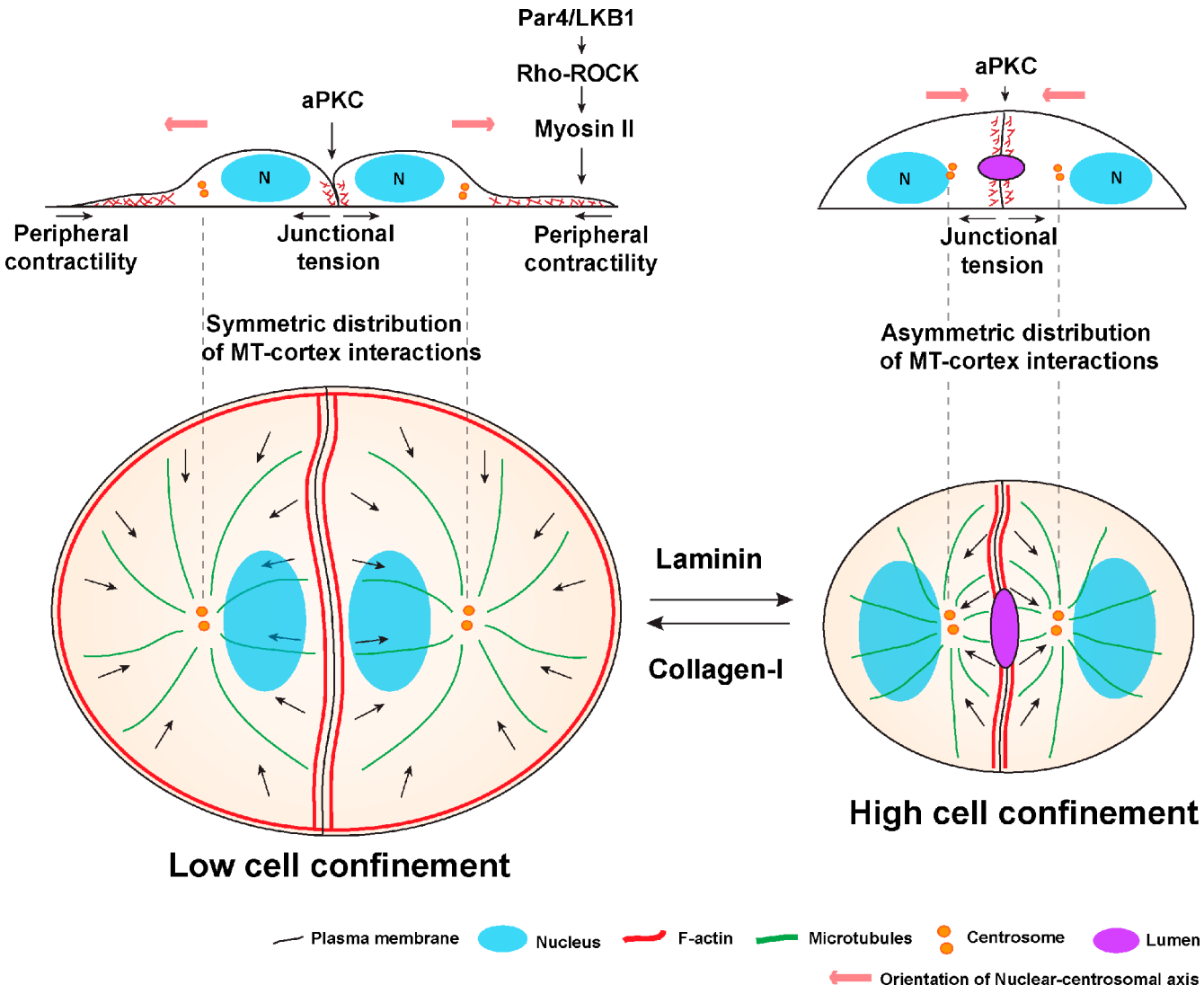

Figure 8. **Model for cell confinement regulation of lumen morphogenesis.** In highly adhesive substrates, such as collagen I, low cell confinement induces cell spreading, promoting formation of peripheral nuclear and cortical actin fibers and maintaining the centrosome positioned at the cell center and nuclei close to the junctions. Cell confinement prevents cell spreading, contractility is reduced, and centrosomes reposition toward the cell junctions where the initial lumen forms. Peripheral actin contractility depends on LKB1-mediated regulation of myosin II activity through Rho–ROCK, whereas contractility-independent centrosome positioning is controlled by aPKC activity at the junctions. MT, microtubule; N, nuclei.

components, exhibit increased cell migration and invasion capabilities (Butcher et al., 2009; Samuel et al., 2011). Further studies are required to clarify the role of LKB1 and its relationship with Rho-mediated contractility in cell polarity and cancer initiation and progression.

Materials and methods

Cell culture

MDCK cells (NBL2 clone) were cultured using 10% fetal bovine serum–supplemented complete MEM, containing 50 µm/ml penicillin-streptomycin and 2 mM L-Gln (Gibco), and passaged according to American Type Culture Collection instructions. Stably transfected MDCK cells (Lifeact-GFP) were grown and maintained in 0.5 mg/ml G418 or 0.1 mg/ml hygromycin B. To grow cells on agar substrate, a cell culture–tested agar solution was incubated on coverslips, and cells were seeded at 40,000 cells/cm^2. For lumen initiation experiments, cells were cultured in the presence of 2% Matrigel (BD) to induce cyst morphogenesis. MDCK cells stably expressing Venus-LKB1 and pLV-shLKB1 were gifts from the G. Walz laboratory (University of Freiburg, Freiburg, Germany; Boehlke et al., 2010).

Micropatterned cell culture

MDCK cells were cultured on micropatterned CYTOOchips using proprietary technology obtained from CYTOO, Inc. Disk-shaped micropatterns of different surface area size were used for most experiments (small = 700 µm^2; medium = 1,100 µm^2; large = 1,600 µm^2). Cells were seeded at 20,000 cells/ml (80,000 cells/chip) in complete MEM and then washed and incubated according to the manufacturer's instructions.

Plasmids, reagents, antibodies, and inhibitors

Life-actin probe cDNA was cloned into the pEGFP-N1 vector. pEGFP-C1-RhoV14 was a gift from I. Correas (Universidad Autónoma de Madrid, Madrid, Spain). pEGFP-C1-RLC2 mutants were gifts from M. Vicente-Manzanares (Universidad Autónoma de Madrid, Madrid, Spain). For ECM coating, CYTOOchips were incubated with collagen I (from rat tail; Sigma-Aldrich) or laminin (from ECM extracts; Sigma-Aldrich) at 20 µg/ml for 1 h and washed twice with 20 ml PBS before use. Antibodies used were gp135/podocalyxin (1:5,000, 3B8; gift from G. Ojakian, State University of New York Downstate Medical Center, New York, NY), α-tubulin (1:2,000, DM1A [Sigma-Aldrich]; 1:1,000, YL1/2 [gift from J. Kilmartin, Medical Research Council, Cambridge, England, UK]), γ-tubulin (1:1,000, GT-88; Sigma-Aldrich), β-catenin (1:1,000; Santa Cruz Biotechnology, Inc.), paxillin (1:1,000; BD), vinculin (1:1,000; BD), RhoA (1:1,000; BD),

and p-PKC-ζ (Thr410; 1:500, sc-12894; Santa Cruz Biotechnology, Inc.). Phalloidin-FITC and -TRITC were used to stain F-actin (1:5,000), and DAPI (1:1,000), Hoechst 33842 (1:10,000), and Topro-3 (1:500) were used to stain nuclei (Molecular Probes; Invitrogen). MDCK cells were treated with 40 µg/ml aPKC-PS (EMD Millipore), 50 µM BB (Sigma-Aldrich), or 20 µM Y27632 (Sigma-Aldrich) at the indicated times. Dox (Sigma-Aldrich) was used for inducible expression plasmids (0.1 µg/ml).

RNAi

The LKB1-targeting shRNA for MDCK cells was previously characterized (Boehlke et al., 2010). Inducible LKB1 silencing was verified by quantitative RT-PCR using specific primers (forward, 5′-CTGAGGAGATTACGGCACAA-3′; and reverse, 5′-CGCAGTACTCCATCACCATATA-3′).

Immunofluorescence and quantifications

MDCK cells were fixed at different time points and stained by immunofluorescence using the indicated primary antibodies. Pacific blue (405)– or Alexa Fluor 488/555/647–conjugated anti–rabbit and anti–mouse were used as secondary antibodies (Life Technologies). Images were acquired using inverted/vertical confocal microscopes (LSM 510 or LSM 710; Carl Zeiss) using the ZEN software (Carl Zeiss). Objectives used were 63×/NA 1.4 oil Plan Apochromat and 100×/NA 1.4 oil Plan Apochromat (Carl Zeiss). Then, images were treated using ImageJ software (National Institutes of Health) for producing x-z orthogonal slices, z-stack projections, and 3D deconvolution. For quantifications, more than three experiments were quantified (analyzing ∼50 cells per condition) using different CYTOOchips. Accumulation of a gp135 after 24 h in a single membrane patch at cell–cell junctions was used to quantify normal initiating lumens. For centrosome positioning, we analyzed the angle between the two nuclei and γ-tubulin staining to determine the position of the centrosome. Centrosomes oriented within 90° from the nuclei–nuclei axis were considered to be correctly oriented toward the cell–cell junctions. Significance was calculated using a paired, two-tailed Student's *t* test, and significant p-values are indicated in each experiment.

Rho-GTP pull-down experiments

In brief, cells plated at low confluence (10,000 cells/ml) on collagen-coated 10-cm dishes were lysed using TBS (1% Triton X-100 and 0.1% SDS) with 25 mM $MgCl_2$ and protease inhibitors. Lysates were loaded with Sepharose-glutathione beads bound to the purified Rhotekin-binding domain and 100 µg/ml lysate, incubated for 20 min (4°C), and washed twice with lysis buffer. Beads were dried by aspiration, and bound protein was eluted with 50 µl Laemmli loading buffer (95°C). Band intensity in a Western blot was quantified by optical densitometry (ImageJ).

Live-cell imaging

For live-cell imaging, MDCK cells were seeded on CYTOOchips and incubated in CYTOOchambers for different times, according to manufacturer's instructions. Live imaging experiments were performed using incubator chamber accessories for each system at 37°C and 5% CO_2. Imaging medium was red-free complete MEM (Life Technologies) supplemented with 2% Matrigel. Images were acquired with a 63×/NA 1.2 oil immersion objective using a video microscope (Eclipse Ti; Nikon) or with a 40×/NA 0.60 dry objective using a microscope (AF6000 LX [Leica]; camera [885 EM; Andor]). MetaMorph software (Nikon) or Leica Application Suite (Leica) was used for acquisition and video analysis.

Online supplemental material

Fig. S1 shows focal adhesions, Golgi apparatus, and tight junction stainings in micropatterned cysts and laminin distribution in different confinement conditions at 24 h. Fig. S2 shows that cell confinement controls time of lumen initiation and centrosome positioning but not spindle orientation in cell division. Fig. S3 shows the myosin II inhibition effects on Golgi polarization and vinculin staining. Fig. S4 shows that ROCK inhibition mimics BB effects on micropatterned cysts. Fig. S5 shows the LKB1-knockdown (KD) phenotype in mature MDCK cysts. Video 1 shows MDCK cyst formation in micropatterns using wide-field light microscopy. Video 2 shows Life-actin GFP staining of a micropatterned MDCK cyst growing in high confinement conditions. Video 3 shows Life-actin GFP staining of a micropatterned MDCK cyst growing in low confinement conditions. Online supplemental material is available at http://www.jcb.org/cgi/content/full/jcb.201203075/DC1.

We thank Carmen M. Ruiz-Jarabo for comments on the manuscript and members of the Alonso and Martin-Belmonte laboratory for discussion. We thank Miguel Vicente-Manzanares for RLC2-(T18D,S19D) plasmids and reagents and George Ojakian for the gp135/podocalyxin antibody.

This work was supported by grants from the Human Frontiers Science Program (Human Frontiers Science Program Career Development Award 00011/2009), Marie Curie (IRG-209382), Ministerio de Ciencia e Innovación (BFU2008-01916 and BFU2011-22622), and CONSOLIDER (CSD2009-00016) to F. Martín-Belmonte. A.E. Rodríguez-Fraticelli is the recipient of a Junta para la Ampliación de Estudios fellowship from Consejo Superior de Investigaciones Científicas. An institutional grant from Fundación Ramón Areces to Centro de Biología Molecular Severo Ochoa is also acknowledged.

Submitted: 15 March 2012
Accepted: 16 August 2012

References

Amin, N., A. Khan, D. St Johnston, I. Tomlinson, S. Martin, J. Brenman, and H. McNeill. 2009. LKB1 regulates polarity remodeling and adherens junction formation in the *Drosophila* eye. *Proc. Natl. Acad. Sci. USA*. 106:8941–8946. http://dx.doi.org/10.1073/pnas.0812469106

Asada, N., K. Sanada, and Y. Fukada. 2007. LKB1 regulates neuronal migration and neuronal differentiation in the developing neocortex through centrosomal positioning. *J. Neurosci.* 27:11769–11775. http://dx.doi.org/10.1523/JNEUROSCI.1938-07.2007

Boehlke, C., F. Kotsis, V. Patel, S. Braeg, H. Voelker, S. Bredt, T. Beyer, H. Janusch, C. Hamann, M. Gödel, et al. 2010. Primary cilia regulate mTORC1 activity and cell size through Lkb1. *Nat. Cell Biol.* 12:1115–1122. http://dx.doi.org/10.1038/ncb2117

Bornens, M. 2012. The centrosome in cells and organisms. *Science*. 335:422–426. http://dx.doi.org/10.1126/science.1209037

Bornens, M., M. Paintrand, and C. Celati. 1989. The cortical microfilament system of lymphoblasts displays a periodic oscillatory activity in the absence of microtubules: implications for cell polarity. *J. Cell Biol.* 109:1071–1083. http://dx.doi.org/10.1083/jcb.109.3.1071

Bryant, D.M., and K.E. Mostov. 2008. From cells to organs: building polarized tissue. *Nat. Rev. Mol. Cell Biol.* 9:887–901. http://dx.doi.org/10.1038/nrm2523

Bryant, D.M., A. Datta, A.E. Rodríguez-Fraticelli, J. Peränen, F. Martín-Belmonte, and K.E. Mostov. 2010. A molecular network for de novo generation of the apical surface and lumen. *Nat. Cell Biol.* 12:1035–1045. http://dx.doi.org/10.1038/ncb2106

Burakov, A., E. Nadezhdina, B. Slepchenko, and V. Rodionov. 2003. Centrosome positioning in interphase cells. *J. Cell Biol.* 162:963–969. http://dx.doi.org/10.1083/jcb.200305082

Butcher, D.T., T. Alliston, and V.M. Weaver. 2009. A tense situation: forcing tumour progression. *Nat. Rev. Cancer*. 9:108–122. http://dx.doi.org/10.1038/nrc2544

Chartier, N.T., D.P. Salazar Ospina, L. Benkemoun, M. Mayer, S.W. Grill, A.S. Maddox, and J.C. Labbé. 2011. PAR-4/LKB1 mobilizes nonmuscle myosin through anillin to regulate *C. elegans* embryonic polarization and cytokinesis. *Curr. Biol.* 21:259–269. http://dx.doi.org/10.1016/j.cub.2011.01.010

Datta, A., D.M. Bryant, and K.E. Mostov. 2011. Molecular regulation of lumen morphogenesis. *Curr. Biol.* 21:R126–R136. http://dx.doi.org/10.1016/j.cub.2010.12.003

de Anda, F.C., G. Pollarolo, J.S. Da Silva, P.G. Camoletto, F. Feiguin, and C.G. Dotti. 2005. Centrosome localization determines neuronal polarity. *Nature*. 436:704–708. http://dx.doi.org/10.1038/nature03811

Desai, R.A., L. Gao, S. Raghavan, W.F. Liu, and C.S. Chen. 2009. Cell polarity triggered by cell-cell adhesion via E-cadherin. *J. Cell Sci.* 122:905–911. http://dx.doi.org/10.1242/jcs.028183

Discher, D.E., P. Janmey, and Y.L. Wang. 2005. Tissue cells feel and respond to the stiffness of their substrate. *Science*. 310:1139–1143. http://dx.doi.org/10.1126/science.1116995

DuFort, C.C., M.J. Paszek, and V.M. Weaver. 2011. Balancing forces: architectural control of mechanotransduction. *Nat. Rev. Mol. Cell Biol.* 12:308–319. http://dx.doi.org/10.1038/nrm3112

Etienne-Manneville, S., and A. Hall. 2003. Cdc42 regulates GSK-3beta and adenomatous polyposis coli to control cell polarity. *Nature*. 421:753–756. http://dx.doi.org/10.1038/nature01423

Etienne-Manneville, S., J.B. Manneville, S. Nicholls, M.A. Ferenczi, and A. Hall. 2005. Cdc42 and Par6–PKCζ regulate the spatially localized association of Dlg1 and APC to control cell polarization. *J. Cell Biol.* 170:895–901. http://dx.doi.org/10.1083/jcb.200412172

Ferrari, A., A. Veligodskiy, U. Berge, M.S. Lucas, and R. Kroschewski. 2008. ROCK-mediated contractility, tight junctions and channels contribute to the conversion of a preapical patch into apical surface during isochoric lumen initiation. *J. Cell Sci.* 121:3649–3663. http://dx.doi.org/10.1242/jcs.018648

Fink, J., N. Carpi, T. Betz, A. Bétard, M. Chebah, A. Azioune, M. Bornens, C. Sykes, L. Fetler, D. Cuvelier, and M. Piel. 2011. External forces control mitotic spindle positioning. *Nat. Cell Biol.* 13:771–778. http://dx.doi.org/10.1038/ncb2269

Georgiou, M., E. Marinari, J. Burden, and B. Baum. 2008. Cdc42, Par6, and aPKC regulate Arp2/3-mediated endocytosis to control local adherens junction stability. *Curr. Biol.* 18:1631–1638. http://dx.doi.org/10.1016/j.cub.2008.09.029

Gomes, E.R., S. Jani, and G.G. Gundersen. 2005. Nuclear movement regulated by Cdc42, MRCK, myosin, and actin flow establishes MTOC polarization in migrating cells. *Cell*. 121:451–463. http://dx.doi.org/10.1016/j.cell.2005.02.022

Heasman, S.J., and A.J. Ridley. 2008. Mammalian Rho GTPases: new insights into their functions from in vivo studies. *Nat. Rev. Mol. Cell Biol.* 9:690–701. http://dx.doi.org/10.1038/nrm2476

Hezel, A.F., S. Gurumurthy, Z. Granot, A. Swisa, G.C. Chu, G. Bailey, Y. Dor, N. Bardeesy, and R.A. Depinho. 2008. Pancreatic LKB1 deletion leads to acinar polarity defects and cystic neoplasms. *Mol. Cell. Biol.* 28:2414–2425. http://dx.doi.org/10.1128/MCB.01621-07

Jaffe, A.B., N. Kaji, J. Durgan, and A. Hall. 2008. Cdc42 controls spindle orientation to position the apical surface during epithelial morphogenesis. *J. Cell Biol.* 183:625–633. http://dx.doi.org/10.1083/jcb.200807121

Li, R., and G.G. Gundersen. 2008. Beyond polymer polarity: how the cytoskeleton builds a polarized cell. *Nat. Rev. Mol. Cell Biol.* 9:860–873. http://dx.doi.org/10.1038/nrm2522

Luxton, G.W., and G.G. Gundersen. 2011. Orientation and function of the nuclear-centrosomal axis during cell migration. *Curr. Opin. Cell Biol.* 23:579–588. http://dx.doi.org/10.1016/j.ceb.2011.08.001

Luxton, G.W., E.R. Gomes, E.S. Folker, E. Vintinner, and G.G. Gundersen. 2010. Linear arrays of nuclear envelope proteins harness retrograde actin flow for nuclear movement. *Science*. 329:956–959. http://dx.doi.org/10.1126/science.1189072

Manneville, J.B., and S. Etienne-Manneville. 2006. Positioning centrosomes and spindle poles: looking at the periphery to find the centre. *Biol. Cell*. 98:557–565. http://dx.doi.org/10.1042/BC20060017

Martin-Belmonte, F., A. Gassama, A. Datta, W. Yu, U. Rescher, V. Gerke, and K. Mostov. 2007. PTEN-mediated apical segregation of phosphoinositides controls epithelial morphogenesis through Cdc42. *Cell*. 128:383–397. http://dx.doi.org/10.1016/j.cell.2006.11.051

Mirouse, V., and M. Billaud. 2011. The LKB1/AMPK polarity pathway. *FEBS Lett.* 585:981–985. http://dx.doi.org/10.1016/j.febslet.2010.12.025

Mirouse, V., L.L. Swick, N. Kazgan, D. St Johnston, and J.E. Brenman. 2007. LKB1 and AMPK maintain epithelial cell polarity under energetic stress. *J. Cell Biol.* 177:387–392. http://dx.doi.org/10.1083/jcb.200702053

O'Brien, L.E., T.S. Jou, A.L. Pollack, Q. Zhang, S.H. Hansen, P. Yurchenco, and K.E. Mostov. 2001. Rac1 orientates epithelial apical polarity through effects on basolateral laminin assembly. *Nat. Cell Biol.* 3:831–838. http://dx.doi.org/10.1038/ncb0901-831

Ojakian, G.K., W.J. Nelson, and K.A. Beck. 1997. Mechanisms for de novo biogenesis of an apical membrane compartment in groups of simple epithelial cells surrounded by extracellular matrix. *J. Cell Sci.* 110:2781–2794.

Paluch, E., J. van der Gucht, and C. Sykes. 2006. Cracking up: symmetry breaking in cellular systems. *J. Cell Biol.* 175:687–692. http://dx.doi.org/10.1083/jcb.200607159

Pitaval, A., Q. Tseng, M. Bornens, and M. Théry. 2010. Cell shape and contractility regulate ciliogenesis in cell cycle–arrested cells. *J. Cell Biol.* 191:303–312. http://dx.doi.org/10.1083/jcb.201004003

Rodriguez-Fraticelli, A.E., S. Vergarajauregui, D.J. Eastburn, A. Datta, M.A. Alonso, K. Mostov, and F. Martín-Belmonte. 2010. The Cdc42 GEF Intersectin 2 controls mitotic spindle orientation to form the lumen during epithelial morphogenesis. *J. Cell Biol.* 189:725–738. http://dx.doi.org/10.1083/jcb.201002047

Rodríguez-Fraticelli, A.E., M. Gálvez-Santisteban, and F. Martín-Belmonte. 2011. Divide and polarize: recent advances in the molecular mechanism regulating epithelial tubulogenesis. *Curr. Opin. Cell Biol.* 23:638–646. http://dx.doi.org/10.1016/j.ceb.2011.07.002

Samuel, M.S., J.I. Lopez, E.J. McGhee, D.R. Croft, D. Strachan, P. Timpson, J. Munro, E. Schröder, J. Zhou, V.G. Brunton, et al. 2011. Actomyosin-mediated cellular tension drives increased tissue stiffness and β-catenin activation to induce epidermal hyperplasia and tumor growth. *Cancer Cell*. 19:776–791. http://dx.doi.org/10.1016/j.ccr.2011.05.008

Schlüter, M.A., C.S. Pfarr, J. Pieczynski, E.L. Whiteman, T.W. Hurd, S. Fan, C.J. Liu, and B. Margolis. 2009. Trafficking of Crumbs3 during cytokinesis is crucial for lumen formation. *Mol. Biol. Cell*. 20:4652–4663. http://dx.doi.org/10.1091/mbc.E09-02-0137

Sebbagh, M., M.J. Santoni, B. Hall, J.P. Borg, and M.A. Schwartz. 2009. Regulation of LKB1/STRAD localization and function by E-cadherin. *Curr. Biol.* 19:37–42. http://dx.doi.org/10.1016/j.cub.2008.11.033

Sfakianos, J., A. Togawa, S. Maday, M. Hull, M. Pypaert, L. Cantley, D. Toomre, and I. Mellman. 2007. Par3 functions in the biogenesis of the primary cilium in polarized epithelial cells. *J. Cell Biol.* 179:1133–1140. http://dx.doi.org/10.1083/jcb.200709111

Stinchcombe, J.C., E. Majorovits, G. Bossi, S. Fuller, and G.M. Griffiths. 2006. Centrosome polarization delivers secretory granules to the immunological synapse. *Nature*. 443:462–465. http://dx.doi.org/10.1038/nature05071

Strilić, B., T. Kucera, J. Eglinger, M.R. Hughes, K.M. McNagny, S. Tsukita, E. Dejana, N. Ferrara, and E. Lammert. 2009. The molecular basis of vascular lumen formation in the developing mouse aorta. *Dev. Cell*. 17:505–515. http://dx.doi.org/10.1016/j.devcel.2009.08.011

Théry, M. 2010. Micropatterning as a tool to decipher cell morphogenesis and functions. *J. Cell Sci.* 123:4201–4213. http://dx.doi.org/10.1242/jcs.075150

Théry, M., V. Racine, A. Pépin, M. Piel, Y. Chen, J.B. Sibarita, and M. Bornens. 2005. The extracellular matrix guides the orientation of the cell division axis. *Nat. Cell Biol.* 7:947–953. http://dx.doi.org/10.1038/ncb1307

Vicente-Manzanares, M., M.A. Koach, L. Whitmore, M.L. Lamers, and A.F. Horwitz. 2008. Segregation and activation of myosin IIB creates a rear in migrating cells. *J. Cell Biol.* 183:543–554. http://dx.doi.org/10.1083/jcb.200806030

Wallace, S.W., J. Durgan, D. Jin, and A. Hall. 2010. Cdc42 regulates apical junction formation in human bronchial epithelial cells through PAK4 and Par6B. *Mol. Biol. Cell*. 21:2996–3006. http://dx.doi.org/10.1091/mbc.E10-05-0429

Watanabe, T., H. Hosoya, and S. Yonemura. 2007. Regulation of myosin II dynamics by phosphorylation and dephosphorylation of its light chain in epithelial cells. *Mol. Biol. Cell*. 18:605–616. http://dx.doi.org/10.1091/mbc.E06-07-0590

Wilkinson, S., H.F. Paterson, and C.J. Marshall. 2005. Cdc42-MRCK and Rho-ROCK signalling cooperate in myosin phosphorylation and cell invasion. *Nat. Cell Biol.* 7:255–261. http://dx.doi.org/10.1038/ncb1230

Williams, T., and J.E. Brenman. 2008. LKB1 and AMPK in cell polarity and division. *Trends Cell Biol.* 18:193–198. http://dx.doi.org/10.1016/j.tcb.2008.01.008

Xu, X., T. Omelchenko, and A. Hall. 2010. LKB1 tumor suppressor protein regulates actin filament assembly through Rho and its exchange factor Dbl independently of kinase activity. *BMC Cell Biol.* 11:77. http://dx.doi.org/10.1186/1471-2121-11-77

Yu, W., A. Datta, P. Leroy, L.E. O'Brien, G. Mak, T.S. Jou, K.S. Matlin, K.E. Mostov, and M.M. Zegers. 2005. Beta1-integrin orients epithelial polarity via Rac1 and laminin. *Mol. Biol. Cell*. 16:433–445. http://dx.doi.org/10.1091/mbc.E04-05-0435

Yu, W., A.M. Shewan, P. Brakeman, D.J. Eastburn, A. Datta, D.M. Bryant, Q.W. Fan, W.A. Weiss, M.M. Zegers, and K.E. Mostov. 2008. Involvement of RhoA, ROCK I and myosin II in inverted orientation of epithelial polarity. *EMBO Rep.* 9:923–929. http://dx.doi.org/10.1038/embor.2008.135

Zagórska, A., M. Deak, D.G. Campbell, S. Banerjee, M. Hirano, S. Aizawa, A.R. Prescott, and D.R. Alessi. 2010. New roles for the LKB1-NUAK pathway in controlling myosin phosphatase complexes and cell adhesion. *Sci. Signal.* 3:ra25. http://dx.doi.org/10.1126/scisignal.2000616

Rodríguez-Fraticelli et al., http://www.jcb.org/cgi/content/full/jcb.201203075/DC1

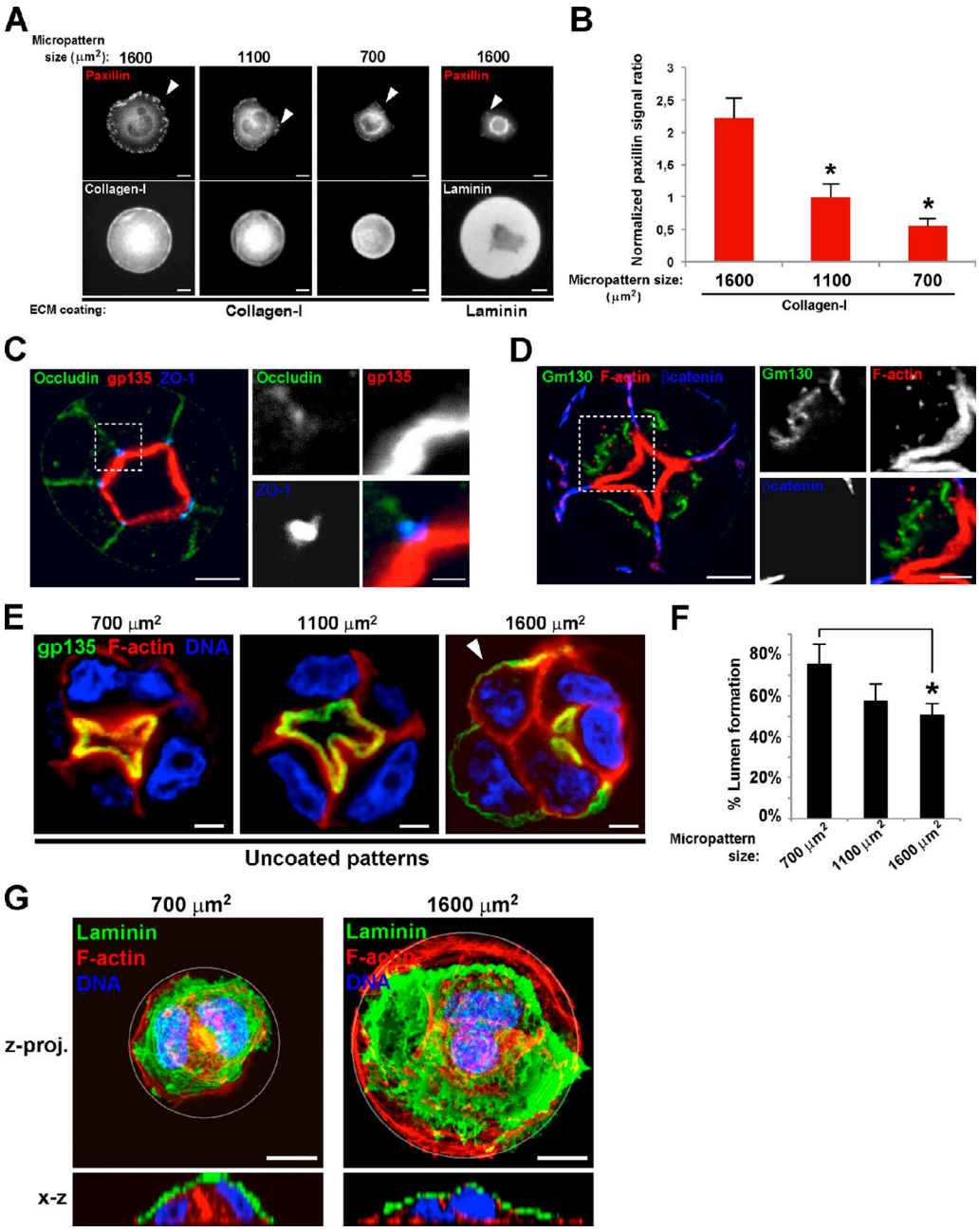

Figure S1. **Cell spreading and lumen formation in confined 3D cell cultures.** (A) Focal adhesion formation in MDCK cells on collagen I micropatterns or laminin micropatterns. MDCK cells were seeded on disk-shaped collagen I micropatterns or laminin micropatterns of different sizes, fixed 5 h after seeding, and stained to detect paxillin. Bottom images show ECM staining for collagen I or laminin. Arrowheads show focal adhesions. (B) Quantification of focal adhesions in collagen I micropatterns of different sizes. Total paxillin signal in A was quantified to analyze focal adhesion formation in spreading MDCK cells. $n \geq 10$ cells/experiment. (C) Localization of tight junctions and apical membrane. Micropatterned MDCK cysts were stained to detect gp135, occludin, and ZO-1. Dotted box shows magnification area. (D) Localization of Golgi apparatus, adherens junctions, and actin. Micropatterned MDCK cysts were stained to detect Gm130, β-catenin, or F-actin. Dotted box shows magnification area. (E) Lumen formation in MDCK cysts micropatterned without a biological substrate. MDCK cells were seeded on uncoated CYTOOchips of different sizes (1,600 μm^2, 1,100 μm^2, and 700 μm^2) and grown to form cysts. Cysts were fixed after 60 h and stained to detect gp135, F-actin, and DNA. Arrowheads indicate inverted apical membrane polarity (dorsal apical polarity). (F) Quantification of lumen formation efficiency in MDCK cysts micropatterned without biological substrate. MDCK cells were cultured to form micropatterned cysts on uncoated CYTOOchips. Cysts were fixed at 60 h, and normal lumen formation was quantified. $n \geq 30$ cysts/experiment. (G) Laminin distribution in different confinement conditions. MDCK cells seeded on collagen I–coated micropatterns of different size (1,600 μm^2 and 700 μm^2) were grown to form cysts for 24 h. Cells were fixed and stained to detect laminin, F-actin, and DNA. Full z-stack projections (proj.) and x-z cross sections are shown. Values are means ± SD from three independent experiments. *, $P < 0.005$. Bars: (A, C, D, and G) 10 µm; (E) 5 µm.

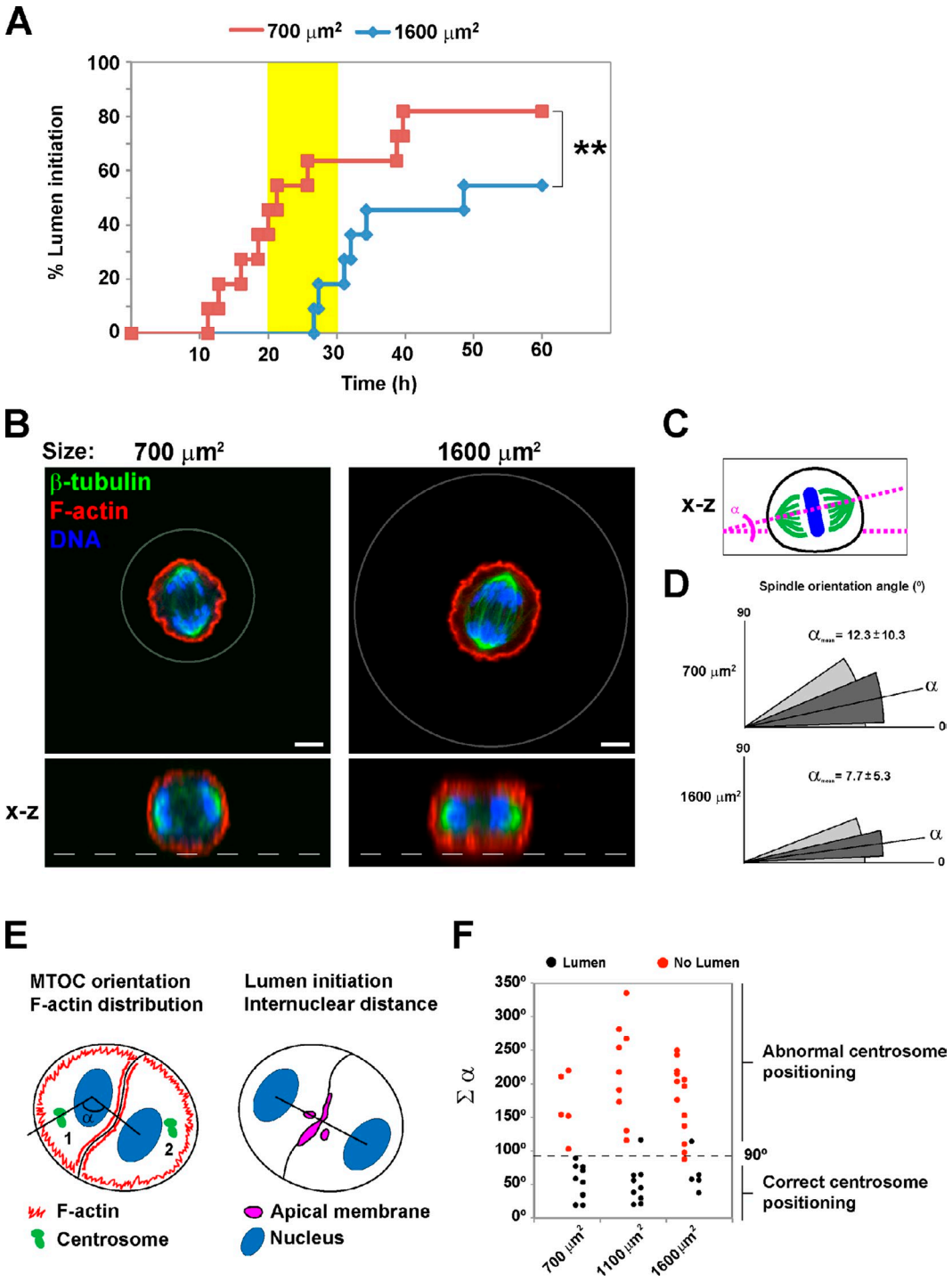

Figure S2. **Cell confinement control of lumen formation, F-actin polarization, and centrosome positioning but not spindle orientation in cell division.** (A) Delay in lumen opening in low confinement conditions. MDCK cells were seeded on collagen-coated micropatterns of different sizes to grow cysts and recorded by bright-field video microscopy for 60 h. Time until lumen opening was determined de visu and quantified (n = 11; **, P < 0.0005). Yellow color indicates the time frame in which the largest difference between high and low confinement conditions is observed. (B) Orientation of cell divisions in different confinement conditions. MDCK cells were seeded on collagen I–coated micropatterns of different sizes (1,600 μm² and 700 μm²) and grown to form cysts for 10 h. Cells were fixed and stained to detect β-tubulin, F-actin, and DNA. An x-z cross section is shown. Gray circles indicate pattern shape. Bars, 5 μm. (C) Scheme for quantification of spindle angle. The spindle orientation angle was calculated between the spindle axis and the bottom of the CYTOOchip in cells in anaphase. (D) Quantification of spindle orientation angle in high confinement (700 μm²) versus low confinement (1,600 μm²). The charts show the spindle angle orientation (α) mean values ± SD (dark gray). Light gray shows maximum/minimum spindle angle values (n = 3 and $n \geq 10$ cells/experiment). (E) Method for quantification of centrosome positioning, F-actin distribution, and lumen position after the first cell division. β-Tubulin distribution was used to position the centrosome and the angle between the nucleus–centrosome axis, and the nucleus–nucleus axis (α) was used to quantify centrosome orientation. The total value of nucleus–centrosome axis angle between both cells was the sum of α of each cell in the doublet (Σα). Σα values <90° were considered correct centrosome orientation. F-actin intensity signal was quantified at the cell–cell junction and at the peripheral cell cortex. Localization of gp135 was used to define the apical membrane in cells initiating a lumen. MTOC, microtubule-organizing center. (F) Identification of lumen-initiating centrosome position in 24-h micropatterned cysts using the method in E. The plot indicates normal lumens (black dots) and inverted cysts (red dots). The threshold considered for normal centrosome positioning was a 90° angle, which is the one that best discriminates normal and defective lumen initiation.

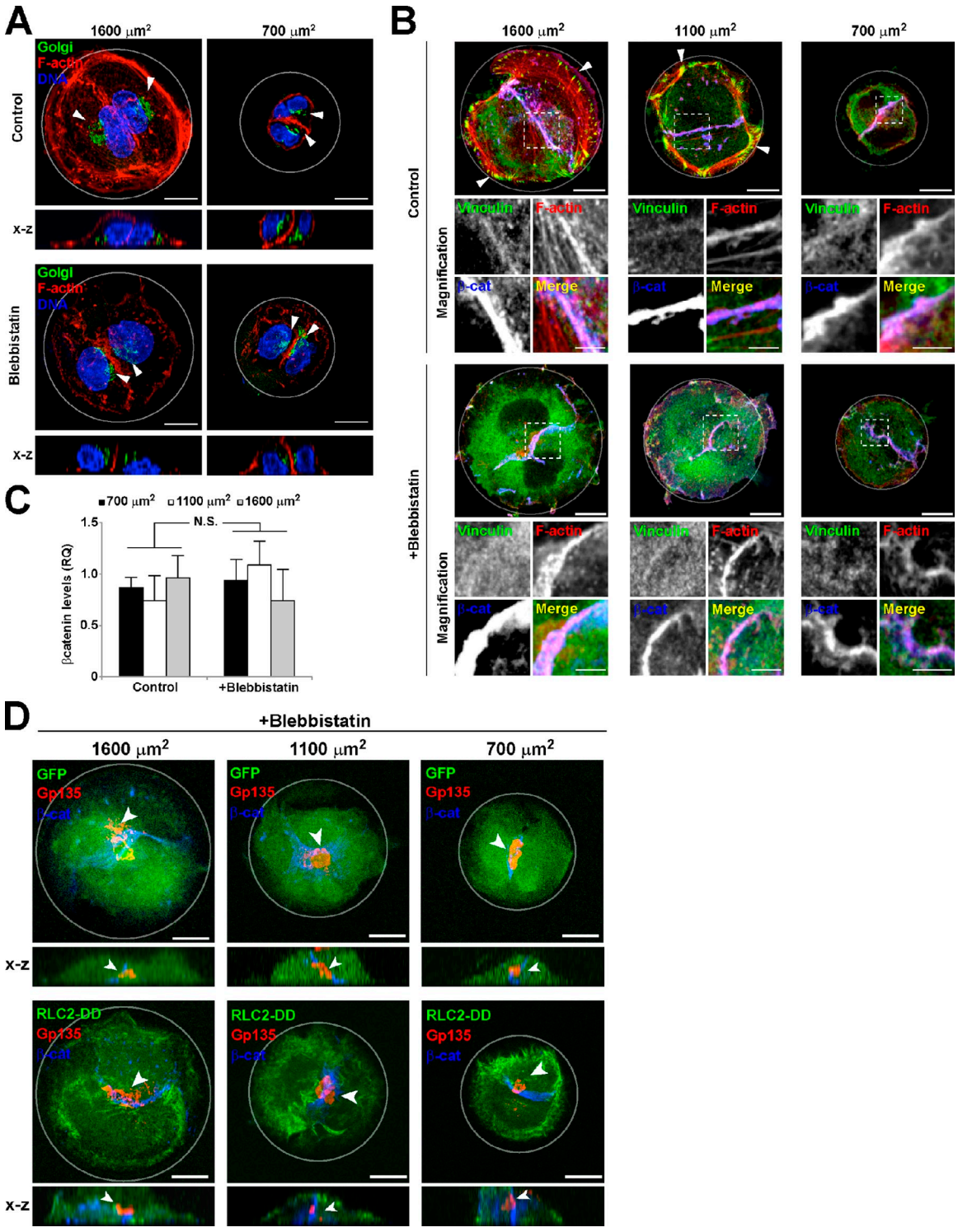

Figure S3. **Additional effects of myosin II inhibition.** (A) Effect of cell confinement on Golgi apparatus positioning. MDCK cells were seeded on collagen I micropatterns of different sizes to form cysts. After 24 h, cysts were treated with 50 μm BB for 30 min and then fixed and stained to detect the Golgi apparatus (Gm130), F-actin, and DNA. Arrowheads shows Golgi apparatus. (B) Localization of vinculin and β-catenin in control and BB-treated cells. MDCK cells were seeded on collagen I micropatterns of different sizes to form cysts. After 24 h, cysts were treated with 50 μm BB for 30 min and then fixed and stained to detect vinculin, F-actin, and β-catenin (β-cat). Cells were analyzed by confocal microscopy. Arrowheads indicate vinculin staining in focal adhesions. Dotted boxes show areas of magnification. (C) Relative quantification (RQ) of β-catenin junctional levels in micropatterned cysts. MDCK cells were seeded on collagen-coated micropatterns of different sizes (700 μm^2, $n = 7$; 1,100 μm^2 $n = 6$; 1,600 μm^2, $n = 7$) to grow cysts and stained for β-catenin. Cells were analyzed by confocal microscopy, and whole-cyst stack projections were analyzed to subtract background and measure integrated density in a selected region of interest between the two adjacent cells. Values are means ± SD and represent a relative quantification normalizing values to one of the samples ($P = 0.31$). (D) BB rescue of RLC2-DD expression effects. MDCK cells expressing GFP-tagged myosin II regulatory light chain phosphomimetic mutant Thr18-Asp and Ser-19-Asp (RLC2-DD) were seeded on collagen I micropatterns of different sizes to form cysts. After 24 h, cysts were treated with BB and then fixed and stained to detect gp135 and β-catenin. Arrowheads indicate position of the apical membrane (gp135). Gray circles indicate pattern shape. Bars: (A, B [main images], and D) 10 μm; (B, magnifications) 2 μm.

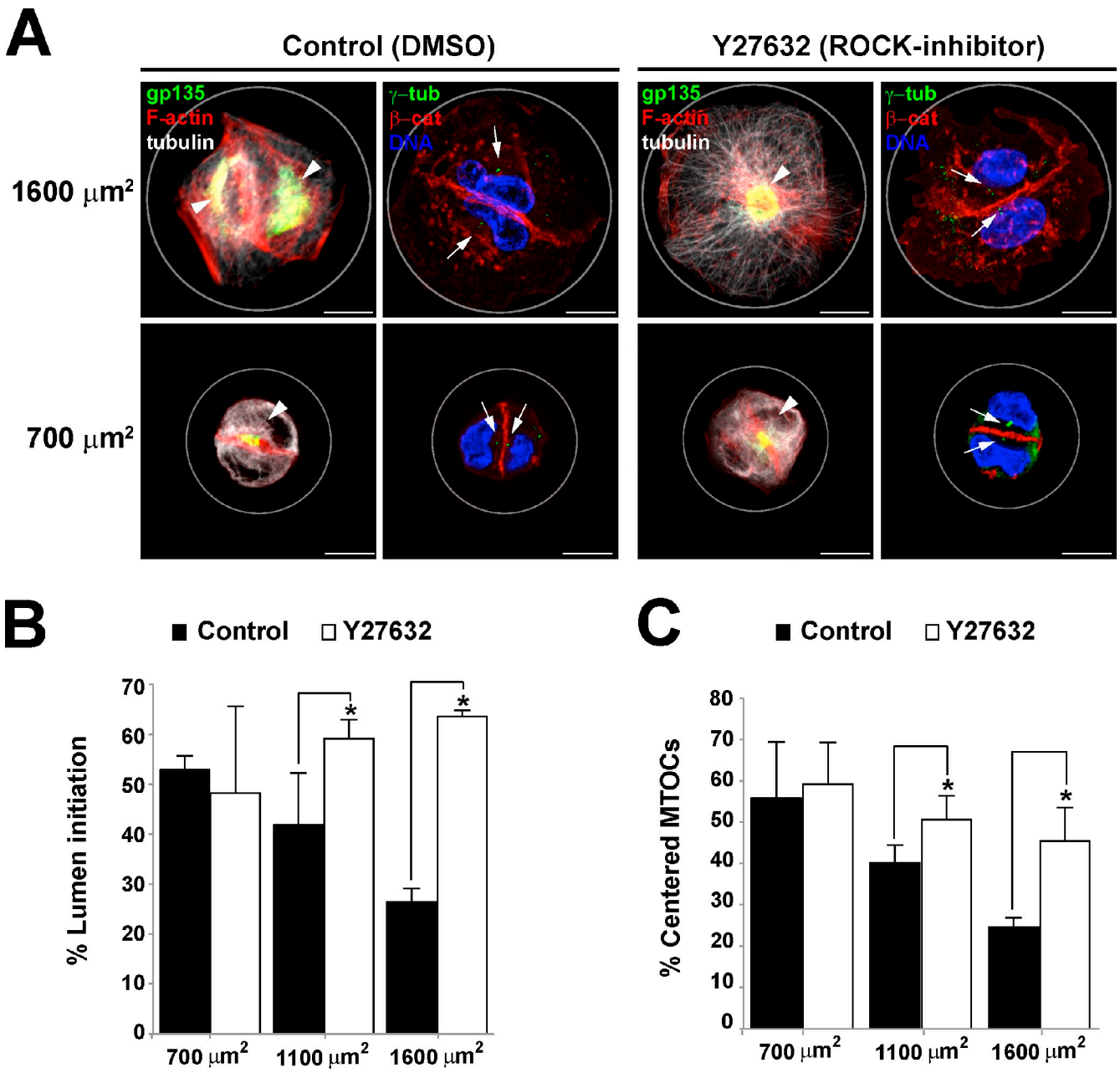

Figure S4. **Peripheral actin contractility is ROCK dependent.** (A) Effect of ROCK inhibition on lumen initiation on low confinement. MDCK cells were seeded on collagen I micropatterns of different sizes to form cysts. After 24 h, cysts were treated with ROCK inhibitor (Y27632) for 1 h and then fixed and stained to detect gp135, F-actin, and α-tubulin (gray) or γ-tubulin (γ-tub), β-catenin (β-cat), and DNA. Arrowheads indicate position of the apical membrane. Arrows indicate centrosome localization. Gray circles indicate pattern shape. Bars, 10 µm. (B) Quantification of lumen initiation in ROCK inhibitor–treated cells. (C) Quantification of centrosome positioning of ROCK inhibitor treated–cells. Values are means ± SD from three independent experiments ($n \geq 50$ cysts/experiment; *, $P < 0.005$). MTOC, microtubule-organizing center.

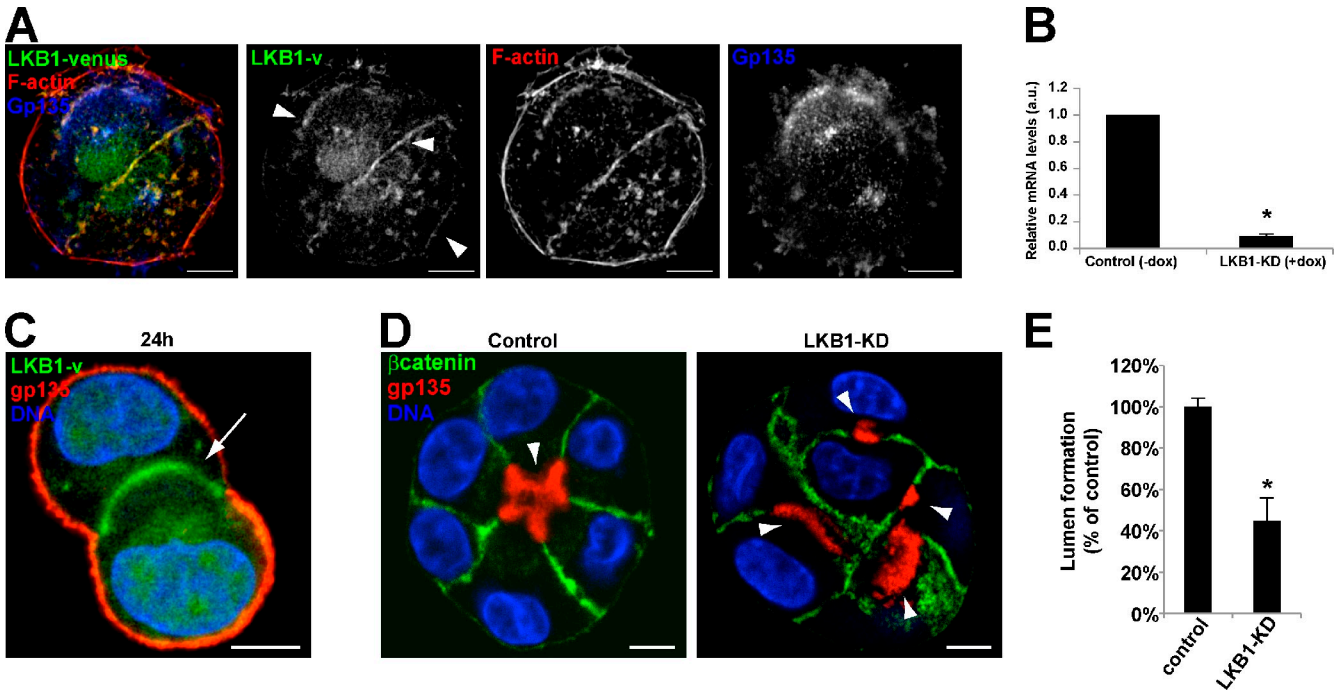

Figure S5. **Phenotype of LKB1 silencing in 3D MDCK cysts.** (A) Localization of LKB1 in MDCK cells. MDCK cells stably expressing fluorescent Venus-LKB1 (LKB1-v) were seeded on 1,700-μm^2 micropatterns and fixed after 24 h. Cysts were stained for F-actin and gp135. Arrowheads indicate localization of LKB1 in the nucleus, at cell junctions, and at the cell periphery. (B) Inducible silencing of LKB1 in MDCK cells. MDCK cells stably expressing LKB1 shRNA under the tetracycline-inducible promoter were grown for 24 h with or without dox. RNA silencing efficiency was analyzed by performing quantitative RT-PCR with LKB1-specific primers. Values are relative mRNA level means ± SD from three independent experiments. a.u., arbitrary unit. (C) Localization of LKB1 in MDCK cysts (24 h). MDCK cells stably expressing fluorescent Venus-LKB1 were seeded on Matrigel and fixed after 24 h. Cysts were stained for gp135 and nuclei (blue). Arrow indicates localization of LKB1 at cell junctions. (D) Effect of LKB1-KD in cyst formation. MDCK cells stably expressing LKB1 shRNA were seeded on Matrigel and fixed after 48 h. Cysts were stained to detect gp135, β-catenin, and DNA. Arrowheads show multiple closed lumens. (E) Quantification of the effect of LKB1-KD in lumen formation in D. Values are means ± SD from three independent experiments (n > 100 cysts/experiment, $P < 0.005$). Bars: (A and D) 10 μm; (C) 5 μm.

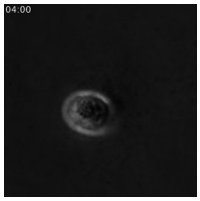

Video 1. **Bright-field microscopy analysis of epithelial cyst formation in a micropatterned surface.** MDCK cells were seeded on 1,100-μm^2 micropatterns to grow cysts and analyzed by time-lapse wide-field microscopy with a microscope (Eclipse Ti; 63× oil immersion objective). Frames were taken every 5 min for 60 h. Time is given in hours and minutes.

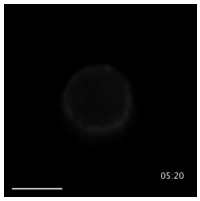

Video 2. **Actin localization in an epithelial cyst developing in low spreading (high confinement) conditions.** MDCK cells stably expressing Life-actin-GFP (gray) were seeded on 700-μm^2 collagen I–coated micropatterns to grow cysts and analyzed by time-lapse epifluorescence microscopy with a microscope (AF6000 LX; 40× dry objective). Frames were taken every 10 min for 48 h. After 48 h, DNA was stained with cell-permeable Hoechst at the end of the video recording. Time is given in hours and minutes. Bar, 10 μm.

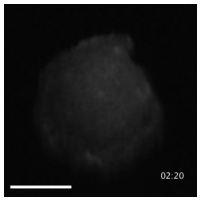

Video 3. **Actin localization in an epithelial cyst developing in high spreading (low confinement) conditions.** MDCK cells stably expressing Life-actin-GFP (gray) were seeded on 1,600-μm^2 collagen I micropatterns to grow cysts and analyzed by time-lapse epifluorescence microscopy with a microscope (AF6000 LX; 40× dry objective). Frames were taken every 10 min for 48 h. After 48 h, DNA was stained with cell-permeable Hoechst at the end of the video recording. Time is given in hours and minutes. Bar, 10 μm.

THE CDC42 GEF INTERSECTIN-2 CONTROLS MITOTIC SPINDLE ORIENTATION TO FORM THE LUMEN DURING EPITHELIAL MORPHOGENESIS

***Alejo E. Rodriguez-Fraticelli**, Silvia Vergarajauregui, Dennis J. Eastburn, Anirban Datta, Miguel A. Alonso, Keith E. Mostov, Fernando Martín-Belmonte.*

Publicado en The Journal of Cell Biology *189*; págs. 725-38.

PRESENTACION

La familia Rho de GTPasas monoméricas es crucial para la regulación de los procesos de adquisición de polaridad celular. La GTPasa Cdc42 cumple un papel fundamental en el desarrollo de la polaridad celular epitelial. En particular, Cdc42 se activa en la membrana apical en una ruta que requiere Annexin 2 y PTEN, a través de la segregación apical del *PtdIns(4,5)p2*. Cdc42 es necesario para regular la orientación del huso mitótico en cultivos tridimensionales de células CaCo2. Cuando las células epiteliales se dividen, lo hacen posicionando los polos del huso mitótico perpendicularmente al eje apicobasal. De este modo, la división simétrica origina dos células que mantienen la arquitectura de monocapa del epitelio tubular. Las células en las que la expresión de Cdc42 ha sido bloqueada mediante siRNA, no son capaces de orientar correctamente el huso mitótico, y fracasan en la formación de cistos tridimensionales con un único lumen.

Las GTPasas ciclan entre un estado "inactivo", unidas a GDP, y un estado "activado", unidas a GTP, en el que se unen a efectores con dominios de unión a GTPasas, entre los que se encuentran muchos reguladores del citoesqueleto. El equilibrio entre el estado unido a GTP y el estado unido a GDP está regulado por actividades GEF (que promueven el estado activo) y actividades GAP (que promueven el estado inactivo). Para esclarecer qué GEFs podrían estar regulando a Cdc42 durante la formación de cistos de MDCK, empleamos una librería de shRNA que interfiriera la expresión de todas las GEFs de Cdc42 expresadas en MDCK. La GEF Intersectin 2 (ITSN2) fue el candidato que presentaba el fenotipo más similar a la propia interferencia de Cdc42.

Luego de confirmar que ITSN2 se comportaba como un GEF de Cdc42 en nuestro modelo, nos propusimos a estudiar el mecanismo molecular de ITSN2. Sorprendentemente, ITSN2 se localizaba en el centrosoma, en lugar de en la membrana plasmática. Además, ITSN2 interaccionaba con componentes del motor de

microtúbulos, dineina-dinactina, sugiriendo que su transporte hacia el centrosoma estaba mediado por interacción al citoesqueleto de microtúbulos. Estudiando la localización de Cdc42 e ITSN2 en interfase y mitosis, descubrimos que ITSN2 y Cdc42 se localizaban en los polos del huso mitótico durante la división. Repetimos los experimentos midiendo la orientación del huso mitótico en células deplecionadas de ITSN2 y/o Cdc42. En estos experimentos, además de comprobar que Cdc42 era necesaria para la orientación perpendicular del huso al eje apicobasal, comprendimos que ITSN2 regulaba a Cdc42 en este mismo proceso, y las células interferidas para ITSN2 perdían la localización de Cdc42 en la membrana plasmática, sugiriendo que Cdc42 era transportado mediante reciclaje entre el compartimento pericentrosomal, donde era activado por ITSN2, y el compartimento de membrana plasmática.

Además de esclarecer el mecanismo molecular de Cdc42, y dilucidar el primer regulador GEF de esta GTPasa en órganos epiteliales, estos experimentos nos permitieron comprender que el papel de los fosfoinosítidos podía estar controlando muchos diversos aspectos necesarios para el mantenimiento la arquitectura epitelial. De este modo, sería necesario un estudio menos sesgado por los mecanismos previamente descritos para comprender mejor el mecanismo de formación del lumen.

Published May 17, 2010

The Cdc42 GEF Intersectin 2 controls mitotic spindle orientation to form the lumen during epithelial morphogenesis

Alejo E. Rodriguez-Fraticelli,[1] Silvia Vergarajauregui,[1] Dennis J. Eastburn,[2] Anirban Datta,[2] Miguel A. Alonso,[1] Keith Mostov,[2] and Fernando Martín-Belmonte[1]

[1]Centro de Biología Molecular Severo Ochoa, Consejo Superior de Investigaciones Científicas, Madrid 28049, Spain
[2]Department of Anatomy, University of California, San Francisco, San Francisco, CA 94143

Epithelial organs are made of tubes and cavities lined by a monolayer of polarized cells that enclose the central lumen. Lumen formation is a crucial step in the formation of epithelial organs. The Rho guanosine triphosphatase (GTPase) Cdc42, which is a master regulator of cell polarity, regulates the formation of the central lumen in epithelial morphogenesis. However, how Cdc42 is regulated during this process is still poorly understood. Guanine nucleotide exchange factors (GEFs) control the activation of small GTPases. Using the three-dimensional Madin–Darby canine kidney model, we have identified a Cdc42-specific GEF, Intersectin 2 (ITSN2), which localizes to the centrosomes and regulates Cdc42 activation during epithelial morphogenesis. Silencing of either Cdc42 or ITSN2 disrupts the correct orientation of the mitotic spindle and normal lumen formation, suggesting a direct relationship between these processes. Furthermore, we demonstrated this direct relationship using LGN, a component of the machinery for mitotic spindle positioning, whose disruption also results in lumen formation defects.

Introduction

During development, epithelial cells develop apicobasal polarity, a specific type of constitutive cell polarity which is regulated by different mechanisms, including membrane transport, cytoskeleton organization, and cellular junction formation (Bryant and Mostov, 2008). The deregulation of apicobasal polarity is associated with major diseases such as polycystic kidney disease and cancer (Lee and Vasioukhin, 2008). Rho GTPases are molecular switches that control a wide variety of signaling pathways critical for the acquisition of the polarized phenotype. For instance, the orientation of epithelial cell polarity is controlled by the opposing actions of Rac1 and RhoA (O'Brien et al., 2001; Yu et al., 2003, 2005, 2008). Cdc42, which is a master regulator of cell polarity, controls the formation of a single lumen in MDCK cells. For this, Cdc42 is activated at the apical plasma membrane in a pathway regulated by annexin2 (Anx2) and PTEN, which mediate the enrichment of phosphatidylinositol-4,5-bisphosphate (PtdInsP2) at the apical domain (Martín-Belmonte et al., 2007). Additionally, Cdc42 activity has also been shown to regulate epithelial morphogenesis by controlling other processes such as vesicle traffic and exocytosis (Kroschewski et al., 1999; Müsch et al., 2001; Rojas et al., 2001; Wu et al., 2008) and, more recently, the mitotic spindle orientation (Jaffe et al., 2008). Therefore, Cdc42 appears to control different pathways and/or mechanisms for epithelial morphogenesis. How Cdc42 is regulated during these processes is currently unknown.

Rho guanine nucleotide exchange factors (GEFs) constitute the main activators of Rho GTPases. Rho GEFs are multidomain proteins modulated by different signals, whose number in the human genome greatly exceeds the number of Rho family proteins. This suggests that different Rho GEFs could be regulating where and how a Rho GTPase is activated to control different cellular processes (Jaffe and Hall, 2005). Intersectin (ITSN) is a multimodular protein that is mainly expressed in two splicing variants: ITSN short (ITSN-S) and ITSN long (ITSN-L). Only

Correspondence to Fernando Martín-Belmonte: fmartin@cbm.uam.es

Abbreviations used in this paper: DIC, dynein intermediate chain; Dox, doxycycline; EH, Eps15 homology; GEF, guanine nucleotide exchange factor; ITSN, Intersectin; KD, knockdown; MT, metaphase time; MTOC, microtubule-organizing center; N-WASP, neural WASP; vhITSN2, Venus–human ITSN2; WASP, Wiskott-Aldrich syndrome protein.

Supplemental Material can be found at:
http://jcb.rupress.org/content/suppl/2010/05/17/jcb.201002047.DC1.html
Original image data can be found at:
http://jcb-dataviewer.rupress.org/jcb/browse/2856

The Rockefeller University Press $30.00
J. Cell Biol. Vol. 189 No. 4 725–738
www.jcb.org/cgi/doi/10.1083/jcb.201002047

Published May 17, 2010

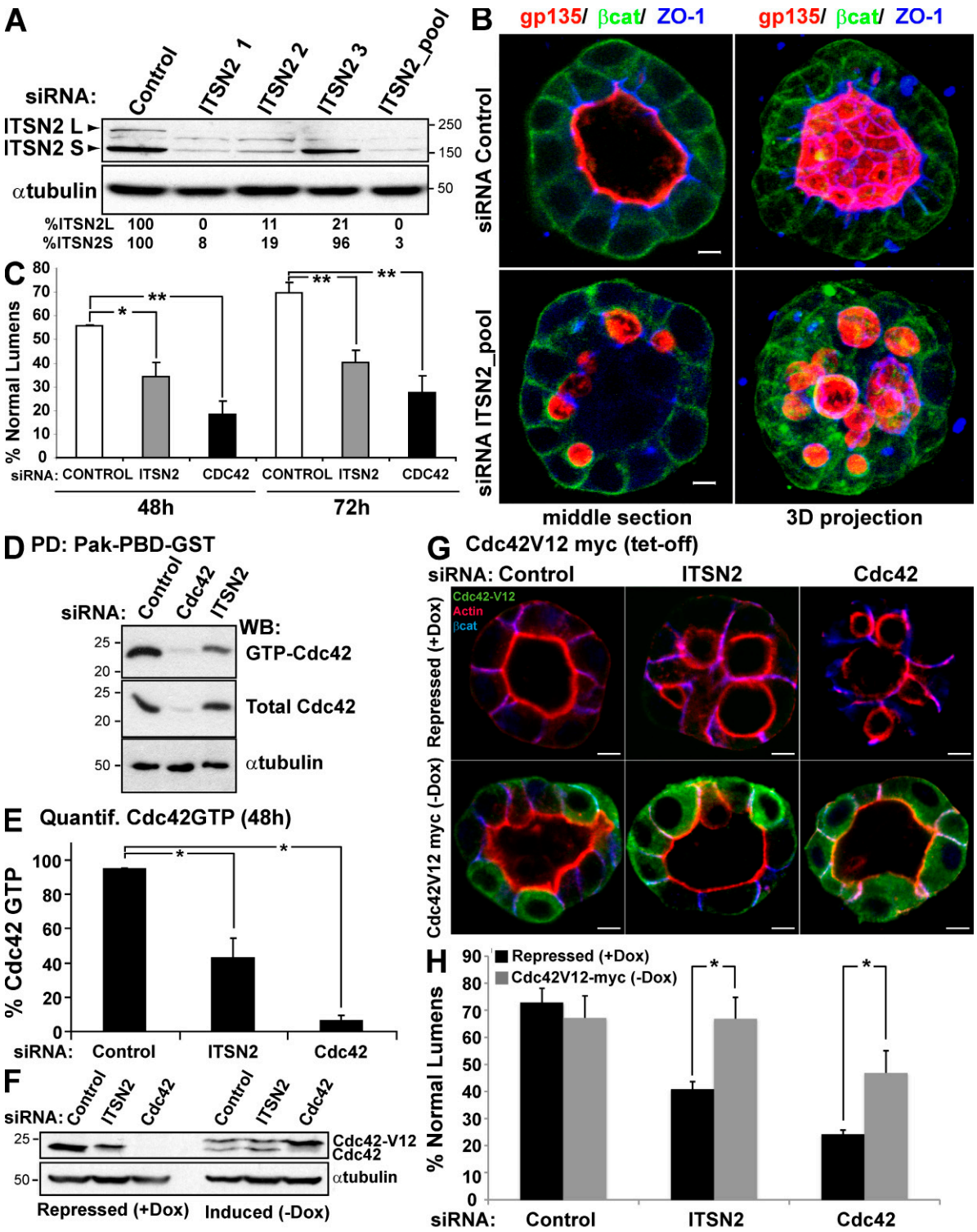

Figure 1. **ITSN2 silencing abrogates lumen formation and reduces GTP-bound Cdc42 levels.** (A) Down-regulation of ITSN2 by siRNA. MDCK cells were transfected with siRNA ITSN2-1, ITSN2-2, ITSN2-3, and a pooled combination of all three or with control siRNA and allowed to form cysts for 72 h. Total lysates were blotted for ITSN2 and tubulin. (B) Confocal microscopy images of the effect of ITSN2 siRNA–mediated silencing on lumen formation. Cells were transfected with ITSN2 siRNA pool or control siRNA and plated to form cysts for 72 h. Cells were stained to detect gp135, β-catenin (βcat), and ZO-1. (C) Quantification of cysts with normal lumens in cells transfected with control siRNA, Cdc42 siRNA, or ITSN2 siRNA pool. Values are mean ± SD from five different experiments (n = 100 cysts/experiment; *, $P < 0.05$; **, $P < 0.005$). (D) siRNA-mediated silencing of ITSN2 inhibits activation of Cdc42. Cells were transfected with ITSN2 siRNA pool, Cdc42 siRNA, or control siRNA. Extracts from these cells were pulled down with Pak-PBD-GST. Total and GTP-bound Cdc42 was detected by immunoblotting with specific antibodies to Cdc42 or tubulin. PD, pull-down; WB, Western blot. (E) Quantification of Cdc42-GTP levels in ITSN2-silenced cells. The ratios of GTP-bound to total protein were calculated relative to tubulin content. Values shown are mean ± SD from three different experiments (*, $P < 0.005$). (F) Down-regulation of ITSN2 by siRNA in cells with the inducible expression of Cdc42V12-myc. MDCK cells stable expressing Cdc42V12-myc under the control of the tet-off repressor were transfected with siRNA to ITSN2 pool or Cdc42 or with control siRNA and allowed to form cysts for 72 h in the presence of Dox (Cdc42V12-myc expression repressed) or not (induced). Total lysates were Western blotted for

Published May 17, 2010

ITSN-L contains the Dbl domain at the C-terminal region of ITSN and functions as a specific GEF for Cdc42 (Hussain et al., 2001). ITSN-L has two isoforms in mammals, ITSN1-L, which is differentially expressed in brain, and ITSN2-L, which is ubiquitously expressed (Pucharcos et al., 2000). ITSN interacts with Wiskott-Aldrich syndrome protein (WASP) and neural WASP (N-WASP) through its SH3 domains to trigger actin polymerization together with Cdc42 (Hussain et al., 2001; McGavin et al., 2001; Irie and Yamaguchi, 2002). ITSNs have been proposed to be a connection between endocytosis and exocytosis because they bind to multiple endocytic and exocytic proteins such as dynamin and SNAP25 and -23 (Okamoto et al., 1999). In fact, the ability of ITSNs to interact with multiple components suggests that they might act as scaffolding proteins necessary for the formation of signaling platforms.

In this work, we have characterized ITSN2 as a specific GEF for Cdc42 activation in epithelial morphogenesis using the organotypic 3D MDCK cell system. We have found out that ITSN2 localizes to centrosomes and is required for the correct orientation of the mitotic spindle and for correctly positioning the apical surface during epithelial morphogenesis. In addition, we have demonstrated a direct relation between lumen formation and spindle orientation. Disruption of LGN, a component of the machinery which regulates spindle movements and orientation, interferes with lumen formation in MDCK cells forming cysts.

Results

ITSN2 is required for normal lumen morphogenesis

In our previous work, we have described that Cdc42 must be activated to induce the formation of the apical domain and the central lumen in 3D MDCK cysts (Martín-Belmonte et al., 2007). A candidate screening for Cdc42 GEFs using RNAi was performed to identify Cdc42-specific GEFs associated with epithelial lumen formation using the apical marker gp135/podocalyxin and the actin cytoskeleton integrity as readout to detect luminal defects in the 3D MDCK model. Using this system, ITSN2 emerged as a candidate for regulating the Cdc42 activity controlling lumen formation (unpublished data). To confirm the function of ITSN2, we designed three siRNA heteroduplexes to deplete endogenous ITSN2 levels. The siRNA directed against the C-terminal region (ITSN2-3) specifically reduced the levels of the long isoform, whereas siRNAs ITSN2-1 and ITSN2-2, directed against the middle and N-terminal region of ITSN2, respectively, were able to reduce the expression of both isoforms (Fig. 1 A). The pool of the three siRNAs dramatically reduced both isoforms as well (Fig. 1 A) and was used for all of the following experiments to silence ITSN2. When siRNA-transfected cells were plated to form cysts, most control cells formed normal lumens at 72 h (70%; Fig. 1 B); MDCK cysts with reduced ITSN2 formed cysts of similar size, but only 41% of them had normal lumens at 72 h. Instead, most cysts with reduced ITSN2 had multiple small lumens, although the basolateral marker β-catenin and tight junctions marker ZO-1 localized normally (Fig. 1, B and C). This phenotype very closely resembles that obtained by silencing Cdc42 in MDCK cysts (Fig. 1 C; Martín-Belmonte et al., 2007). To further confirm these results, we prepared RNAi pPRIME lentiviral system carrying short hairpin RNAs targeted specifically to silence the canine isoform of ITSN2 and obtained consistent results (Fig. S1). To investigate the GEF function of ITSN2 in 3D MDCK cysts, we analyzed GTP-bound Cdc42 levels in ITSN2 and Cdc42 knockdown (KD) cells by GST pull-down assays. Cells silenced for ITSN2 showed a significant reduction in Cdc42-GTP levels, which might explain the aberrant phenotype observed in cyst morphogenesis (Fig. 1, D and E; and Fig. S1 D).

To confirm the specificity of ITSN2 function on Cdc42 activation, we prepared MDCK cells expressing the constitutively active form of Cdc42, Cdc42V12-GFP under the control of a tetracycline-repressible promoter (tet-off; Fig. 1 F), and we tested the ability for lumen formation in ITSN2- and Cdc42-silenced cells. The expression of Cdc42V12 was able to restore the normal formation of the lumen in cells silenced for ITSN2 and also, although to lesser extent, of cells silenced for Cdc42 (Fig. 1, G and H). Together, these results suggest that ITSN2 is required for the activation of Cdc42 to form the lumen.

ITSN2 localizes at centrosomes

Next, we characterized the localization of ITSN2 in MDCK cysts. Staining with several antibodies available for ITSN2 did not serve to identify the localization of the endogenous protein (unpublished data). Therefore, we prepared MDCK cells stably expressing a fusion of the fluorescent protein Venus and human ITSN2 (vhITSN2). In interphase cells, vhITSN2 localized to intracellular clusters close to the apical membrane, which was stained with the apical marker gp135 in MDCK cysts (Fig. 2 A, arrows). vhITSN2 colocalized with the centrosomal markers pericentrin (Fig. 2 B, arrows) and γ-tubulin (not depicted). In mitotic cells, vhITSN2 also distributed at the edge of the spindle poles, stained with acetylated tubulin (Fig. 2 C, arrows), and colocalized with the centrosomal marker pericentrin (not depicted). Because vhITSN2 is an siRNA-resistant form of ITSN2 (Fig. 2 D), we used these cells to validate the specific effect of ITSN2 silencing on lumen formation. We observed that vhITSN2 expression restored the normal phenotype in lumen formation in cells silenced for endogenous ITSN2 (Fig. 2, E and F).

To confirm that the localization of ITSN2 to centrosomes was not an artifact caused by the ectopic expression of vhITSN2, we obtained centrosome-enriched fractions of MDCK cells using centrifugation in Ficoll gradients (Blomberg-Wirschell

Cdc42 and α-tubulin. (A, D, and F) Molecular mass is indicated in kilodaltons. (G) Confocal microscopy images of the rescue effect of Cdc42V12-myc in cells silenced for ITSN2, Cdc42, or control on lumen formation. Cells were transfected with ITSN2 pool, control, or Cdc42 siRNAs and plated to form cysts for 72 h in the presence (Cdc42V12 repressed) or the absence (induced) of 20 µmol Dox. Cells were stained to detect actin, Cdc42V12-myc, and β-catenin. (H) Quantification of cysts with normal lumens in cells expressing or not Cdc42V12-myc and transfected with the control, Cdc42, or ITSN2 pool siRNAs. Values are mean ± SD from three different experiments ($n \geq 100$ cysts/experiment; *, $P < 0.005$). Bars, 5 µm.

Published May 17, 2010

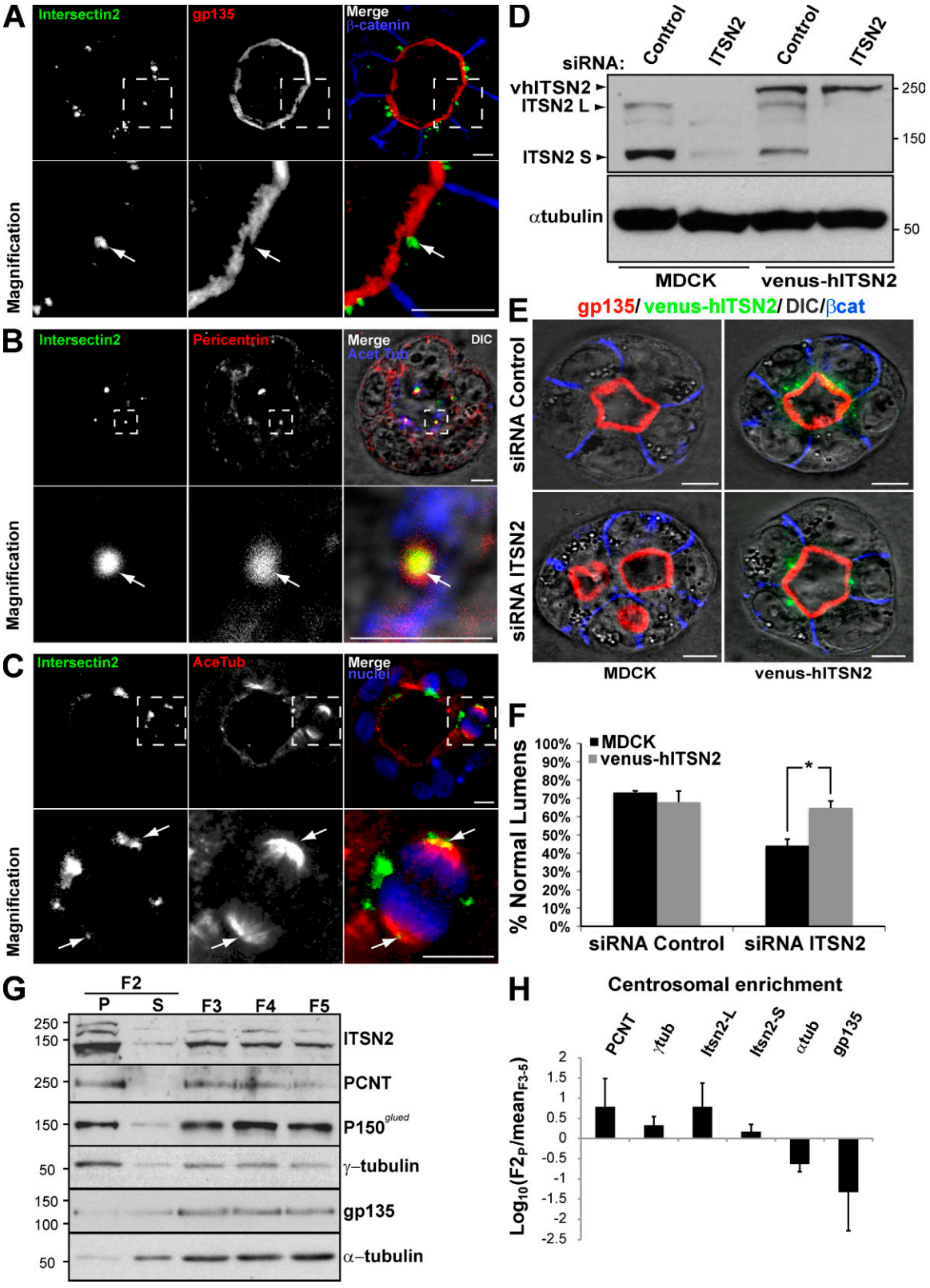

Figure 2. **The siRNA-resistant form of ITSN2, vhITSN2, rescues normal lumen formation.** (A) vhITSN2 is apically localized in MDCK cysts. Cells expressing vhITSN2 (green) were plated to form cysts for 72 h. Cysts were stained with gp135 and β-catenin (top). (B) ITSN2 colocalizes with pericentrin at centrosomes in interphase MDCK cells. Cells expressing vhITSN2 (green; left) were stained with pericentrin (centrosomal marker; middle) and acetylated tubulin (Acet Tub; right with DIC and merge). (C) ITSN2 localizes at spindle poles in mitotic MDCK cells. Cells expressing vhITSN2 (green; left) were stained with acetylated tubulin (AceTub; middle) and chromatin (blue; right and merge). (A–C) Bottom panels show the magnification image of the boxed areas indicated in the top panels. Arrows indicate ITSN2 localization. (D) Down-regulation of ITSN2 by siRNA in cells stably expressing vhITSN2. MDCK cells stable expressing vhITSN2 were transfected with siRNA to ITSN2 pool or with control siRNA and allowed to form cysts for 72 h. Total lysates were blotted for ITSN2 and α-tubulin. (E) Confocal microscopy images of the rescue effect of vhITSN2 in cells silenced for ITSN2 on lumen formation. Cells stably expressing

Published May 17, 2010

and Doxsey, 1998). We detected endogenous ITSN2 in the sediments positive for γ-tubulin/pericentrin and negative for α-tubulin/gp135 (Fig. 2 G, left lane, F2-P). The quantitative analysis showed that both ITSN isoforms (ITSN2-L and ITSN2-S) were highly enriched in the centrosomal fraction together with other centrosomal proteins (Fig. 2 H). To characterize whether the association of centrosomes with ITSN2 is dependent on its association with microtubules or, conversely, whether ITSN2 associates with centrosomes independently of the microtubules, we performed depolymerization/repolymerization experiments using nocodazole (Hung et al., 2000). Microtubules were depolymerized using nocodazole for 4 h, and the subsequent pattern of microtubule regrowth was determined (Fig. S2 A). In nocodazole, interphase microtubules were depolymerized. However, compared with untreated cells, no significant decrease in the concentration of ITSN2 was observed in nocodazole-treated cells (Fig. S2 A). To ensure that ITSN2 is indeed located at the centrosomes where microtubule growth is initiated, the nocodazole-treated cells were washed out to permit microtubule regrowth. After increasing times of regrowth (0–45 min), cells were fixed and stained to detect α- and γ-tubulin, and confocal images were analyzed. As shown in Fig. S2 A, microtubule growth started at the centrosomes, where ITSN2 is located.

Altogether, these results indicate that ITSN2 localizes to centrosomes, and it could activate Cdc42 in this region to form the lumen. Because Cdc42 regulates cell polarity through different effectors that control vesicle trafficking, actin organization, and microtubule stabilization (Etienne-Manneville, 2004), we next focused on characterizing the process in which ITSN2 activates Cdc42.

The exocytosis of apical gp135/podocalyxin and apical junction formation are both dependent on Cdc42 but independent of ITSN2

Activated Cdc42 can associate with numerous effectors that regulate vesicle traffic, mainly through the regulation of the actin cytoskeleton. Accumulated evidence supports the idea that ITSNs are adaptors that coordinate Cdc42-dependent membrane trafficking events in different cells (Hussain et al., 2001; Irie and Yamaguchi, 2002; Malacombe et al., 2006). To evaluate whether ITSN2 functions in exocytosis during lumen formation, we analyzed apical vesicle exocytosis using calcium switch experiments. For these experiments, we used MDCK stably expressing GFP-tagged Anx2 (Anx2-GFP), a peripheral membrane protein which associates with the plasma membrane in a calcium-dependent manner (Rescher and Gerke, 2004), and the apical marker gp135/podocalyxin. Control or MDCK cells silenced for ITSN2 or Cdc42 were polarized in monolayers. After 48 h, the cells were treated overnight with normal (Fig. 3 A) or low-calcium medium (Fig. 3 B). Low-calcium conditions induced the internalization of the apical protein gp135 and Anx2-GFP in a vesicular apical compartment (Fig. 3 B), as described previously (Vega-Salas et al., 1987, 1988). The restitution of normal calcium levels induced the exocytic translocation of gp135 and Anx2-GFP to the plasma membrane in control cells (Fig. 3 C). In contrast, Cdc42 KD cells did not restore the apical compartment after returning to normal calcium conditions (Fig. 3 C), inducing a phenotype very similar to that produced by silencing Cdc42 in the 3D MDCK cyst model (Martín-Belmonte et al., 2007, 2008). Importantly, the restitution of normal calcium levels in ITSN2 KD cells resulted in normal exocytosis of gp135 and Anx2-GFP to the plasma membrane (Fig. 3 C). Previous experiments have shown that activated Cdc42 is implicated in the formation of normal tight junctions at epithelial cell–cell contacts (Joberty et al., 2000; Hurd et al., 2003; Wells et al., 2006). To test whether ITSN2 could activate Cdc42 to form apical junctions, we performed a calcium switch experiment and analyzed the recovery of transepithelial resistance in vivo using an electrical cell-substrate impedance system (Lo et al., 1995). Again, the recovery of normal transepithelial resistance levels was delayed in cells knocked down for Cdc42, whereas cells knocked down for ITSN2 showed a recovery profile similar to that of control cells (Fig. 3 D). Furthermore, the staining of the tight junction protein ZO-1 also showed a specific effect of Cdc42 in the recovery of tight junction integrity in the calcium switch experiment (Fig. 3, A–C). Finally, we also observed that ITSN2 and Cdc42 were not implicated in the orientation of the microtubule-organizing center (MTOC; Fig. S3, A and B) or in the formation of the primary cilium (not depicted). These results suggest that ITSN2 activation of Cdc42 does not affect either vesicle trafficking or tight junction formation in MDCK cell morphogenesis.

With the goal of identifying the possible role of Cdc42 in which ITSN2 is involved during the process of lumen formation, we further investigated the phenotypes of ITSN2 KD and Cdc42 KD in MDCK cysts. First, we quantified the proportion of internal vesicles with apical markers and intercellular lumens in siRNA-transfected cells. For this quantification, we assumed that the intracellular lumens were similar to the vesicular apical compartments that appeared in the calcium switch experiments (Fig. 3 B) and, therefore, could indicate flaws in the process of exocytosis. ITSN2 KD cysts had a significantly reduced proportion of intracellular gp135-loaded vesicles compared with Cdc42 KD cysts, which contained both intercellular lumens and intracellular gp135-loaded vesicles (Fig. 3, E and F). Collectively,

vhITSN2 were transfected with ITSN2 pool or control siRNAs and plated to form cysts for 72 h. Cells were stained to detect gp135, vhITSN2, and β-catenin (βcat). (F) Quantification of cysts with normal lumens in cells expressing vhITSN2 and transfected with the control or ITSN2 pool siRNAs. Values are mean ± SD from three different experiments ($n \geq 100$ cysts/experiment; *, $P < 0.005$). (G) Endogenous ITSN2 is present in centrosome-enriched fractions. MDCK cells were plated to reach confluence and then treated with 0.3 µM nocodazole and 1 µg/ml cytochalasin D for 4 h. A rapid isolation of centrosomes was performed using Ficoll gradient centrifugation of lysates, and then, centrosomes in the F2 fraction were precipitated by ultracentrifugation. The F2 supernatant (S) and pellet (P) were loaded together with fractions F3, F4, and F5, containing cytosolic and membrane proteins. The fractions were immunoblotted for ITSN2 and centrosomal, cytosolic, and membrane markers. (D and G) Molecular mass is indicated in kilodaltons. (H) Densitometry quantification of fractional enrichment represented as $\log_{10}(F2_P/mean_{F3-5})$. Values are mean ± SD from three different experiments. PCNT, pericentrin. Bars, 5 µm.

Published May 17, 2010

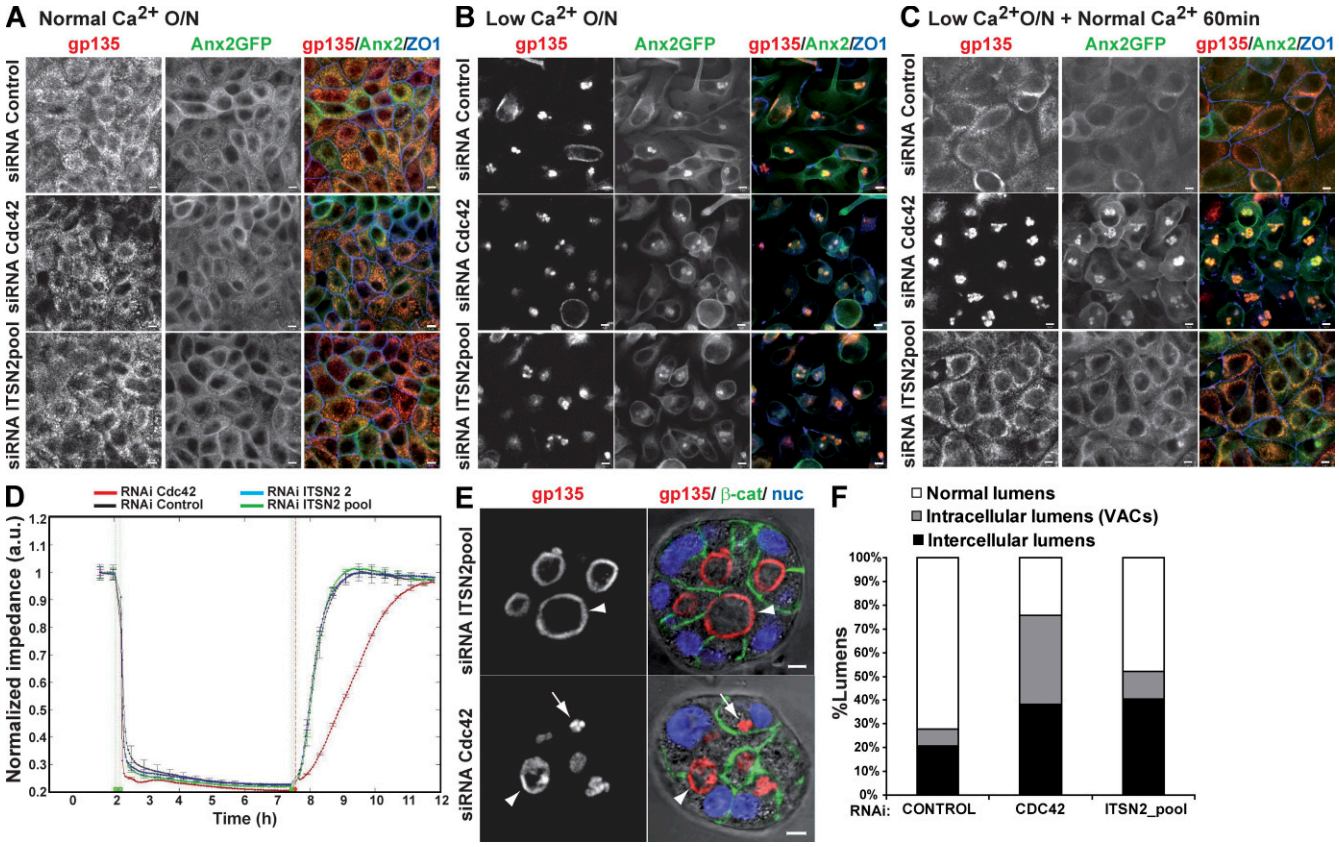

Figure 3. **Apical exocytosis is affected in Cdc42 KD cells but not in ITSN2 KD cells.** (A–C) Effect of Cdc42 and ITSN2 silencing on gp135 and Anx2 exocytosis in calcium switch experiments. Anx2-GFP cells were transfected with Cdc42 siRNA (middle), ITSN2 siRNA pool (bottom) or control siRNA (top) and plated after 48 h to form a confluent monolayer (A). Cells were treated with calcium-free medium overnight (O/N; B) and then treated with complete medium for 60 min (C). Cells were fixed after each step and stained to detect gp135 and ZO-1. (D) Quantification of monolayer impedance. Control (black line)-, Cdc42 (red line)-, and ITSN2-silenced cells (blue and green lines) were plated on electrode plates and allowed to form a confluent monolayer. Cells were treated as described for A–C, and impedance was measured in real time to determine epithelial permeability. Values shown are mean ± SD from three different experiments. (E) Lumen formation phenotypes of Cdc42 and ITSN2 silencing. Cdc42 and ITSN2 KD cells were plated to form cysts for 72 h. Cells were stained to detect gp135 (left), β-catenin (β-cat), and nuclei (nuc). Arrows indicate intracellular lumens (vesicular apical compartments [VACs]), and arrowheads indicate intercellular lumens. (F) Quantification of cysts with normal lumens or with multiple intercellular and intracellular lumens in cells transfected with control siRNA, Cdc42 siRNA, or ITSN2 siRNA pool. Values shown are means from three different experiments ($n \geq 100$ cysts/experiment; *, $P < 0.005$ for intracellular lumens of Cdc42 vs. control or ITSN2; **, $P < 0.06$ for intercellular lumens of ITSN2 vs. control; ***, $P < 0.07$ for intercellular lumens of Cdc42 vs. control). Bars, 5 µm.

these results indicated that ITSN2 does not detectably function to activate Cdc42 for vesicular trafficking or the formation of tight junctions, but it could be necessary for other processes such as mitotic spindle orientation, in which defects in the activation of Cdc42 results in multiple lumen phenotypes.

ITSN2 and CDC42 are both required for normal positioning of the mitotic spindle in 3D MDCK cultures

Recent work performed in Caco-2 epithelial cells suggested that Cdc42 is required for the orientation of the mitotic spindle to position the apical surface in cells forming 3D cysts (Jaffe et al., 2008). We analyzed the orientation of the mitotic spindle in dividing cells using cysts of MDCK cells with reduced levels of Cdc42 or ITSN2 and compared them with control cells. We transfected MDCK cells with control or siRNA heteroduplexes targeting Cdc42 or ITSN2 (Fig. 4 A) and then measured the angle formed between the apicobasal axis and the spindle pole axis in three dimensions, which was calculated as described in the schematic drawing of Fig. 4 B. Most of the mitotic spindles analyzed in control cells were normal (Fig. 4 B, right). However, cysts with reduced levels of both Cdc42 and ITSN2 had a significant increase in abnormally positioned spindle poles, the effect being stronger in cells silenced for Cdc42 (Fig. 4, B [left and middle] and C). These results suggest that the defect in mitotic spindle rotation and/or positioning in cells silenced for Cdc42 might generate the defects observed in lumen formation. To test this hypothesis, we analyzed mitotic spindle dynamics in metaphase by confocal time-lapse microscopy using 3D MDCK cells expressing GFP–α-tubulin. We observed that in control cells, there was an ~90° rotation of the spindle from the apicobasal axis to the plane of the epithelium (Fig. 4 D, top; and Video 1), which was described previously in MDCK cysts (Yu et al., 2003). However, in cells silenced for Cdc42 or ITSN2, there was a disruption of this spindle rotation, which resulted in the translocation of one of the dividing cells to the center of the cyst, narrowing the luminal space (Fig. 4 D, middle and bottom; and Videos 2 and 3). Moreover, the impairment in spindle rotation also induced a delay

Published May 17, 2010

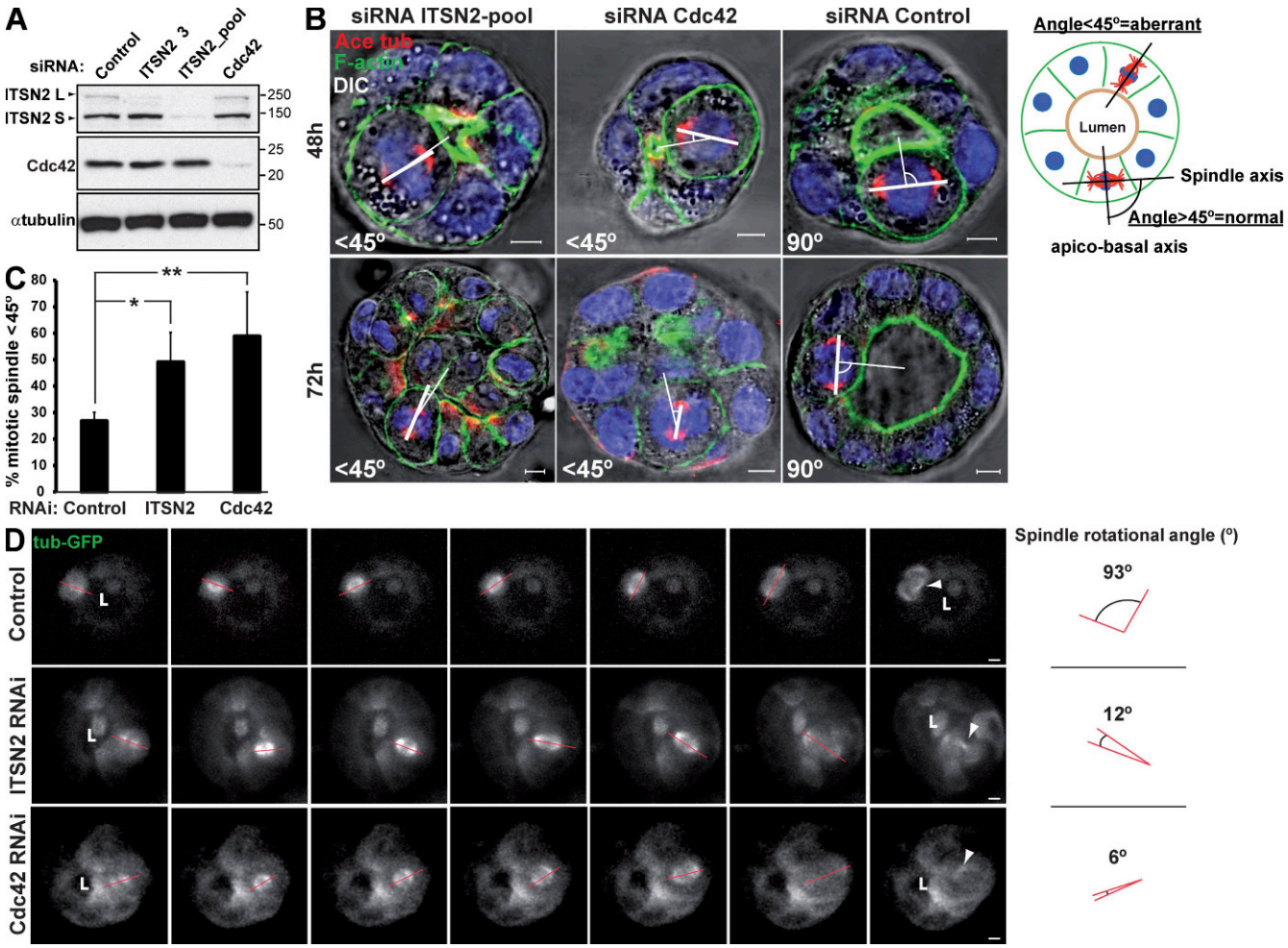

Figure 4. **Cells silenced for Cdc42 or ITSN2 present spindle orientation defects.** (A) Down-regulation of ITSN2 and Cdc42 by siRNA. Cells were transfected with Cdc42, ITSN2, or control siRNA and allowed to form cysts for 72 h, and then total cell lysates were Western blotted for Cdc42 and α-tubulin (control). Molecular mass is indicated in kilodaltons. (B) Effect of Cdc42 and ITSN2 siRNA in spindle orientation. Cells were transfected with ITSN2 siRNA pool (left), Cdc42 siRNA (middle), or control siRNA (right) and plated to form cysts for 48 (top) or 72 h (bottom). Cells were stained to detect actin, acetylated tubulin (Ace tub), and chromatin (blue). The apicobasal axis (thin line) and the spindle axis (thick line) are drawn in white. (C) Quantification of misoriented spindles in 48-h cysts silenced with Cdc42, ITSN2, or control siRNA. The angle between the apicobasal axis and spindle axis was measured. Angles <45° were counted as abnormal. Values shown are mean ± SD from five different experiments (n = 30 cysts/experiment; *, $P < 0.01$; **, $P < 0.05$). (D) Spindle orientation defects in Cdc42- and ITSN2-silenced cells. MDCK cells stably expressing α-tubulin–GFP were transfected with control (top), ITSN2 (middle), or Cdc42 siRNA (bottom) and plated to form cysts. Live cells were analyzed by 3D video confocal microscopy from early metaphase until anaphase at 0.5 frames/min. Quantification of angle deviation in control and cells knocked down for Cdc42 or knocked down for ITSN2 is shown. Arrowheads indicate the localization of the midbodies after cytokinesis. Red lines indicate the orientation of the mitotic spindle. "L" indicates localization of the lumen. Bars, 5 μm.

in the metaphase to anaphase transition, which we characterized in MDCK 2D monolayers for statistics (Fig. S3 C). Metaphase time (MT) was affected in cells silenced for Cdc42 (MT = 27.3 ± 7.7 min) and cells silenced for ITSN2 (MT = 31.2 ± 11.5 min), as compared with control cells (MT = 16.9 ± 4.6 min; Fig. S3, C and D). These results indicate that ITSN2 and Cdc42 are both required for normal mitotic spindle orientation during cell division. In particular, they seem to control the normal rotation of the mitotic spindle in mitotic cells.

In summary, we have shown that ITSN2 activates Cdc42, which in turn controls the orientation of the mitotic spindle during mitosis. Although our results can explain the phenotype of multiple lumens observed in cells silenced for ITSN2 or Cdc42, it sheds no light on the subjacent molecular mechanism. To identify the possible mechanism of action of ITSN2, we characterized the domain responsible for targeting ITSN2 to centrosomes. ITSN2 contains two EH (Eps15 homology) domains, a central coiled-coil region, and five consecutive SH3 domains. Additionally, ITSN-L presents an extended C-terminal region containing a DH (Dbl homology), a PH (pleckstrin homology), and a C2 domain (Fig. 5 A). We prepared GFP-fused constructs comprising different domains of ITSN2 and characterized their subcellular localization in MDCK cells (Fig. 5, A and B). We observed that when overexpressed, the EH domains of ITSN2 targeted GFP to the centrosomes in MDCK cells (Fig. 5 B, left; arrows show the colocalization of EH domains with pericentrin). In contrast, the rest of the domains analyzed distributed in the cytoplasm, forming clumps that did not colocalize with centrosomal markers (Fig. 5 B, bottom right). Previous results have shown the ability of ITSNs to interact with multiple components

Published May 17, 2010

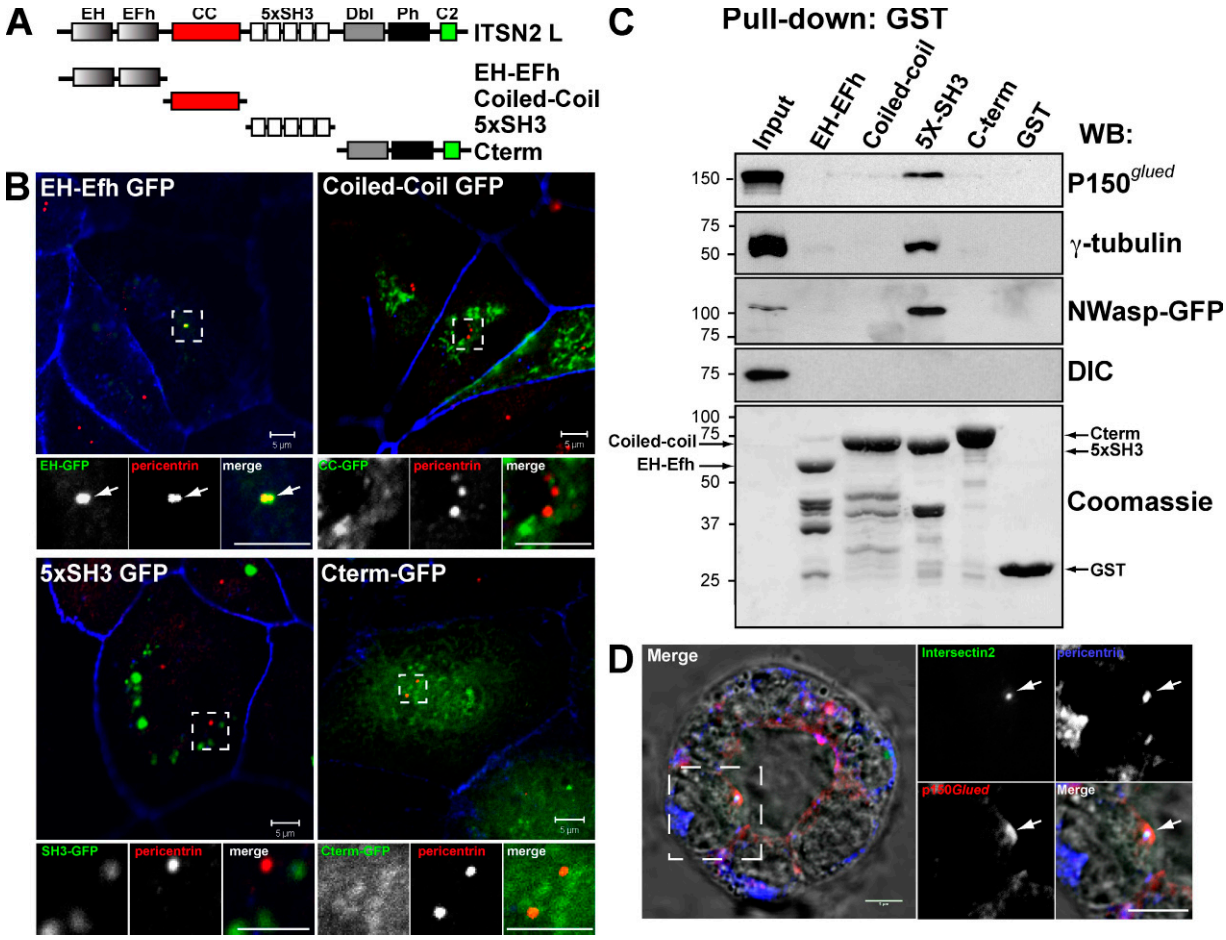

Figure 5. **ITSN2 is partially localized at centrosomes through the EH domains and interacts with centrosomal proteins through the SH3 domains.** (A) Schematic diagram of the different ITSN2-L domains (called EH-EFh, coiled-coil [CC], 5xSH3, and C terminus) and the GFP and GST constructs generated with them. (B) EH-Efh domains target ITSN2 to the centrosomes. MDCK cell were transfected with GFP-tagged protein constructs of ITSN2 (EH, coiled-coil, 5xSH3, and C terminus) and analyzed by confocal microscopy. Cells were stained to detect pericentrin and actin (blue). Bottom panels show the magnification image of the boxed areas indicated in the top panels. Arrows indicate the localization of EH-GFP to the centrosome (pericentrin) (C) ITSN2 interacts with the centrosomal proteins γ-tubulin and p150^{Glued}. Total cell lysates were incubated with beads preloaded with GST-tagged protein constructs of ITSN2 (EH, coiled-coil, 5xSH3, and C terminus) or with GST. Pulled down fractions were immunoblotted to detect γ-tubulin, p150^{Glued}, N-WASP–GFP (positive control), and DIC or stained with Coomassie blue to detect the total amount of the GST-fused proteins used as bait. Molecular mass is indicated in kilodaltons. WB, Western blot. (D) ITSN2 colocalizes with γ-tubulin and p150^{Glued} in cysts. Cysts expressing vhITSN2 (green) were stained for p150^{Glued} and pericentrin merged with DIC in the left panel. Right panels are the magnification of the boxed area in the left panel. Arrows indicate the colocalization of ITSN2 and p150^{Glued} at the centrosome (pericentrin). Bars, 5 μm.

of the endocytic machinery, which suggests that ITSNs might act as scaffolding proteins necessary for the formation of signaling platforms (Yamabhai et al., 1998; Okamoto et al., 1999; Pucharcos et al., 2000; Hussain et al., 2001). To characterize the possible role of ITSN2 as a scaffolding protein at centrosomes, we performed pull-down assays using GST fusions of the various aforementioned domains of ITSN2 (Fig. 5 A). ITSN2 was found to interact through the SH3 domains with p150^{Glued}, one of the subunits of the dynactin complex, and with γ-tubulin but not with other members of the complex such as dynein intermediate chain (DIC; Fig. 5 C). As a control, we analyzed the interaction of ITSN2 with N-WASP through the SH3 domains of ITSN2 (Fig. 5 C), as described previously for ITSN2 and WASP in T cells (McGavin et al., 2001). The dynein–dynactin complex is an essential regulator of spindle orientation and cell division (Quintyne et al., 1999). Previous studies have indicated that Cdc42 activation is involved in the reorientation of the MTOC during cell migration through a pathway dependent on the dynein–dynactin complex (Palazzo et al., 2001; Gomes et al., 2005). We observed that vhITSN2 colocalized with p150^{Glued} and pericentrin at the centrosome in 3D cysts (Fig. 5 D). These results suggest that ITSN2, which is targeted to the centrosome through its EH domains, mediates the activation of Cdc42 in this region, which in turn would control the orientation of the spindle through the activity of other centrosomal proteins such as the dynein–dynactin complex.

Next, we analyzed the localization of Cdc42 in different phases of the cell cycle using MDCK cells expressing Cdc42-GFP (Fig. 6). It has been reported that the localization of Cdc42 is associated with the plasma membrane and the Golgi in different cell types (Itoh et al., 2002; Yoshizaki et al., 2003). The stable expression of Cdc42-GFP caused a significant reduction of the endogenous Cdc42, so the final levels of total Cdc42 were similar to the endogenous protein in these cells (Fig. 6 B).

Published May 17, 2010

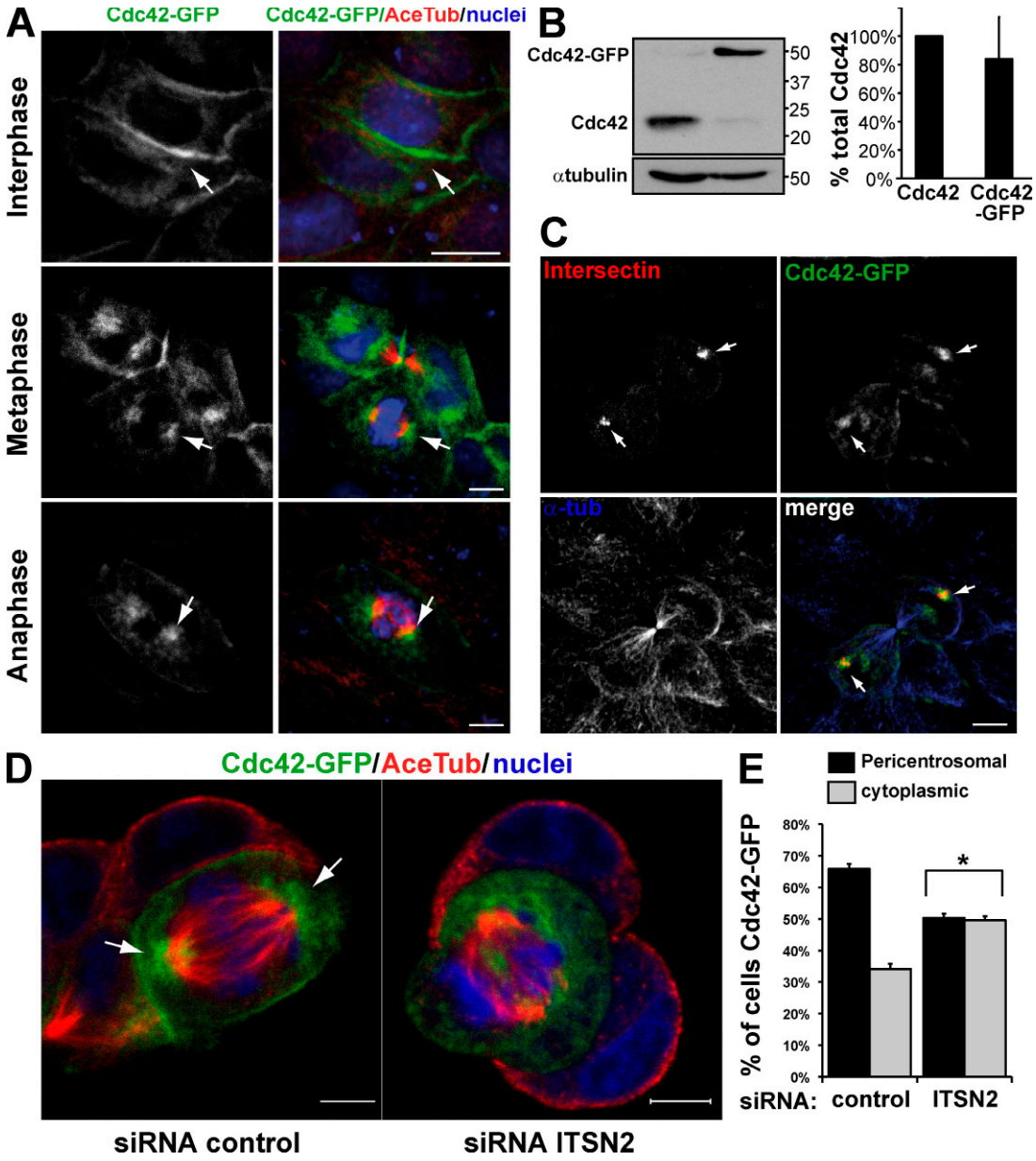

Figure 6. **Cdc42 localizes near centrosomes during mitosis.** The localization of Cdc42 in mitosis depends on ITSN2. (A) Confocal images of Cdc42 localization in MDCK cells in different phases of the cell cycle. MDCK Cdc42-GFP cells were plated in a monolayer and stained for acetylated tubulin (Ace Tub) and chromatin (blue). Cells in interphase (top), metaphase (middle), and anaphase (bottom) are shown. (B) Cdc42 levels are regulated in Cdc42-GFP cells. Total cell lysates of wild-type MDCK cells and Cdc42-GFP cells were immunoblotted for Cdc42, and total Cdc42 levels were quantified using α-tubulin as a control. Molecular mass is indicated in kilodaltons. Values shown are mean ± SD from three different experiments (Western blots). (C) Confocal images of ITSN2 colocalizing with Cdc42 in dividing cells. Cdc42-GFP cells were transfected with ITSN2-Cherry (red) and stained for α-tubulin (α-tub). Arrows indicate the localization of ITSN2 and Cdc42. (D) Confocal images showing that the localization of Cdc42 in mitosis depends on ITSN2. MDCK cells stably expressing Cdc42-GFP were silenced with siRNA oligonucleotides to ITSN2 (right) or control (left) and plated to form cysts for 24 h. Cells with Cdc42-GFP were stained for acetylated tubulin and chromatin (blue). (A and D) Arrows indicate Cdc42 localization. (E) Quantification of Cdc42-GFP associated with the mitotic spindles in control cell or cells silenced for ITSN2. Cells with Cdc42-GFP concentrated at the spindle poles or dispersed throughout the cytoplasm were quantified. Values shown are mean ± SD from three different experiments (n = 100 cysts/experiment; *, $P < 0.001$ for cytoplasmic/pericentrosomal Cdc42-GFP localization in ITSN2 KD vs. control cells). Bars, 5 µm.

Cdc42-GFP–expressing cells formed normal cysts as we showed previously (Martín-Belmonte et al., 2007). As expected, Cdc42-GFP localized mainly to the plasma membrane in interphase cells (Fig. 6 A, top); however, we detected an important fraction of Cdc42-GFP in close proximity to the mitotic spindles during different phases of cell division in MDCK cells (Fig. 6 A, middle and bottom). Interestingly, we observed that Cdc42 colocalized with ITSN2 at the mitotic spindles in dividing MDCK cells (Fig. 6 C, arrows). Therefore, during cell division, Cdc42 is localized to the region of the spindle pole and is activated by ITSN2 to control the orientation of the spindle. To investigate whether the presence of ITSN2 is necessary not only for the activation but also for the localization of Cdc42, we analyzed the effect of silencing ITSN2 on the localization of Cdc42 in MDCK cells in mitosis. In control cells, the localization of Cdc42 was concentrated at the spindle poles in cells in mitosis, but in

Published May 17, 2010

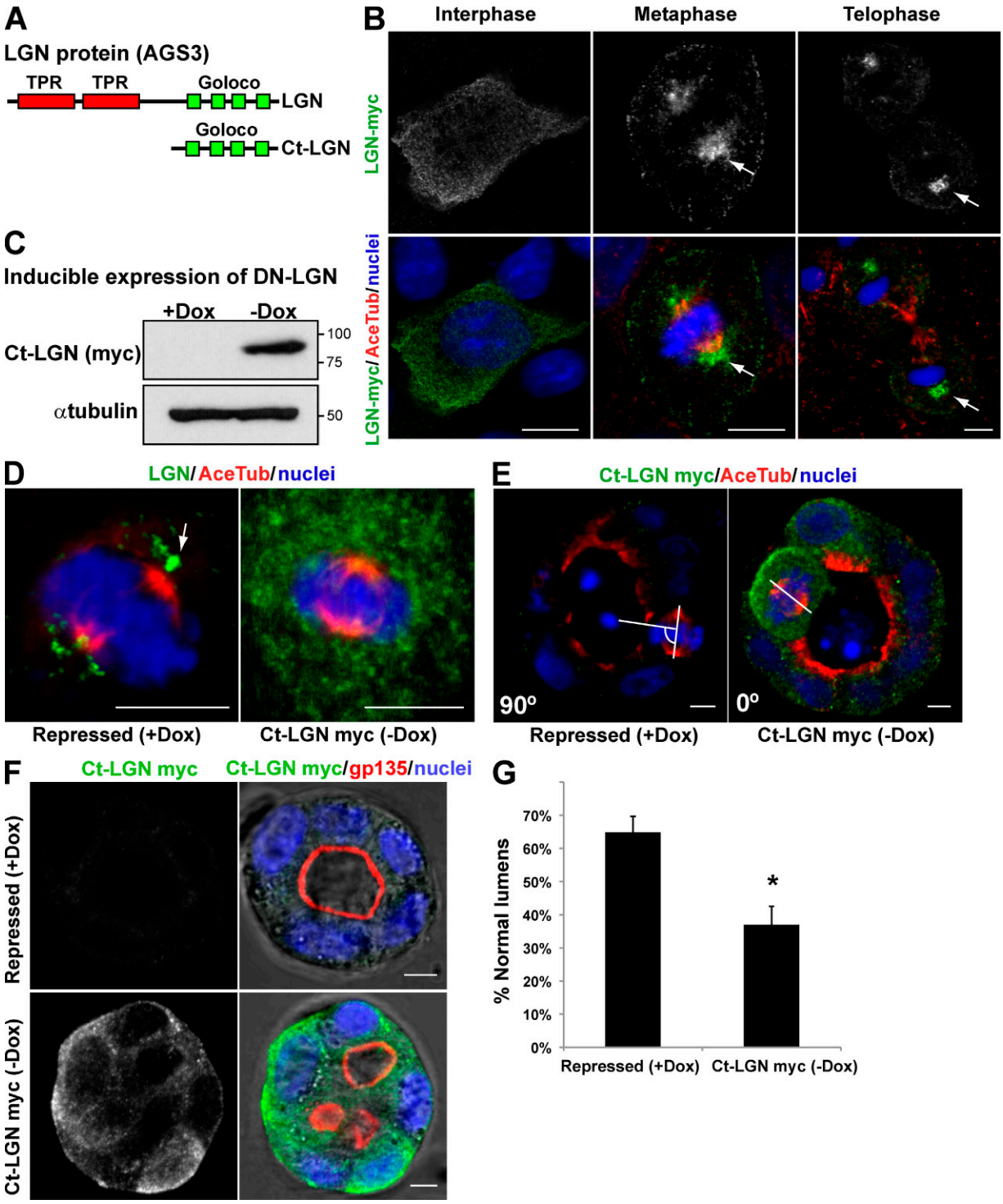

Figure 7. **Expression of a dominant-negative form of LGN in MDCK cells disrupts mitotic spindle organization in cysts and interferes with normal lumen formation.** (A) Schematic diagram of LGN protein domains and the C-terminal region (Ct-LGN) containing the four GoLoco domains that were used as the dominant-negative form of LGN. (B) Confocal images of LGN-myc localization in MDCK cells in different phases of the cell cycle. MDCK cells expressing LGN-myc (top) were plated in a monolayer and stained for acetylated tubulin (Ace Tub) and chromatin (blue; merge images in bottom panels). In cells in interphase (left), LGN localized to the cytoplasm. In cells in metaphase (middle) and telophase (right), LGN localized to the spindle poles. Arrows indicate the localization of LGN-myc. (C) Inducible expression of the dominant-negative (DN) form of LGN (Ct-LGN–myc). MDCK cells expressing Ct-LGN–myc under the control of the tet-off repressor were plated to form cysts for 72 h in the presence of Dox (Ct-LGN–myc expression repressed) or not (induced). Total lysates were Western blotted for myc (top) or α-tubulin (bottom). Molecular mass is indicated in kilodaltons. (D) Confocal microscopy images of the effect of Ct-LGN on endogenous LGN localization. Cells expressing Ct-LGN–myc were plated to form monolayers for 72 h in the presence (Ct-LGN–myc repressed) or the absence (Ct-LGN–myc induced) of 20 µmol Dox. Cells were stained to detect acetylated tubulin, LGN, and chromatin (blue). The arrow indicates the localization of LGN. (E) Confocal microscopy images of the effect of Ct-LGN on mitotic spindle orientation in cysts. Cells expressing Ct-LGN–myc were plated to form cysts for 72 h in the presence (Ct-LGN–myc repressed) or the absence (Ct-LGN–myc induced) of 20 µmol Dox. Cells were stained to detect acetylated tubulin, myc (green), and chromatin (blue). The angles between the apicobasal axis and the spindle axis (white lines) are indicated in the lower

Published May 17, 2010

cells silenced for ITSN2, Cdc42 was dispersed throughout the cytoplasm (Fig. 6, D [arrows] and E). These data suggest that ITSN2 is required for the localization and activation of Cdc42 at the spindle poles of mitotic cells, which in turn regulates the proper orientation of the mitotic spindle.

Disruption of LGN, a regulator of the mitotic spindle orientation, interferes with lumen formation

The data presented in this paper and previous results suggest a correlation between the orientation of the mitotic axis, regulated by Cdc42, and the formation of a single central lumen (Jaffe et al., 2008). However, to further demonstrate this relationship more convincingly, we investigated the effect of the alteration of another component of the machinery specific for mitotic spindle orientation on lumen formation. LGN, which is part of the machinery that controls the spindle orientation, contains two tetratricopeptide repeat motifs in its N-terminal region and four Gαi/o-Loco (GoLoco) motifs near the C terminus (Fig. 7 A). Tetratricopeptide repeat motifs are involved in protein–protein interactions, whereas GoLoco motifs have been implicated as inhibitors of GDP dissociation from heterotrimeric G protein α-subunits. The expression of the GoLoco motifs can act as a dominant-negative form of LGN (Ct-LGN; Fig. 7 A; Morin et al., 2007). LGN, which is expressed in MDCK cells, localizes at the cytoplasm in interphase but translocates to the cell cortex and spindle poles in mitosis (Du et al., 2001). We confirmed this localization for LGN-myc in MDCK cells (Fig. 7 B; arrows indicate LGN localization at the spindle poles). LGN regulates mitotic spindle movements and orientation, so interfering with its function randomizes the plane of division and disrupts the orientation of the mitotic spindle in epithelial and neuroepithelial cells (Du and Macara, 2004; Morin et al., 2007). To disrupt LGN function, we expressed Ct-LGN in MDCK cells under the control of an inducible promoter (tet-off; Fig. 7 C). We confirmed that Ct-LGN expression was sufficient to disperse the normal localization of LGN from the mitotic spindles (Fig. 7 D) and the normal orientation of the mitotic spindle in 3D MDCK cysts (abnormal spindles in control cells [+doxycycline (Dox)], 25.5%; abnormal spindles in Ct-LGN–induced cells [−Dox], 54.2%; Fig. 7 E), as was described previously in chick neuroepithelial cells (Morin et al., 2007). Interestingly, we also found that the expression of Ct-LGN disrupted the formation of normal lumens in MDCK cells forming cysts (Fig. 7, F and G). In sum, when we alter the orientation of the axis with the expression of a dominant-negative form of LGN, a protein essential for the orientation of the mitotic spindles in different models of cell division, the formation of the lumen results also altered. Therefore, with these experiments, we have demonstrated a direct relationship between the orientation of the mitotic axis and the formation of the lumen.

Discussion

Collectively, the results presented in this study suggest that ITSN2 is involved in the activation of Cdc42 to regulate spindle orientation during mitosis. To perform this function, ITSN2 localizes to the centrosomes, both in interphase cells and in cells in mitosis. The EH domains of ITSN2 mediate the localization of ITSN2 at the centrosomes. Thus, ITSN2 operates as a spatial regulator for Cdc42 activity, which is also associated to the spindle poles during cell division. Then, Cdc42 is required somehow for the normal function of the spindle machinery, which is involved in regulating the orientation of the mitotic spindle at the centrosomes and for the normal formation of the lumen in epithelial morphogenesis.

The mechanisms and external factors that regulate spindle orientation in epithelial cells are poorly understood. The majority of these studies have been performed using asymmetric division models (for review see Siller and Doe, 2009). However, it has been postulated that the main players of this process in mammalian epithelial cells may be the same, including the dynein–dynactin complex, Gα proteins, LGN, NuMA (nuclear mitotic apparatus protein), the Par complex, and the Rho GTPase Cdc42 (for review see Siller and Doe, 2009). The molecular mechanism associated with the function of Rho GTPases is generally related to its subcellular localization (Iden and Collard, 2008). We have shown that Cdc42 localizes to the mitotic spindle in the centrosomal region, where it can activate downstream effectors that control the mitotic spindle machinery. An essential question is how Cdc42 associates with the spindle poles. We found that ITSN2 is localized in centrosomes, through the EH domains of ITSN2. Therefore, ITSN2 could recruit and activate Cdc42 at the spindle poles. In fact, silencing of ITSN2 significantly reduces the amount of active Cdc42 and that of the Cdc42 associated with the spindle poles. In addition, ITSN2 seems to mediate protein–protein interactions with other centrosomal proteins through the SH3 domains, and thus, it might scaffold signaling platforms for Cdc42 at this location. Therefore, a potential mechanism for Cdc42 function in the orientation of the mitotic spindles might be mediated by ITSN2, which would be responsible not only for activating Cdc42 in the centrosomal region but also for scaffolding proteins involved in downstream signaling.

In addition to the data presented in this study for the role of Cdc42 by controlling mitotic spindle orientation in the MDCK cells, Cdc42 activity was also recently described to regulate epithelial morphogenesis and spindle orientation in Caco-2 cells, a mammalian intestinal model of epithelial morphogenesis (Jaffe et al., 2008). However, the link between Cdc42, spindle orientation, and the formation of the lumen described previously was strictly correlative (Jaffe et al., 2008). To clarify this issue, we have shown that disruption of LGN, a known essential component of the spindle orientation machinery, also caused a defect

left corners. (F) Confocal microscopy images of the effect of Ct-LGN in MDCK cysts on lumen formation. Cells expressing Ct-LGN–myc were plated to form cysts for 72 h in the presence (Ct-LGN–myc repressed) or the absence (Ct-LGN–myc induced) of 20 µmol Dox. Cells were stained to detect gp135, myc (green), and nuclei. (G) Quantification of cysts with normal lumens in cells expressing or not Ct-LGN–myc. Values are mean ± SD from three different experiments (n = 100 cysts/experiment; *, $P < 0.001$). Bars, 5 µm.

Published May 17, 2010

lumen formation similar to the defect caused by the silencing of ITSN2 and Cdc42, which suggests a direct relationship between these two processes.

The mechanism of spindle rotation may involve centrosome movement directed by interactions between the astral microtubules and the cell cortex. Therefore, the connection of astral microtubules to centrosomes and the cell cortex must be fully coordinated. A role for the actin cytoskeleton and motors such as the dynein–dynactin complex has been proposed in this process (Schuyler and Pellman, 2001; Kunda and Baum, 2009). The actin cytoskeleton is one of the main downstream effects of Rho GTPase function. To stabilize the interaction between the cell cortex, centrosomes, and the astral microtubules, Cdc42 regulates actin remodeling via different effectors such as Pak (p21-activated kinase), N-WASP, and formins in mammalian cells (Narumiya and Yasuda, 2006). Moreover, in yeast, a Cdc42 GEF complex (Bem1–cdc24p, functionally similar to ITSN) interacts with PAK and regulates the polarization of the cell division machinery (Heil-Chapdelaine et al., 1999). A previous study has elucidated a route in which Cdc42 may regulate the activation of Pak2 at the centrosomes, which in turn regulates the spindle assembly machinery, including Aurora A, dynein–dynactin, and NuMA (Mitsushima et al., 2009). In other series of experiments, Cdc42 and its effector mammalian Dia3 have been shown to regulate the biorientation of the chromosomes, which involved attachment of the plus ends of microtubules to kinetochores, to ensure alignment of chromosomes during metaphase and their correct segregation during anaphase (Yasuda et al., 2004). Therefore, although the function of Cdc42 in spindle positioning is clear, the effectors involved and the molecular mechanism acting downstream of Cdc42 remain to be identified.

Different epithelial tissues undergo events of massive membrane trafficking in the initial steps of morphogenesis (Bryant and Mostov, 2008). Previous data have demonstrated a role for Cdc42 in vesicle trafficking in polarized epithelial cells (Müsch et al., 2001). We have observed a function for Cdc42 in the exocytosis of gp135-containing vesicles and the remodeling of tight junctions in calcium switch experiments. In addition, we have found a greater effect of silencing Cdc42 on lumen formation and mitotic spindle orientation than silencing ITSN2. Our present data suggest the existence of another GEF as regulator for Cdc42 during this process. Interestingly, we have detected ITSN2 at intracellular locations in MDCK cells, which might be endosomal membranes. Multiple studies have demonstrated an important function for ITSN2 during endocytosis (Pucharcos et al., 2000; McGavin et al., 2001). Recently, it has been shown that endocytosis can act to promote cell polarity in different models (Georgiou et al., 2008, Harris and Tepass, 2008; Leibfried et al., 2008). Even more, some proteins associated with endocytosis have been described to be required for spindle positioning in mitosis (Royle et al., 2005; Liu and Zheng, 2009). The possibility that ITSN2 regulates cell polarity through endocytosis remains to be investigated.

In summary, we have identified ITSN2 as an activator of Cdc42 at the centrosomes to regulate spindle orientation during mitosis. It has been recently described that the apical membrane and the lumen originate from the place where the midbody is formed during cytokinesis (Schlüter et al., 2009). Therefore, the regulation of the orientation of the mitotic spindle, which determines the location of the midbody, would be essential to ensure the formation of a single lumen.

Materials and methods

Reagents

Antibodies against ITSN2 (Novus Biologicals), N-WASP (Santa Cruz Biotechnology, Inc.), Cdc42 (BD), pericentrin (Covance), mLGN/GPSM2/AGS3 (Abnova), α-tubulin (Sigma-Aldrich), γ-tubulin (Sigma-Aldrich), $p150^{Glued}$ (BD), GFP (Sigma-Aldrich), β-catenin (Sigma-Aldrich), and acetylated tubulin (Sigma-Aldrich) were used as primary antibodies. Gp135 antibody was a gift from the Ojakian laboratory (State University of New York Downstate Medical Center, Brooklyn, NY). Peroxidase-conjugated donkey anti–mouse IgG and anti–rabbit IgG were used as secondary antibodies for Western blots (Jackson ImmunoResearch Laboratories, Inc.). Alexa Fluor–conjugated secondary antibodies (Alexa Fluor 488, 555, or 647; Invitrogen) and TOPRO-3 (for nuclear/DNA staining) were used in microscopy protocols. Nocodazole (Sigma-Aldrich) and cytochalasin D (Sigma-Aldrich) depolymerized tubulin and actin cytoskeleton, respectively.

Vectors

N-WASP–GFP was cloned in a pEGFP-C1 vector (Takara Bio Inc.). GFP-tagged ITSN2 constructs (EH/EH, coiled-coil, SH3, and C terminus) were cloned in a pEGFP-C2 vector (Takara Bio Inc.). Human ITSN2-Cherry was a gift from S. de la Luna (Centre de Regulació Genòmica, Barcelona, Spain). Human ITSN2-L–GFP, GST-EH/EH, GST–coiled-coil, GST-5xSH3, and GST–C terminus were gifts from K. Kaibuchi (Nagoya University, Chikusa-ku, Nagoya, Japan). vhITSN2 vector was a contribution from I. Macara (University of Virginia School of Medicine, Charlottesville, VA). Myc-tagged Ct-LGN inducible and LGN-myc vector were a gift from X. Morin (École Normale Supérieure, Paris, France).

Cells

MDCK cells were grown as described previously (Martín-Belmonte et al., 2007). MDCK cells stably expressing β-tubulin–GFP, Cdc42-GFP, vhITSN2-L, inducible Cdc42V12-myc or inducible Ct-LGN–myc were made by cotransfection with blasticidin-resistant gene and selection for 10 d with 20 ng/ml Dox and 0.5 mg/ml blasticidin. To prepare cysts in Matrigel, cells were trypsinized to a single cell suspension of 2×10^4 cells/ml in 2% Matrigel and plated in coverglass chambers (Thermo Fisher Scientific) covered with Matrigel. Cysts were grown for 3–5 d.

Microscopy

Immunofluorescence of cysts was previously described (Martín-Belmonte et al., 2007). Cysts were analyzed on a confocal microscope (510 or 710 LSM; Carl Zeiss, Inc.) using a 63× NA 1.4 oil Plan-Apochromat objective and a 63× NA 1.2 water C-Apochromat Corr (for live cell and cyst imaging). The imaging acquisition system used was ZEN software suite (Carl Zeiss, Inc.). For image processing, we used ImageJ (National Institutes of Health) and ZEN software suite. For videomicroscopy and 3D reconstitutions, we processed maximum projections of all stacks and then reduced background using ImageJ software. Fixed cyst imaging was performed in PBS medium or mounted using ProLong Gold antifade reagent. Fixed cells in monolayers were analyzed in Fluoromount medium. Cysts with actin/gp135 staining at the interior surface and β-catenin facing the ECM were identified as normal lumens (interior apical pole). Cysts that had actin/gp135 absent, in small multiple lumens, or at the periphery were considered as abnormal lumens. Per condition, >100 cysts/experiment were analyzed, SD was calculated, and statistical significance was determined by paired Student's *t* test. For spindle orientation analysis, cysts were stained with acetylated tubulin, and the angle formed by the spindle and the apicobasal axis was measured. Divisions with angles <45° were considered abnormal. Per condition, >30 cysts/experiment were analyzed. For videomicroscopy, cells stably expressing β-tubulin–GFP were analyzed using an LSM 510 with incubation chamber at 5% CO_2 and 37°C. Stacks of five images were taken every 2 min, and videos were rendered at 2 frames/s from centrosome duplication until cells achieved telophase.

RNAi

25 nucleotide stealth siRNA duplexes targeting mRNA sequences of canine Cdc42 and ITSN2 were purchased from Invitrogen. Sequences were submitted to BLAST search to ensure targeting specificity. The specificity

Published May 17, 2010

of Cdc42 and ITSN2 was further checked by Western blot analysis. MDCK cells were trypsinized and then nucleofected (Lonza) with either Cdc42 or ITSN2 siRNA duplexes or scrambled siRNA. After 24-h incubation, cells were resuspended and plated in 12-well plates and in coverglass chambers to grow cysts. Total cell lysates were analyzed by Western blotting as described previously (Martín-Belmonte et al., 2007) to confirm siRNA efficiency.

Calcium switch and microtubule repolymerization assays

Calcium switch was performed by incubating cells overnight in a calcium-free MEM medium (supplemented with dialyzed FCS) and then restoring normal calcium conditions with complete MEM for 120 min. Microtubule depolymerization was performed by incubating cells in 20 µg/ml nocodazole-supplemented MEM for 240 min. Then, nocodazole was washed out by incubating cells in normal MEM for 15–45 min.

Centrosome purification

Centrosomes were purified using fast isolation of centrosomes (Blomberg-Wirschell and Doxsey, 1998). 5×10^8 cells were treated during 180 min with 20 µg/ml nocodazole and 1 µg/ml cytochalasin D. Cells were washed in cold PBS, 8% sucrose, 0.1× PBS, and then 8% sucrose and finally lysed using 0.5% Triton X-100 and 0.1% 2-mercaptoethanol in Tris-HCl buffer, pH 8.0, for 10 min at 4°C. Cell debris and nuclei were removed by fast centrifugation at 1,500 *g* for 5 min at 4°C and 33-µm filters. The lysate was loaded on top of a 1.5-ml 20% Ficoll 400 cushion and centrifuged at 25,000 *g* for 20 min at 4°C. Five 1-ml fractions were collected, and then fractions were diluted 1:4 in Pipes-EDTA buffer and centrifuged at 25,000 *g* for 20 min at 4°C. The sediment was resuspended in Laemmli buffer and loaded. Supernatants and top fractions were loaded as control.

GTPase activation

Cysts were lysed in 500 µl of 4°C 2× gold lysis buffer (2% Triton X-100, 40 mM Tris HCl, pH 7.5, 150 mM NaCl, 20 mM $MgCl_2$, 30% glycerol, 1 mM DTT, and EDTA-free protease inhibitors; Roche) and centrifuged at 15,000 rpm for 5 min. A 50-µl sample from the supernatant was set aside for determination of Cdc42 and tubulin levels in the total lysate, and GTP loading on Cdc42 was determined with GST-Pak3-CRIB pull-down.

ITSN2 pull-down assays

Cysts grown in 100,000 cells/ml on top of Matrigel-coated dishes were lysed in 0.1% SDS, 1% Triton X-100, 0.5 mM DTT, and 1× TBS buffer with protease inhibitor cocktail and NaOV. Cell debris was removed by fast cold centrifugation at 14,000 *g* for 2 min, and cleared lysates were incubated in rotation with protein-GST–loaded beads for 30 min. Beads were centrifuged and washed four times, dried using aspiration, and resuspended in Laemmli buffer.

Online supplemental material

Fig. S1 shows the effect of ITSN2 silencing using stable short hairpin RNA expression. Fig. S2 shows that ITSN2 localization to centrosomes is independent of microtubules. Fig. S3 shows that MTOC orientation is not affected by ITSN2 or Cdc42 silencing. Videos 1, 2, and 3 show spindle dynamics in control MDCK, ITSN2-silenced, and Cdc42-silenced cells, respectively. Online supplemental material is available at http://www.jcb.org/cgi/content/full/jcb.201002047/DC1.

We thank C.M. Ruiz-Jarabo and I. Correas for comments on the manuscript and members of the F. Martín-Belmonte, J. Millán, and M.A. Alonso laboratories for discussion. We also thank I. Macara for the plasmid of vhITSN2, X. Morin for the plasmids of LGN-myc and CH-LGN–myc, S. de la Luna for the plasmid of hITSN2, and K. Kaibuchi for the plasmids of GST-tagged domains of ITSN2.

This work was supported by grants from the Human Frontier Science Program (HFSP-CDA 00011/2009) and Marie Curie (IRG-209382) to F. Martín-Belmonte, National Institutes of Health grants (R01 DK067153 and R01 DK074398) to K. Mostov, and grants from the Ministerio de Ciencia e Innovación to F. Martín-Belmonte (BFU2008-01916) and M.A. Alonso (BFU2006-01925) and to F. Martín-Belmonte and M.A. Alonso (CONSOLIDER CSD2009-00016). An institutional grant from the Fundación Ramón Areces to the Centro de Biología Molecular Severo Ochoa is also acknowledged.

Submitted: 9 February 2010
Accepted: 20 April 2010

Note added in proof. In this issue, Qin et al. (2010. *J. Cell Biol.* doi:10.1083/jcb.201002097) have characterized the role of Tuba, another GEF specific for Cdc42, to be involved in spindle orientation and epithelial cyst formation, suggesting that Cdc42 must be regulated at different levels to control epithelial morphogenesis.

Also, during the editing process, Zheng et al. (2010. *J. Cell Biol.* doi:10.1083/jcb.200910021) characterized the role of LGN in spindle orientation and epithelial cyst formation, which corroborates the results presented in this paper.

References

Blomberg-Wirschell, M., and S.J. Doxsey. 1998. Rapid isolation of centrosomes. *Methods Enzymol.* 298:228–238. doi:10.1016/S0076-6879(98)98022-3

Bryant, D.M., and K.E. Mostov. 2008. From cells to organs: building polarized tissue. *Nat. Rev. Mol. Cell Biol.* 9:887–901. doi:10.1038/nrm2523

Du, Q., and I.G. Macara. 2004. Mammalian Pins is a conformational switch that links NuMA to heterotrimeric G proteins. *Cell*. 119:503–516. doi:10.1016/j.cell.2004.10.028

Du, Q., P.T. Stukenberg, and I.G. Macara. 2001. A mammalian Partner of inscuteable binds NuMA and regulates mitotic spindle organization. *Nat. Cell Biol.* 3:1069–1075. doi:10.1038/ncb1201-1069

Etienne-Manneville, S. 2004. Cdc42—the centre of polarity. *J. Cell Sci.* 117:1291–1300. doi:10.1242/jcs.01115

Georgiou, M., E. Marinari, J. Burden, and B. Baum. 2008. Cdc42, Par6, and aPKC regulate Arp2/3-mediated endocytosis to control local adherens junction stability. *Curr. Biol.* 18:1631–1638. doi:10.1016/j.cub.2008.09.029

Gomes, E.R., S. Jani, and G.G. Gundersen. 2005. Nuclear movement regulated by Cdc42, MRCK, myosin, and actin flow establishes MTOC polarization in migrating cells. *Cell*. 121:451–463. doi:10.1016/j.cell.2005.02.022

Harris, K.P., and U. Tepass. 2008. Cdc42 and Par proteins stabilize dynamic adherens junctions in the *Drosophila* neuroectoderm through regulation of apical endocytosis. *J. Cell Biol.* 183:1129–1143. doi:10.1083/jcb.200807020

Heil-Chapdelaine, R.A., N.R. Adames, and J.A. Cooper. 1999. Formin' the connection between microtubules and the cell cortex. *J. Cell Biol.* 144:809–811. doi:10.1083/jcb.144.5.809

Hung, L.Y., C.J. Tang, and T.K. Tang. 2000. Protein 4.1 R-135 interacts with a novel centrosomal protein (CPAP) which is associated with the gamma-tubulin complex. *Mol. Cell. Biol.* 20:7813–7825. doi:10.1128/MCB.20.20.7813-7825.2000

Hurd, T.W., L. Gao, M.H. Roh, I.G. Macara, and B. Margolis. 2003. Direct interaction of two polarity complexes implicated in epithelial tight junction assembly. *Nat. Cell Biol.* 5:137–142. doi:10.1038/ncb923

Hussain, N.K., S. Jenna, M. Glogauer, C.C. Quinn, S. Wasiak, M. Guipponi, S.E. Antonarakis, B.K. Kay, T.P. Stossel, N. Lamarche-Vane, and P.S. McPherson. 2001. Endocytic protein intersectin-l regulates actin assembly via Cdc42 and N-WASP. *Nat. Cell Biol.* 3:927–932. doi:10.1038/ncb1001-927

Iden, S., and J.G. Collard. 2008. Crosstalk between small GTPases and polarity proteins in cell polarization. *Nat. Rev. Mol. Cell Biol.* 9:846–859. doi:10.1038/nrm2521

Irie, F., and Y. Yamaguchi. 2002. EphB receptors regulate dendritic spine development via intersectin, Cdc42 and N-WASP. *Nat. Neurosci.* 5:1117–1118. doi:10.1038/nn964

Itoh, R.E., K. Kurokawa, Y. Ohba, H. Yoshizaki, N. Mochizuki, and M. Matsuda. 2002. Activation of rac and cdc42 video imaged by fluorescent resonance energy transfer-based single-molecule probes in the membrane of living cells. *Mol. Cell. Biol.* 22:6582–6591. doi:10.1128/MCB.22.18.6582-6591.2002

Jaffe, A.B., and A. Hall. 2005. Rho GTPases: biochemistry and biology. *Annu. Rev. Cell Dev. Biol.* 21:247–269. doi:10.1146/annurev.cellbio.21.020604.150721

Jaffe, A.B., N. Kaji, J. Durgan, and A. Hall. 2008. Cdc42 controls spindle orientation to position the apical surface during epithelial morphogenesis. *J. Cell Biol.* 183:625–633. doi:10.1083/jcb.200807121

Joberty, G., C. Petersen, L. Gao, and I.G. Macara. 2000. The cell-polarity protein Par6 links Par3 and atypical protein kinase C to Cdc42. *Nat. Cell Biol.* 2:531–539. doi:10.1038/35019573

Kroschewski, R., A. Hall, and I. Mellman. 1999. Cdc42 controls secretory and endocytic transport to the basolateral plasma membrane of MDCK cells. *Nat. Cell Biol.* 1:8–13. doi:10.1038/8977

Kunda, P., and B. Baum. 2009. The actin cytoskeleton in spindle assembly and positioning. *Trends Cell Biol.* 19:174–179. doi:10.1016/j.tcb.2009.01.006

Lee, M., and V. Vasioukhin. 2008. Cell polarity and cancer—cell and tissue polarity as a non-canonical tumor suppressor. *J. Cell Sci.* 121:1141–1150. doi:10.1242/jcs.016634

Leibfried, A., R. Fricke, M.J. Morgan, S. Bogdan, and Y. Bellaiche. 2008. *Drosophila* Cip4 and WASp define a branch of the Cdc42-Par6-aPKC pathway regulating E-cadherin endocytosis. *Curr. Biol.* 18:1639–1648. doi:10.1016/j.cub.2008.09.063

Liu, Z., and Y. Zheng. 2009. A requirement for epsin in mitotic membrane and spindle organization. *J. Cell Biol.* 186:473–480. doi:10.1083/jcb.200902071

Lo, C.M., C.R. Keese, and I. Giaever. 1995. Impedance analysis of MDCK cells measured by electric cell-substrate impedance sensing. *Biophys. J.* 69:2800–2807. doi:10.1016/S0006-3495(95)80153-0

Malacombe, M., M. Ceridono, V. Calco, S. Chasserot-Golaz, P.S. McPherson, M.F. Bader, and S. Gasman. 2006. Intersectin-1L nucleotide exchange factor regulates secretory granule exocytosis by activating Cdc42. *EMBO J.* 25:3494–3503. doi:10.1038/sj.emboj.7601247

Martín-Belmonte, F., A. Gassama, A. Datta, W. Yu, U. Rescher, V. Gerke, and K. Mostov. 2007. PTEN-mediated apical segregation of phosphoinositides controls epithelial morphogenesis through Cdc42. *Cell*. 128:383–397. doi:10.1016/j.cell.2006.11.051

Martín-Belmonte, F., W. Yu, A.E. Rodríguez-Fraticelli, A.J. Ewald, A. Ewald, Z. Werb, M.A. Alonso, and K. Mostov. 2008. Cell-polarity dynamics controls the mechanism of lumen formation in epithelial morphogenesis. *Curr. Biol.* 18:507–513. doi:10.1016/j.cub.2008.02.076

McGavin, M.K., K. Badour, L.A. Hardy, T.J. Kubiseski, J. Zhang, and K.A. Siminovitch. 2001. The intersectin 2 adaptor links Wiskott Aldrich Syndrome protein (WASp)-mediated actin polymerization to T cell antigen receptor endocytosis. *J. Exp. Med.* 194:1777–1787. doi:10.1084/jem.194.12.1777

Mitsushima, M., F. Toyoshima, and E. Nishida. 2009. Dual role of Cdc42 in spindle orientation control of adherent cells. *Mol. Cell. Biol.* 29:2816–2827. doi:10.1128/MCB.01713-08

Morin, X., F. Jaouen, and P. Durbec. 2007. Control of planar divisions by the G-protein regulator LGN maintains progenitors in the chick neuroepithelium. *Nat. Neurosci.* 10:1440–1448. doi:10.1038/nn1984

Müsch, A., D. Cohen, G. Kreitzer, and E. Rodriguez-Boulan. 2001. cdc42 regulates the exit of apical and basolateral proteins from the trans-Golgi network. *EMBO J.* 20:2171–2179. doi:10.1093/emboj/20.9.2171

Narumiya, S., and S. Yasuda. 2006. Rho GTPases in animal cell mitosis. *Curr. Opin. Cell Biol.* 18:199–205. doi:10.1016/j.ceb.2006.02.002

O'Brien, L.E., T.S. Jou, A.L. Pollack, Q. Zhang, S.H. Hansen, P. Yurchenco, and K.E. Mostov. 2001. Rac1 orientates epithelial apical polarity through effects on basolateral laminin assembly. *Nat. Cell Biol.* 3:831–838. doi:10.1038/ncb0901-831

Okamoto, M., S. Schoch, and T.C. Südhof. 1999. EHSH1/intersectin, a protein that contains EH and SH3 domains and binds to dynamin and SNAP-25. A protein connection between exocytosis and endocytosis? *J. Biol. Chem.* 274:18446–18454. doi:10.1074/jbc.274.26.18446

Palazzo, A.F., H.L. Joseph, Y.J. Chen, D.L. Dujardin, A.S. Alberts, K.K. Pfister, R.B. Vallee, and G.G. Gundersen. 2001. Cdc42, dynein, and dynactin regulate MTOC reorientation independent of Rho-regulated microtubule stabilization. *Curr. Biol.* 11:1536–1541. doi:10.1016/S0960-9822(01)00475-4

Pucharcos, C., X. Estivill, and S. de la Luna. 2000. Intersectin 2, a new multimodular protein involved in clathrin-mediated endocytosis. *FEBS Lett.* 478:43–51. doi:10.1016/S0014-5793(00)01793-2

Quintyne, N.J., S.R. Gill, D.M. Eckley, C.L. Crego, D.A. Compton, and T.A. Schroer. 1999. Dynactin is required for microtubule anchoring at centrosomes. *J. Cell Biol.* 147:321–334. doi:10.1083/jcb.147.2.321

Rescher, U., and V. Gerke. 2004. Annexins—unique membrane binding proteins with diverse functions. *J. Cell Sci.* 117:2631–2639. doi:10.1242/jcs.01245

Rojas, R., W.G. Ruiz, S.M. Leung, T.S. Jou, and G. Apodaca. 2001. Cdc42-dependent modulation of tight junctions and membrane protein traffic in polarized Madin-Darby canine kidney cells. *Mol. Biol. Cell*. 12:2257–2274.

Royle, S.J., N.A. Bright, and L. Lagnado. 2005. Clathrin is required for the function of the mitotic spindle. *Nature*. 434:1152–1157. doi:10.1038/nature03502

Schlüter, M.A., C.S. Pfarr, J. Pieczynski, E.L. Whiteman, T.W. Hurd, S. Fan, C.J. Liu, and B. Margolis. 2009. Trafficking of Crumbs3 during cytokinesis is crucial for lumen formation. *Mol. Biol. Cell*. 20:4652–4663. doi:10.1091/mbc.E09-02-0137

Schuyler, S.C., and D. Pellman. 2001. Search, capture and signal: games microtubules and centrosomes play. *J. Cell Sci.* 114:247–255.

Siller, K.H., and C.Q. Doe. 2009. Spindle orientation during asymmetric cell division. *Nat. Cell Biol.* 11:365–374. doi:10.1038/ncb0409-365

Vega-Salas, D.E., P.J. Salas, and E. Rodriguez-Boulan. 1987. Modulation of the expression of an apical plasma membrane protein of Madin-Darby canine kidney epithelial cells: cell-cell interactions control the appearance of a novel intracellular storage compartment. *J. Cell Biol.* 104:1249–1259. doi:10.1083/jcb.104.5.1249

Vega-Salas, D.E., P.J. Salas, and E. Rodriguez-Boulan. 1988. Exocytosis of vacuolar apical compartment (VAC): a cell-cell contact controlled mechanism for the establishment of the apical plasma membrane domain in epithelial cells. *J. Cell Biol.* 107:1717–1728. doi:10.1083/jcb.107.5.1717

Wells, C.D., J.P. Fawcett, A. Traweger, Y. Yamanaka, M. Goudreault, K. Elder, S. Kulkarni, G. Gish, C. Virag, C. Lim, et al. 2006. A Rich1/Amot complex regulates the Cdc42 GTPase and apical-polarity proteins in epithelial cells. *Cell*. 125:535–548. doi:10.1016/j.cell.2006.02.045

Wu, H., G. Rossi, and P. Brennwald. 2008. The ghost in the machine: small GTPases as spatial regulators of exocytosis. *Trends Cell Biol.* 18:397–404. doi:10.1016/j.tcb.2008.06.007

Yamabhai, M., N.G. Hoffman, N.L. Hardison, P.S. McPherson, L. Castagnoli, G. Cesareni, and B.K. Kay. 1998. Intersectin, a novel adaptor protein with two Eps15 homology and five Src homology 3 domains. *J. Biol. Chem.* 273:31401–31407. doi:10.1074/jbc.273.47.31401

Yasuda, S., F. Oceguera-Yanez, T. Kato, M. Okamoto, S. Yonemura, Y. Terada, T. Ishizaki, and S. Narumiya. 2004. Cdc42 and mDia3 regulate microtubule attachment to kinetochores. *Nature*. 428:767–771. doi:10.1038/nature02452

Yoshizaki, H., Y. Ohba, K. Kurokawa, R.E. Itoh, T. Nakamura, N. Mochizuki, K. Nagashima, and M. Matsuda. 2003. Activity of Rho-family GTPases during cell division as visualized with FRET-based probes. *J. Cell Biol.* 162:223–232. doi:10.1083/jcb.200212049

Yu, W., L.E. O'Brien, F. Wang, H. Bourne, K.E. Mostov, and M.M. Zegers. 2003. Hepatocyte growth factor switches orientation of polarity and mode of movement during morphogenesis of multicellular epithelial structures. *Mol. Biol. Cell*. 14:748–763. doi:10.1091/mbc.E02-06-0350

Yu, W., A. Datta, P. Leroy, L.E. O'Brien, G. Mak, T.S. Jou, K.S. Matlin, K.E. Mostov, and M.M. Zegers. 2005. Beta1-integrin orients epithelial polarity via Rac1 and laminin. *Mol. Biol. Cell*. 16:433–445. doi:10.1091/mbc.E04-05-0435

Yu, W., A.M. Shewan, P. Brakeman, D.J. Eastburn, A. Datta, D.M. Bryant, Q.W. Fan, W.A. Weiss, M.M. Zegers, and K.E. Mostov. 2008. Involvement of RhoA, ROCK I and myosin II in inverted orientation of epithelial polarity. *EMBO Rep.* 9:923–929. doi:10.1038/embor.2008.135

Rodriguez-Fraticelli et al., http://www.jcb.org/cgi/content/full/jcb.201002047/DC1

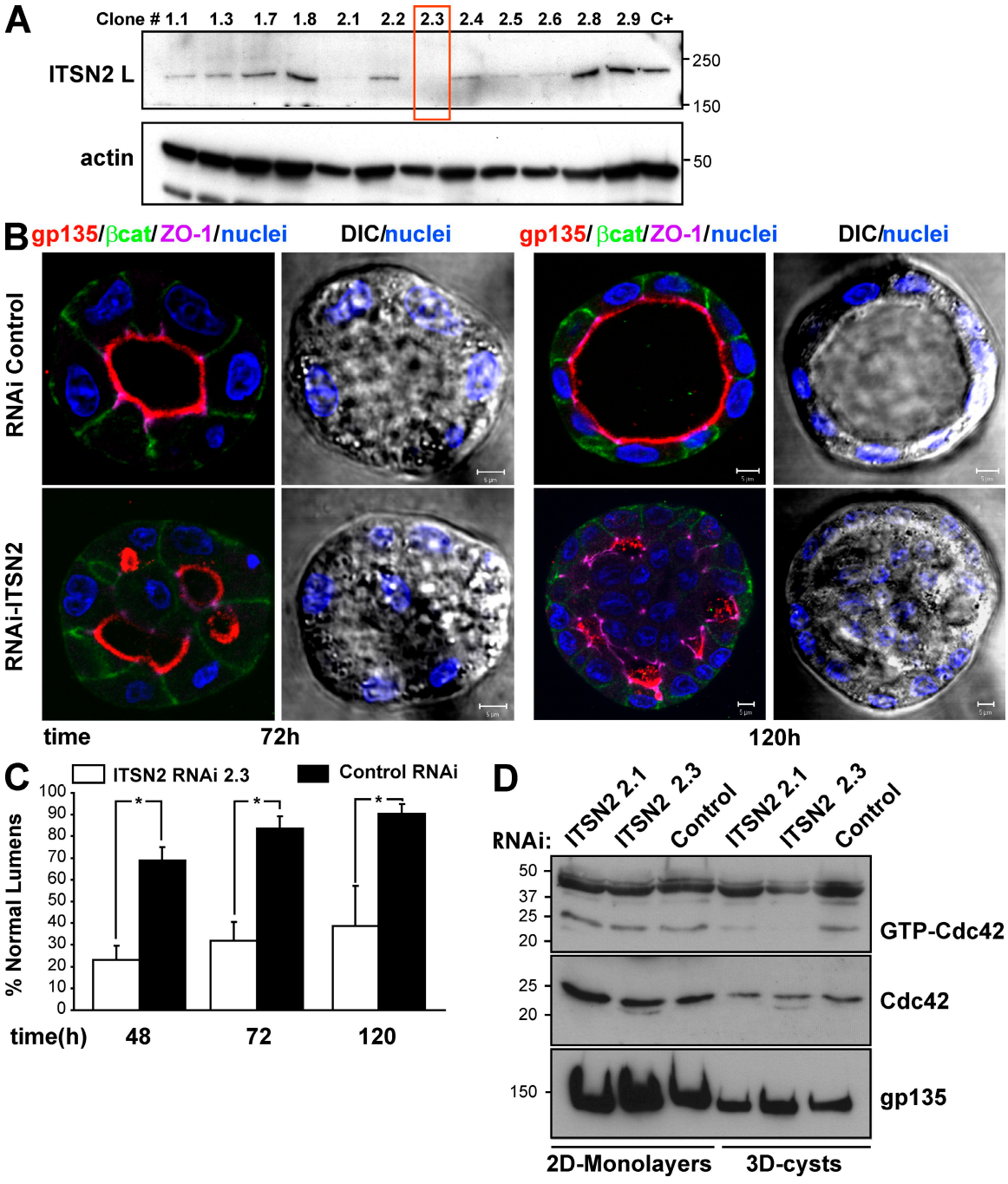

Figure S1. **Effect of ITSN2 silencing using stable short hairpin RNA expression.** (A) Western blot of ITSN2 short hairpin RNA clones. MDCK cells were transfected with pSUPER-ITSN2 short hairpin RNA, and clones were selected and expanded with G418. Cells were grown forming cysts for 48 h, and total cell lysates were immunoblotted to detect ITSN2 and actin. The boxed area indicates the ITSN2 KD clone of MDCK cells selected to analyze cyst formation. (B) Effect of stable ITSN2 silencing in cyst formation. Mock short hairpin RNA–expressing MDCK cells (top) and 2.3 ITSN2 short hairpin RNA MDCK (bottom) cells were plated to form cysts for 72 and 120 h and stained for detecting gp135, β-catenin (βcat), ZO-1, and nuclei. (C) Quantification of cyst formation in short hairpin RNA ITSN2 cells. Control MDCK cells and short hairpin RNA ITSN2 cells from clone 2.3 were plated to form cysts for 48, 72, and 120 h, and normal lumens were quantified using gp135 as an apical marker. Values shown are mean ± SD of three different experiments (for each experiment, $n = 100$; *, $P < 0.05$). (D) Effect of stable ITSN2 silencing in Cdc42-GTP levels. Selected ITSN2 short hairpin RNA clones were seeded to form 2D monolayers (left lanes) or cysts (right lanes) for 48 h. Total cell lysates were incubated with GST-Pak3-CRIB–preloaded beads, and bound Cdc42 was detected by immunoblotting (top). As a control, total cell lysates were loaded to detect total levels of Cdc42 (middle) and gp135 (bottom). (A and D) Molecular mass is indicated in kilodaltons. Bars, 5 µm.

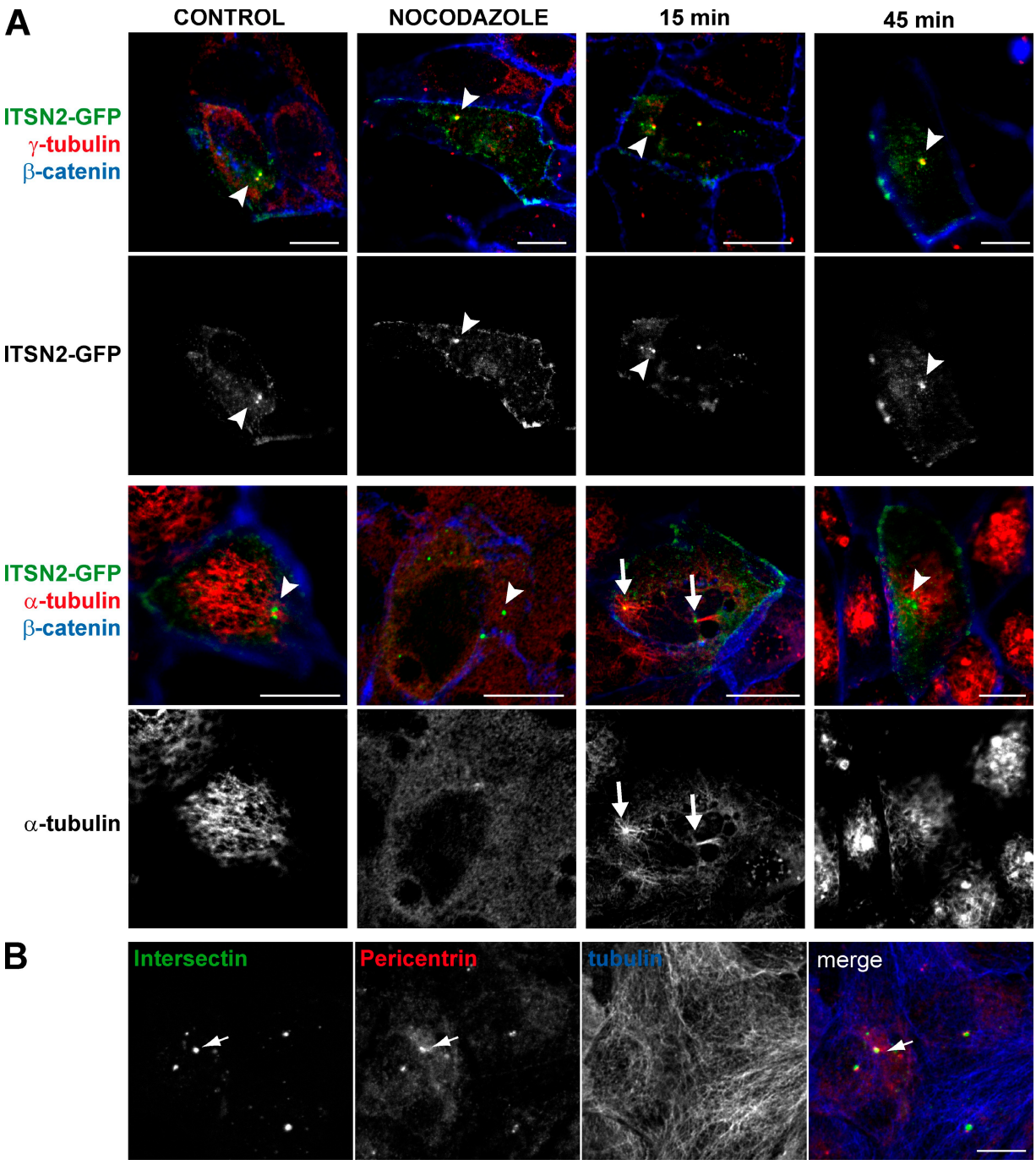

Figure S2. **ITSN2 localization to centrosomes is independent of microtubules.** (A) ITSN2 colocalization with γ-tubulin is independent of microtubules. Cells were transfected with ITSN2-GFP and plated for 24 h to form confluent monolayers. Cells were treated with 20 μg/ml nocodazole for 4 h, and then nocodazole was washed out by incubating cells with complete medium for up to 45 min. Cells were then stained for γ-tubulin and β-catenin (top) or α-tubulin and β-catenin (bottom). Arrows indicate the localization of MTOC. Arrowheads indicate the localization of ITSN2. (B) vhITSN2 localizes to centrosomes in MDCK cells forming monolayers. Cells expressing vhITSN2 (green; first panel) were stained with pericentrin (centrosomal marker; second panel) and tubulin (third panel). The right panel shows the merge image with the colocalization of vhITSN2 with centrosomal proteins. Arrows indicate the localization of ITSN2 and centrosomes (pericentrin). Bars, 5 μm.

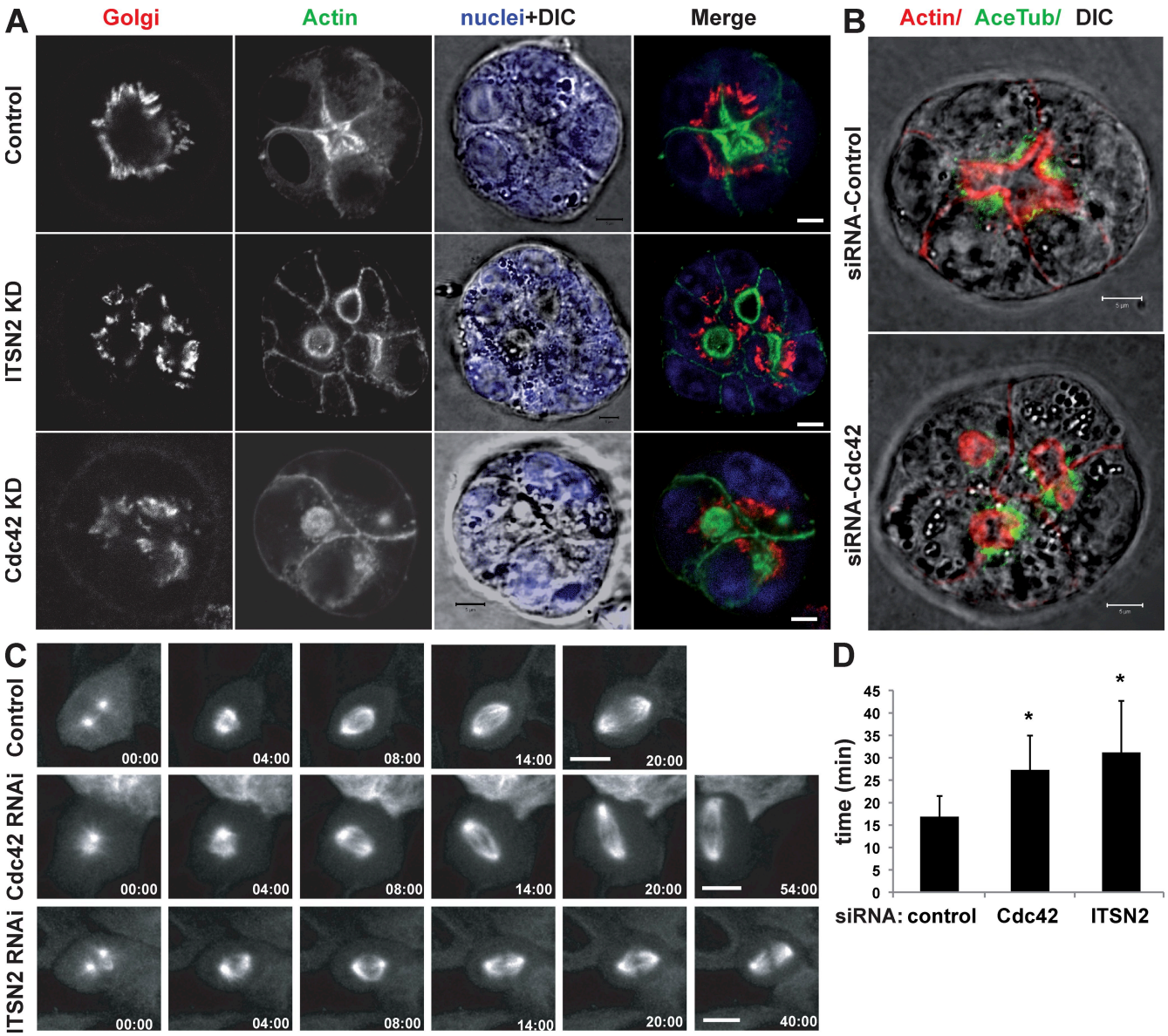

Figure S3. **MTOC orientation is not affected by ITSN2 or Cdc42 silencing.** (A) Golgi is normally oriented in Cdc42- or ITSN2-silenced cells. MDCK cells were transfected with control siRNA (top), ITSN2 siRNA pool (middle), or Cdc42 siRNA (bottom) and were seeded to form cysts for 48 h. Cells were stained to detect Golgi protein GM130 (red), actin, and nuclei (blue merged with DIC). (B) Acetylated tubulin is normally distributed in cysts. MDCK cells were transfected with control (top) or Cdc42 siRNA (bottom) and grown to form cysts for 48 h and then stained for detecting actin and acetylated tubulin (Ace Tub). (C) Spindle orientation defects in Cdc42- and ITSN2-silenced cells. MDCK cells stably expressing β-tubulin–GFP were transfected with control (top), Cdc42 (middle), or ITSN2 siRNA (bottom) and plated to form monolayers. Live cells were analyzed by 3D video confocal microscopy from early metaphase until anaphase at 0.5 frames/min. (D) Quantification of MT in control or cells knocked down for Cdc42 or knocked down for ITSN2. Time in metaphase transition was measured from centrosome duplication to anaphase. Values shown are mean ± SD of three different experiments (*, $P < 0.02$). Bars, 5 μm.

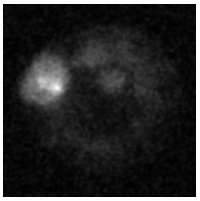

Video 1. **Spindle dynamics in control MDCK cells.** MDCK cells stably expressing tubulin-GFP (white) were transfected with control siRNA and plated to form cysts (Fig. 4) or a subconfluent monolayer (Fig. S3). Images were analyzed by time-lapse confocal microscopy using an LSM 510 laser-scanning confocal microscope. Frames were taken every 2 min until cells entered anaphase. The video is shown at 4 frames/s.

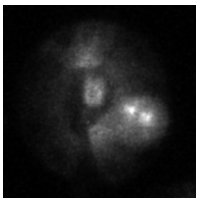

Video 2. **Spindle dynamics in ITSN2 RNAi cells.** MDCK cells stably expressing tubulin-GFP (white) were transfected with Cdc42 siRNA and plated to form cysts (Fig. 4) or a subconfluent monolayer (Fig. S3). Images were analyzed by time-lapse confocal microscopy using an LSM 510 laser-scanning confocal microscope. Frames were taken every 2 min until cells entered anaphase. The video is shown at 4 frames/s.

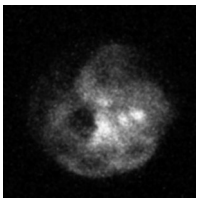

Video 3. **Spindle dynamics in Cdc42 RNAi cells.** MDCK cells stably expressing tubulin-GFP (white) were transfected with ITSN2 siRNA pool and plated to form cysts (Fig. 4) or a subconfluent monolayer (Fig. S3). Images were analyzed by time-lapse confocal microscopy using an LSM 510 laser-scanning confocal microscope. Frames were taken every 2 min until cells entered anaphase. The video is shown at 4 frames/s.

SYNAPTOTAGMIN-LIKE PROTEINS CONTROL THE FORMATION OF A SINGLE APICAL MEMBRANE DOMAIN IN EPITHELIAL CELLS

Manuel Gálvez-Santisteban, **Alejo E. Rodriguez-Fraticelli***, David M. Bryant, Silvia Vergarajauregui, Takao Yasuda, Inmaculada Bañón-Rodríguez, Ilenia Bernascone, Anirban Datta, Natalie Spivak, Kitty Young, Christian L. Slim, Paul Brakeman, Mitsunori Fukuda, Keith E. Mostov, Fernando Martín-Belmonte.*

Publicado en agosto de 2012 en Nature Cell Biology *14,* págs. 838-49.

*contribución equivalente

PRESENTACION

La formación de órganos epiteliales depende de la coordinación de la polaridad apicobasal de todas las células del tejido, para conseguir formar un único lumen central. Durante la formación de un lumen, cada célula provee los componentes de una única membrana apical. Este transporte de proteinas apicales está regulado por la presencia asimétrica de dos fosfoinosítidos, *PtdIns(4,5)p2* y *PtdIns(3,4,5)p3*, enriquecidos en la membrana apical y basolateral respectivamente. Se sabe que esta polaridad en los fosfoinosítidos es necesaria para la activación de Cdc42/Par6/aPKC y la formación de un único lumen. Sin embargo, no se sabe cual es el mecanismo molecular por el que los fosfoinosítidos controlan el tráfico apical.

Para descubrir mecanismos que pudieran regular la formación de la membrana apical, estudiamos la expresión diferencial de genes en células MDCK cultivadas en 2D y en 3D a tiempos tempranos (36h), mediante el uso de microarrays y RT-PCR cuantitativa. Encontramos un grupo de 1597 genes inducidos más de 2 veces en 3D, de los cuales elegimos 100 candidatos con funciones relacionadas con mecanismos involucrados previamente en la formación de la membrana apical: regulación/interacción con GTPasas, regulación de SNAREs, regulación del exocisto, regulación de fosfoinosítidos, regulación de la ciliogénesis, y regulación del citoesqueleto.

Conseguimos validar el patrón de expresión de 47 de estos genes por RT-PCR, y diseñamos experimentos de interferencia de expresión con siRNA para estudiar el requerimiento de estos genes en el proceso de la formación del lumen. Entre estos 47 genes, encontramos 14 reguladores nuevos del proceso de formación del lumen (FRZB, NHERF1, ARHGAP24, PI3KR1, CHE11, SMTNL2, STARD10, SYTL2, FUZ, TB2/DP1, CADH16, SNX5, IFT172), y 2 que habían sido previamente descritos

(Claudin-2 y Rho-U/Wrch-1). De entre los 14 nuevos reguladores, el producto del gen SYTL2 (Synaptotagmin-like 2), Slp2-a, era el mejor candidato para regular el tráfico apical: era un efector de Rabs (Rab27), su localización estaba regulada por *PtdIns(4,5)p2* y controlaba el citoesqueleto de actina. Además, su homólogo en *Drosophila melanogaster, btsz* (bitesize), había sido descrito como regulador de la morfogénesis epitelial previamente. Por estos motivos, nos decidimos a estudiar el papel de las proteínas synaptotagmin-like (Slp) en la formación del lumen.

Encontramos que, mientras que Slp2-a se inducía durante los pasos iniciales de la morfogénesis, otro gen de la misma familia, Slp4, se inducía a tiempos más tardíos. Aún siendo ambos necesarios para la formación del lumen, presentaban mecanismos diferentes. Slp2-a se regula principalmente por *PtdIns(4,5)p2*, aunque requiere de la unión a Rab27 en vesículas apicales para su función en la formación de un único lumen central. Mientras tanto, Slp4 no se regula por fosfoinosítidos, y principalmente depende de la unión a Rab27 y a la tSNARE-apical, Syntaxin-3 para su localización y función.

Mediante estudios de siRNA y rescate de fenotipo empleando mutantes de cada Slp para cada una de sus interacciones, describimos el mecanismo que mejor explica el papel de las Slp durante la formación del lumen. Slp2-a dirige las vesículas Rab27+, cargadas con marcadores apicales, hacia parches de membrana enriquecidos en *PtdIns(4,5)p2*. Este direccionamiento de vesículas Rab27+, arrastra a Slp4, cuya localización depende de su anclaje a Rab27 y a la t-SNARE apical Syntaxin-3. La sobreexpresión de Slps retrasa el desarrollo del lumen, sugiriendo que su mecanismo molecular es el de un regulador negativo de la secreción apical, probablemente a través de la inhibición de Syntaxin-3. Este mecanismo, por deletéreo que pudiera parecer, es necesario para controlar que se forme una única membrana apical por célula.

nature cell biology

Synaptotagmin-like proteins control the formation of a single apical membrane domain in epithelial cells

Manuel Gálvez-Santisteban[1,6], Alejo E. Rodriguez-Fraticelli[1,6], David M. Bryant[2], Silvia Vergarajauregui[1,7], Takao Yasuda[3], Inmaculada Bañón-Rodríguez[1], Ilenia Bernascone[1], Anirban Datta[2], Natalie Spivak[2,4], Kitty Young[2], Christiaan L. Slim[2,7], Paul R. Brakeman[2,4], Mitsunori Fukuda[3], Keith E. Mostov[2,5] and Fernando Martín-Belmonte[1,8]

The formation of epithelial tissues requires both the generation of apical–basal polarity and the coordination of this polarity between neighbouring cells to form a central lumen. During *de novo* lumen formation, vectorial membrane transport contributes to the formation of a singular apical membrane, resulting in the contribution of each cell to only a single lumen. Here, from a functional screen for genes required for three-dimensional epithelial architecture, we identify key roles for synaptotagmin-like proteins 2-a and 4-a (Slp2-a/4-a) in the generation of a single apical surface per cell. Slp2-a localizes to the luminal membrane in a PtdIns(4,5)P_2-dependent manner, where it targets Rab27-loaded vesicles to initiate a single lumen. Vesicle tethering and fusion is controlled by Slp4-a, in conjunction with Rab27/Rab3/Rab8 and the SNARE syntaxin-3. Together, Slp2-a/4-a coordinate the spatiotemporal organization of vectorial apical transport to ensure that only a single apical surface, and thus the formation of a single lumen, occurs per cell.

Epithelia represent the most fundamental tissue in metazoa, forming complex layers of cells such as the skin or kidney tubules. The epithelial plasma membrane is divided into two domains: apical and basolateral, separated by cellular junctions, dependent on the asymmetric delivery and segregation of membrane proteins and lipids[1,2]. Such plasma membrane asymmetry allows the formation of a central lumen, and hence the evolution of specialized functions for different metazoan tissues[3]. Epithelial cells create lumens through an array of morphogenetic mechanisms. Despite this diversity, a series of common molecular events creates biological tubes: vectorial transport to a nascent apical domain, *de novo* apical plasma membrane biogenesis, and secretion and expansion of the luminal space[4,5]. Transport of apical proteins to the initial site for apical-membrane formation, at which the Par3–aPKC–Cdc42 polarity complex is established, is controlled by a Rab11a/8a GTPase cascade and its effectors, the exocyst and Myo5B (refs 6,7). At the lumen, phosphoinositide asymmetry is concomitantly established with PtdIns(4,5)P_2 and PtdIns(3,4,5)P_3 localizing to, and specifying, the apical and basolateral domains, respectively[8,9]. How vectorial exocytic transport is coordinated and directed so that each cell has a single apical initiation site, and thus the tube has a single lumen, however, is largely unclear. Similarly, how such machineries are controlled at the transcriptional level during morphogenesis of epithelial tissues is poorly understood[3].

Here, we report a functional screen for regulators of three-dimensional (3D) epithelial polarity using MDCK cyst cultures, based on transcriptional, RNA-mediated interference (RNAi) and morphogenetic analysis.

Synaptotagmin-like proteins (Slps) 1-5 are a family of Rab effectors involved in regulated exocytosis[10]. Slps harbour an amino-terminal Rab-binding domain (also called the Slp homology domain SHD) and tandem carboxy-terminal C2 domains involved in Ca^{2+} and phospholipid binding, and function in tethering secretory vesicles to the plasma membrane[11]. In *Drosophila melanogaster*, a single divergent Slp paralogue, bitesize (Btsz), functions in epithelial polarization[12], although whether mammalian Slps function in polarity generation is unknown.

We demonstrate that Slp2-a and related family member Slp4-a function in distinct, but complementary, steps of apical transport

[1]Centro de Biología Molecular Severo Ochoa, Consejo Superior de Investigaciones Científicas (CSIC), C/Nicolás Cabrera 1, Madrid 28049, Spain. [2]Department of Anatomy, University of California San Francisco, California 94143-2140, USA. [3]Department of Developmental Biology and Neurosciences, Graduate School of Life Sciences, Tohoku University, Aobayama, Aoba-ku, Sendai, Miyagi 980-8578, Japan. [4]Department of Pediatrics, University of California San Francisco, California 94143-2140, USA. [5]Department of Biochemistry and Biophysics, University of California San Francisco, California 94143-2140, USA. [6]These authors contributed equally to this work. [7]Present addresses: National Heart, Lung and Blood Institute (NHLBI), National Institutes of Health (NIH) Bethesda, Maryland 20824-0105, USA (S.V.); Department of Cell Biology, University Medical Center Groningen, Antonius Deusinglaan 1, Groningen 9713 AV, Holland (C.L.S.). [8]Correspondence should be addressed to F.M-B. (e-mail: fmartin@cbm.uam.es)

Received 21 September 2011; accepted 14 June 2012; published online 22 July 2012; DOI: 10.1038/ncb2541

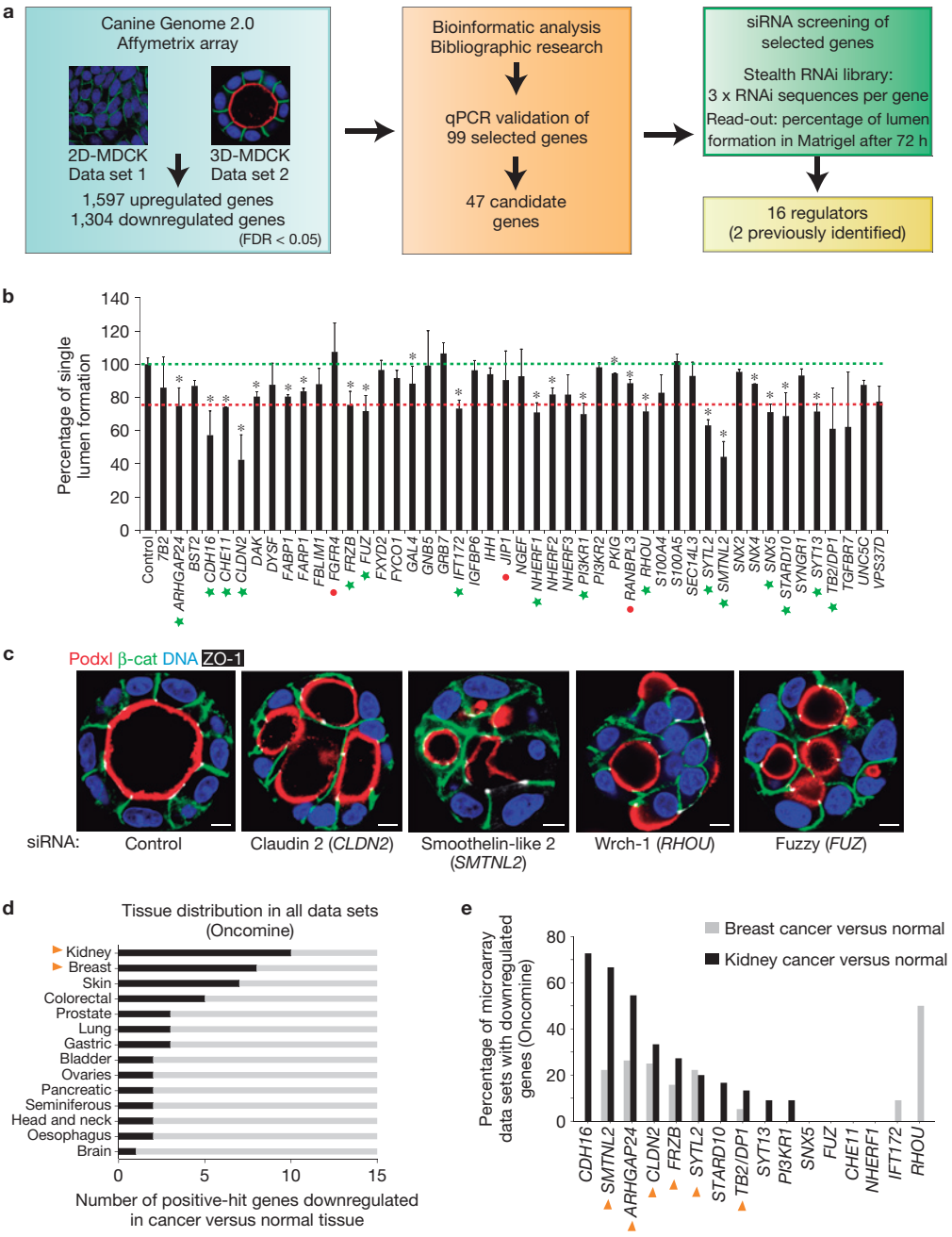

Figure 1 A screen for regulators of 3D epithelial polarization. (**a**) Experimental design for the function screen of regulators of 3D epithelial polarity. MDCK cells were cultured for 36 h in 2D or 3D ($n = 3$), and control (2D) and experimental (3D) RNA samples were analysed using the Affymetrix Canine Genome 2.0 platform. The significance of the data was determined by LiMMA analysis (false discovery rate (FDR) < 0.05). A set of significantly upregulated (>2-fold) genes was pooled with other genes of interest and then gene overexpression was validated by RT–qPCR. Bioinformatic pathway analyses revealed that some genes were connected in common functional pathways. A final set of 47 candidates was selected for stealth siRNA design. MDCK cells were transfected with siRNAs individually or in pools and cultured to grow cysts. The silencing efficiency of the siRNA was determined by RT–qPCR. Then, cells were fixed and stained for Podxl, β-catenin and nuclei to quantify normal lumen formation. The RNAi screening finally resulted in 16 positive hits (see Methods). (**b**) RNAi screening for polarization regulation. Lumen formation efficiency was quantified for each of the listed 47 siRNA treatments. Green dotted line, normal levels as found in control; red dotted line, the threshold considered for the definition of a positive hit (lumen formation $< 75\%$ of control; $P < 0.05$); green stars, positive hits; red dots, knockdowns where the efficiency was below 60%. $^*P < 0.05$; $n = 3$; error bars represent s.d. (**c**) Examples of phenotypes induced by RNAi in the screen. Seventy-two hour MDCK cysts transfected with siRNA from four positive candidates (*SMTNL2*, *CLDN2*, *RHOU* and *FUZ*) and stained for the apical marker Podxl (red), the basolateral marker β-catenin (β-cat; green), the tight junction marker ZO-1 (white) and nuclei (blue). Scale bars, 5 μm. (**d**) Epithelial cancers with a downregulated 3D polarity gene set. The expression levels of the candidate gene set in all cancer versus normal expression data sets were analysed using Oncomine (www.oncomine.org). The graph shows the number of downregulated genes per type of indicated epithelial cancers ($P < 0.05$, n varies in each tissue). (**e**) Frequency of gene downregulation in breast and kidney cancer data sets. The graph indicates the percentage of data sets with downregulated candidate genes in breast and kidney cancer versus normal tissue microarray data sets (Oncomine, $P < 0.05$). The yellow arrowheads denote genes downregulated in both breast and kidney cancer.

Table 1 Localization and function of synaptotagmin-like proteins, and their mutants, in MDCK cyst formation.

Protein	Construct	Cell localization			Mutant effect	Phenotype rescue
		Early aggregate	Lumen initiation	Open lumen		
Slp2-a	Full length	Unpolarized PM	Junctions PM	Apical PM		Yes
	SHD	Vesicle/cytosolic	Vesicle/cytosolic	Vesicle/cytosolic		-
	ΔC2AB	Vesicle/endosome	Vesicle/endosome	Subapical		-
	Linker	Cytosol	Cytosol	Cytosol		-
	ΔSHD	Unpolarized PM	Junctions PM	Apical PM		No
	C2AB	Unpolarized PM	Junctions PM	Apical PM		-
	mut E11A/R32A	Unpolarized PM	Junctions PM	Apical PM	No Rab binding	No
	mut V18A	Unpolarized PM	Junctions PM	Apical PM	No Rab3/8 binding	Yes
Slp4-a	Full-length	Apical PM	Vesicles	Apical PM		Yes
	SHD	nuc/cytosol	nuc/cytosol	nuc/cytosol		-
	ΔC2AB	Cytosol	Cytosol	Cytosol		-
	Linker	Cytosol	Cytosol	Cytosol		-
	ΔSHD	Unpolarized PM	Unpolarized PM	Unpolarized PM		-
	C2AB	Unpolarized PM	Unpolarized PM	Unpolarized PM		-
	mut I18A	Unpolarized PM	Vesicles/junctions PM	Subapical/junctions PM	No Rab3/8 binding	No
	mut V21A	Vesicles	Vesicles	Subapical	No Rab3 binding	No
	mut W118S	Cytosol	Cytosol	Cytosol	No Rab binding	No
	mut K > Q	Vesicles	Vesicles	Subapical	No lipid binding	Partial
	Slp454a	Unpolarized PM	Vesicles/PM	Subapical/junctions PM	No SNARE binding	No
	Δ305–354	Unpolarized PM	Vesicles/PM	Junctions PM	No SNARE binding	No

This table represents a qualitative summary of results regarding WT or mutant Slp protein localization (at different time points) and its ability to rescue the silencing of endogenous protein expression. PM, plasma membrane; nuc, nucleus; mut, mutant.

to form a lumen *de novo*. Slp2-a controls the positioning of Slp4-a/Rab27-positive vesicles to target exocytosis to a single PtdIns(4,5)P_2-enriched lumen. Slp4-a regulates the tethering of these vesicles, through the association with the apical SNARE syntaxin-3 (Stx3), to mediate vesicle delivery to the lumen. Thus, through a functional, multi-step screen, we have identified a previously uncharacterized mechanism for coordinated vectorial transport, crucial to form a single apical domain.

RESULTS

Identification of 14 previously uncharacterized regulators of epithelial morphogenesis

We performed a multi-step, functional screen for regulators specifically of 3D epithelial architecture and morphogenesis. We first conducted a microarray-based differential expression analysis comparing the transcriptome of MDCK cells undergoing apical–basolateral polarization either in the traditional monolayer culture (2D), or as 3D cysts grown in basement membrane extract (3D), wherein MDCK cells self-assemble to form a 3D monolayer (Fig. 1a). Notable transcriptional differences were observed during 3D morphogenesis with 1,597 upregulated, and 1,304 downregulated probes detected (Supplementary Fig. S1). To prioritize functional analyses, upregulated genes were subjected to bioinformatic analysis to reconstruct potential molecular pathways and known components of epithelial polarization. Using this approach, a set of 99 upregulated genes was selected for secondary validation by quantitative PCR (qPCR; Supplementary Fig. S2 and Table S1). Finally, 47 candidate genes were targeted through short interfering RNA (siRNA), including the known polarity regulators claudin-2 (*CLDN2*) and Wrch-1 (*RHOU*) as internal controls[13,14](Fig. 1b and Supplementary Table S2). We found a set of 14 genes previously uncharacterized to be required for this process (Fig. 1b,c, green stars and Supplementary Table S3). These included tight and adherens junctions, Rho GTPases, lipid signalling and membrane trafficking proteins.

To analyse a possible relevance of these genes *in vivo*, we analysed whether this gene set was downregulated in human cancers, suggesting an importance in the maintenance of a differentiated epithelial phenotype *in vivo* (Fig. 1d). Notably, renal, breast and skin cancers presented with the strongest downregulation of this gene set. We selected one of these genes, *SYTL2* (encoding the protein Slp2-a), which was significantly downregulated in several epithelial cancer data sets (Fig. 1e), to characterize its role in lumen formation.

Slp2-a associates with, and regulates the formation of, the luminal membrane

The mammalian Slp family has been shown to regulate primarily Rab27-dependent membrane trafficking and secretion[15–17], but the function of these proteins in mammalian epithelial morphogenesis is unknown. We confirmed that Slp2-a protein levels were upregulated in 3D when compared with 2D cultures by western blot (14-fold enrichment at 72 h; Fig. 2a), validating the qPCR data (Supplementary Fig. S2). Next, we characterized Slp2-a localization in MDCK cysts. On plating MDCK into 3D, the apical podocalyxin (Podxl) localized to the peripheral surface of early aggregates, before it is internalized into vesicles and delivered to the contact between two cells, where lumen is formed *de novo*[7,9,18]. In early aggregates, Slp2-a localized to the plasma membrane, enriched at cellular junctions (Fig. 2b and Table 1). A pool of Slp2-a became apparent on internalized Podxl-positive transcytosing vesicles near the cell–cell contact (Fig. 2b, 16–20 h). On lumen formation (24–48 h), Slp2-a localized to the apical membrane (Fig. 2b, 48 h).

Slp2-a depletion perturbed 3D lumen formation in a dose-dependent manner (Fig. 2c,e), without affecting the cell polarity in cells growing in monolayers (Supplementary Fig. S3A). Slp2-a depletion results in abnormal morphology with multiple small lumens, and the accumulation of Podxl (Fig. 2d), that we identify as transcytotic vesicles (Supplementary Fig. S5C). Notably, stable expression of RNAi-resistant human Slp2-a (GFP–Slp2-a; Fig. 2f) completely

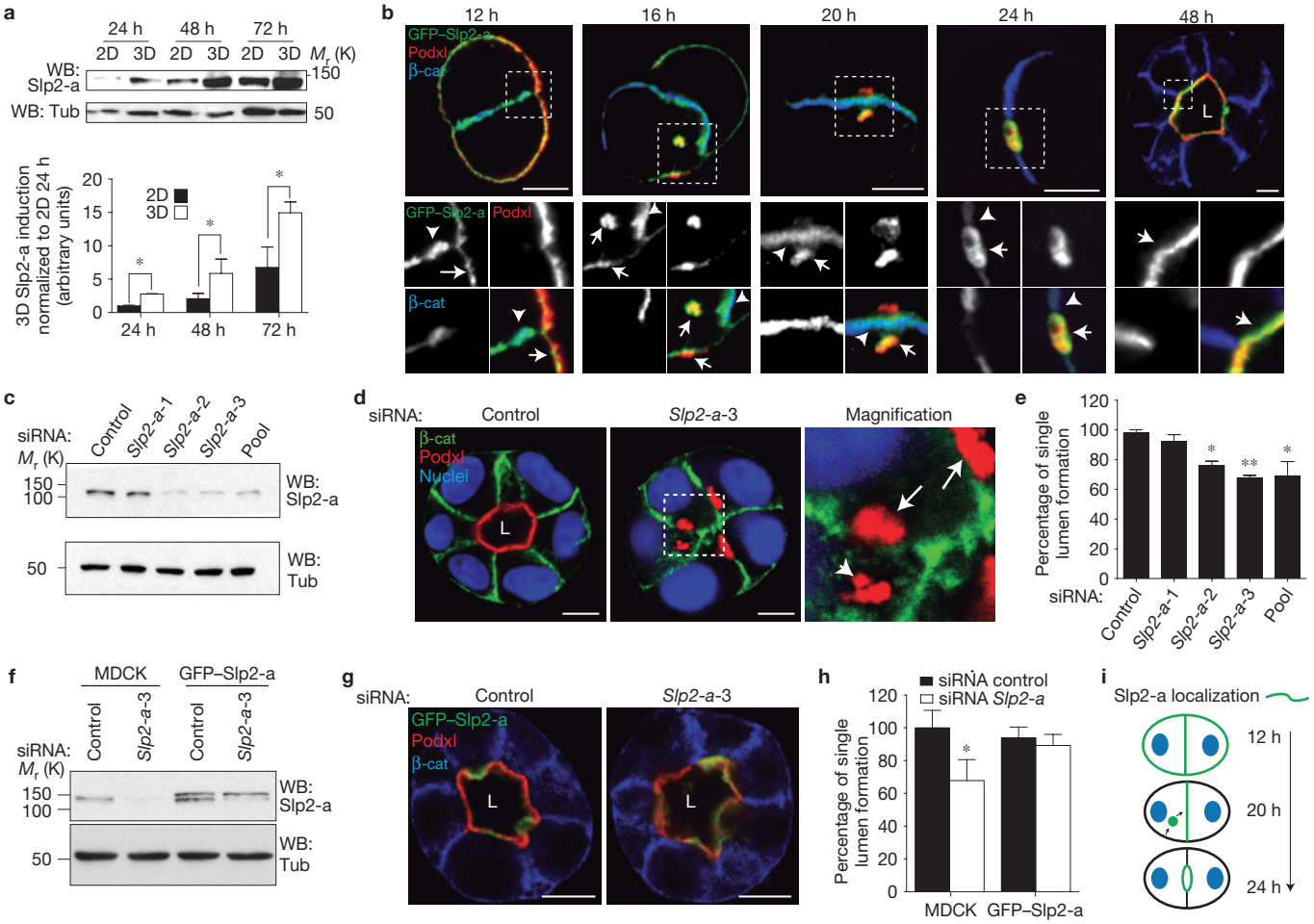

Figure 2 Slp2-a is required for epithelial morphogenesis. (**a**) Top, western blot (WB) showing the induction of Slp2-a in MDCK cells growing in 2D and 3D at different time points (24–72 h). Bottom, expression quantified by densitometry ($n = 4$). (**b**) Localization of GFP–Slp2-a during lumen formation. MDCK cells stably expressing GFP–Slp2-a were grown in 3D and fixed at different time points. Cysts were stained with Podxl (red) and β-catenin (β-cat; blue). The arrows indicate localization to apical plasma membrane; the arrowheads indicate localization to cell–cell junctions; scale bar, 5 μm. (**c**) Downregulation of *Slp2-a* by siRNA. MDCK cells were transfected with three different siRNA duplexes targeting canine *Slp2-a*, and siRNA efficiency was analysed by western blotting. (**d**) Effect of *Slp2-a* siRNA-mediated silencing on lumen formation. Cells were transfected with a pool of siRNA to knockdown *Slp2-a* or siRNA control and plated to form cysts for 72 h. Markers are Podxl (red), β-catenin (green) and nuclei (blue). The arrows indicate apical membrane localization; the arrowheads indicate localization to intracellular apical vesicles. Scale bars, 5 μm. (**e**) Quantification of cysts with normal lumens in cells transfected with control siRNA or *Slp2-a* siRNA. Values are mean ± s.d. ($n = 5$; ≥100 cysts per experiments). (**f**) Knockdown of *Slp2-a* by siRNA in cells stably expressing GFP–Slp2-a. MDCK cells stably expressing GFP–Slp2-a were transfected with *Slp2-a* or control siRNAs. Total lysates were blotted for Slp2-a using α-tubulin as a loading control. (**g**) Rescue effect of GFP–Slp2-a in cells silenced for *Slp2-a* on lumen formation. Cells were stained for Podxl (red) and β-catenin (blue). Scale bars, 10 μm. (**h**) Quantification of cysts with normal lumens in cells expressing GFP–Slp2-a and transfected with control or *Slp2-a* siRNAs, $n = 3$. (**i**) Slp2-a localization during lumen initiation. In early aggregates (12 h), Slp2-a localizes to cell–cell junctions at sites of apical vesicle fusion. After the lumen is initiated (24 h), Slp2-a remains polarized at the apical membrane. Green lines, Slp2-a; blue ovals, nuclei; black lines, basolateral membrane. In all panels error bars represent s.d.; $^{*}P < 0.05$; $^{**}P < 0.005$; L, lumen; areas outlined in micrographs are magnified in the associated images. Uncropped images of blots are shown in Supplementary Fig. S8.

rescued lumen formation and morphogenesis of cysts with endogenous *Slp2-a* knockdown (Fig. 2g,h). Moreover, these results indicate that Slp2-a is the predominant variant required for epithelial morphogenesis in 3D-MDCK (ref. 19).

The SHD and C2 domains play non-redundant roles in targeting Slp2-a to membranes

Slp-family proteins share an N-terminal Rab27-binding domain (the SHD), a linker region and two c-terminal tandem C2 domains (phospholipid and/or protein interaction sites)[20,21]. Slp2-a could potentially therefore connect Rab GTPases and phosphoinositides during lumen formation[7–9]. To elucidate the control of Slp2-a localization, we analysed Slp2-a domains during cyst formation. In early aggregates, the C2 domains localized to the plasma membrane and to cell–cell junctions, but not to Podxl vesicles (Fig. 3a and Supplementary Fig. S4b, 12–20 h). Once lumens formed, the C2A/B fragment localized exclusively to the apical membrane (Fig. 3a and Supplementary Fig. S4b, 24–48 h). In contrast, the SHD fragment was predominantly cytoplasmic, and partially localized to Podxl vesicles in early aggregates and subapically in mature cysts (Fig. 3a, bottom panels). Deletion of the C2 domains (GFP–Slp2-a$^{\Delta C2A/B}$) resulted in a similar localization to the SHD, whereas the linker region

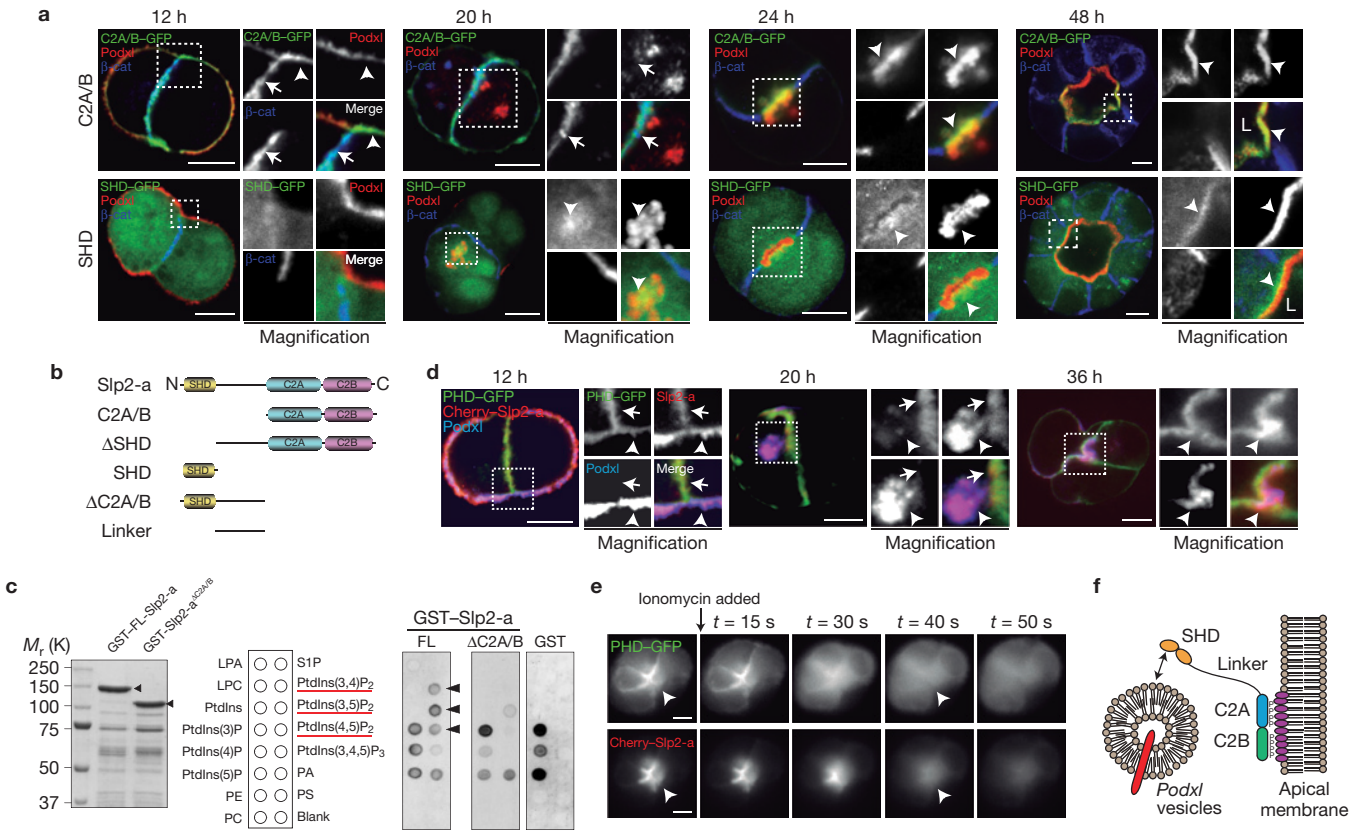

Figure 3 Slp2-a requires SHD and C2A/B domains for correct localization. (**a**) Localization of GFP–Slp2-a C2A/B, and SHD during lumen morphogenesis. MDCK cells stably expressing different GFP–Slp2-a constructs were grown in 3D to form cysts. Cysts were fixed at different time points (12, 20, 24 and 48 h) and co-stained to detect Podxl (red) and β-catenin (β-cat; blue). The arrowheads indicate apical membrane; the arrows indicate localization to cell–cell junctions. Scale bars, 5 μm. (**b**) Scheme of the Slp2-a constructs used. Different domains and truncated forms of Slp2-a were cloned for characterizing Slp2-a function. (**c**) PIP-binding ability of Slp2-a. GST-tagged full-length Slp2-a (GST–FL-Slp2-a) and ΔC2A/B (GST–Slp2-a$^{\Delta C2A/B}$), which should be unable to bind phospholipids, were expressed and purified in bacteria. PIP-strip membranes were incubated with 1 μg ml^{-1} of GST (control), GST–FL-Slp2-a or GST–Slp2-a$^{\Delta C2A/B}$ and then membranes were blotted with anti-GST. A scheme of the PIP-strip membrane is shown. The arrowheads indicate specific PIP_2 binding. The red lines highlight the PIP_2 species. LPA, lysophosphatidic acid. LPC, lysophosphatydilcholine. PI, phosphatidylinositol. PE, phosphatidylethanolamine. PC, phosphatidylcholine, S1P, sphingosine-1-phosphate. PA, phosphatidic acid. PS, phosphatidylserine. (**d**) Co-localization of Cherry–Slp2-a and PtdIns(4,5)P_2 during early cyst formation. MDCK cells stably expressing Cherry–Slp2-a were transfected with the PtdIns(4,5)P_2 probe (PHD–GFP) and grown in cysts. Cysts were fixed at different time points (12, 20, 36 h) and co-stained to detect Podxl (blue). The arrowheads indicate apical membranes; the arrows indicate cell–cell junction membrane localization. Scale bars, 5 μm. (**e**) Apical Slp2-a localization depends on PtdIns(4,5)P_2. Cysts expressing PHD–GFP (top panels) and Cherry–Slp2-a (bottom panels), were treated with ionomycin, which stimulates endogenous PLC activity to deplete membrane PtdIns(4,5)P_2, and were analysed by video-microscopy (0.1 s exposure every 1 s). Still images at different time points after ionomycin addition are presented. The arrowheads indicate apical membrane localization. Scale bars, 10 μm. (**f**) Schematic of Slp2-a association with the apical plasma membrane. Slp2-a C2A/B domains bind PIP_2 and localize Slp2-a to the lumen initiation site and the apical membrane. The SHD domain binds apical vesicles. For all panels, areas outlined in micrographs are magnified in the associated images. Uncropped images of blots are shown in Supplementary Fig. S8.

was cytoplasmic (Supplementary Fig. S4). These results suggest that whereas the SHD binds to apical vesicles, the C2 domains target Slp2-a to membranes.

Notably, the distribution of the C2 domains resembles PtdIns(4,5)P_2 localization during cyst formation[9]. Furthermore, Slp2-a, and paralogues, bind selectively to PtdIns(4,5)P_2 (refs 12,17), although it could bind also to phosphatidylserine[16]. We found that C2 domains bound specifically to PIP_2 species, but not to phosphatidylserine (Fig. 3c). Lact-C2–GFP, a probe for phosphatidylserine, presents non-polarized membrane localization in cysts (Supplementary Fig. S4e). Given the established role of PtdIns(4,5)P_2 in apical membrane specification[9], and higher cellular abundance[22], we reasoned that PtdIns(4,5)P_2 may target Slp2-a to plasma membranes. During cyst formation, Slp2-a and PtdIns(4,5)P_2 co-localized at the plasma membrane, becoming progressively enriched to the lumen in morphogenesis (Fig. 3d). Both PtdIns(4,5)P_2 and Cherry–Slp2-a disappeared rapidly from the apical membranes on ionomycin treatment, which causes PIP depletion at the membrane[23] (Fig. 3e and Supplementary Video S1). Taken together, these results confirm that Slp2-a requires the C2 domains for PtdIns(4,5)P_2 binding and apical membrane localization, whereas the SHD region targets Slp2-a to apically destined vesicles (Fig. 3f).

Slp2-a targets Rab27 vesicles to the lumen initiation site to form the lumen

Nearly all described functions of mammalian Slps required the SHD domain[21]. In contrast, Btsz, the sole Slp paralogue in *Drosophila*, does not require a Rab-binding domain for epithelial

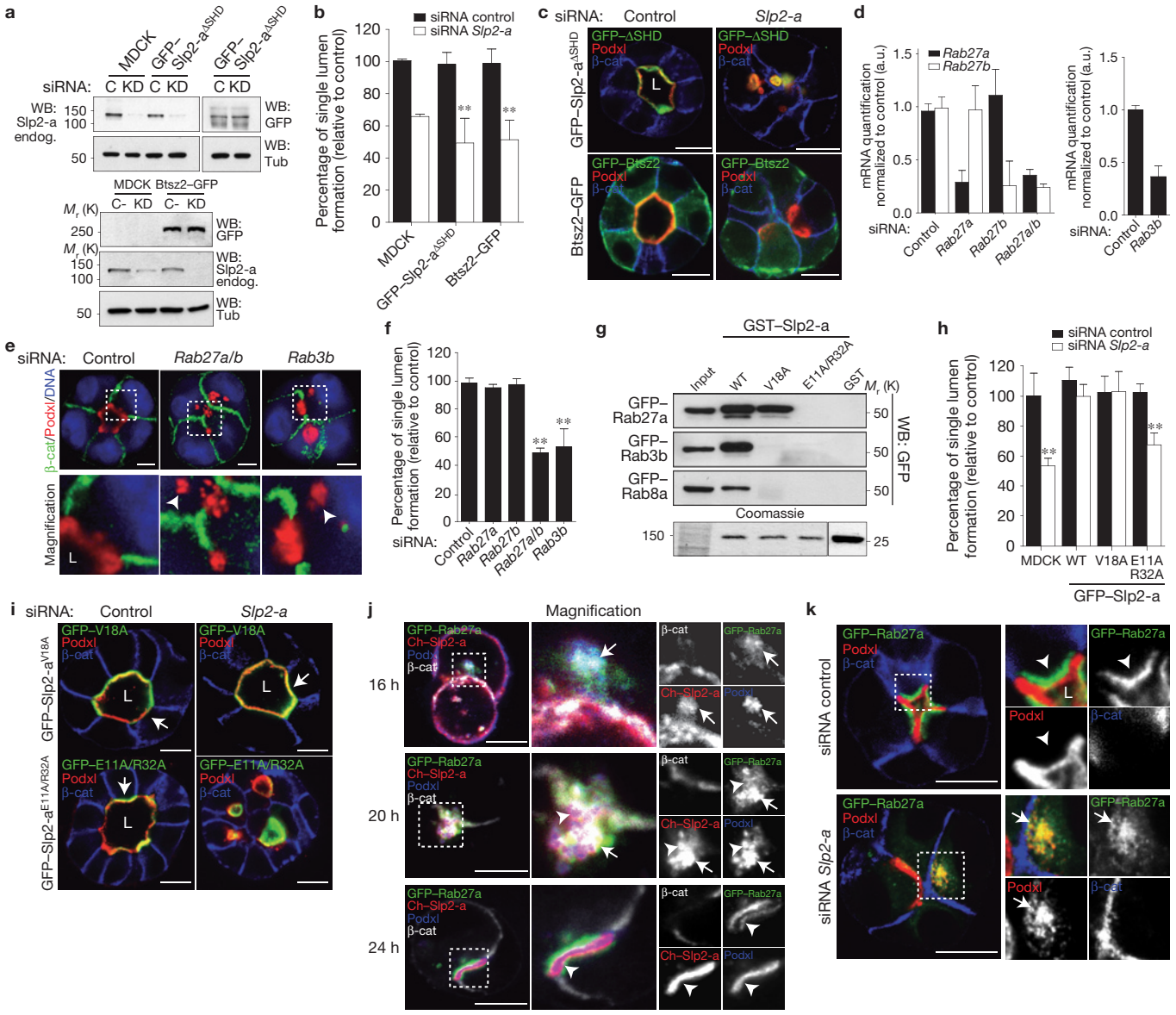

Figure 4 Slp2-a binds Rab27 to form the apical membrane. (**a**) Knockdown of *Slp2-a* in cells stably expressing GFP–Slp2-a$^{\Delta SHD}$ or Btsz2–GFP (Btsz2) at 72 h after siRNA transfection. C, control; KD, knockdown; endog, endogenous; WB, western blot. (**b**) Quantification of cysts with normal lumens in cells expressing GFP–Slp2-a$^{\Delta SHD}$ or Btsz2–GFP and transfected with siRNA to *Slp2-a* or control ($n = 3$). (**c**) Rescue effect of GFP–Slp2-a$^{\Delta SHD}$ and Btsz2–GFP in cells knocked down for *Slp2-a* on lumen formation at 72 h post siRNA transfection. PodxI, red; β-catenin (β-cat), blue. Note, Btsz2–GFP localization is not polarized on the plasma membrane of cysts. (**d**) Knockdown of *Rab27a/b* and *Rab3b* by siRNA. MDCK cells were transfected with different siRNA duplexes targeting canine *Rab27a, Rab27b* or *Rab3b.* After 72 h RNA extracts were quantified by RT–qPCR; $n = 3$. (**e**) Effect of *Rab27a/b* or *Rab3b* knockdown on cyst formation. Cysts were fixed 48 h after transfection. Silencing of *Rab27a/b* or *Rab3b* was sufficient to disrupt cyst formation and accumulate PodxI in vesicles (arrowheads). PodxI, red; β-catenin, green; nuclei, blue. (**f**) Quantification of cysts with normal lumens in cells transfected with siRNA targeting *Rab27a, Rab27b, Rab27a/b* or *Rab3b* ($n = 3$). (**g**) Rab–GTPase interaction with Slp2-a mutants V18A and E11A/R32A. GST (control) or GST–Slp2-a (WT, V18A and E11A/R32A) beads were used to pulldown fluorescent protein-tagged Rab3b, Rab8a or Rab27a from total cell lysates. Bottom lane, Coomassie staining of an independent polyacrylamide gel loaded with GST–Slp2-a constructs and a representative input. (**h**) Quantification of normal cysts in cells expressing GFP–Slp2-a WT, V18A and E11A/R32A mutants transfected with siRNA against *Slp2-a* or control ($n = 3$). (**i**) Images of GFP–Slp2-a V18A and E11A/R32A cysts after *Slp2-a* knockdown. Cysts were fixed 48 h after transfection. PodxI, red; β-catenin, blue. The arrows indicate apical membrane. (**j**) Co-localization of Rab27 and Slp2-a during cyst morphogenesis. MDCK cells stably expressing Cherry (Ch)–Slp2-a and GFP–Rab27a were grown as cysts and fixed after 16, 20, or 24 h. PodxI, blue; β-catenin, white. (**k**) Effect of the downregulation of *Slp2-a* on GFP–Rab27a cells 36 h after siRNA transfection. The arrowheads indicate Rab27a subapical localization; the arrows indicate co-localization of PodxI and Rab27a. In all panels values are means ± s.d. of *n* independent experiments; $^*P < 0.05$; $^{**}P < 0.005$; L, lumen; scale bars, 10 μm; areas outlined in micrographs are magnified in the associated images. Uncropped images of blots are shown in Supplementary Figs S8 and S9.

morphogenesis[12] (Supplementary Fig. S5b), suggesting Rab–Slp interactions may be dispensable for epithelial polarity. To address this possibility, we expressed the epithelial Btsz protein (Btsz2–GFP) and an SHD-deleted Slp2-a mutant (GFP–Slp2-a$^{\Delta SHD}$). Importantly, neither GFP–Slp2-a$^{\Delta SHD}$ nor Btsz2–GFP was able to rescue the defects caused by endogenous *Slp2-a* knockdown (Fig. 4a–c and

Supplementary Fig. S4b) . These results reveal that the SHD region is required for epithelial morphogenesis in MDCK cysts.

To determine which Rab GTPase interactions are required for Slp2-a function, we analysed Rabs that interact with other Slps (ref. 10). Slp2-a bound to Rab3b, Rab8a, Rab27a and to a lower extent Rab3a (Supplementary Fig. S5A). Although Rab8a/b are required for cyst formation[7,18], only knockdown of both *Rab27a/b* strongly perturbed lumen formation (Fig. 4d–g), confirming partial isoform redundancy noted from knockout mice[24]. In contrast, although Rab3a-d isoforms are expressed in MDCK (data not shown), silencing of Rab3b was sufficient to disrupt cyst formation (Fig. 4d–g), suggesting Rab3b may have subtle non-redundant roles in apical transport[25,26], and epithelial polarity. These results suggested that Slp2-a could mediate the targeting of apical vesicles loaded with Rab27a/b, Rab3b and/or Rab8a/b.

Next, we generated Slp2-a SHD mutants to disrupt the interaction with specific Rabs based on the structure of the Slp2-a/Rab27 interaction[20]. The introduction of a V18A mutation in Slp2-a completely abolished the interaction with Rab3b and Rab8a, while preserving Rab27a binding; E11A/R32A mutations also disrupted the binding to Rab27 (Fig. 4g). Although both mutants retain apical localization (Fig. 4i and Table 1), GFP–Slp2-a^{V18A}, but not GFP–Slp2-a$^{E11A/R32A}$, completely rescued the *Slp2-a* knockdown phenotype (Fig. 4h,i and Supplementary Fig. S5f). Together, these data indicate that although Slp2-a can bind multiple Rabs, Rab27a/b is necessary and sufficient for Slp2-a function in lumen morphogenesis.

Next, we analysed Rab27 localization. Before lumen formation, GFP–Rab27a co-localized with Podxl and Slp2-a in vesicles transcytosing to the lumen (Fig. 4j, top and middle panels and Supplementary Fig. S5c). Once lumen initiation was completed, Rab27a localized to a subapical compartment, whereas Slp2-a localized apically (Fig. 4j, bottom panels and Supplementary Fig. S5c,e). Finally, *Slp2-a* knockdown caused the scattering of Rab27a vesicles close to the plasma membrane (Fig. 4k, bottom panels). Thus, Slp2-a is required to localize Rab27a. Taken together, these results indicate that Slp2-a binds to Rab27a-loaded apical vesicles and targets them to initiate the lumen.

Slp4-a also functions in lumen biogenesis

In addition to Slp2-a, mammalian cells express four other Slp-family proteins (Slp1-5), and four closely related Slac2s (Slp homologue lacking C2 domains)[10]. To determine whether other Slp proteins function in epithelial polarization, we analysed their expression during lumen formation. Notably, whereas Slp2-a was the sole Slp upregulated in 3D at early times (Fig. 5a, 3D-14 h), Slp1 and Slp4-a were upregulated at later times (Fig. 5a, 3D-36 h).

In contrast to Slp1, Slp4-a silenced cysts presented acute defects with the formation of multiple lumens and internal vesicles (Fig. 5b,c). In addition, *Slp4-a* knockdown did not affect polarity or ciliogenesis in monolayers (Supplementary Fig. S3a,b). Moreover, we observed that Slp2-a is specifically induced before Slp4-a in 3D cultures (Fig. 5d), suggesting that Slp2-a is required earlier than Slp4 in lumenogenesis.

We next examined the localization of Slp4-a. Endogenous Slp4a/b and GFP–Slp4-a associated with apical membranes at all stages of polarization (Fig. 5e and Supplementary Fig. S6d), thus presenting a different localization pattern from Slp2-a (Fig. 3 and Table 1). Next, we examined Slp4-a domains in cysts. The C2 domains (C2A/B), either alone or in tandem, localized to apical and basolateral plasma membranes (Fig. 5f, left panels, Supplementary Fig. S6e and Table 1), suggesting that they confer nonspecific plasma membrane localization. In support of this, GST–Slp4-a C2 domains bound promiscuously to PtdIns(4,5)P_2 and PtdIns(3,4,5)P_3 (Fig. 5g,h and Supplementary Fig. S6c). In contrast, the C2A domain of Slp2-a bound specifically to PtdIns(4,5)P_2 and localized apically (Supplementary Fig. S4d), suggesting that only Slp2-a is able to tether Rab27 vesicles to apical PtdIns(4,5)P_2-enriched plasma membrane. Together, these data highlight a requisite of the SHD-linker region for apical targeting of Slp4-a, representing a major difference from Slp2-a, and suggesting non-redundant roles for Slp2-a and Slp4-a in lumen formation.

Slp4-a apical localization and function depend on Rab and syntaxin interaction

Slp4-a functions in docking of secretory granules with the plasma membrane, a function modulated by the SHD region, which interacts with Rab3, Rab8 and Rab27 family members[10]. Therefore, we examined the contribution of Rab binding to Slp4-a function.

To elucidate the role of Rab binding, we examined the ability of SHD mutations to bind to Rab27/3/8 and to rescue the phenotype of endogenous *Slp4-a* knockdown (Fig. 6a,b)[27]. In contrast to apical wild-type (WT)-Slp4-a, removal of the Rab-interacting region of Slp4-a$^{\Delta SHD}$ resulted in both cytoplasmic and non-polarized membrane localization of Slp4-a (Fig. 6c, Supplementary Fig. S6e and Table 1), as for Slp4-a^{W118S} (no Rab binding) expression (Fig. 6a–c, Supplementary Fig. S6f and Table 1). Uncoupling of Slp4-a from Rab3b (V21A) resulted in subapical localization (Fig. 6c and Supplementary Fig. S6f). In contrast, co-uncoupling of Rab8 and Rab3b (I18A) resulted in the targeting of a pool of Slp4-a to the basolateral membrane, in addition to subapical vesicles (Fig. 6a–c, Supplementary Fig. S6f and Table 1). Whereas WT-Slp4-a was able to rescue endogenous *Slp4-a* knockdown, none of the Rab-binding mutants was able to restore lumen formation (Fig. 6b,c and Table 1). These results indicate that Rab27, Rab8 and Rab3 binding are required for Slp4-a localization and function. The different localization of the mutants also suggests that Rab27 is required for Slp4-a targeting to vesicles, Rab8 would be necessary to exclude Slp4-a from the basolateral membrane, and Rab3 may be important for subsequent Slp4-a transport to the lumen initiation membrane.

Next we analysed the role of phospholipid binding for Slp4-a, using a phospholipid-uncoupled mutant (K > Q; ref. 16). Slp4-a$^{K>Q}$ localized to subapical puncta of apical membranes (Supplementary Fig. S6g and Table 1), and conferred a partial rescue to morphogenesis (Fig. 6b), suggesting that although the C2 domains can confer membrane localization, interaction of Slp4-a with other factors (Rabs and SNARE complexes) may partially compensate for the lack of C2 domain function.

Slp4, in contrast to other Slps, binds to SNARE proteins by its linker domain[28,29]. To analyse SNARE binding, we generated a chimaeric construct of Slp4-a bearing a Slp5 linker domain (*Slp454*) that was unable to bind to Stx3 (Fig. 6d). *Slp454* showed a subapical and basolateral localization, and failed to rescue lumen formation on endogenous *Slp4-a* knockdown (Fig. 6e,f and Supplementary Fig. S6i and Table 1), suggesting an important role for Stx3 binding to Slp4-a. Next, we mapped the Stx3-binding domain of Slp4-a, and

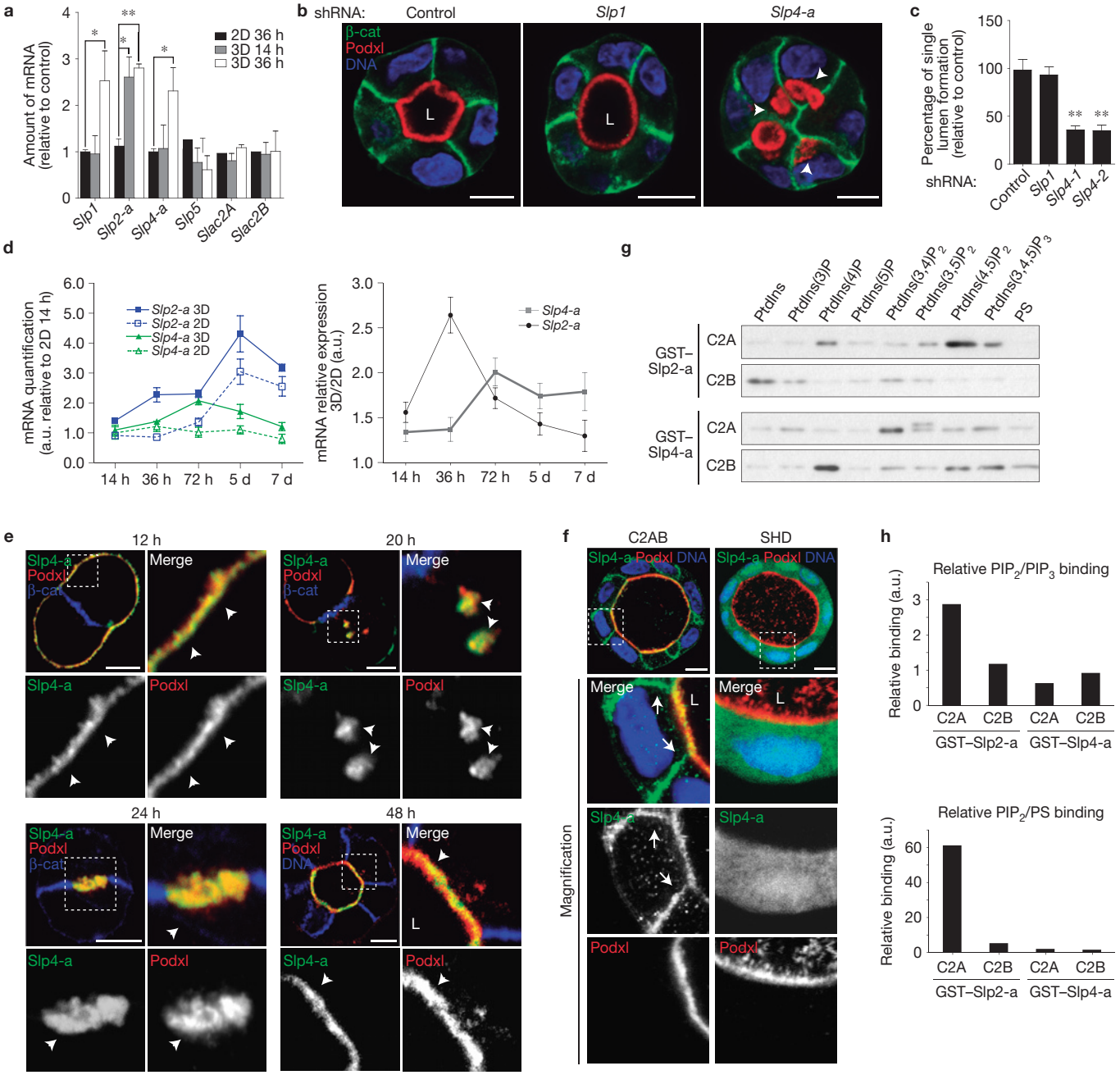

Figure 5 Slp4-a is required for epithelial morphogenesis. (**a**) Analysis of *Slps* and *Slac2s* expression in 2D versus 3D. *Slp1, Slp2-a, Slp4-a, Slp5, Slac2A* and *Slac2B* expression was evaluated at different time points (14 and 36 h) by RT–qPCR in MDCK cells grown in 2D and 3D. Slp3, Slac2C and the related Rab27 effectors Noc2 and rabphilin3 were not expressed in MDCK ($n = 4$). (**b**) Effect of *Slp4-a* silencing on lumen formation. Cells stably expressing *Slp4, Slp1* or scramble shRNA were plated to form cysts for 72 h. Cells were stained to detect Podxl (red), β-catenin (β-cat; green) and nuclei (blue). The arrowheads indicate intracellular Podxl vesicles. (**c**) Quantification of cysts with normal lumens in cells expressing scramble, Slp1 or *Slp4-a* shRNA ($n = 3$). (**d**) Quantification of *Slp2-a* and *Slp4-a* mRNA in cells grown on filters or in Matrigel. MDCK cells were grown on filters to confluence (2D) or in Matrigel (3D). mRNA expression was evaluated at different times by RT–qPCR. Data were normalized to 2D levels at 14 h post-plating. Left panel, *Slp2-a* (blue lines) and *Slp4-a* (green lines) mRNA expression patterns in 2D (solid lines) or 3D (dashed lines). Right panel, mRNA expression as the 3D/2D coefficient at different time points ($n = 3$). (**e**) Localization of GFP–Slp4-a in stably expressing cells during lumen formation. Cysts were stained for Podxl (red) and β-catenin (blue). The arrowheads indicate Slp4-a co-localization with Podxl. (**f**) Localization of GFP–Slp4-a C2A/B and SHD during lumen morphogenesis. Cysts were fixed at 96 h and co-stained to detect Podxl (red) and β-catenin (blue). The arrows indicate the basolateral plasma membrane. (**g**) Phospholipid-binding ability of Slp2-a and Slp4-a C2 domains. Purified GST-tagged Slp2-a and Slp4-a C2A and C2B domains were incubated with beads covered with phosphoinositides or phosphatidylserine (PS). (**h**) Quantification of relative binding of phosphoinositides and PS to Slp2-a and Slp4-a C2 domains. The panels show the PIP_2/PIP_3 (top) and PS/PIP_2 binding ratios (bottom). Note, the Slp2-a C2A domain binds mainly to PIP_2, whereas other C2 domains show similar binding abilities to PIP_2, PIP_3 or PS. In all panels values are means ± s.d. of n independent experiments; $^{*}P < 0.05$; $^{**}P < 0.005$; L, lumen; scale bars, 10 μm; areas outlined in micrographs are magnified in the associated images. Uncropped images of blots are shown in Supplementary Fig. S9.

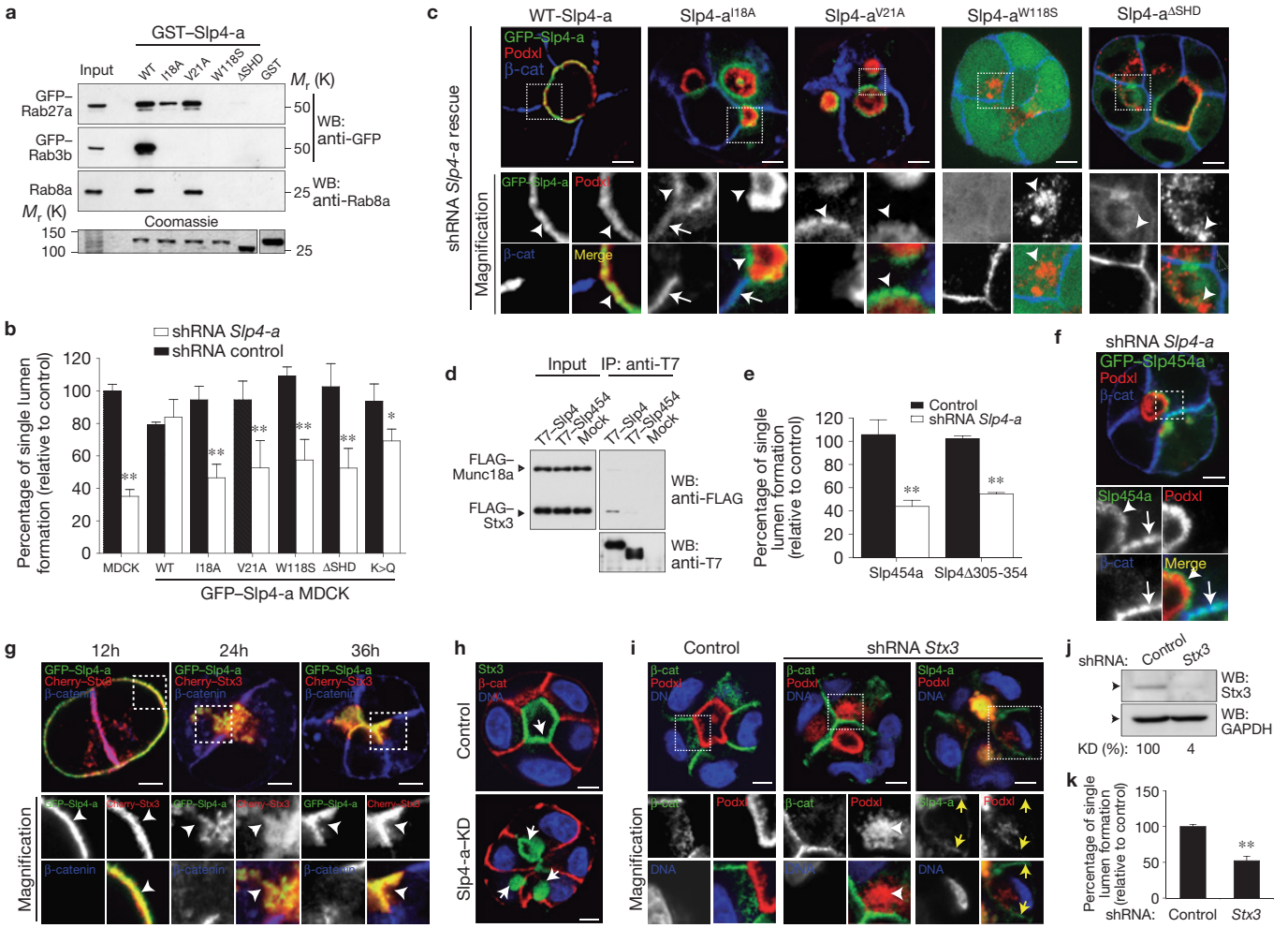

Figure 6 Slp4-a binding to the plasma membrane, Rabs and Stx3 is required for apical membrane formation. (**a**) Rab–GTPase binding to Slp4-a mutants. Purified GST-tagged Slp4-a (WT, I18A, V21A, W118S and ΔSHD) or GST (control) proteins were used to pulldown fluorescent-protein-tagged Rab3b, Rab8a or Rab27a from total cell lysates. Membranes were blotted with anti-GFP or anti-Rab8a. Bottom lane, Coomassie staining of an independent polyacrylamide gel loaded with different GST–Slp4-a constructs and inputs. WB, western blot. (**b**) Quantification of cysts with normal lumens in GFP–Slp4-a (WT, ΔSHD, I18A, V21A, W118S and K > Q) cells expressing scramble or *Slp4-a* shRNA ($n = 3$). (**c**) Rescue effect of GFP–Slp4-a WT, Rab-binding defective mutants or membrane-binding defective Slp4-a$^{K>Q}$. MDCK cysts (72 h) expressing GFP–Slp4-a WT, ΔSHD, I18A, V21A, W118S or K > Q were knocked down (KD) for *Slp4-a*, and stained for Podxl (red) and β-catenin (β-cat; blue). Arrowheads indicate co-localization with Podxl; arrows indicate co-localization with β-catenin. (**d**) Co-immunoprecipitation assay of Slp4a binding to Stx3. T7–Slp4-a or T7–Slp454 beads were incubated with FLAG–Munc18-2 and FLAG–Stx3 lysates. FLAG-tagged proteins were detected with HRP-conjugated anti-FLAG. Input 1:10 of immunoprecipitate (IP) volume. (**e**) Quantification of cysts with normal lumens in the absence of the Stx3–Slp4 interaction using cells expressing GFP–Slp454 or GFP–Slp4-a$^{Δ305–354}$ and knocked down for *Slp4-a* ($n = 3$). (**f**) Localization of GFP–Slp454 in *Slp4-a* silenced cells. Podxl, red; β-catenin, blue. Arrowheads show vesicular localization; arrows show basolateral membrane. (**g**) Localization of Cherry–Stx3 and GFP–Slp4-a during cyst development. Cherry–Stx3 co-localized with GFP–Slp4-a at the periphery of early aggregates (arrowheads), intracellular vesicles and cell–cell contacts. As lumens formed, Cherry–Stx3 concentrated at the nascent luminal membrane with GFP–Slp4-a (arrowheads). Nuclei (blue). (**h**) Intracellular localization of GFP–Stx3 (arrows) in *Slp4-a* knockdown cysts (72 h). β-catenin, red; nuclei, blue. (**i**) GFP–Slp4-a localization in 48 h cysts knocked down for *Stx3*. Podxl (red), β catenin (green) and nuclei (blue). Note the Slp4-a basolateral mis-localization in the *Stx3* knockdown cysts (yellow arrows). The arrowheads indicate Podxl vesicles. (**j**) Downregulation of Stx3 in MDCK cells stably expressing *Stx3* shRNA. Total lysates were blotted for Stx3 and GAPDH (loading control). (**k**) Quantification of the effect of Stx3 silencing in cyst formation ($n = 3$). In all panels values are means ± s.d of *n* independent experiments; $^{*}P < 0.05$; $^{**}P < 0.005$; scale bars, 5 μm; areas outlined in micrographs are magnified in the associated images. Uncropped images of blots are shown in Supplementary Fig. S10.

identified amino acids 305–354 to be essential for Stx3 binding (Supplementary Fig. S6h). Consistently, expression of a construct lacking amino acids 305–354 of Slp4-a (GFP–Slp4-a^{Δ305}–354) also failed to localize to the apical plasma membrane and to rescue lumen formation on endogenous *Slp4-a* knockdown (Fig. 6e and Supplementary Fig. S6j and Table 1).

Stx3 functions as a critical apical[30] SNARE. In cysts, GFP–Stx3 co-localized with Slp4-a at the nascent luminal membrane (Fig. 6g). Notably, *Stx3* knockdown resulted in disruption of lumen formation and the redistribution of a pool of GFP–Slp4-a to the basolateral membrane (Supplementary Fig. S6i–k), and a similar localization observed on the removal of the Stx-binding region of *Slp4-a* (Supplementary Fig. S6i,j).

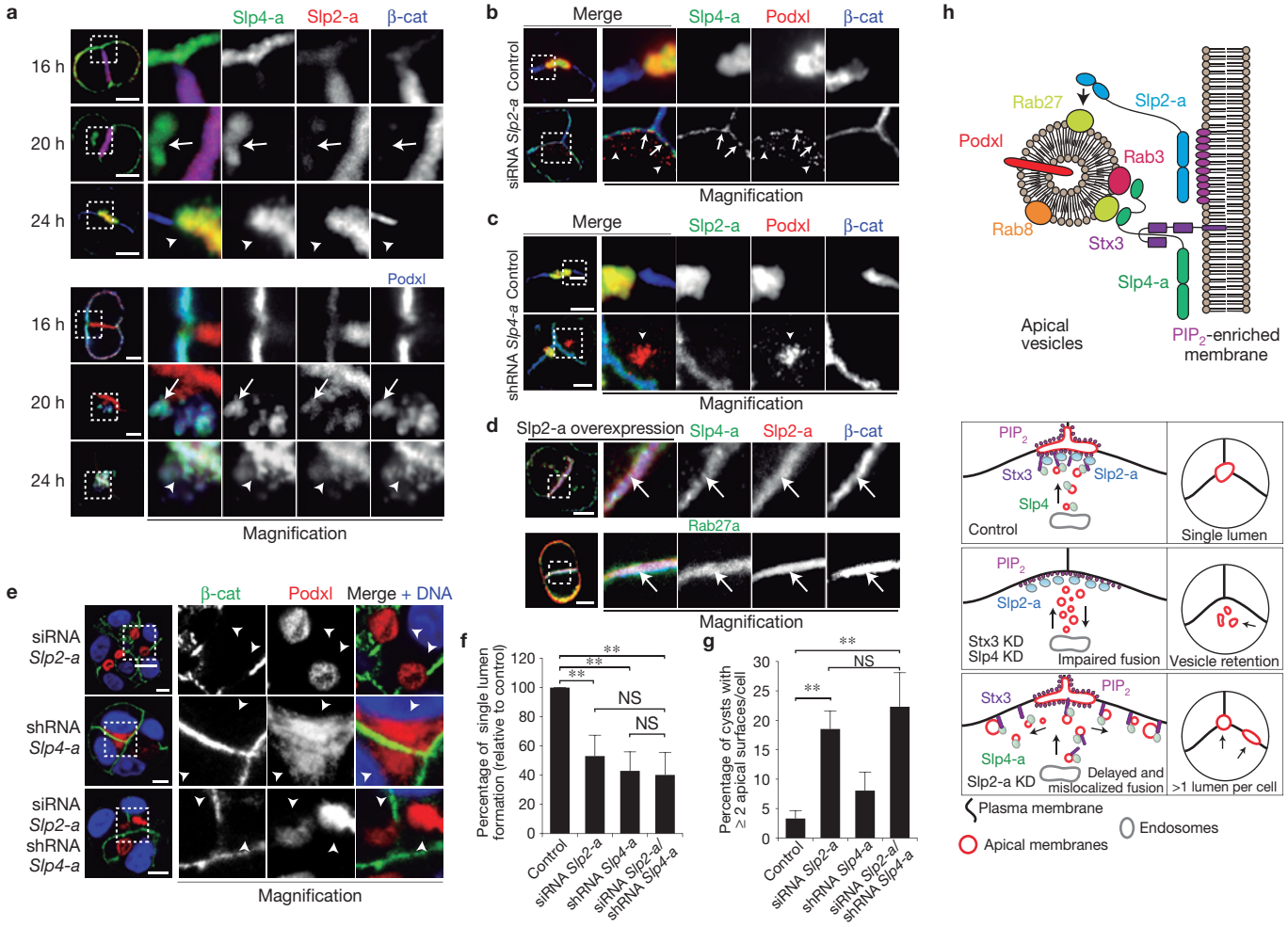

Figure 7 Slp2-a regulates Slp4-a targeting to determine single apical membrane formation. (**a**) Slp2-a and Slp4-a localization during lumen initiation. Cysts stably expressing GFP–Slp4-a and Cherry–Slp2-a were fixed after 16, 20 and 24 h. Podxl (blue, bottom panels) and β-catenin (β-cat; blue, top panels). The arrows indicate vesicular Slp4-a; the arrowheads indicate Slp2-a/Slp4-a co-localization at the nascent luminal membrane. (**b**) Effect of *Slp2-a* knockdown (KD) on Slp4-a localization. Slp4-a localization becomes basolateral after *Slp2-a* knockdown and co-localizes partially with Podxl (red) in vesicles (arrows). The arrowheads indicate scattered Podxl vesicles. (**c**) Effect of *Slp4-a* knockdown on *Slp2-a* localization. After *Slp4-a* knockdown, Slp2-a localization at cellular junctions is unaffected. Note the accumulation of Podxl (red) in vesicles (arrowheads). (**d**) Effect of Slp2-a overexpression on GFP–Slp4-a and GFP–Rab27 in 24 h cysts. Slp4-a or Rab27a co-localized with Slp2-a and β-catenin (blue) at cellular junctions (arrows). (**e**) Effect of double *Slp2-a/Slp4-a* knockdown on lumen formation. Cells knocked down for *Slp4-a*, *Slp2-a* or *Slp4-a/Slp2-a* for 48 h were fixed and stained for nuclei (blue), Podxl (red) and β-catenin (green). The arrowheads indicate apical plasma membranes. (**f**) Quantification of cysts with normal lumens in control, *Slp2-a* knockdown, *Slp4-a* knockdown or *Slp2-a/4-a* double knockdown ($n = 3$). (**g**) Quantification of cysts presenting two or more apical surfaces per cell in control, *Slp2-a* knockdown, *Slp4-a* knockdown or *Slp2-a/4-a* double knockdowns ($n = 3$). In all panels values are mean ± s.d. from n independent experiments; NS, not significant; $^{**}P < 0.005$; scale bars, 5 μm; areas outlined in micrographs are magnified in the associated images. (**h**) Model of Slp2-a/4-a function in epithelial polarization. Top panel, Slp2-a targets Rab27-positive endosomes to the PIP_2-enriched membrane. Slp4-a binds to Rab3 and Stx3 to be delivered to the lumen initiation site in Rab27-positive vesicles. As Slp4-a is delivered in Rab27-positive vesicles, its targeting depends on Slp2-a function. Therefore, Slp2-a directs localization of the Slp4-a/Stx3-influenced vesicle tethering activity to the single PIP_2-enriched initiation site, and thus a single lumen per cell. Bottom panel, when Slp4-a or Stx3 are perturbed, vesicles cannot be correctly tethered and apical vesicles accumulate. When Slp2-a is disrupted, vesicles are tethered ectopically to different positions of the plasma membrane, resulting in multiple apical domains in the same cell.

In contrast, *Slp4-a* knockdown did not disrupt the apical localization of Stx3 (Fig. 6h). These data suggest that Stx3 association with Slp4-a, by interaction with the linker domain, directs recruitment of Slp4-a to apically destined vesicles, and initiation of *de novo* lumen formation.

Slp2-a regulates Slp4-a function to produce a single apical surface per cell

Our data thus far indicate that Slp2-a and Slp4-a function in distinct, non-redundant steps in Rab-dependent transport to form the lumen. We thus examined their localization during lumen formation. In early aggregates, Slp2-a localized mainly to cell–cell junctions, whereas Slp4-a co-localized with Podxl at the cell–extracellular matrix interface (Fig. 7a, 16 h, top panels and Supplementary Fig. S7c). As internalized Podxl transcytosed to the cell–cell contact, Slp4-a co-localized to these vesicles, whereas Slp2-a was mainly at the cell–cell junctions (Fig. 7a, 20 h and Supplementary Fig. S7c). Finally, Slp2-a/4-a co-localization was evident once lumens formed (Fig. 7a, 24 h and Supplementary Fig. S7c).

Next we examined whether their activities were mutually dependent. Knockdown of *Slp2-a* caused the scattered distribution of small Podxl vesicles and the redistribution of GFP–Slp4-a to the lateral plasma membrane, partially co-localizing with Podxl vesicles (Fig. 7b, arrows). In contrast, *Slp4-a* knockdown cysts presented clusters of Podxl vesicles (Fig. 7c), but GFP–Slp2-a localized normally to cell–cell contacts, suggesting that Slp2-a localization and function are independent, or upstream, of Slp4-a. Furthermore, overexpression of GFP–Slp2-a forced endogenous Rab27a and Slp4-a mis-recruitment to cell–cell contacts at early time points (Fig. 7d), whereas the converse effect of GFP–Rab27a on Slp2-a was not observed (not shown). These results suggest that Slp2-a functions to regulate the positioning of Rab27 vesicles upstream of Slp4-a-mediated vesicle docking, thus controlling the position of the apical membrane and subsequent lumen.

To test this hypothesis, we silenced Slp2-a and Slp4-a alone or together (Fig. 7e–g). Strikingly, we observed that whereas *Slp4-a* knockdown induced accumulation of Podxl vesicles close to the membrane (Fig. 7e, middle panels), *Slp2-a* knockdown cysts possessed some cells simultaneously developing more than one apical membrane (Fig. 7e, top panels, quantification Fig. 7g). Moreover, although dual knockdown cysts presented a mixture of both phenotypes (Fig. 7e, bottom panels), they perturbed single lumen formation to a level resembling that of *Slp4-a* knockdown alone, supporting the notion that Slp4-a functions downstream of Slp2-a (Fig. 7f). Although cysts with multiple lumens have been observed previously on knockdown of trafficking proteins, the knockdown of Slp2-a is unique in that this is the first time, to our knowledge, that a cell can participate simultaneously in the generation of multiple luminal surfaces.

These results indicate that Slp2-a and Slp4-a form part of a core apical transport pathway that controls the positioning of Rab27a/b vesicles, and their subsequent Rab8/Rab3b/Stx3-dependent fusion with the apical plasma membrane, respectively, to form a single PtdIns(4,5)P_2-enriched apical membrane and lumen during *de novo* apical domain biogenesis (Fig. 7h).

DISCUSSION

One of the central, unsolved questions in epithelial biology concerns how apical–basolateral polarity is coordinated between neighbouring cells to form a common, single luminal region. Making use of the fact that MDCK can undergo polarization into either in 2D or 3D, we have uncovered a gene set that specifically facilitates the transition to the 3D architecture. Interestingly, most of this gene set is downregulated in some glandular epithelial cancers, indicating a potential clinical relevance in maintaining a polarized phenotype (Fig. 1).

During the development of 3D polarity, apical membrane components are delivered to the site for lumen initiation, between neighbouring cells, to initiate a luminal space *de novo*[7,31]. What had remained unclear, though, was how this trafficking pathway was organized to direct vectorial transport to a singular position, thus allowing formation of a single apical membrane per cell. Here, we have identified a molecular pathway specifically upregulated during 3D morphogenesis that controls the formation and positioning of a single apical membrane per cell, through the complementary functions of Slp2-a and Slp4-a (Fig. 7h). We demonstrate that Slp2-a controls the clustering of apically destined vesicles through the interaction with Rab27a/b and the association with PtdIns(4,5)P_2 at the nascent apical membrane. Subsequently, Slp4-a acts as an effector of Rab27a/b, Rab8a/b and Rab3b on vesicles, to couple the vesicles to Stx3-mediated fusion events at the plasma membrane to create the lumen. Inhibition of this Slp2-a/4-a pathway perturbs this transport and ultimately causes the formation of multiple apical membranes. These data support our model that Slp2-a and Slp4-a function in a spatiotemporal cascade to control vectorial apical transport (Fig. 7h), a fact supported by their sequential transcriptional upregulation during cyst formation.

An interesting question is how Slp2-a/4-a may coordinate this vectorial transport to form a single lumen. In non-polarized cells, both Slp2-a and Slp4-a are considered as negative regulators of secretion, on the basis of the fact that their overexpression attenuates secretory granule release[15–17,27,32]. Indeed, Slp4-a can interact with the closed (non-fusion-forming) conformation of SNARE complexes[29]. To this end, transient overexpression of Slp2-a or Slp4-a in the presence of endogenous protein consistently reduced single-lumen-formation rates (Supplementary Fig. S7A,B), a trend that could be strongly reversed by expression of SHD-deleted Slp2-a/4-a, suggesting that they may act as negative regulators of vesicle trafficking. However, Slp2-a/4-a are also clearly required for single lumen formation, thus suggesting a scenario where, rather than being considered as negative or positive regulators of exocytosis, Slp2-a/4-a act as molecular traffic wardens[32], controlling vectorial exocytosis through ensuring vesicles dock and fuse only at singular membrane domains to form a single, coordinated luminal space between neighbouring cells.

We identified, for the first time, a transcriptionally regulated molecular pathway that controls the formation of a single apical surface per cell, addressing a major, long-term unanswered question in cell biology. The study of the transcriptional machinery responsible for lumenogenesis *in vivo* presents a major future challenge to both cell and developmental biology. □

METHODS

Methods and any associated references are available in the online version of the paper.

Note: Supplementary Information is available in the online version of the paper

ACKNOWLEDGEMENTS

We thank C. M. Ruiz-Jarabo for comments on the manuscript, and members of the Martin-Belmonte laboratory for discussion. We thank M. ter Beest, J. Peränen, and K. Simons, Max Planck Institute of Molecular Cell Biology and Genetics (MPI-CBG), Dresden, Germany, for generous gifts of reagents, and the Mostov laboratory for kind assistance. This work was supported by grants from the Human Frontiers Science Program (HFSP-CDA 00011/2009), Marie Curie (IRG-209382), MICINN (BFU2008-01916), (BFU2011-22622) and CONSOLIDER (CSD2009-00016) to F.M-B.; by NIH R01DK074398, R01AI25144 and R01DK91530 to K.M., and The March of Dimes Basil O'Connor Starter Research Award to P.R.B. A.E.R-F. is the recipient of a JAE fellowship, from CSIC; M.G-S. is the recipient of a FPI fellowship, from MICINN; and I.B-R. is the recipient of an AECC fellowship. An institutional Grant from the Fundación Ramón Areces to CBMSO is also acknowledged.

AUTHOR CONTRIBUTIONS

M.G-S., A.E.R-F., D.M.B., S.V. and F.M-B. designed the experiments. M.G-S., A.E.R-F., D.M.B., S.V., T.S., I.B.R., I.B., A.D., N.S., K.Y. and C.L.S. did the experimental work. M.G-S., A.E.R-F., D.M.B., K.E.M. and F.M-B. analysed the experiments. P.R.B. and M.F. provided reagents. F.M-B., D.M.B. M.G-S. and A.E.R-F. wrote the manuscript.

COMPETING FINANCIAL INTERESTS

The authors declare no competing financial interests.

Published online at www.nature.com/doifinder/10.1038/ncb2541
Reprints and permissions information is available online at www.nature.com/reprints

1. Mostov, K., Su, T. & ter Beest, M. Polarized epithelial membrane traffic: conservation and plasticity. *Nat. Cell Biol.* **5,** 287–293 (2003).
2. Rodriguez-Boulan, E., Musch, A. & Le Bivic, A. Epithelial trafficking: new routes to familiar places. *Curr. Opin. Cell Biol.* **16,** 436–442 (2004).
3. Bryant, D. M. & Mostov, K. E. From cells to organs: building polarized tissue. *Nat. Rev. Mol. Cell Biol.* **9,** 887–901 (2008).
4. Datta, A., Bryant, D. M. & Mostov, K. E. Molecular regulation of lumen morphogenesis. *Curr. Biol.* **21,** R126–R136 (2011).
5. Lubarsky, B. & Krasnow, M. A. Tube morphogenesis: making and shaping biological tubes. *Cell* **112,** 19–28 (2003).
6. Roland, J. T. *et al.* Rab GTPase-Myo5B complexes control membrane recycling and epithelial polarization. *Proc. Natl Acad. Sci. USA* **108,** 2789–2794 (2011).
7. Bryant, D. M. *et al.* A molecular network for *de novo* generation of the apical surface and lumen. *Nat. Cell Biol.* **12,** 1035–1045 (2010).
8. Gassama-Diagne, A. *et al.* Phosphatidylinositol-3,4,5-trisphosphate regulates the formation of the basolateral plasma membrane in epithelial cells. *Nat. Cell Biol.* **8,** 963–970 (2006).
9. Martin-Belmonte, F. *et al.* PTEN-mediated apical segregation of phosphoinositides controls epithelial morphogenesis through Cdc42. *Cell* **128,** 383–397 (2007).
10. Kuroda, T. S., Fukuda, M., Ariga, H. & Mikoshiba, K. The Slp homology domain of synaptotagmin-like proteins 1-4 and Slac2 functions as a novel Rab27A binding domain. *J. Biol. Chem.* **277,** 9212–9218 (2002).
11. Ishii, N. *et al.* A case of recurrent gall bladder cancer responding to chemotherapy with gemcitabine after endoscopic metallic biliary stent implantation. *Gan To Kagaku Ryoho* **35,** 1403–1405 (2008).
12. Pilot, F., Philippe, J. M., Lemmers, C. & Lecuit, T. Spatial control of actin organization at adherens junctions by a synaptotagmin-like protein. *Nature* **442,** 580–584 (2006).
13. Bagnat, M., Cheung, I. D., Mostov, K. E. & Stainier, D. Y. Genetic control of single lumen formation in the zebrafish gut. *Nat. Cell Biol.* **9,** 954–960 (2007).
14. Brady, D. C., Alan, J. K., Madigan, J. P., Fanning, A. S. & Cox, A. D. The transforming ρ family GTPase Wrch-1 disrupts epithelial cell tight junctions and epithelial morphogenesis. *Mol. Cell Biol.* **29,** 1035–1049 (2009).
15. Holt, O. *et al.* Slp1 and Slp2-a localize to the plasma membrane of CTL and contribute to secretion from the immunological synapse. *Traffic* **9,** 446–457 (2008).
16. Kuroda, T. S. & Fukuda, M. Rab27A-binding protein Slp2-a is required for peripheral melanosome distribution and elongated cell shape in melanocytes. *Nat. Cell Biol.* **6,** 1195–1203 (2004).
17. Yu, M. *et al.* Exophilin4/Slp2-a targets glucagon granules to the plasma membrane through unique Ca2+-inhibitory phospholipid-binding activity of the C2A domain. *Mol. Biol. Cell* **18,** 688–696 (2007).
18. Sato, T. *et al.* The Rab8 GTPase regulates apical protein localization in intestinal cells. *Nature* **448,** 366–369 (2007).
19. Fukuda, M., Saegusa, C. & Mikoshiba, K. Novel splicing isoforms of synaptotagmin-like proteins 2 and 3: identification of the Slp homology domain. *Biochem. Biophys. Res. Commun.* **283,** 513–519 (2001).
20. Chavas, L. M. *et al.* Elucidation of Rab27 recruitment by its effectors: structure of Rab27a bound to Exophilin4/Slp2-a. *Structure* **16,** 1468–1477 (2008).
21. Fukuda, M. Versatile role of Rab27 in membrane trafficking: focus on the Rab27 effector families. *J. Biochem.* **137,** 9–16 (2005).
22. Di Paolo, G. & De Camilli, P. Phosphoinositides in cell regulation and membrane dynamics. *Nature* **7112,** 651–657 (2006).
23. Zoncu, R. *et al.* Loss of endocytic clathrin-coated pits upon acute depletion of phosphatidylinositol 4,5-bisphosphate. *Proc. Natl Acad. Sci. USA* **104,** 3793–3798 (2007).
24. Bolasco, G. *et al.* Loss of Rab27 function results in abnormal lung epithelium structure in mice. *Am. J. Physiol. Cell Physiol.* **300,** 466–476 (2011).
25. van IJzendoorn, S. C., Tuvim, M. J., Weimbs, T., Dickey, B. F. & Mostov, K. E. Direct interaction between Rab3b and the polymeric immunoglobulin receptor controls ligand-stimulated transcytosis in epithelial cells. *Dev. Cell* **2,** 219–228 (2002).
26. Schlülter, O. M., Schmitz, F., Jahn, R., Rosenmund, C. & Südhof, T. C. A complete genetic analysis of neuronal Rab3 function. *J. Neurosci.* **24,** 6629–6637 (2004).
27. Fukuda, M., Kanno, E., Saegusa, C., Ogata, Y. & Kuroda, T. S. Slp4-a/granuphilin-a regulates dense-core vesicle exocytosis in PC12 cells. *J. Biol. Chem.* **277,** 39673–39678 (2002).
28. Tsuboi, T. & Fukuda, M. The Slp4-a linker domain controls exocytosis through interaction with Munc18-1.syntaxin-1a complex. *Mol. Biol. Cell* **17,** 2101–2112 (2006).
29. Fukuda, M., Imai, A., Nashida, T. & Shimomura, H. Slp4-a/granuphilin-a interacts with syntaxin-2/3 in a Munc18-2-dependent manner. *J. Biol. Chem.* **280,** 39175–39184 (2005).
30. Low, S. H. *et al.* The SNARE machinery is involved in apical plasma membrane trafficking in MDCK cells. *J. Cell Biol.* **141,** 1503–1513 (1998).
31. Schluter, M. A. *et al.* Trafficking of Crumbs3 during cytokinesis is crucial for lumen formation. *Mol. Biol. Cell* **20,** 4652–4663 (2009).
32. Gomi, H., Mizutani, S., Kasai, K., Itohara, S. & Izumi, T. Granuphilin molecularly docks insulin granules to the fusion machinery. *J. Cell Biol.* **171,** 99–109 (2005).

DOI: 10.1038/ncb2541

METHODS

Two-step functional screening (microarrays, RT–qPCR, RNAi, Oncomine). A microarray-based differential expression analysis was conducted using the Affymetrix Canine Genome 2.0 platform. MDCK type II cells were grown in P100 dishes to form 2D monolayers or 3D cysts in Matrigel (at 10^5 cells ml^{-1}). Total RNA was isolated at 36 h and purified using RNeasy (Qiagen) and 5 μg of RNA was submitted for microarray analysis ($n = 3$) using the Affymetrix platform at Parque Científico de Madrid (Cantoblanco). The raw microarray data are deposited in NCBI GEO (Gene Expression Omnibus), accessible online using the number GSE32495. A LiMMA (false discovery rate < 0.05) analysis revealed a set of 1,597 upregulated genes. The resulting data set was analysed to select a maximum of 100 upregulated genes for qPCR validation. To further examine this selection, we used bioinformatic/bibliographic searches to analyse all 1,597 upregulated genes for previously published references into function, and Gene Ontology terms from human or mouse orthologues in NCBI databases. We selected genes with Gene Ontology terms, or references into function related to processes or mechanisms involved in changes in cell signalling, cell architecture and organ morphogenesis.

The list included a comprehensive list of Gene Ontology terms related to cell polarity, membrane trafficking, cell-to-cell junction assembly and remodelling, cell cycle regulation, cytoskeleton regulation and cell division, among others (complete list on demand). The second selection approach used STRING software (http://string-db.org/) to select genes interacting with pathways previously known to have a role in epithelial architecture or morphogenesis. From the resulting list, we selected 99 genes on the basis of bibliographic research and designed specific primers to perform qPCR analysis validation of their overexpression pattern in 3D cyst formation.

After qPCR validation, a stealth siRNA library was custom designed to target 47 validated candidate genes (Invitrogen). To perform the siRNA screening, MDCK cells were transfected with siRNA using Nucleofector-II (Lonza). Transfected cells were cultured for two days in 3D conditions and RNA extracts were analysed by RT-qPCR to check the silencing efficiency (Supplementary Table S2). Gene expression silencing was verified by RT–qPCR procedures (SYBR RT-qPCR premix, Applied Biosystems), and normalizing to GAPDH or HPRT expression. For functional analyses, transfected MDCK cells were grown for three days in Matrigel to form cysts, and lumen formation efficiency was quantified by confocal microscopy using the following markers to assess lumen formation: localization of the apical protein Podxl, integrity of the actin cytoskeleton (F-actin; phalloidin), adherens junctions (β-catenin), tight junctions (ZO-1), nuclei (DNA; DAPI).

Antibodies. Antibodies against α-tubulin (1:5,000; T9026, Sigma-Aldrich), Rab27a (1:200; R4655, Sigma-Aldrich), GFP (1:500; a5455, Invitrogen), Rab8a (1:1,000, 610845, BD Biosciences), mRFP/Cherry (1:250; PM005, MBL), Stx3 (1:200; Ab4113, Abcam), GST (1:5,000; sc138), β-catenin (1:1,000, sc7199) and Slp4-a (1:100; 34448) from Santa Cruz Biotechnology were commercial primary antibodies. The Slp2-a antibody was raised as a polyclonal serum against the Slp2-a^{SHD} region and used as previously described[33]. Podxl antibody was a gift from the Ojakian laboratory (State University of New York Downstate Medical Center, USA). ZO-1 (1:500; R4076) was from DSHB. Peroxidase-conjugated donkey anti-mouse IgG and anti-rabbit IgG were used as secondary antibodies for western blots (Jackson ImmunoResearch Laboratories). Alexa Fluor-conjugated secondary antibodies (Alexa Fluor 405, 488, 555 or 647; Invitrogen) and TOPRO-3 or DAPI (for nuclear/DNA staining) were used in the microscopy protocols.

Plasmids. Slp2-a and Slp4-a (full length and mutants) were cloned into either pEGFP-C1/C2 or pmCherry-C1 vector (Takara Bio). The human Slp4-a complementary DNA template was from Open Biosystems (Thermo Fisher). Plasmids provided were: pEGFP-Slp1 (J. Peränen, University of Helsinki, Finland), pEGFP-STX3a (M. ter Beest, University of Chicago, Illinois, USA), pENTR-Rab3a/b/c/d (B. Goud, Institut Curie, Paris, France), pEGFP-Rab8a (M. Montoya, CNIC, Madrid, Spain) and pEGFP-Rab27a/b (WT and dominant negative) (J. Hammer, NIH, USA). For bacterial expression of GST-tagged full-length and mutant proteins, Slp2-a and Slp4-a were cloned into pGEX-4T1 vector (Promega) or pDEST15 (Invitrogen). Slp2-a (V18A, E11A/R32A; ref. 16), and Slp4-a (V21A, W118S, I18A, K > Q; refs 17,27) mutants were generated using Quickchange XL (Stratagene). To disrupt C2 domain–lipid interactions in Slp4-a (C2AB K > Q; K410Q, K412Q, K416Q, K564Q, K566Q, K571Q), three of four lysine residues of the PIP-binding consensus motifs present in synaptotagmin and synaptotagmin-like family C2 domains [K(K/R)KTXXK(K/R)] were mutated to glutamine in both C2 domains, as reported for Slp2-a (ref. 16). To disrupt Stx interactions in Slp4-a, the linker domain of Slp4-a was substituted for the linker domain of Slp5 (GFP–Slp454a) by subcloning the chimaeric SHD$_{Slp4}$-linker$_{Slp5}$ fragment from a previously reported Slp454b construct[28] into a GFP–Slp4-a^{C2AB} plasmid. T7-tagged Slp4-a, Slp454a and Slp4-a linkers were used for *in vitro* Stx3 binding experiments as previously reported[28,29]. The Slp4-a construct lacking the Stx3-interacting amino acids of the linker domain (Δ305–354) was cloned into pEGFP-C1. All constructs were verified by sequencing.

Cells and 3D culture. T23-MDCKII and MDCKII cells were grown as described previously[9]. MDCK cells stably expressing GFP–Slp2-a (full length and mutants), Cherry–Slp2-a, GFP–Rab27a, GFP–Rab8a and PLCδ-PH–GFP (PHD–GFP) were made by co-transfection with the blasticidin-resistant gene and selected for ten days with 0.5 μg ml^{-1} blasticidin. MDCK cells stably expressing GFP–Slp1, GFP–Stx3 or GFP–Slp4-a (full length and mutants) were selected for ten days using G418 (0.5 mg ml^{-1}). Cysts and Transwell cultures were prepared as described before[34].

Microscopy. Immunofluorescence microscopy of cysts was performed as previously described[9,34]. Per condition, >100 cysts per experiment were analysed. For early time points, cysts were grown up to 24 h and two/three-cell stage cysts were classified on the basis of Podxl and β-catenin localization either as: formed preapical-patch or presence of internal vesicles.

RNAi. The RNAi sequences and qPCR primers are listed in Supplementary Table S3. Briefly, 25 nucleotide stealth siRNA duplexes targeting messenger RNA sequences of canine Slp2-a were purchased from Invitrogen. Sequences were submitted to BLAST search to ensure targeting specificity. For siRNA transfection, MDCK cells were trypsinized and then nucleofected (Lonza) with siRNA duplexes or scrambled siRNA. After 24-h incubation, cells were resuspended and plated in 12-well plates and in coverglass chambers coated with Matrigel to grow cysts. Total cell lysates from 3D cultures were analysed by western blotting or RT-qPCR to confirm the siRNA efficiency.

Stable RNAi was achieved by viral short hairpin RNA (shRNA), essentially as previously described[7]. In all instances, knockdown was verified by western blot or RT-qPCR procedures (Brilliant-II SYBR Green Kit, Agilent), and normalizing to GAPDH expression. RNAi and RT-qPCR primers are presented in Supplementary Table S3. *Stx3* shRNA is as described previously[35]. *Slp1* and *Slp4-a* shRNA lentiviruses were constructed in pLKO.1-puro according to the Addgene pLKO.1 protocol (www.addgene.org) using iRNAi (www.mekentosj.com), and target sequences were based on an (AA)N19 algorithm. RNAi sequences were submitted to BLAST (NCBI) to verify target specificity, with SYTL4 sequences targeting common regions to Slp4-a and Slp4-b transcripts. GFP-tagged human Slp4-a, which is not targeted by anti-canine shRNA, was used for Slp4-a knockdown and rescue experiments.

Virus production and transduction. Lentivirus production was performed essentially as previously described[7]. For lentivirus transductions, subconfluent MDCK cultures, 1–4 h after plating, were infected with virus-containing supernatants for 12–16 h at 37 °C. Viral supernatants were then diluted 1:1 with growth medium, and cultured for a further 48 h. Transduced cells were selected by passage into appropriate antibiotic-containing medium. Puromycin (5 μg ml^{-1}), and blasticidin (12.5 μg ml^{-1}) were used.

Statistics. Single lumen formation was quantified as previously described[7]. The percentage of cysts with a single lumen was determined, and normalized to control cysts as 100%. Values are mean ± s.d. from ≥3 replicate experiments, with $n \geq 100$ cysts per replicate. For RT-qPCR experiments, the percentage of remaining mRNA in each knockdown condition was normalized to the HPRT level, and represented as a percentage of the control (scramble shRNA) mRNA levels. The significance was calculated using a paired, two-tailed Student's *t*-test. $^{*}P < 0.05$, $^{**}P < 0.001$.

Rab–GTPase pulldown. Rab GTPase–Slp protein pulldowns were performed using HEK293T cells overexpressing GFP-tagged Rab proteins, and GST-tagged Slp proteins. HEK293T cells expressing GFP-tagged Rab proteins were lysed in 0.1% SDS, 1% Triton X-100, 0.5 mM dithiothreitol and ×1 TBS buffer with a protease inhibitor cocktail and sodium orthovanadate. Cell debris and nuclei were removed by centrifugation at 14,000*g* for 2 min at 4 °C, and lysates were precleared and incubated in rotation with 100 ng of the relevant GST protein-loaded beads (GE Amersham) for 30 min, using GST alone as the control, in the presence of a non-hydrolysable GTP analogue (Sigma). Beads were centrifuged and washed five times, dried using aspiration, and resuspended in 40 μl Laemmli buffer before western blot analysis.

Co-immunoprecipitation assays. Co-immunoprecipitation assays in COS-7 cells were performed essentially as described previously[28,29]. In brief, pEF-FLAG-Stx3, pEF-FLAG-Munc18-2, pEF-T7-Slp454 (a linker domain-swapping construct between Slp4-a and Slp5 (ref. 28)) or pEF-T7-Slp4a linker deletion constructs (that is, linker, amino acids 144–354; F1, amino acids 144–240; F2, amino acids 215–304; and F3, amino acids 272–354) were transfected into COS7 cells by using Lipofectamine 2000 (Invitrogen) according to the manufacturer's instructions.

Cells were collected 48 h after transfection and homogenized in a homogenization buffer[28,29]. After removal of insoluble materials by centrifugation, cell lysates were obtained. The associations between T7-tagged proteins and FLAG-tagged Stx3/Munc18-2 in the cell lysates were evaluated by immunoprecipitation using anti-T7 tag antibody-conjugated agarose beads (Merck Biosciences) as described previously[36]. Immunoreactive bands were visualized with horseradish peroxidase (HRP)-conjugated anti-T7 tag antibody (1:10,000 dilution; Novagen, 69522-4) and HRP-conjugated anti-FLAG tag M2 antibody (1:10,000 dilution; Sigma-Aldrich, A8592) and detected by enhanced chemiluminescence (GE Healthcare). The Rab–GTPase co-immunoprecipitation assay was performed as previously described[7].

PIP-strip and lipid bead protein binding assays. A solution of 1 μg ml^{-1} of purified protein (GST, GST–Slp2-a, GST–Slp4-a) was incubated with PIP-strip membranes according to the instructions of the manufacturer (Echelon Bioscience). Lipid beads (Echelon) prepared with different phosphoinositides or phosphatidylserine were incubated with 2 μg of purified GST–C2A or GST–C2B from Slp2-a or Slp4-a, washed five times, dried and resuspended in 100 μl sample buffer before western blot analysis. Enhanced chemiluminescence blotting of membranes was developed by immunostaining with an anti-GST antibody (Sigma-Aldrich) and HRP-conjugated donkey anti-mouse IgG (Jackson Immunoresearch).

33. Imai, A., Yoshie, S., Nashida, T., Shimomura, H. & Fukuda, M. The small GTPase Rab27B regulates amylase release from rat parotid acinar cells. *J. Cell Sci.* **117,** 1945–1953 (2004).
34. Rodriguez-Fraticelli, A. E. *et al.* The Cdc42 GEF Intersectin 2 controls mitotic spindle orientation to form the lumen during epithelial morphogenesis. *J. Cell Biol.* **189,** 725–738 (2010).
35. Schuck, S., Manninen, A., Honsho, M., Fullekrug, J. & Simons, K. Generation of single and double knockdowns in polarized epithelial cells by retrovirus-mediated RNA interference. *Proc. Natl Acad. Sci. USA* **101,** 4912–4917 (2004).
36. Fukuda, M. & Kanno, E. Analysis of the role of Rab27 effector Slp4-a/Granuphilin-a in dense-core vesicle exocytosis. *Methods Enzymol.* **403,** 445–457 (2005).

DOI: 10.1038/ncb2536

nature cell biology

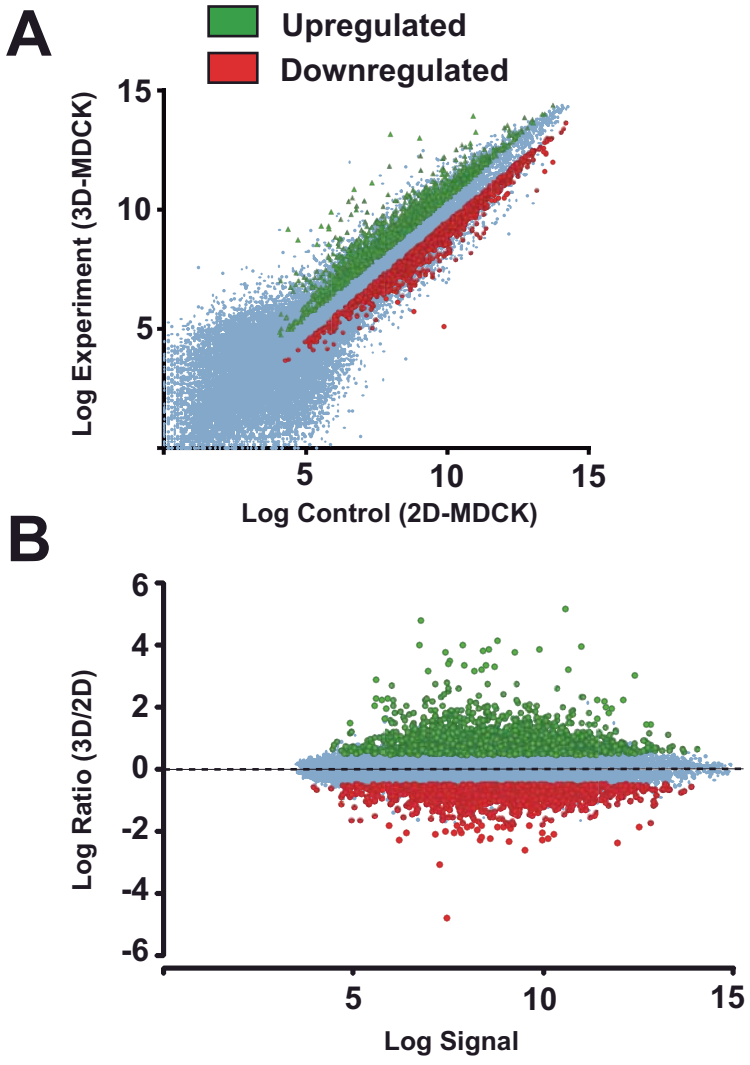

Figure S1 Transcriptional profiling of 3D vs. 2D MDCK cultures. **(A)** MDCK cells were grown in 2D and 3D conditions and purified RNA extracts were submitted for Canine Genome 2.0 Affymetrix cDNA chip microarray analysis. Mean results of overexpressed (green) and downregulated (red) genes are plotted. Significance of upregulated and downregulated genes was calculated using FDR-LiMMA analysis (FIESTA software). **(B)** Signal-ratio (3D/2D) M-A plot of microarray results presented in A.

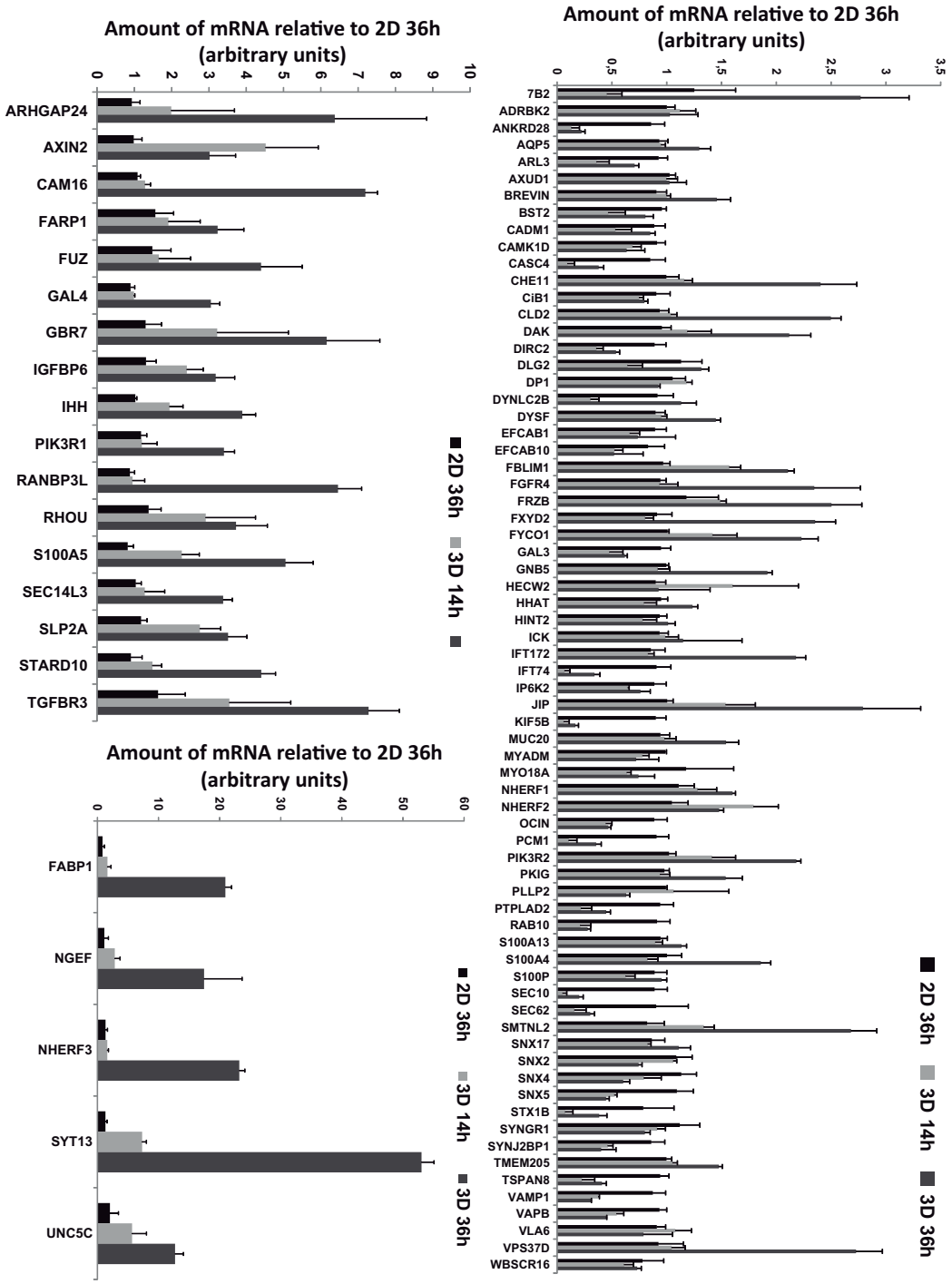

Figure S2 RT-qPCR validation of selected genes. Relative mRNA expression of a selected group of genes upregulated during cyst formation. MDCK cells were plated either in 2D, or 3D to grow cysts and lysates were collected for 2D at 36h, and at 14 and 36h in 3D. After mRNA extraction and cDNA polymerization, samples were analyzed by qPCR using gene-specific exon-spanning reactions and quantitative data was analyzed using SDS software (Applied Biosystems), and normalized to 2D expression levels. Different charts are used to distribute results in different scales using relative arbitrary units (top chart, ≤2-fold; bottom-left, ≤10-fold; bottom-right >10-fold). N=4.

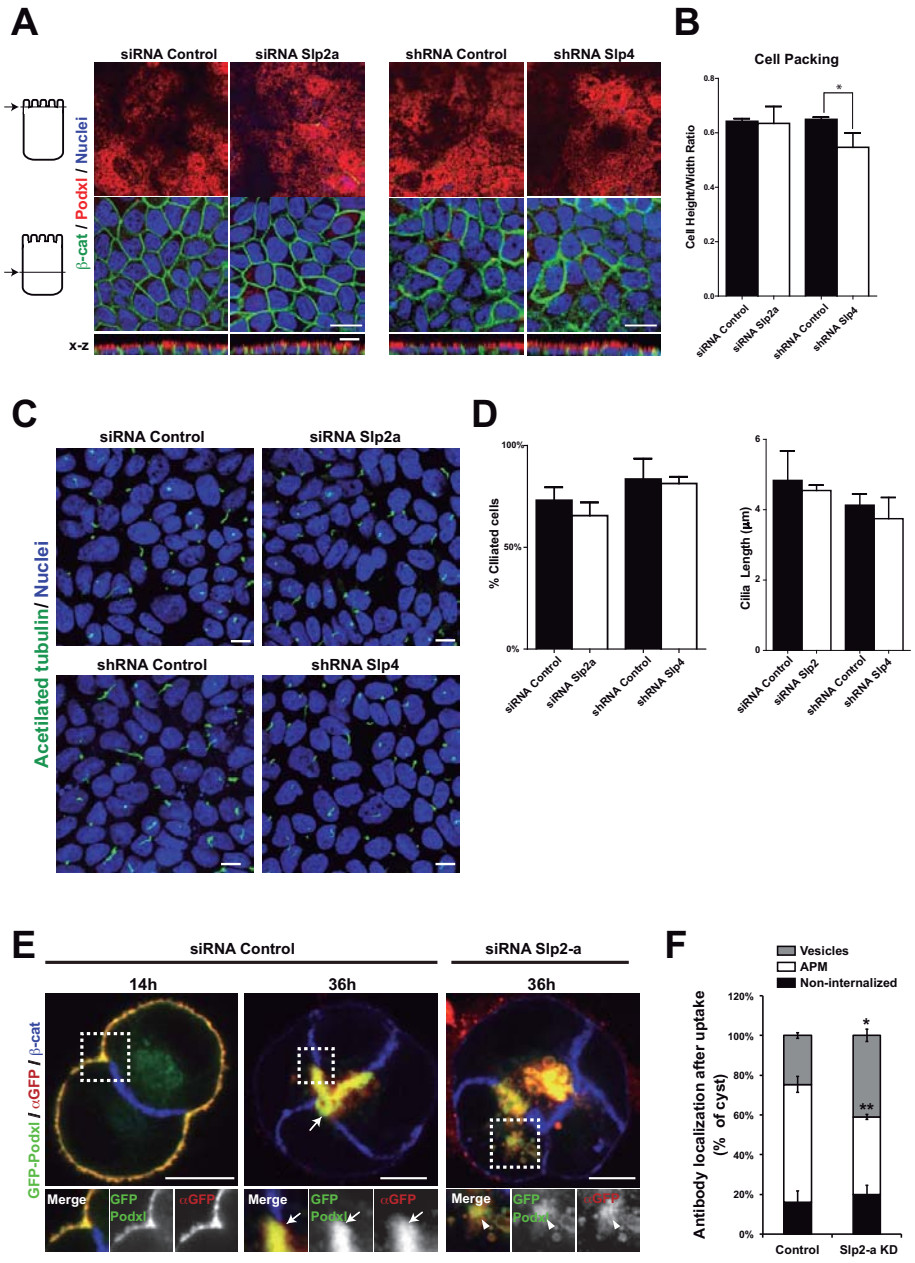

Figure S3 Slp-family proteins are not essential for 2D cell polarity or ciliogenesis. **(A)** Confocal microscopy images of 6d culture of MDCK cells in transwells. Cells transfected with Slp2-a siRNA or Slp4-a shRNA or controls were grown in a 2D-monolayer in transwells for 6d, fixed and stained to detect Podxl (red), β-catenin (green) and DNA (blue). Three confocal sections are shown for each treatment. Top panels show x-y apical section. Middle panels show x-y mid-height section. Bottom panels show x-z section. Bars, 20 μm. **(B)** Quantification of cell packing in monolayers shown in A. Cell packing measurements are cell height-width ratios of control (black bars) or Slp-KD cells (white bars). Values represent the average of three different experiments ± S.D. N=3 (> 150 cells/experiment, * P<0.05). **(C)** Confocal microscopy images of 6d culture of MDCK cells in transwells. Cells treated as in A were fixed and stained to detect primary cilia using acetyl-tubulin as a marker (green) and DNA (blue). Bars, 10 μm. **(D)** Quantification of ciliated cells and cilia length in monolayers shown in C. Values represent the average of three different experiments ± S.D. N=3 (> 100 cells/experiment). **(E)** Localization of apical and basolateral proteins in control cysts or silenced for Slp2-a. 14 hours after plating, cysts were treated with α-GFP for 30' at 4ºC, after washing, they were grown for 24 hours more, allowing lumen development to occur. Then, they were fixed and staining for β-catenin (blue) and a secondary antibody to detect the uptaken α-GFP. Inmediately after binding (14h), control and Slp2-a silenced cysts showed peripheral GFP-PCX (green) and α-GFP (red). 24 hours after treatment, control cysts presented podocalyxin, mainly in the apical plasma membrane (arrows), revealing PCX-GFP is transcytosed from peripheral membranes to the new developed apical membrane. However, Slp2-a knock-down cysts showed accumulations of vesicles containing GFP-PCX (green) and α-GFP (red), suggesting a defect in trafficking of transcytosed PCX. Yellow, colocalization of podocalyxin and bound antibodies, blue indicates β-catenin. Bar, 10 μm. **(F)** Quantification of antibody localization after uptake in control or Slp2-a KD cysts. Cysts in Figure A were analyzed by confocal microscopy. Cysts were classified as "vesicles", "apical plasma membrane" (APM) or "not-internalized" depending on the localization presented by the α-GFP (Red) antibody was found in internal vesicles, apical membrane or peripherally, respectively. Values are mean ± SD from three different experiments. N=3 (>100 cysts/experiment; **, P < 0.005; *, P<0.05).

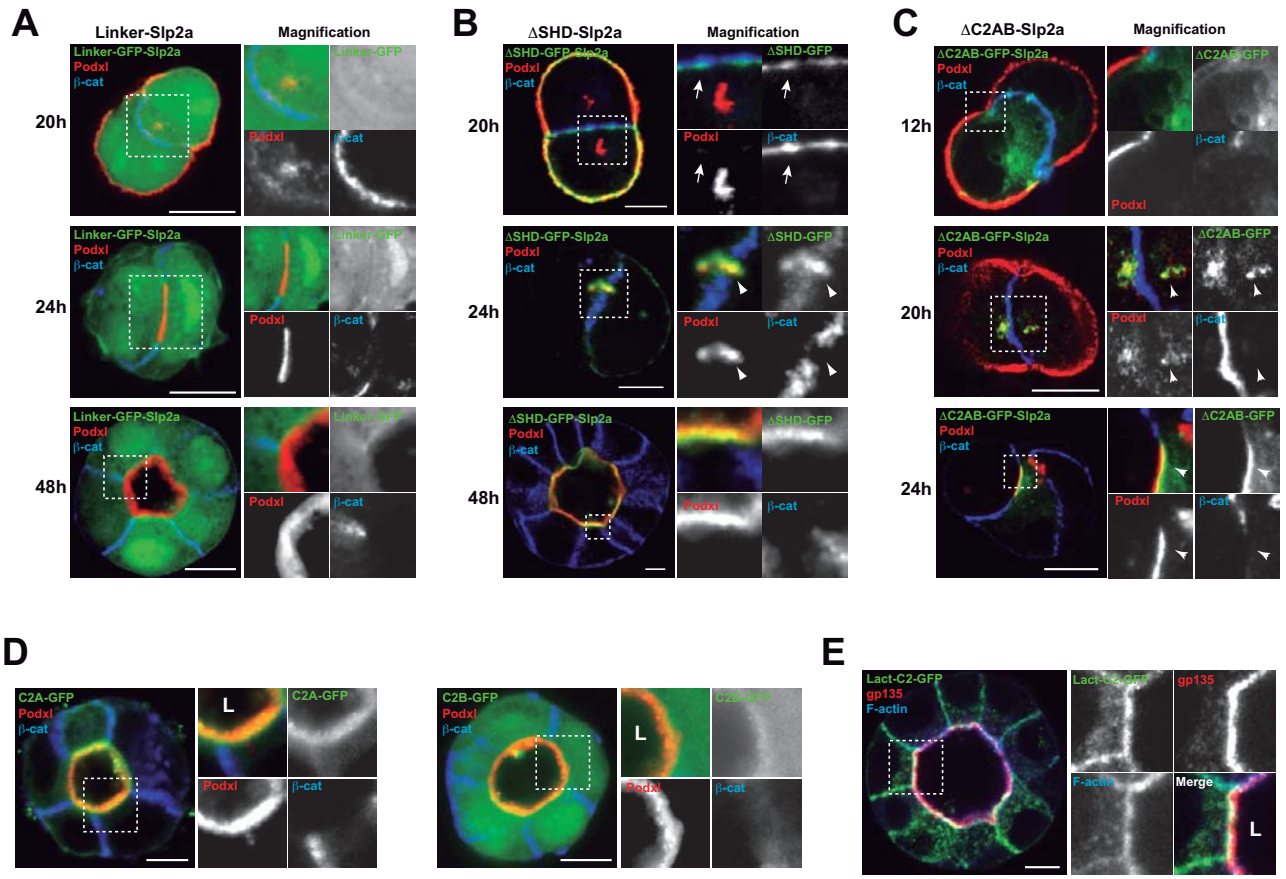

Figure S4 Slp2-a-ΔC2AB, Slp2-a-ΔSHD, Slp2-a-linker and PS-probe localization. **(A)** Confocal microscopy images of cysts stably expressing GFP-Slp2-a linker domain. Cells were plated to form cysts for 20-24-48h, fixed and stained to detect Podxl (red) and β–catenin (blue). Bar, 10 μm. **(B)** Confocal microscopy images of cysts stably expressing GFP- Slp2-a ΔSHD. Cells were plated to form cysts for 20-24-48h, fixed and stained to detect Podxl (red) and β–catenin (blue). Bar, 10 μm. **(C)** Confocal microscopy images of cysts stably expressing GFP- Slp2-a ΔC2AB. Cells were plated to form cysts for 12-24h, fixed and stained to detect Podxl (red) and β–catenin (blue). Bar, 10 μm. **(D)** Confocal microscopy images of cysts stably expressing GFP- Slp2-a C2A (left panels) and C2B (right panels). Cells were plated to form cysts for 12-24h, fixed and stained to detect Podxl (red) and β–catenin (blue). Bar, 10 μm. **(E)** Confocal microscopy images of cysts stably expressing a phosphatidylserine (PS) fluorescent probe (Lact-C2-GFP). Cells were plated to form cysts for 72h, fixed and stained to detect Podxl (red) and F-actin (blue). Note the lack of asymmetric polarization of PS at the PM. Bar, 10 μm.

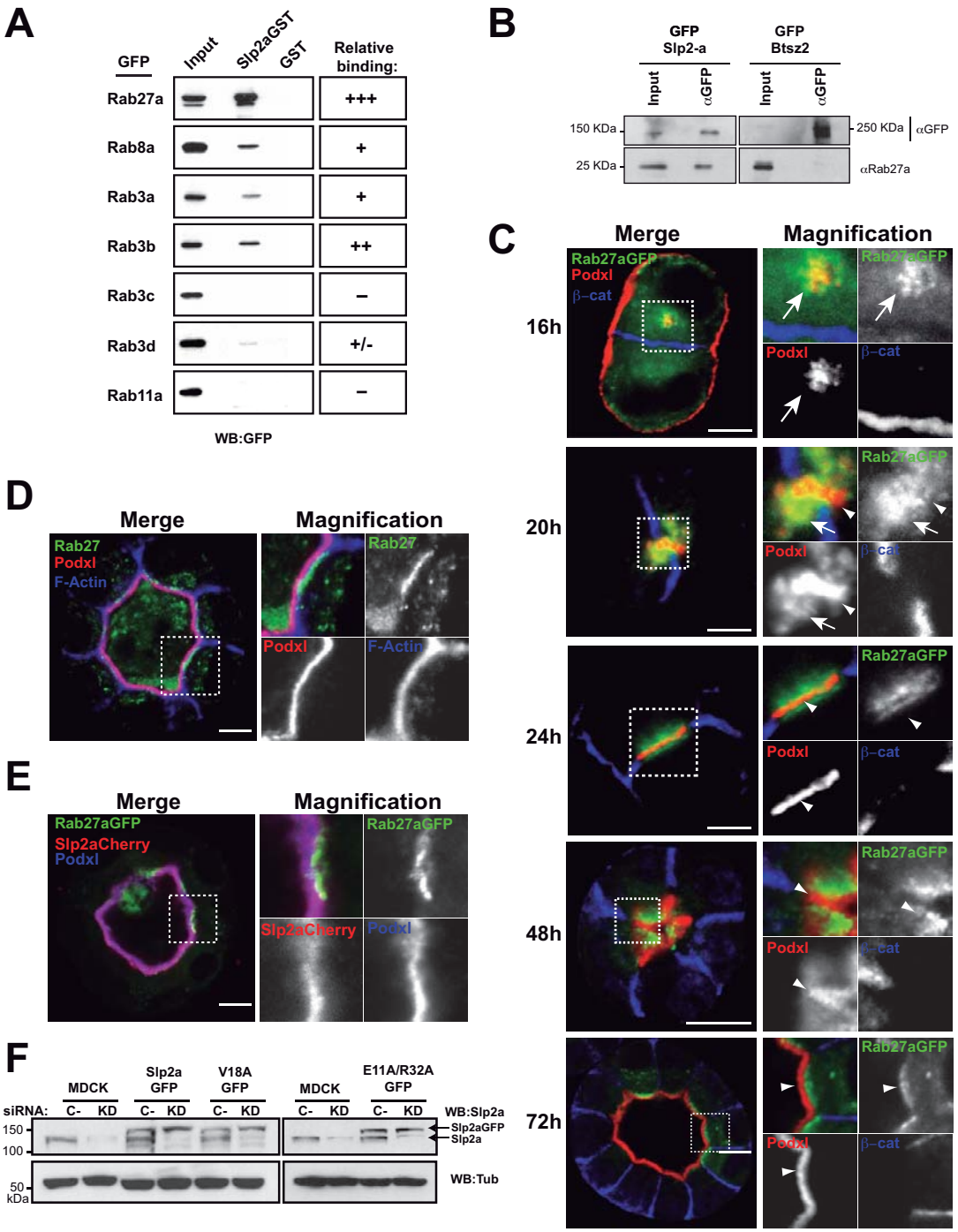

Figure S5 Slp2-a controls apical membrane trafficking through interaction with Rab27a. **(A)** Slp2-a-interacting Rab GTPases. GST-Slp2-a or GST (control) beads were used to pull-down fluorescent protein-tagged Rab3a/b/c/d, Rab8a, Rab11a or Rab27a from total cell lysates. The table indicates relative binding results from 3 different experiments. **(B)** Immunoprecipitation of Rab27-GTP in GFP-Slp2-a or GFP-Btsz2 MDCK cysts. GFP-Slp2-a or GFP-Btsz2 were immunoprecipiated using anti-GFP (or control) beads and analyzed to detect binding of endogenous Rab27. **(C)** Localization of GFP-Rab27a during cyst morphogenesis. MDCK cells stably expressing GFP-Rab27a were grown to form cysts and fixed after 16, 20, 24, 48 and 72h. Samples were stained for Podxl (red), and β-catenin (blue). Confocal microscopy images correspond to five different stages of lumen initiation (AP vesicle aggregation [16h], vesicle fusion [20h], preapical-patch formation [24h], lumen expansion [48h], and mature cyst [72h]). Arrowheads, Podxl-positive vesicles; arrows, lumen. Bar, 5 μm (left panels).**(D)** Confocal microscopy images of endogenous Rab27a/b. MDCK cells were plated to form cysts for 72h and stained to detect Rab27 (green), Podxl (red) and F-actin (blue). Bar, 10 μm. **(E)** Confocal microscopy images of Slp2-a and Rab27 in cysts at 72h. MDCK cells stably expressing Cherry-Slp2-a and GFP-Rab27a were grown as cysts and fixed at 4d and stained to detect Podxl (blue). Bar, 10 μm. **(F)** Western-blot of Slp2-a downregulation by siRNA in WT, V18A or E11A/R32A-Slp2-a-GFP stably expressing MDCK cells. Tubulin was used as loading control.

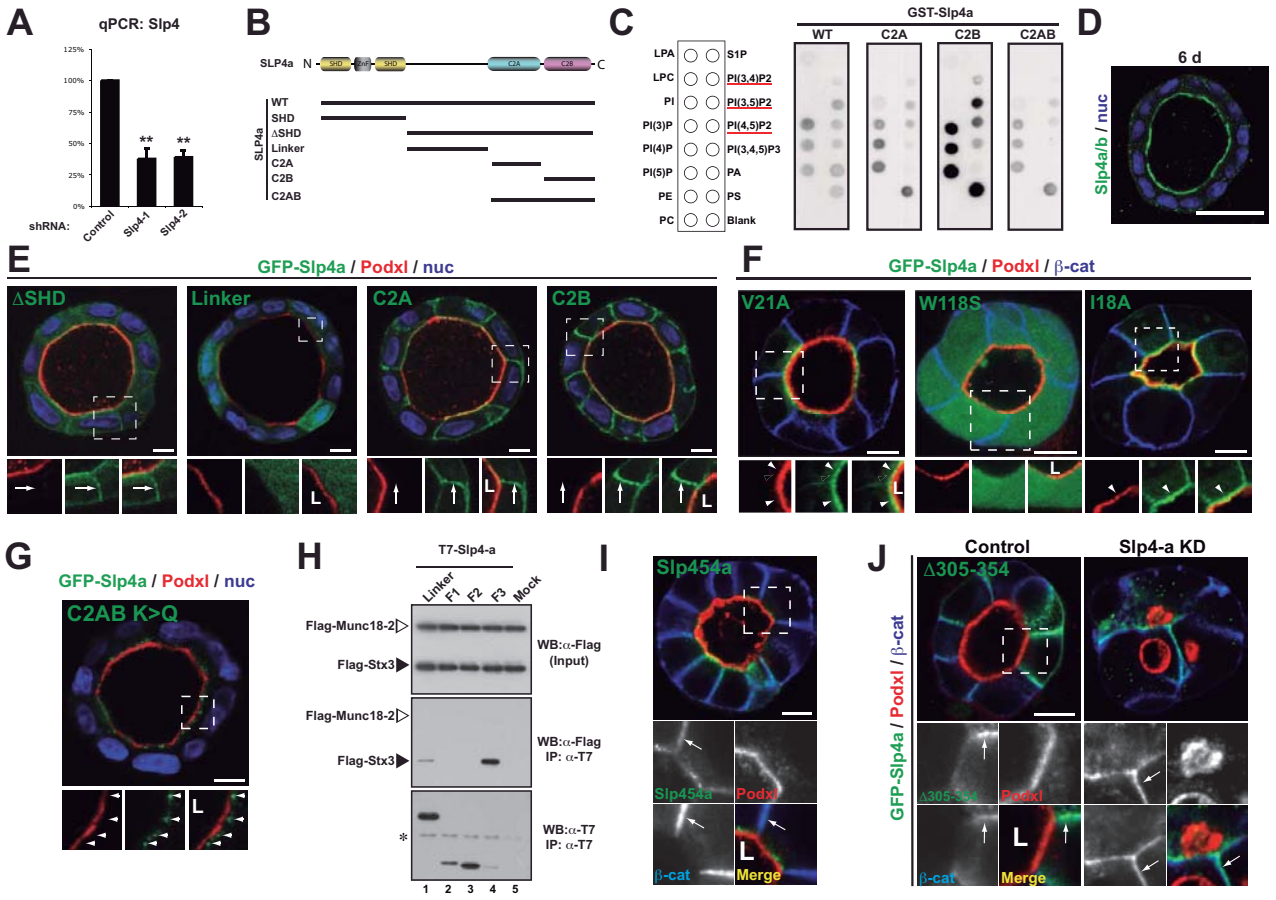

Figure S6 Localization of other mutants and constructs of Slp4-a. **(A)** Quantification of the silencing of Slp4-a by RT-qPCR. Values represent the average of ≥ three different experiments ± S.D., normalized to control levels (**, $P < 0.005$). **(B)** Scheme of Slp4-a/b, and Slp4-a domain fragments utilized. **(C)** PIP-binding assay. GST-tagged Slp4-a WT and C2A, C2B or C2AB were expressed and purified in bacteria. PIP-strip membranes were incubated with 1 μg/ml concentration of either GST-Slp4-a WT, C2A, C2B or C2AB fusion proteins and then membranes were blotted with an anti-GST antibody. A scheme of the PIP-strip membrane is shown (left panel). **(D)** Confocal microscopy images of 72h cysts stained with anti-Slp4-a antibody (green) and nuclei (blue). Note apical localization of Slp4-a. Bar, 20 μm. **(E)** Confocal microscopy images of cells stably transfected with GFP-Slp4-a fragments. Cells stably expressing GFP-Slp4-a linker, C2A, C2B or ΔSHD fragments were plated to form cysts for 72 h, fixed and stained to detect Podxl (red) and nuclei (blue). Arrowheads, subapical vesicular localization of Slp4-a. Arrows, BL PM localization of Slp4-a. Bar, 10 μm. **(F)** Confocal microscopy images of cells stably transfected with GFP-Slp4-a Rab GTPase mutants. Cells stably expressing GFP-Slp4-a V21A, W118S or I18A mutants were plated to form cysts for 48 h, fixed and stained to detect Podxl (red) and β-catenin (blue). Arrowheads, subapical vesicular localization of Slp4-a. Bar, 10 μm. **(G)** Confocal microscopy images of cells stably transfected with GFP-Slp4-a K>Q mutant which uncouples phospholipid binding. Cells were plated to form cysts for 48 h, fixed and stained to detect Podxl (red) and nuclei (blue). Arrowheads, subapical vesicular localization of Slp4-a. Bar, 10 μm. **(H)** Mapping of Slp4-a syntaxin binding site. Beads coupled with each T7-Slp4a linker deletion mutant (i.e., AA144-240; AA215-304; and, AA272-354) were incubated with FLAG-Munc18-2 and FLAG-Stx3, and co-immunoprecipitated FLAG-tagged proteins were detected with HRP-conjugated anti-FLAG antibody (Blot: anti-FLAG, middle panel). The asterisk indicates non-specific bands of immunoglobulin light chain used for the IP. Note that only the F3 construct exhibited Munc18-2-dependent Stx3 binding activity (lane 4), indicating that amino acids 305-354 of the Slp4a linker domain are required for Stx3 binding. **(I)** Confocal microscopy images of scramble shRNA expressing cells stably expressing GFP-Slp4-5-4-a chimera. Cells were plated to form cysts for 48 h, fixed and stained to detect Podxl (red) and βcatenin (blue). Arrows, lateral plasma membrane localization of Slp4-5-4-a. Bar, 10 μm. **(J)** Confocal microscopy images of Slp4-a or scramble shRNA expressing cells stably transfected with GFP-Slp4-aΔ305-354. Cells were plated to form cysts for 48 h, fixed and stained to detect Podxl (red) and βcatenin(blue). Arrows, lateral plasma membrane localization of GFP-Slp4-aΔ305-354. Bar, 10 μm.

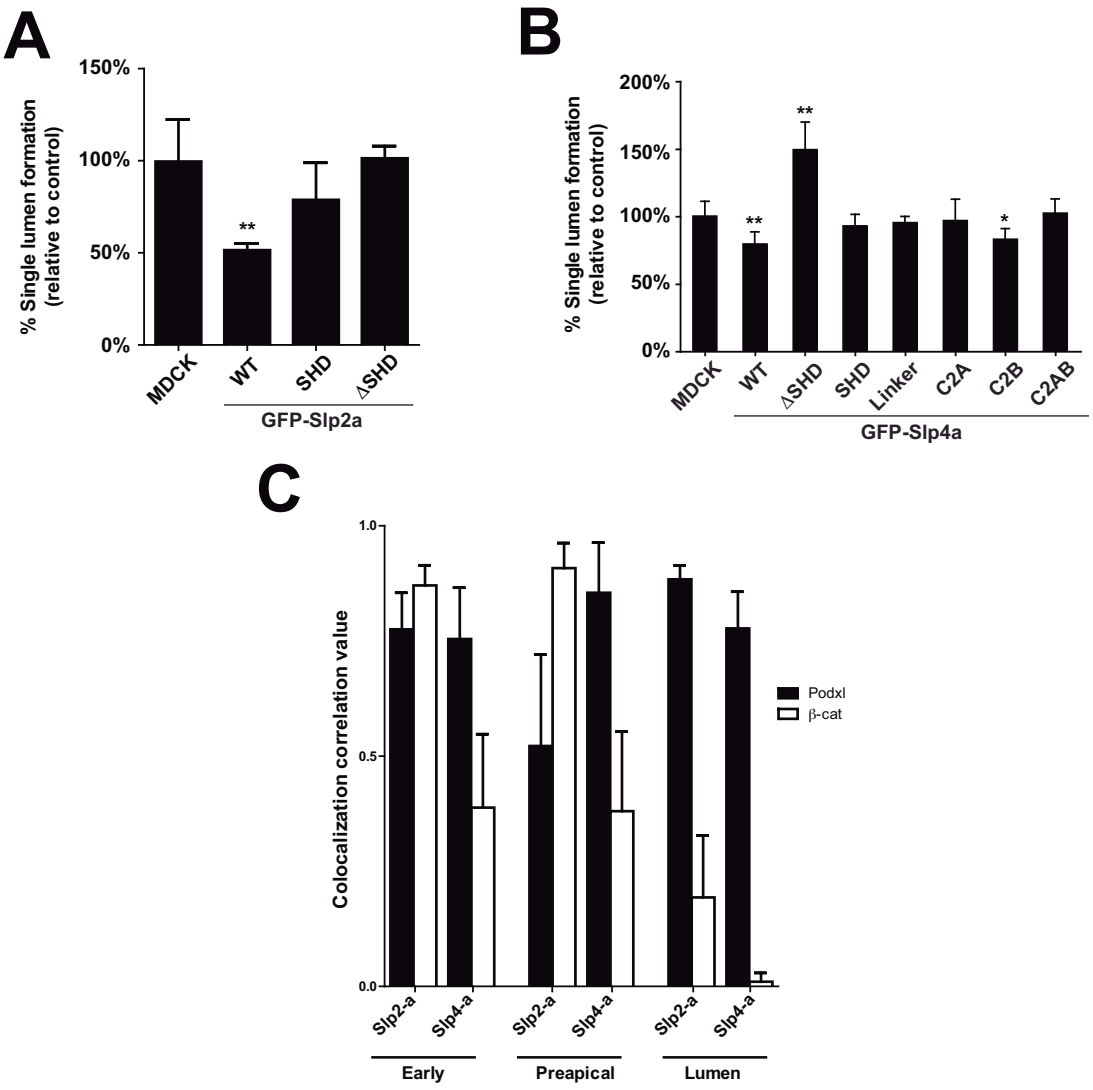

Figure S7 Overexpression and colocalization analysis of Slp2-a and Slp4-a during cyst morphogenesis. (A) Quantification of cysts with normal lumens in cells transiently overexpressing GFP (control), or GFP-Slp2-a constructs (WT, ΔSHD, or SHD). Values are mean ± SD from three different experiments. N=3(>100 cysts/experiment; *, $P < 0.05$; **, $P < 0.005$). (B) Quantification of cysts with normal lumens in cells stably overexpressing GFP (control), or GFP-Slp4-a constructs (WT, ΔSHD, SHD, Linker, C2A, C2B and C2AB-GFP). Values are mean ± SD from three different experiments. N=3 (>100 cysts/experiment; *, $P < 0.05$; **, $P < 0.005$). (C) Correlation analysis for Slp2-a and Slp4-a quantitative-colocalization using Podxl (black bars, apical membrane marker) and β-catenin (white bars, basolateral marker) in three different stages during cyst morphogenesis. GFP-Slp2-a or GFP-Slp4-a expressing cells were grown to form cysts for 12 (early), 24 (preapical) or 72h (lumen), fixed and stained to analyze Podxl or β-catenin localization. Quantitative colocalization analysis between GFP signal and each marker was performed using ImageJ. Values are mean ± SD from three independent cyst cultures. N=3 (>10 cysts/experiment).

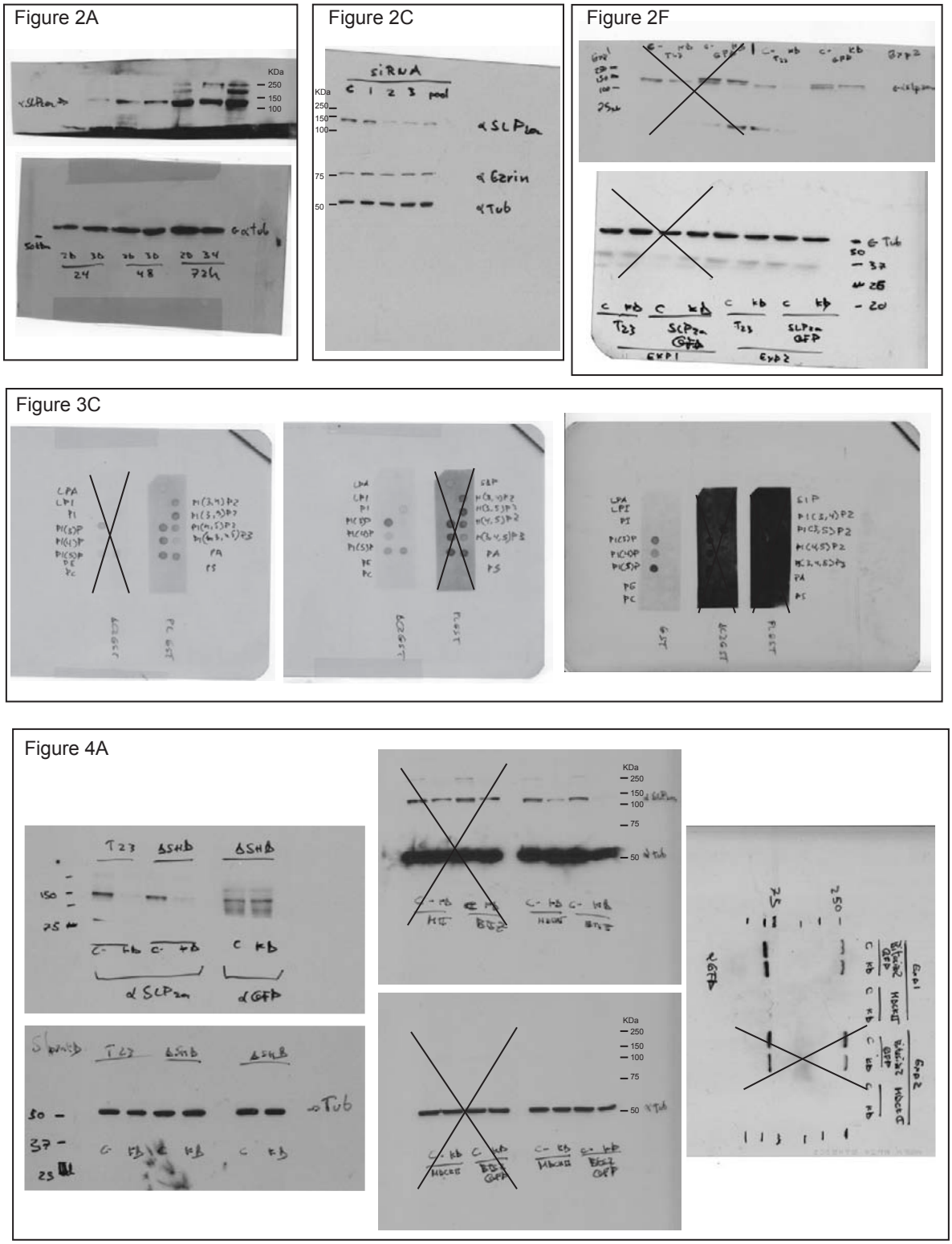

Figure S8 Scans of uncropped blots.

Figure 4G

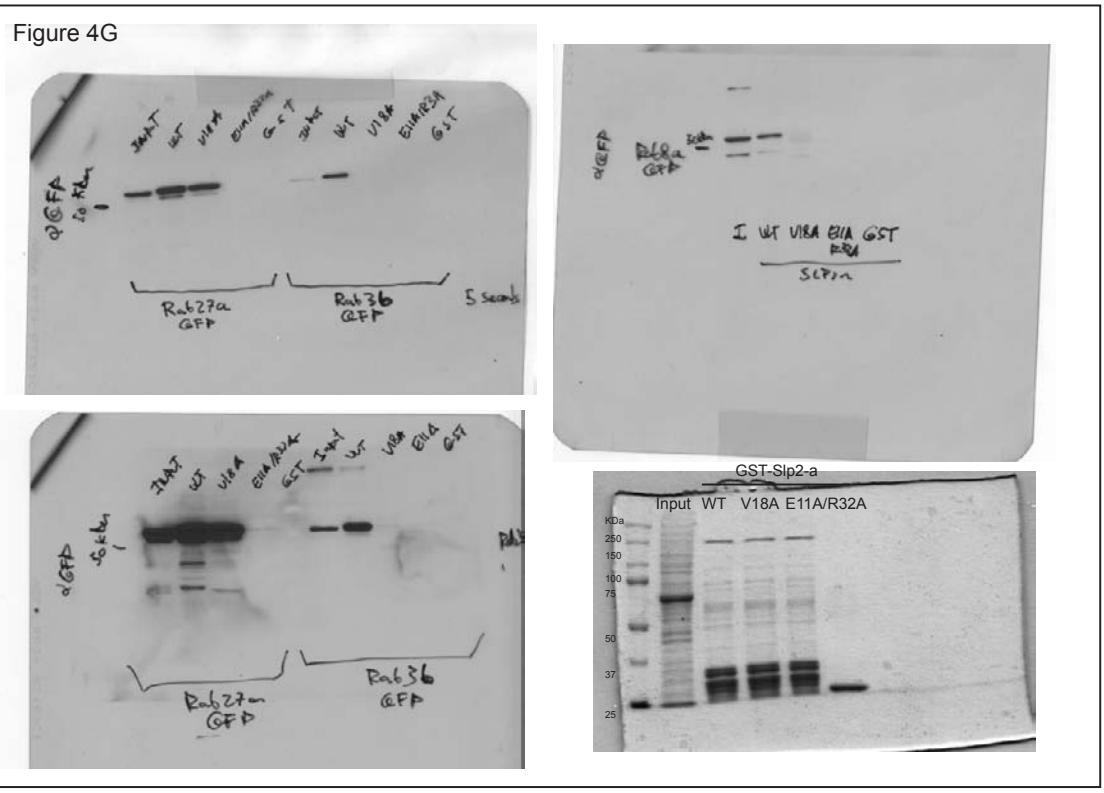

Figure 5G

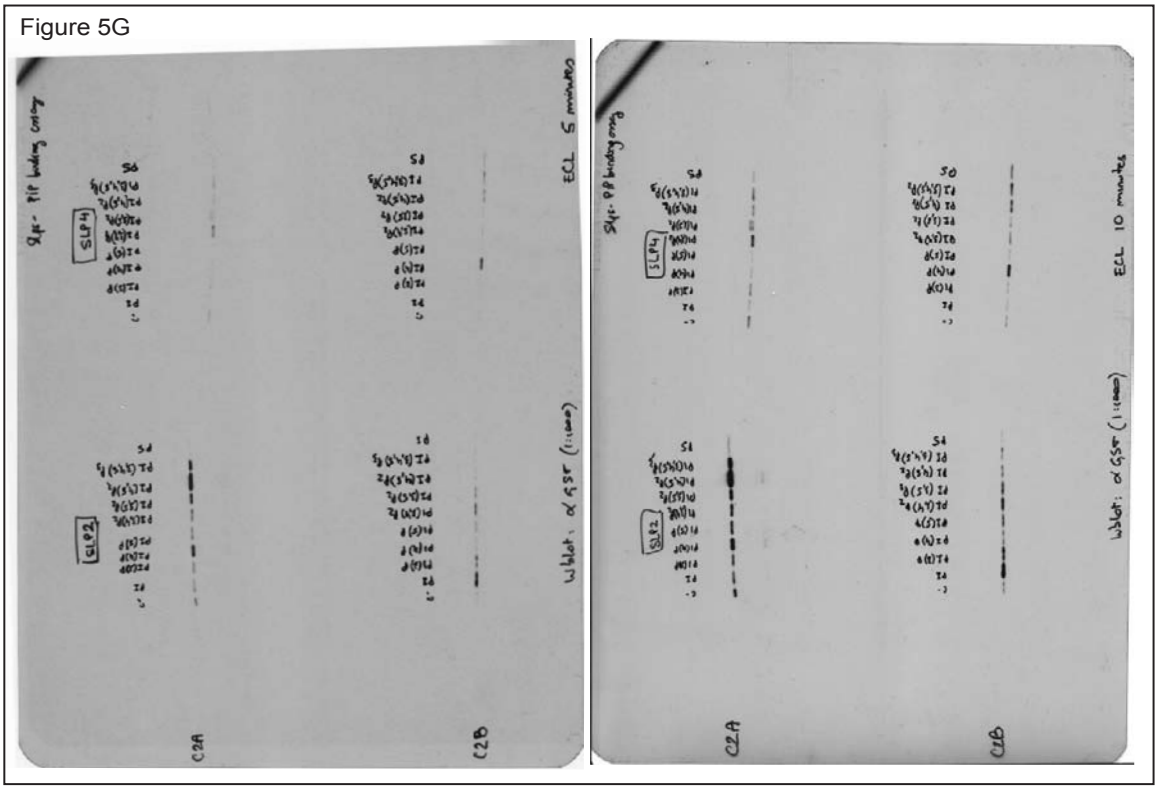

Figure S8 continued

Figure 6A

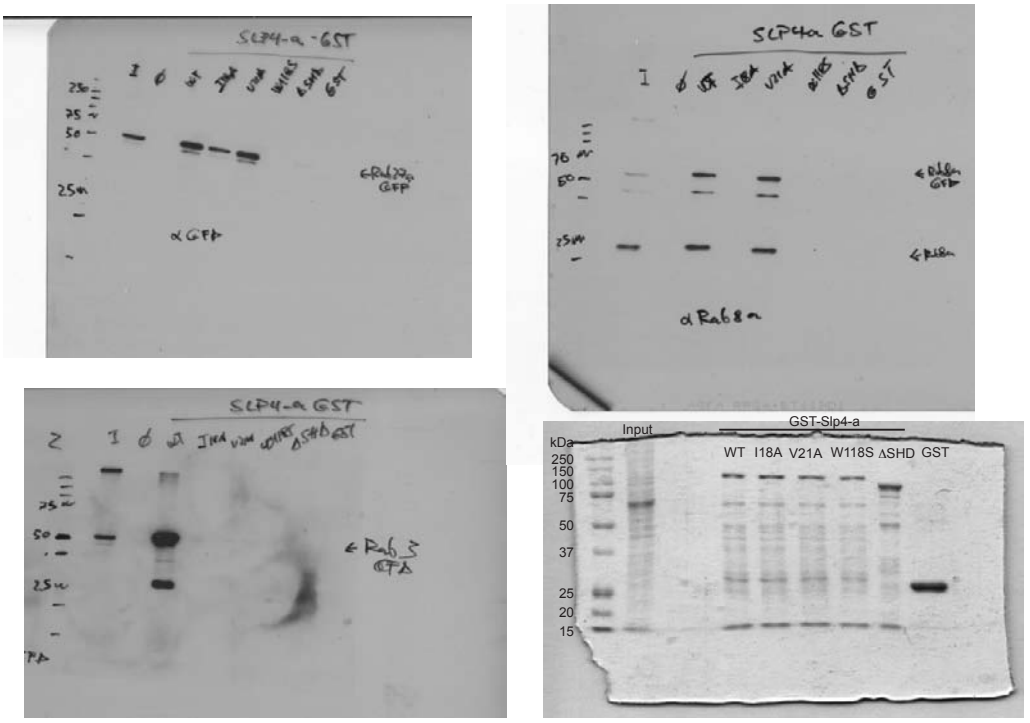

Figure 6D

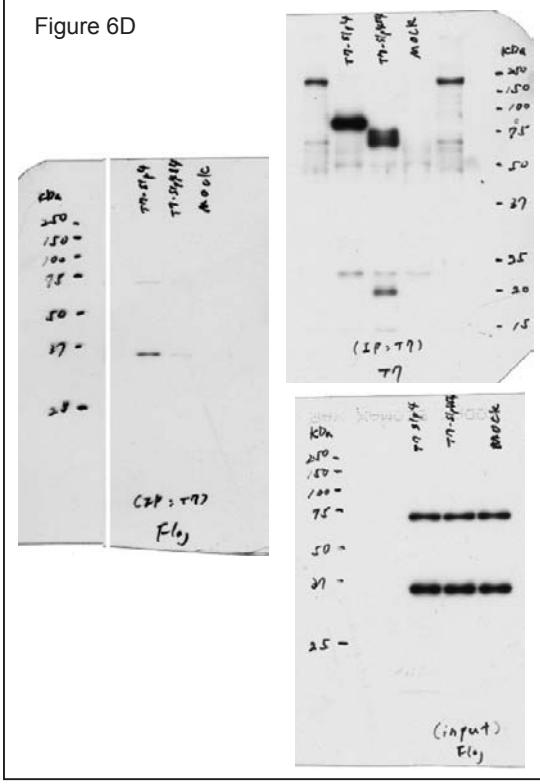

Figure 6J

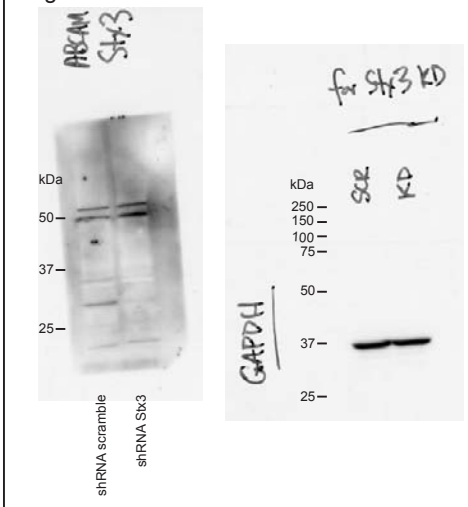

Figure S8 continued

Figure S5A

Figure S5B

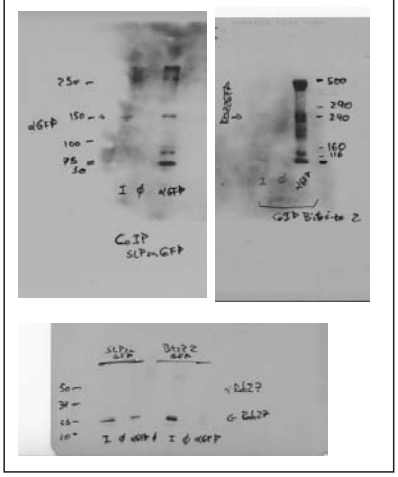

Figure S5F

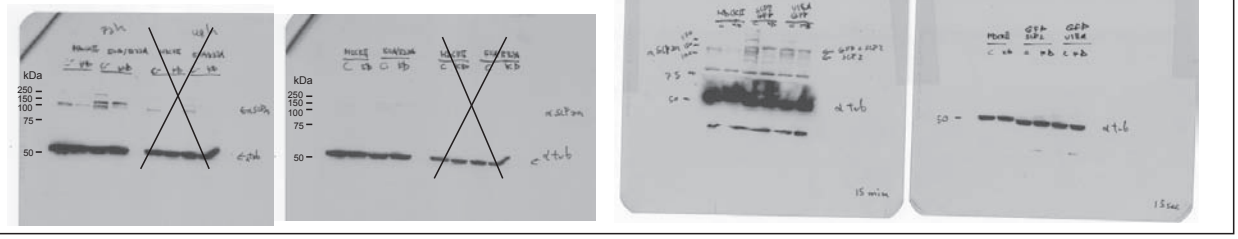

Figure S8 continued

Figure S6C

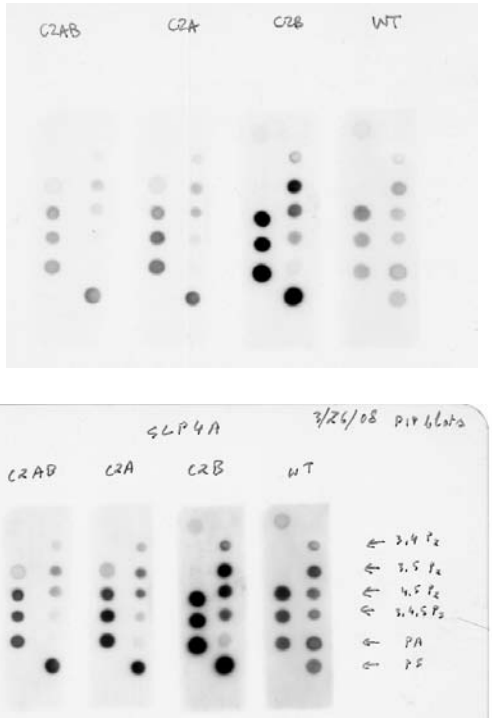

Figure S6H

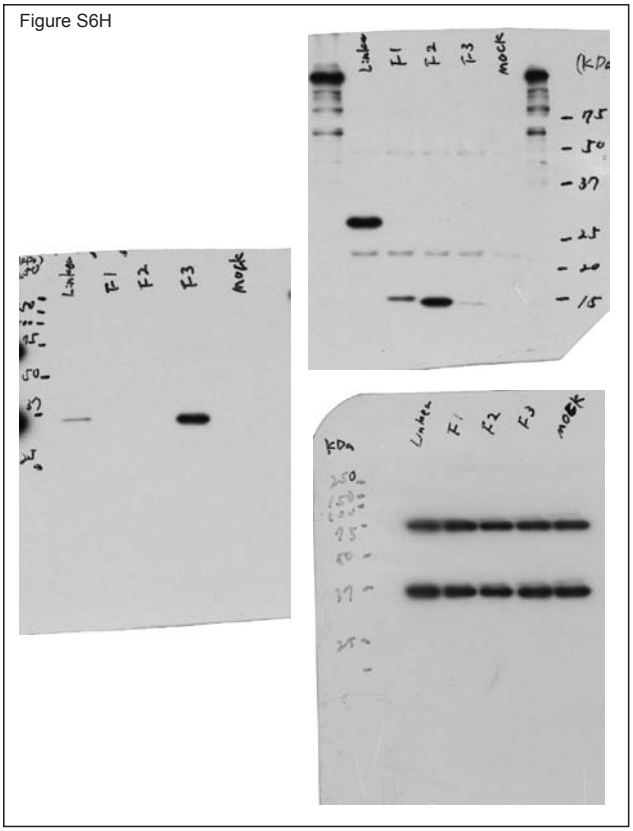

Figure S8 continued

Supplementary Table 1 RTqPCR validation of gene overexpression (2D, 14h, 36h)
Supplementary Table 2 RNAi and RNA expression analysis in silencing experiments
Supplementary Table 3 Quantification of lumen morphogenesis (RNAi screening)

Supplementary Video 1 Slp2-a apical localization depends on PIPs. MDCK cells stably expressing PHD-GFP and Slp2-Cherry were grown in cysts and set up for videomicroscopy. Cysts were treated with Ionomycin for 5 minutes during recording.

DEVELOPMENTAL REGULATION OF APICAL ENDOCYTOSIS IN VERTEBRATE TUBULAR EPITHELIA

***Alejo E. Rodriguez-Fraticelli**, Jennifer Bagwell, Minerva Bosch-Fortea, Gaelle Boncompain, Natalia Reglero-Real, Germán Andrés, Miguel A. Alonso, Jaime Millán, Franck Perez, Michel Bagnat y Fernando Martín-Belmonte.*

- enviado a Cell (junio de 2014)

PRESENTACION

Los órganos epiteliales se desarrollan gracias a un control exquisito de la proliferación y la diferenciación de células epiteliales. La endocitosis juega un papel decisivo en el control de la proliferación y la polaridad celular durante la morfogénesis epitelial en *Drosophila*. En vertebrados, sin embargo, el papel de la endocitosis en estos procesos no ha sido esclarecido aún.

En este artículo, nos propusimos dilucidar qué proteínas controlan el proceso de endocitosis durante el desarrollo de órganos epiteliales. Para ello, estas proteínas debían estar expresándose a bajos niveles en células no polarizadas, y deberían inducirse durante la morfogénesis epitelial en tres dimensiones. Utilizando el modelo de 3D-MDCK y el modelo del desarrollo del tubo intestinal del pez cebra, encontramos un gen, Plasmolipin (PLLP), común a ambos procesos, que se inducía más de 5 veces respecto a las células de partida. Para estudiar la función de PLLP, desarrollamos un alelo mutante *pllp*^{pd1116}, mediante el uso de edición genómica dirigida por TALENs, y un transgénico BAC, TgBAC(*pllp-spGFP*), reemplazando el codón de terminación de la secuencia codificante por un espaciador unido a GFP, mediante recombinación homóloga en bacterias.

Con estas herramientas, demostramos que PLLP es necesaria para la endocitosis apical en células intestinales, y su deficiencia causa defectos en la morfogénesis epitelial del intestino. Aprovechándonos de que las células MDCK expresaban PLLP en 3D, utilizamos este modelo para esclarecer el mecanismo molecular más finamente. La formación de un único lumen en cistos MDCK también requiere de PLLP. Subcelularmente PLLP se asocia a endosomas de reciclaje apicales, Rab11-positivos, y endosomas tardíos, Rab7-positivos. PLLP interacciona con un adaptador de clatrina, EpsinR, cuya función es reciclar receptores de fusión de membrana, SNAREs, desde los endosomas tardíos. Estudiando esta interacción, describimos que las funciones de PLLP

y EpsinR son fundamentales para el reciclaje de la SNARE de endosomas apicales Syntaxin 7.

El déficit en la expresión de PLLP ocasiona defectos en la maduración y acidificación endosomal, y esto conlleva un bloqueo en la endocitosis de receptores apicales, como Crumbs y Notch, tanto *in vivo* como *in vitro*, explicando los defectos en morfogénesis y diferenciación intestinal observados. Postulamos, de este modo, que la expresión de PLLP, regulada de forma precisa durante el desarrollo de órganos epiteliales, es necesaria para la morfogénesis y diferenciación epitelial.

TITLE: **Developmental regulation of apical endocytosis controls epithelial morphogenesis and differentiation in vertebrate tubular epithelia**

Authors:

Alejo E. Rodríguez-Fraticelli[1], Jennifer Bagwell[2], Minerva Bosch-Fortea[1], Gaelle Boncompain[3], Natalia Reglero-Real[5], Germán Andrés[4], Miguel A. Alonso[5], Jaime Millán[5], Franck Perez[3], Michel Bagnat[2*]and Fernando Martín-Belmonte[1†]

Affiliation:

[1]Department of Development and Differentiation, Centro de Biología Molecular "Severo Ochoa", CSIC-UAM, Madrid, 28049, SPAIN

[2]Department of Development and Cell Biology, Duke University, NC, 27708, USA

[3]Department of Subcellular Structure and Cellular Dynamics, UMR144, Institut Curie, Paris, 75005, FRANCE

[4]Electron Microscopy Core, Centro de Biología Molecular "Severo Ochoa", CSIC-UAM, Madrid, 28049, SPAIN

[5]Department of Immunology and Cell Biology, Centro de Biología Molecular "Severo Ochoa", CSIC-UAM, Madrid, 28049, SPAIN

Correspondence:

[†]fmartin@cbm.csic.es

[*] m.bagnat@cellbio.duke.edu

Highlights:

- PLLP is a novel protein that marks differentiation of posterior midgut absorptive cells of zebrafish larvae
- PLLP is required for apical endocytosis in the posterior midgut
- PLLP controls apical SNARE recycling in the endolysosomal pathway through the binding of the clathrin adaptor Epsin-R
- PLLP regulates Crumbs and Notch signaling by promoting endocytosis

Keywords: Endocytosis, Epithelial morphogenesis, SNARE, Cell polarity

SUMMARY

Epithelial organs develop through tightly coordinated events of cell proliferation and differentiation in which endocytosis seems to play a major role. Despite recent advances, how endocytosis is regulated during development in time and space is still not well understood. Here we found that Plasmolipin (PLLP), which marks a specific population of highly polarized absorptive zebrafish gut cells, is developmentally upregulated to induce apical endocytosis during epithelial morphogenesis. To perform this role, PLLP interacts with recycling adaptor EpsinR and the SNARE machinery at late endosomes to control the recycling and proper sorting of endosomal SNAREs into apical Rab11-positive compartment, which is essential to properly feed endocytosis. Furthermore, PLLP expression induces apical Crumbs (Crb) internalization and the activation of the Notch signaling pathway, which are crucial steps in the acquisition of cell polarity and differentiation of epithelial cells. We thus postulate that expression of PLLP promotes endocytosis to control epithelial morphogenesis and differentiation of the posterior midgut.

INTRODUCTION

Epithelial cells establish functional barriers which are essential for a wide variety of physiological processes, such as gas exchange in the lungs, or nutrient absorption in the intestine (Rodriguez-Boulan and Macara, 2014). To perform these roles the plasma membrane of epithelial tissues form specialized cellular junctions that separate different highly specialized membrane domains, apical or basolateral, preventing their lateral mixing. This in turn results in the segregation of physiological transport functions to the each membrane domain, as certain channels, receptors, and endocytic machineries are frequently found polarized to one of these domains (Apodaca et al., 2012). Endocytosis is one of such processes that become highly polarized (Eaton and Martin-Belmonte, 2014). Indeed, recent studies have described that immature epithelial sheets have a reduced rate of apical endocytosis that intensifies along development (Fabrowski et al., 2013), which suggests that epithelial cells acquire the ability to internalize material

specifically from the apical pole during differentiation. Interestingly, this apical endocytosis controls polarity and proliferation through regulation of Crb and Notch surface levels and signaling in Drosophila epithelial cells (Lu and Bilder, 2005; Richardson and Pichaud, 2010). As a result, developmental regulation of endocytosis in time and space could coordinate the events of proliferation and differentiation that take place during epithelial morphogenesis (Bokel and Brand, 2014). However, the molecular mechanisms of this endocytic regulation in epithelial organ development have not been previously characterized in vertebrates. To unveil developmentally regulated proteins that may control the process of apical endocytosis we used the zebrafish gut morphogenesis model (Alvers et al., 2014; Bagnat et al., 2007; Horne-Badovinac et al., 2003). We describe the role of the MARVEL protein Plasmolipin (Pllp), which is induced in the posterior midgut (a.k.a segment II) of the zebrafish intestine during morphogenesis, and is required for the generation of a highly endocytic enterocyte population during gut differentiation. We also characterized the molecular mechanism of PLLP role in endocytosis using the 3D-MDCK model. Using the bioID technique in 3D-MDCK cells, we found that PLLP interacts with EpsinR (EpsR), an AP1B-binding clathrin adaptor, which regulates the recycling of the endosomal SNARE Stx7. Together, PLLP and EpsR are required for the sorting of Syntaxin 7 into the apical recycling compartment to properly feed the endocytic uptake of apical cargo. Finally, we demonstrate that this role of PLLP is essential for Crb endocytic downmodulation and Notch activation in order to promote absorptive cell differentiation.

RESULTS

Plasmolipin (Pllp), is induced during epithelial tube formation in zebrafish and localizes to a highly endocytic compartment of the midgut

Gut morphogenesis is a genetically regulated process. To unveil new genes developmentally controlled during epithelial gut morphogenesis we used a screen strategy based on the isolation of epithelial cells from the zebrafish gut. GFP-positive gut cells were obtained through FACS sorting from *TgBAC(cldn15la-GFP)*

embryos, which express Cldn15la-GFP in the intestine from 48 hours post fertilization (hpf) onwards (Alvers et al., 2014). We extracted RNA from these cells at different time points, 48, 72 and 120 hpf, and synthetized cDNA to hybridize in custom microarray plates containing a proprietary library of zebrafish cDNAs. We identified Plasmolipin (*pllp*) as one of the genes specifically induced during lumen formation and expansion (Fig. 1A, 120hpf). Pllp is a type III-transmembrane protein of unknown function, containing a 4-transmembrane (4TM) spanning domain and cytoplasmic N- and C- terminal tails, that belongs to the family of MARVEL-domain containing proteins associated with vesicle trafficking and membrane fusion (Sanchez-Pulido, et al et al 2002) (Fig. 1A).

We performed RNA *in situ* hybridization (ISH) with *pllp* antisense probes on fixed embryos and larvae to validate *pllp* expression in the gut (Fig. 1B). *pllp* is expressed in the hatching gland and the pronephric duct as early as 48hpf, and is highly enriched in the gut at 72hpf and 120hpf (Fig. 1B, arrows). To analyze the localization of Pllp protein, we generated a BAC transgenic animal expressing Pllp-GFP, through BAC recombineering (Navis et al., 2013). In *TgBAC(pllp-GFP)pd1115* animals Pllp-GFP is expressed, similar to what we observed by ISH, in the pronephros and the gut (Fig. 1C). In particular, we found that Pllp expression is highly enriched in a specific segment of the posterior midgut (PGS)(Fig. 1C, bottom panel, arrow). At the subcellular level, Pllp-GFP localizes to the apical region of epithelial cells, both in pronephros and gut cells (Fig. 1D, 120hpf, arrows), with a small population associated with internal membranes in more mature and polarized epithelial cells (Fig. 1D, 120hpf, arrowheads). To further evaluate the subcellular localization of the protein, we performed anti-GFP immunogold electron microscopy (EM) in gut sections (Fig. 1E). The majority of Pllp-GFP (65%) localized to small tubules and vesicles (about 70-100 nm wide) present in the first 300 nm below the apical membrane, with a small fraction of PLLP also distributed both to the apical microvilli, and more basal endosomes. Thus, Pllp is an epithelial-specific marker induced during morphogenesis and highly expressed in a specific region of the posterior gut, which at cellular level distributes specifically to subapical tubulovesicles and endosomes.

The polarized localization of Pllp in apical endosomes suggested a function associated with the apical endocytic pathway. Thus, we next analyzed if Pllp is

involved in apical endocytosis in the zebrafish gut by using microgavaging to deliver endocytic tracers directly into the intestinal lumen (Cocchiaro and Rawls, 2013). First, we analyzed the apical uptake of Texas-Red-labeled Dextran (Dextran-TR) in 144hpf *TgBAC(pllp-spGFP*) larvae (Fig. 1F). Interestingly, Dextran-TR was not homogeneously internalized by enterocytes along the whole length of the gut tube, but specifically in the posterior midgut where Pllp is highly enriched (Fig. 1G, arrows). Furthermore, we observed that Lamp2, a late endosomal/lysosomal marker, is specifically enriched in Pllp-positive cells (Fig. 1H, arrows). Thus Pllp is specifically induced in the highly endocytic enterocytes of the posterior midgut on the onset of intestinal differentiation.

.

Pllp is required for apical endocytosis and endosomal maturation in the posterior gut compartment

To analyze if PLLP was required for apical endocytosis in the gut, we generated a mutant allele using TAL-effector nucleases (TALENs). After screening through the founders, we identified one allele that contained an insertion/deletion (*pd1116*), giving rise to a frame-shift mutation and an early STOP codon in the coding sequence, which truncates 85% of the protein structure, including the MARVEL domain (Fig. 2A). We observed that the mutant allele (*pllp*^{pd1116}) presents partial nonsense-mediated mRNA decay (Fig. S1A). To evaluate if apical endocytosis is affected in *pllp*^{pd1116} mutants, we microgavaged Dextran-TR. Homozygous *pllp*^{pd1116} larvae developed normal early gut morphology and intestinal cell numbers (Fig. S1B-C), but presented remarkable defects in dextran internalization, and a reduction in the number of gut cells internalizing this marker (Fig. 2B and 2E). In addition, at 144hpf, *pllp*^{pd1116} intestinal cells were significantly shorter than wild-types (WT) (Fig. 2B, 2C, and 2F), a phenotype that we also observed upon *pllp* knockdown using two different morpholinos designed to target PLLP (Fig. S1D-F). To more precisely evaluate the internalization defects we gavaged *pllp*^{pd1116} larvae with Dextran-TR and BSA-conjugated 15nm gold for ultrastructural analysis. We observed that gut epithelial cells developed an enlarged and void endosomal compartment in *pllp* larvae compared to WT (Fig. 2C, arrows). Furthermore, WT larvae showed gut cells with mature perinuclear endosomes that were filled with

electron dense material and gold particles (Fig. 2D, red endosomes) whereas, in *pllp*^{pd1116} there were untraceable levels of BSA-gold uptake, and larger supranuclear endosomes (>200 nm, green endosomes).

Then, we characterized the effect of *pllp* loss of function in juveniles and we observed that most *pllp*^{pd1116} mutants (75%) presented disrupted intestinal folds at days post fertilization (dpf) (Fig. 2G). Furthermore, the apical plasma membrane of *pllp*^{pd1116} intestinal cells was expanded and bulging towards the lumen (Fig. 2G, magnification in right panels), a phenotype resembling previous observations in *Drosophila* mutants with disrupted apical endocytosis (Lu and Bilder, 2005). Interestingly, the survival of *pllp*^{pd1116} mutants in reduced diet was highly compromised compared to WT juveniles, suggesting that Pllp is necessary for efficient nutrient absorption (Fig. 2H).

We validated the observed phenotypes were specific to *pllp* deficiency by rescue-crossing *pllp*^{pd1116} mutants to *TgBAC(pllp-GFP)* (Fig. 2I-J). Pllp-GFP expression almost completely rescued both the endocytic and the cell-height phenotypes of the *pllp*^{pd1116} mutation, indicating that the lack of *pllp* expression in the mutants is the specific causes of the observed defects in gut cells and that the fusion protein is functional. In summary, these results indicate that Pllp is required for apical endocytosis and epithelial morphogenesis in the gut, which are essential for larval survival, and suggest a function in regulating terminal epithelial differentiation of posterior gut enterocytes.

PLLP is expressed during 3D MDCK cyst morphogenesis, and is required for epithelial morphogenesis and endosomal maturation in MDCK cysts

To dissect more precisely the molecular function of PLLP, we used the 3D-MDCK model. PLLP expression is highly induced during lumen formation and expansion in 3D cultures (Fig. 3A-B), and localizes to a subapical compartment just below the apical marker podocalyxin (Podxl) (Fig. 3A). We also observed a similar pattern of expression in sections of mouse small intestine and kidney (Fig. S2A-B), mimicking the subcellular localization and expression patterns observed in zebrafish. This common pattern of subcellular localization in epithelial tubes suggests a potential similar role in all these tissues.

Then, we characterized the effect of PLLP silencing in 3D-MDCK morphogenesis using siRNAs. Silencing of PLLP (PLLP-KD) resulted in lumen formation defects at 72h (Fig. 3C-E), which we validated using a siRNA-resistant PLLP-GFP (PLLP-GFP(R)) cell line that rescued the normal phenotype (Fig. 3F and Fig. S2D-E). PLLP-GFP presented a similar distribution to the endogenous protein (Fig. 3F). To determine whether PLLP silencing generates endosomal maturation defects in MDCK cysts similar to those observed in the mutant fish, we stained control and PLLP-KD cysts with an acidic-pH probe (Lysotracker-Red), which marks the highly acidic endolysosomal compartment. PLLP-KD cysts present a marked reduction in the number and size of Lysotracker-positive endosomes compared to controls (Fig. 3G and Fig. S2C).

Altogether, these results demonstrate that PLLP is required for epithelial morphogenesis in 3D-MDCK, and suggest that PLLP expression controls the formation of acidic endosomes, and supports a role for PLLP in endocytosis, consistently with the phenotypes observed in the zebrafish gut.

PLLP regulates formation of apical recycling endosomes

The subapical localization of PLLP both in zebrafish and MDCK cells, suggests its association with the apical recycling endosome (ARE), which is required for the recycling of endocytosed protein cargo and receptors back to the plasma membrane (Golachowska et al., 2010). We observed that endogenous Rab11, an ARE marker, colocalized with subapical Pllp in the posterior midgut sections of *TgBAC(pllp-GFP)* animals (Fig. 4A, arrows), but not with the Pllp-positive endosomes that localized more basally (Fig. 4A, arrowheads). Furthermore, subapically-distributed PLLP also colocalized with endogenous Rab11 in 3D MDCK cells (Fig. 4B, arrows).

Next, we investigated whether the integrity of the ARE compartment depends on Pllp. We analyzed Rab11 distribution in WT and *pllp*^{pd1116} larvae (Fig. 4C). We observed that Rab11 mislocalized throughout the cytoplasm in posterior gut epithelial cells of *pllp*^{pd1116} mutants, compared to the WT (Fig. 4C). In addition, EM images showed that apical endosomes in the epithelial gut cells of *pllp*^{pd1116} mutants were devoid of emanating tubules of 100 nm in width, which resembled

recycling or sorting tubules that were present in the WT (Fig. 2D, purple arrowheads). In addition, PLLP-KD MDCK cysts show dispersed Rab11 localization consistently with the effect of the *pllp*^{pd1116} mutation in zebrafish (Fig. 4D).

In conclusion, Pllp is required for Rab11 distribution in epithelial cells both *in vivo* and *in vitro*, suggesting that Pllp is required for the formation or maintenance of the ARE compartment, and possibly for protein recycling during epithelial morphogenesis. Previous data has demonstrated that Rab11 is required for epithelial morphogenesis in MDCK cells (Bryant et al., 2010) and DN-Rab11 expression affects single lumen formation also in the zebrafish gut, through regulation of E-cadherin recycling (Alvers et al., 2014). However, Pllp expression is induced after the formation of single lumens in zebrafish guts, at about 72hpf, which might explain why we do not observe defects in single lumen formation in this model.

Next, we tested if PLLP could be sufficient to induce formation of Rab11-positive tubule-vesicular compartment. Since MDCK cells in monolayers expressed low levels of Pllp protein (Fig. 3A), we performed gain-of-function experiments by transiently expressing Pllp in MDCK monolayers. Indeed overexpression of Pllp-GFP in MDCK cells induced the formation of an enlarged, ARE-like, Rab11-positive compartment, which colocalized with early endosomal marker EEA1, and also the formation of more acidic endosomes in these cells (Fig. S3A). In fact, this Pllp-induced compartment consisted of clusters of vesicles that resembled the ARE tubule-vesicles in shape and size (Fig. S3B). To confirm this phenotype *in vivo* we identified a second founder *TgBAC(pllp-GFP)pd1114* line that overexpresses Pllp-GFP, and also presentes an enlarged subapical endosomal compartment in gut epithelial cells (Fig. S3C). In summary, these experiments suggest that the molecular function of PLLP is to form a subapical Rab11-positive tubule-vesicular compartment with properties of the recycling endosome.

PLLP interacts with EpsR to form recycling vesicles

Taking advantage of the functional activity of PLLP in our *in vitro* system, we used the 3D-MDCK model to better characterize the molecular mechanism associated with PLLP function. To this end we devised an *in vivo* biotinylation assay (bioID) of

PLLP-proximal proteins (Fig. 5A) (Roux et al., 2012). We uncovered 42 proteins likely to interact with PLLP in 3D-MDCK cells from the mass-spectrometry analysis of the biotinylated polypeptides (Fig. 5B) that mostly consisted of SNARE proteins or SNARE regulators that were previously localized to internal membranes (Golgi, vesicles or endosomal compartments).

We identified Clint-1/Epsin-4/EpsR (hereafter termed EpsR) as the principal interacting partner of PLLP. EpsR belongs to the Epsin family of membrane tubulating proteins and it is required for retrograde transport from late endosomes (Hirst et al., 2003; Mills et al., 2003; Saint-Pol et al., 2004). The N-terminal ENTH domain of EpsR has been described to interact with several cargoes, including endosomal SNAREs, and is required for endocytic recycling of SNAREs and maintenance of late endosomes in several cell types (Chidambaram et al., 2004; Chidambaram et al., 2008; Miller et al., 2007). We confirmed the interaction between endogenous PLLP and EpsR, and specifically its C-terminal domain, and not the ENTH (cargo-binding) domain, by pulldown assays (Fig. 5B-C). Indeed, we only identified biotin modifications in C-terminal peptides of EpsR in the bioID assay (Table S1), consistently with this result. We also validated this interaction by co-IP (Fig. 5D-E). Interestingly, the *Drosophila* EpsR homolog, *Liquid-facets related* (*lqfR*) is a regulator of epithelial cell morphology and regulates cell height in the follicle cells of the egg-chamber (Lee et al., 2009; Leventis et al., 2011). Therefore, we investigated and unveiled the role of EpsR, through its interaction with PLLP, during epithelial morphogenesis.

First, we characterized the localization of endogenous EpsR in 3D-MDCK cells. EpsR and PLLP partially colocalized in internal endosomes, but not in the subapical compartment (Fig. 5F, arrows), In fact, EpsR localized to tips of large endosomes containing PLLP (Fig. 5G, arrows), and Rab7, a marker of late endosomes (not shown). These data show that EpsR and PLLP interact in a perinuclear late endosomal compartment, in which they might function to form vesicles and tubules to recycle cargo from the degradative pathway. Indeed, PLLP-KD MDCK cysts presented a dispersed and decreased distribution of both EpsR and Rab7 (Fig. 5H-I), suggesting that PLLP is required for the integrity of Rab7-endosomes and for the binding and recruitment of EpsR to this compartment.

Next, we examined the effect of silencing EpsR in MDCK cysts formation. EpsR silencing disrupted normal lumen formation (Fig. 5J-L), and formation of subapical Rab11 endosomes (Fig. 5M), confirming its functional association with PLLP. Moreover, EpsR was also required for the gain-of-function effects induced by PLLP-overexpression in MDCK monolayers (Fig. S3D). Altogether, these data reveal that EpsR binding to PLLP is required for the formation of tubule-vesicular carriers involved in the recycling of cargo to the Rab11-positive compartment and normal epithelial morphogenesis.

PLLP and EpsR are required to sort endosomal SNARE Stx7 to the apical endocytic network

To investigate how PLLP and EpsR control the recycling of cargo to the Rab11-positive compartment, we analyzed the dynamic distribution of the endosomal SNARE Syntaxin-7 (Stx7), which interacts directly with EpsR as binding cargo (Miller et al., 2007), and was identified in our bioID assay (not shown). We generated an MDCK cell line expressing Stx7, and analyzed its distribution in MDCK cysts. We observed that GFP-Stx7 localized mainly to a subapical compartment in 3D-MDCK cells (Fig. 6A), which is consistent with the endogenous localization of Stx7 in mouse small intestine villar cells (Fig. S4A). Furthermore, Stx7 and PLLP were present in the same membrane domains as we observed using a probe-ligation assay (PLA) (Leuchowius et al., 2011) on MDCK cells expressing GFP-Stx7 (Fig. S4B-C). PLLP formed significantly more PLA-complexes with GFP-Stx7 than with Rab11-GFP (Fig. S4B, arrow), which confirmed the interaction between Stx7 and PLLP in subapical endosomes. Next, we analyzed the dynamic trafficking of Stx7 and PLLP using fluorescence recovery after photobleaching (FRAP) (Fig. 6B-C, Video 1). After photobleaching the subapical pool of Stx7/PLLP, fluorescence recovery was conducted with similar average k_{on} of 0.032 s^{-1} (Stx7) and 0.038 s^{-1} (PLLP), suggesting that both proteins were trafficking in the same carriers to recycle from perinuclear endosomes to the subapical compartment.

Next, we addressed if Stx7 subapical localization requires PLLP and EpsR. We found that both PLLP and EpsR silencing caused a mislocalization of GFP-Stx7, precluding its subapical localization (Fig. 6D). Interestingly, EpsR-KD cysts

presented a mislocalized distribution of Stx7, and also caused an increased accumulation of PLLP in perinuclear Stx7-positive endosomes (Fig. 6D). These experiments suggested that PLLP and EpsR function is required to properly localize the endosomal SNARE Stx7 into the subapical compartment. Importantly, *pllp*^{pd1116} larvae also showed a scattered distribution of Stx7, compared to WTs, resembling the phenotype observed in MDCK cysts (Fig. 6E). Thus, the defects in Stx7 apical recycling in *pllp*^{pd1116} mutants could provide a rational explanation for the observed phenotypes in apical endocytosis and endosomal maturation. Finally, we found that Stx7 silencing in 3D-MDCK cells also leads to epithelial morphogenesis defects, since it caused formation of multiple lumens (Fig. 6F-H) and a drastic reduction in Rab11 apical endosomes (Fig. 6I), a phenotype that was rescued using a GFP-Stx7 stable cell line (Fig. 6H).

Together these results are consistent with a model in which endosomal SNAREs are recycled back from perinuclear mature endosomes (Rab7-positive late endosomes) into the subapical Rab11-positive compartment through the formation of EpsR-mediated tubule-vesicles generated or stimulated by PLLP expression. These data also imply that formation of Rab11 endosomes depends on the maintenance of apical endosomal fusion and a cyclic dependence of both apical endocytosis and the recycling of the SNARE fusion machinery.

PLLP controls endocytic-mediated downmodulation of Crb and is required for Notch signaling during epithelial morphogenesis

Our mechanistic data, together with the endocytic defect observed in zebrafish guts, suggests that PLLP might modulate the endocytosis and degradation of apical protein receptors, through controlling the availability of subapical SNAREs (Stx7) involved in their internalization. Indeed, previous data showed that the Stx7 homolog *avalanche* (*avl)* is required for the endocytosis and degradation of Notch and Crb in *Drosophila* imaginal discs (Lu and Bilder, 2005). Notch and Crb are master regulators of epithelial morphogenesis and differentiation. Thus, we analyzed Crb localization during epithelial morphogenesis in the 3D-MDCK model. Crumbs3a (Crb3) showed overall apical distribution in early MDCK cysts, and later became restricted to the tight junctions (TJ) (Fig. 7A), correlating with the timing

of PLLP induction, and suggesting that PLLP expression might control Crb3 sorting to the TJ. Indeed, MDCK cells silenced for PLLP or Stx7 presented accumulated Crb3 in the apical membrane of mature cysts (Fig. 7B), and higher total levels of Crb3 (Fig. 7C). *In vivo*, *pllp*^{pd1116} mutants also displayed enhanced levels of Crb3 (pan-Crb antibody) in cross sections of 6dpf larvae (Figure 7D-E).

Crb3 mislocalization could be explained by a defect in protein sorting, which in mature cysts could be specifically directed towards the TJ, or by a defect in endocytosis and degradation of Crb3a at the apical plasma membrane. To test these possibilities, we used the RUSH system (Boncompain et al., 2012) to dynamically address GFP-Crb3a localization in MDCK cysts. Interestingly, GFP-Crb3a was not directly sorted to the TJ, but secreted first at the apical plasma membrane in mature cysts (Suppl. video 1), from where Crb3 was slowly relocalized to the TJ (Fig. 7F, top panels, Suppl. video 2). However, in PLLP knockdown cells, Crb3a was normally sorted to the apical membrane, but failed to accumulate later to the TJ (Figure 7F, middle panels, Suppl. video 3). Furthermore, treatment with an endocytosis inhibitor (Dynasore) also disrupted the relocalization of Crb3a from the apical membrane to the TJ (Figure 7F, bottom panels, Suppl. video 4). In addition, we also observed a significant decrease of Crb3 signal in MDCK cells overexpressing PLLP in monolayers, compared to controls (Fig. 7G-H), suggesting that PLLP expression is sufficient to induce Crb3 endocytosis and degradation. These results indicate that Crb3a restricted localization to the TJ is mediated by endocytosis of Crb3a at the apical membrane, and that this process requires PLLP.

Finally, we transiently transfected PLLP-Cherry in MDCK cells expressing a construct of GFP-Crb3a carrying an EGFP tag in the extracellular region of Crb3a, and performed a 90-minute pulse-chase endocytosis assay using anti-GFP antibodies (Abs) (Fig. 7I). We found that cells expressing PLLP-Cherry presented less apical GFP-Crb3a, and that the bound anti-GFP antibodies were endocytosed and localized to endosomes exclusively in PLLP-Cherry cells. These results demonstrate that PLLP regulates endocytosis of certain apical receptors, such as Crb3, which could provide a fine-tuning mechanism to regulate their localization during epithelial morphogenesis. Defects in apical endocytosis may also explain

the enlargement of the apical plasma membrane observed *in vivo* in zebrafish enterocytes.

Previous experiments in fruit fly and zebrafish eye development have shown that Crb expression control Notch signaling during epithelial differentiation and proliferation (Herranz et al., 2006; Ohata et al., 2011; Yan et al., 2009). In addition, the Stx7 homolog, *avl*, is required for Notch signaling in *Drosophila* (Vaccari et al., 2008). We observed that cells silenced for PLLP presented a consistent 43%(±8.4%) reduction in cleaved Notch (NICD) levels in MDCK cysts (Fig. 8A). To analyze whether PLLP affected the localization of Notch, we transfected full length Notch1a-myc and a suboptimal concentration of PLLP siRNA. Interestingly, Notch1a colocalized with PLLP in endosomes, whereas PLLP-KD cells did not present any internal Notch1a-myc signal (Fig. 8B). Furthermore, overexpression of PLLP-GFP induced the internalization of Notch1a-myc in MDCK monolayers (Fig. S5A), where Notch1a partially colocalized with PLLP both in apical and basal endosomes, suggesting they are transported in similar carriers during endocytosis (Fig. S5B). These results suggested that PLLP expression regulates Notch endocytosis and signaling and prompted us to investigate its function *in vivo*.

Notch signaling is required for maintaining the absorptive fate of a subpopulation of epithelial stem cells of the gastrointestinal track, both in vertebrates and invertebrates and Notch-deficient animals show a reduced population of intestinal absorptive cells compared to secretory cell fates (Fre et al., 2011; Ohlstein and Spradling, 2007; van Es et al., 2005; VanDussen et al., 2012). We observed that in WT zebrafish the majority of the cells in the posterior gut presented large supranuclear endosomes and vacuoles, likely constituting the terminally differentiated highly endocytic posterior gut cells (Fig. 8C). In contrast, *pllp*^{pd1116} mutants presented a reduced number of cells with supranuclear vacuoles and a three-fold increase of PAS-positive secretory cells (Fig. 8C-D and S5C). To analyze if Notch signaling is affected in *pllp*^{pd1116} mutants, we measured expression of bona fide Notch-effector genes *hes1* (*her6* and *her9*) and *hes5* (*her15.1*) from dissected adult fish guts. Indeed, *pllp*^{pd1116} mutants showed a marked decrease in Hes5 expression, but not in Hes1 (Figure 8E), similar to what has been previously

reported for Mindbomb (*mib*) mutations, in which Delta-ligands are unable to signal to Notch-positive cells (Crosnier et al., 2005). Altogether, these results indicate that Pllp is required for Notch signaling and terminal differentiation of enterocytes and inhibition of secretory cell differentiation in the posterior midgut.

To analyze if Notch signaling is required for endocytic cell differentiation in the posterior midgut, we used two different strategies. First, we analyzed endocytosis in 6dpf *mib1*^{ta52b} mutant larvae. Secondly, we gavaged 6dpf larvae treated with a Notch-inhibitor (100 μM DAPT) after the single lumen is formed (72hpf). We found that, similar to *pllp*^{pd1116} mutant larvae, both DAPT-treated and *mib1*^{ta52b} larvae exhibited a significant reduction in the number of endocytic cells and the size of endosomes in the posterior midgut compared to WT (Fig. 8F), (Fig. 2B). Altogether, these experiments indicate that Pllp controls Notch activity, which is essential for endocytic enterocyte differentiation in the posterior midgut.

DISCUSSION

Here, we characterized a developmentally regulated mechanism to induce apical endocytosis through the regulation of SNARE recycling which is necessary for epithelial morphogenesis. Decades of intense work showed that SNARE receptor recycling drives the fusion of vesicles in the neurological synapse, which is essential for proper vesicle exocytosis at the presynaptic nerve terminals (Sudhof and Rizo, 2011). Similarly, we propose that endosomal SNARE proteins recycle back from the late endosomal compartment into earlier compartments to promote endosomal fusion along the endocytic pathway. This cyclic behavior of SNAREs depends on their incorporation on specific membrane domains in late endosomes that after budding would form vesicles sorted back to the subapical compartment. We describe that expression of a novel uncharacterized protein PLLP induces SNARE recycling through its interaction with the membrane tubulating clathrin adaptor EpsR. Indeed, PLLP and EpsR are essential for the recycling of the endosomal SNARE Stx7 to the subapical compartment and the proper endosomal maturation in epithelial cells. PLLP, which is a MARVEL-domain containing protein (Sanchez-Pulido et al., 2002) has the potential to oligomerize and form membrane

microdomains (Bosse et al., 2003), which might induce the specific partitioning of selective membrane cargoes for budding and sorting.

Additionally, our experiments demonstrate that PLLP is induced in a time and space-specific manner to regulate Crb endocytosis and Notch signaling for the development of a highly-endocytic absorptive cell population in the zebrafish midgut (Fig. 8G). Epithelial morphogenesis is a finely regulated process in which epithelial cells conduct a delicate balancing act between differentiation and proliferation that becomes deregulated in different types of human carcinomas (Martin-Belmonte and Perez-Moreno, 2012). Epithelial cell differentiation greatly depends on the establishment of cellular junctions and polarity complexes that serve to organize the physiology of mature epithelial tissues. These polarity complexes, such as the Crb complex, crosstalk with proliferation pathways, such as the Notch pathway, in order to prevent overgrowth and, at the same time, to provide a functional population of highly differentiated epithelial cells (Richardson and Pichaud, 2010). Our experiments indicate that PLLP fine-tunes Notch signaling for differentiation of posterior gut absorptive cells. However, *pllp* mutants do not have defects in the formation of goblet cells (Fig. 8G). Interestingly, the highest concentration of mucous-producing secretory goblet cells develops adjacently to the highly absorptive posterior midgut compartment in a timely fashion, suggesting an interesting developmental and functional relationship between mucous secretion and absorption.

In flies, the closest PLLP homolog, CG15211, shares 33% of sequence similarity with the zebrafish protein and was reported to be lethal during a genome-wide RNAi screening for Notch-regulators (Mummery-Widmer et al., 2009). However, the cytoplasmic N and C terminal tails of PLLP poorly resemble the homologous sequences in the CG15211 protein. In contrast, the sequence of vertebrate PLLP, and especially the N-terminal cytoplasmic tail, is remarkably similar to a membrane-adjacent region of the N-terminal tail of Sanpodo, another *Drosophila* four-pass type-III transmembrane protein. Sanpodo is an essential regulator of Notch signaling in flies, with uncharacterized homologs in vertebrates. Interestingly, Sanpodo regulates Notch through control of endocytosis during asymmetric division of the sensory organ precursor (SOP) cells (Upadhyay et al., 2013). However, in the SOP model, Rab11-mediated recycling is required for Delta

activation, but dispensable in Notch-positive cells. It will be interesting to precisely analyze the asymmetric cell divisions in the precursors of zebrafish gut to establish if any similarities with the invertebrate SOP model exist. In this scenario, differential inheritance of Pllp endosomes during asymmetric cell division could dictate Notch activation and establish lateral inhibition mechanisms between secretory and absorptive intestinal precursors.

Pllp is also expressed in several other epithelial-like cell types in zebrafish not described here, such as a subpopulation of skin cells, the sheath cells of the notochord, and the neuromasts of the lateral line (data not shown). Interestingly, asymmetric proliferation and differentiation of these cell types also depend on Notch signaling (Liu et al., 2007; Wibowo et al., 2011; Williams et al., 2011; Yamamoto et al., 2010). Further studies will be directed to understanding the role of PLLP in fine-tuning Notch activity during development of these organs.

Acknowledgements

We thank Carmen M. Ruiz-Jarabo for her comments on the manuscript and members of the Martin-Belmonte lab and Bagnat labs for helpful discussions. We thank Ashley Alvers for helping in the isolation of gut cells, Ben Margolis (University of Michigan) for the Crb3 antibody, Reinhardt Jahn (Max Planck Institute for Biophysical Chemistry) for Stx7 reagents, Margaret Robinson (University of Cambridge) for EpsR plasmids, and Raphael Kopan and Jose Luis de la Pompa (CNIC, Madrid) for Notch plasmids and *mib1*^{ta52b} embryos. This work was supported by grants from the MINECO (BFU2011-22622) and CONSOLIDER (CSD2009-00016) to F.M-B and NIH innovator grant 1DP2OD006486 to M.Ba.

Author contributions

A.R-F, M.Ba. and F.M-B designed the experiments; A.R-F, J.B., M.Bo. and G.A. carried out the experiments; A.R-F. and F.M-B. wrote the manuscript; G.B. and F.P. designed and constructed RUSH experimental tools; N.R., M.A., and J.M. produced and characterized the mammalian PLLP antibody; A.R-F. and G.A. designed and carried out the EM experiments.

EXPERIMENTAL PROCEDURES

Plasmids. Rat Stx7-GFP plasmids were gifts from R. Jahn (Max Planck Institute for Biophysical Chemistry, Göttingen, Germany). Human Rab11a-GFP, canine PLLP-GFP, and canine PLLP-Cherry were constructed by PCR and cloned into pEGFP/Cherry vectors (Clontech). The siRNA#2-resistant (R) variants were generated by introducing synonymous mutations with the Quikchange XLII kit (Stratagene). Canine PLLP-myc/myc-birA* was constructed by PCR and cloned into pCR3.1(+) (Invitrogen). Human EpsR-GFP, GST-N-EpsR and GST-C-EpsR were gifts from S. Robinson (University of Cambridge, UK). Rab7-GFP was from R. Puertollano (NIH, USA). The BAC clones containing *pllp* and *lamp2* genes were obtained from Source Biosciences (*pllp* HUKGB735N1073Q/DKEY-73N10 and *lamp2* HUKGB735N0515Q/DKEY-15N5). The spacer-GFP/RFP sequence was cloned by BAC homologous recombination in bacteria as previously reported (Navis et al., 2013). Full-length Notch1a-myc was obtained from Addgene (plasmid 41728).

Antibodies. The polyclonal antibody (pAb) against mammalian PLLP (1:500 IF on cold MeOH:Acetone fixation, 1:1000 W-b) was designed and generated in rabbits by injecting combination of cytoplasmic peptides from the human PLLP sequence as previously described (Bosse et al., 2003). Podocalyxin/gp135 (1:500 IF, 1:1000 W-b) was a gift from G. Ojakian (NY state, USA). Crb3 pAb (1:250 IF on Acetone fixation, 1:1000 W-b) was a gift from B. Margolis (Pennsylvania, USA). Cleaved Notch1 pAb (#2421, 1:250 W-blot, Cell Signaling), βcatenin pAb (1:500 IF, Santa Cruz Biotechnologies), E-cadherin mAb (1:500 IF, rr1 epitope, DSHB), GFP mAb (1:100 IF, 1:1000 W-b, Roche), GFP pAb (1:1000 IP, 1:1000 IF, 1:2000 W-b, Life technologies), myc 9E10 mAb (1:1000 IF on Acetone fixation, Roche), EpsR mAb (1:100 IF on MeOH:Acetone fixation, 1:500 W-b, Abcam), Stx7 pAb (1:100 on IF on Acetone fixation, 1:500 W-b, Synaptic Systems), Rab11 pAb (1:500 IF, 1:500 W-b, Life technologies) and EEA1 mAb (1:500 IF, BD biosciences) were used as primary antibodies. Peroxidase-conjugated antibodies were used. Alexa405/488/555/647-conjugated Phalloidin or secondary antibodies were used for immunofluorescence. DAPI, ToPRO3, Lysotracker-Red and Dextran-TexasRed were from Life technologies. Dynasore (MERCK) was used at 100µM in culture medium to inhibit

dynamin, and DAPT (Sigma-Aldrich) was used to inhibit γ-secretase cleavage of Notch.

Transgenic animals and mutants. Zebrafish stocks were maintained at 28°C. The zebrafish lines used were EK, *TgBAC(cldn15la-GFP)pd1034* (Alvers et al., 2014), *TgBAC(pllp-GFP)pd1114*, *TgBAC(pllp-GFP)pd1115, TgBAC(lamp2-spRFP)pd1117*, *mib1*^{ta52b} (Schier et al., 1996) and *pllp*^{pd1116}. Zebrafish BAC lines were generated as previously described (Navis et al., 2013).

TALEN-mediated editing. Three TALENs were designed to target the first exon of *pllp* using TALEN targeter (Doyle et al., 2012) and constructed using Golden Gate assembly (Cermak et al., 2011) into the pCS2-TAL3DD/RR vectors using the Addgene v2.0 kit. The TALEN used to generate the *pllp*^{pd1116} mutant allele reported here was designed to target the following sequence of *Danio rerio pllp* exon1: 5'-TTGACATGGGTTTTATcaagagcattcctggaaTACTGCTTATAGCCGA-3', and composed of the following TAL effector domains: pCS2-TAL3DD*_pllpE1* NG NN NI HD NI NG NN NN NN NG NG NG NG NI NG; pCS2-TAL3RR*_pllpE1* HD NN NN HD NG NI NG NI NI NN HD NI NN NG NI. Zebrafish were injected into the yolk at the one-cell stage with 200 pg total TALEN RNA and 100 pg of dsRed RNA to select correctly injected embryos. Mutant alleles were identified by defective BsmI digestion of the PCR product generated with the following primers: FW:5'-CTGGGAAGGTCAGCACTCAG-3'; RV: 5'-ACGGAACAGAAAAGTGGGTGT-3'. The BsmI-undigested PCR band was T/A cloned into the pGEM-T vector for allele sequencing. The experiments shown here were performed on F4/F5 fish and larvae.

Fish gavaging. Zebrafish larvae from 6dpf were tricained for 5 minutes and immersed in 3% methylcellulose. Microforged capillary needles were used to microinject 10 nl of a 1:4:1 Dextran-TexasRed/water/Phenol-red solution. Methylcellulose was washed off and fish were incubated at 28ºC for 2 hours before confocal microscopy analysis or fixation.

Endocytosis assay in cells. MDCK cells stably expressing GFP-Crb3a were cultured as monolayers, washed with cold 1% FBS-supplemented MEM and placed on ice for 15 minutes. Then, coverslips were placed on a 100 ul drop of cold 1%-FBS MEM containing a 1:10000 dilution of the polyclonal GFP antibody at 4ºC for 30 minutes. Coverslips were washed 3 times with 1% FBS-supplemented MEM and

placed on plates containing warm MEM and cultured at 37º for 90 minutes. Cells were washed in Ca/Mg-PBS, fixed and stained for IF.

In situ hybridization. The probe to detect the *pllp* transcript by *in situ* hybridization was PCR amplified from 5dpf larval cDNA and ligated into pGEMT-Easy (Promega, Madison, WI, USA). In situ hybridization was performed as previously described. The plasmids were linearized and digoxygenin-labeled RNA was generated using the DIG labeled nucleotides (Roche) and T7 polymerase (NEB). Stained embryos were imaged on a Discovery.V20 stereoscope (Zeiss, Oberkochen, Germany) with an Achromat S 1.0× lens.

Fish sectioning and analysis. Zebrafish embryos and larvae from different time points were fixed overnight in PBS-buffered 4%PFA (Sigma), washed twice in PBS and embed in PBS-buffered 4% low-melt agarose blocks. Blocks were cut in 200 µm sections using a Vibratome (Leica). Sections were blocked/permeabilized with PBS-3%BSA containing 0.5% Tx100 and then incubated with the indicated antibodies. Stained sections were mounted using DAPI-Fluoromount or DAPI-Vectashield. Sectioned fish were analyzed on a confocal microscope.

Cell culture and stable cell lines. MDCK cells were grown as described previously (Rodriguez-Fraticelli et al., 2010). MDCK cells stably expressing PLLP-GFP, PLLP-Cherry, GFP-Rab7, GFP-Stx7 and EpsR-GFP were made by transfection using Lipofectamine 2000 (Life Technologies) and clones were selected by treating cells with G418 (0.5 mg/ml). Notch1a-myc stable cell line was made by cotransfection with blasticidin-resistant gene (pBlast) and selection for 10 d with 0.5 µg/ml blasticidin. To prepare cysts in Matrigel, cells were trypsinized to a single cell suspension of 2×10^4 cells/ml in 2% Matrigel and plated in coverglass bottom chambers (IBIDI) covered with Matrigel. Cysts were grown and fixed at indicated time points.

Confocal microscopy and videomicroscopy. Immunofluorescence of cysts was previously described (Rodriguez-Fraticelli et al., 2010). Fixed cyst imaging was performed in PBS medium or mounted using ProLong Gold antifade reagent. Fixed cells in monolayers were analyzed mounted in Fluoromount. Cysts were analyzed on a 510 or 710 LSM confocal microscope (Carl Zeiss, Inc.) using a 63× NA 1.4 oil Plan-Apochromat objective and a 63× NA 1.2 water C-Apochromat Corr (for live cell and cyst imaging) and ZEN software suite (Carl Zeiss, Inc.). Fish sections and

whole-mounts were analyzed on a SP5 confocal microscope (Leica) with 10×/0.40 HC PL APO air objective, 20×/0.70 HC PL APO oil objective, and 40×/1.25–0.75 HCX PL APO oil objective, using Application Suite software (Leica). For image processing, we used FIJI/ImageJ (National Institutes of Health). For videomicroscopy and 3D reconstitutions, we processed maximum z-projections of all stacks using ImageJ software. For quantifications of lumen formation, MDCK cysts with a single actin/Podxl staining at the interior surface and β-catenin facing the ECM were identified as normal lumens.

RUSH assay. The RUSH protocol was performed as previously described, with the following modifications. MDCK cysts stably expressing GFP-SBP-Crb3a and Streptavidin-KDEL were grown in Mattek coverglass bottom plates for 72h, washed and incubated with 10 mM Hepes-buffer, 1% serum-supplemented phenol-red-free MEM and imaged using a 510 LSM confocal microscope (Zeiss). 40 μM biotin-supplemented MEM was added at t=0 when image acquisition started.

Electron microscopy. For BSA-Gold endocytosis TEM, 6dpf larvae were gavaged with 15nm gold-conjugated BSA-supplemented Dextran-TR for 2h. Then, larvae were fixed in 2% (w/vol) PFA, 2% (w/vol) glutaraldehyde in 0.2M phosphate buffer (PB, at pH 7.4) for 2h at RT and overnight at 4ºC. Subsequently, posterior midgut sections were embedded in EPON blocks, sectioned using a ultramicrotome (Ultracut E, Leica), and stained with uranyl acetate and lead citrate and imaged at 40,000kV using a JEM1010 Jeol microscope. For immunogold TEM, 6dpf zebrafish larvae were fixed in 2% (w/vol) PFA and 0.2% (w/vol) glutaraldehyde in 0.2 M phosphate buffer (PB, at pH 7.4) for 2h at room temperature and kept in 1% (w/vol) PFA in PB at 4 °C. Subsequently, posterior gut sections were embedded in 10% (w/vol) gelatine, and processed for cryosectioning. Guts were sectioned along the apicobasal axis on an EM FCS cryo-ultramicrotome (Ultracut UCT, Leica) at −120 °C. For immunogold labelling, thawed 75-nm-thick cryosections were incubated with rabbit anti-GFP (1:500, Life technologies) followed by protein A conjugated to 15-nm gold particles (EM Laboratory, Utrecht University). Sections were stained with a mix of 1.8% methylcellulose and 0.4% uranyl acetate.

RNAi. 25 nucleotide stealth siRNA duplexes targeting mRNA sequences of canine PLLP and Stx7 were purchased from Life technologies. 25 nucleotide siRNA duplexes targeting EpsR were purchased from Sigma-Aldrich using dTdT

overhangs. Sequences were submitted to BLAST search to ensure targeting specificity and minimize off-targets. MDCK cells were transfected using AMAXA Nucleofector-II equipment, reagents and protocols (Lonza). Cells were transfected with 10 µl of siRNA (200µM), plated in 6-well plates, cultured for 24h, trypsinized then plated to grow cysts for the indicated time points. Total cell lysates were analyzed by Western blotting to confirm siRNA efficiency.

The siRNAs targeted the following sequences:

Control: 5'-CCUUCGGGUGGAACAUGCUCUCUUU-3'

PLLP_#1: 5'-CUGCUGCAGCUGGUGCUGGGGCUGC-3'

PLLP_#2: 5'-CCUCUGGCUGGUGACAAUCGUCUUU-3'

PLLP_#3: 5'-CCUAAGGAAUCGGGAUCCUUCCUCU-3'

EpsR_#1: 5'-CCUAUGAAUGUGAUGACCCAAAGUU-3',

EpsR_#2: 5'-CAUGAACAUAGGGAUGUCAACUGCU-3',

EpsR_#3: 5'-AAGGAGCAGAUUGAAUGAAGGAUUU-3',

Stx7_#1: 5'-UUCAGGUGAAUCUUGAGGUGUUCCA-3'

Stx7_#2: 5'-CAGAAGAUGACCUCCGCCUUAUUCA-3'

Stx7_#3: 5'-UAGAGAAUGUAGUGCAAUAGUGUGC-3'

Probe ligation assay. The probe ligation assay (O-LINK, Sweden) was performed using anti-PLLP (rabbit polyclonal, Life Technologies) and anti-GFP (mouse, Roche) according to manufacturer's instructions.

In vivo biotinylation of PLLP proximal proteins. MDCK cells stably expressing the promiscuous mutant (R118G) of the humanized bacterial biotin-ligase (birA*) or canine PLLP-myc/myc-birA* constructs were incubated with 50µM biotin for 16h and lysed using 4% SDS, and biotinylated peptides were purified using Streptavidin-coated magnetic beads (Genscript). The bioID technique was performed as previously described (Roux et al., 2012) and eluted peptides were analyzed by liquid chromatography tandem mass spectrometry and peptide-mass fingerprinting, considering up to 2 biotinylations per peptide, in collaboration with the Proteomics unit at Centro Nacional de Biotecnología (CSIC, Spain).

Pulldowns. The full-length EpsR construct is extremely protease sensitive, so the NH2-terminal ENTH domain (amino acids 1–165) and the COOH-terminal domain (amino acids 165–625) of human EpsR were expressed separately as previously published(Hirst et al., 2003). GST-fusion constructs were transformed into BL21 E.

coli and expressed by incubating bacterial clones at 30ºC using 0,5 mM IPTG overnight. Bacterial cultures were collected and lysed at 10,000 psi using a French-press in cold-PBS buffer containing protease inhibitor cocktail (Sigma-Aldrich). Bacterial lysates were incubated with GSH-sepharose beads (GE Amersham) and beads were washed 5 times in PBS before use. MDCK cysts (10^7) grown for 72h were washed twice in cold PBS and lysed in 1ml of TNE buffer (50mM Tris, 250 mM NaCl, 10 mM EDTA, pH 7.4) containing 0.1% NP-40 and protease inhibitor cocktail (Sigma-Aldrich). Each 1 ml of MDCK cyst lysate was incubated with beads containing 100 µg of GST-EpsR (N or C-terminal domains) or GST alone (control) protein for 2h. Beads were washed in TNE buffer 5 times, dried by aspiration and bound proteins were eluted in 100 µl of Laemmli buffer (LB) and analyzed by Western blot.

Coimmunoprecipitation. MDCK cells (10^7) stably expressing PLLP-GFP or EpsR-GFP were grown for 72h were washed once in cold PBS and lysed in 1ml of TNE buffer (50mM Tris, 150 mM NaCl, 10 mM EDTA, pH 7.4) containing 0.5% Triton-X100 and protease inhibitor cocktail (Sigma-Aldrich). Each 1 ml of MDCK cyst lysate was incubated with 2 µg of purified polyclonal anti-GFP (Life Technologies) or 2 µg of rabbit antiserum (control). Beads were washed in TNE buffer 5 times, dried by aspiration and bound proteins were eluted in 100 µl of LB and analyzed by Western blot.

RT-qPCR. Quantitative analysis of gene expression was carried out by real-time quantitative PCR. RNAs were purified from cells or zebrafish guts using the RNAeasy kit (Qiagen) to eliminate genomic DNA contaminations. RNA was converted into cDNA using the RNA-to-cDNA High capacity kit and then qPCR was performed using the ABI-PRISM 7900HT SDS system (Applied biosystems). PCRs were performed on 10 ng template cDNA per well using intron-spanning primers. Specificity was BLAST-analyzed for each primer pair, and we performed a melting curve analysis to ensure that a single PCR product was generated.

Morpholino injections. Morpholinos targeting *pllp* were designed, prepared and injected according to manufacturer's instructions (Genetools, LLC). We injected 4 ng per one-cell embryo in a 1:1:1 dilution with water and Phenol Red. The morpholino sequences were:

pllp AUG-MO (MO1): 5'-ACCTTCCCAGGAAAATCCGCCATTT-3'

pllp SPL-MO (MO2): 5'-GAATAGTCAAAGAGTCTCACCACCA-3'

FIGURE LEGENDS

Figure 1. *pllp* is expressed during zebrafish gut morphogenesis

Identification of *pllp* as a gene induced during gut morphogenesis. Zebrafish guts from *TgBAC(cldn15la-GFP)* animals were dissected at 48, 72 and 120hpf, and GFP+/- cells were sorted by FACS. RNA purification and cDNA synthesis was carried out at each time point and hybridized with a custom cDNA library microarray plate. Selected cDNAs were validated by RT-PCR analysis. Bottom right, scheme of predicted PLLP structure as a type-III transmemebrane protein showing a long N and a short C-terminal cytoplasmic tails.

(B) In situ hybridization of *pllp* probe. Embryos and larvae were collected and fixed at different time points, and incubated with a DIG-labeled PLLP antisense RNA probe and AP-linked anti-DIG antibody. ISH from all different time points were performed at the same time over 3 days and developed for 2h before fixation and cleanup. Arrows indicate gut.

(C) *TgBAC(pllp-GFP)* transgenic zebrafish. A spacer-GFP sequence was recombined in place of the STOP codon using a zebrafish BAC clone carrying the full *pllp* gene. The GFP-tagged BAC was injected in 1-cell embryos to generate stable transgenic lines. Pllp-GFP expression was consistent with RNA ISH data. Transgenic fish were bred and embryos and larvae were analyzed by epifluorescence microscopy. Notice the GFP expression pattern is not homogenous along the anterior-posterior of the gut as the posterior midgut segment contains a population of PLLP^{high} cells (arrow) that is apparent from 120hpf on.

(D) Transverse sections of *TgBAC*(*pllp-GFP*) fish. Sections from the posterior midgut (about 1/3 total gut length before the cloaca) were stained to analyze GFP expression using F-actin (which labels apical microvilli) and DAPI (for DNA). Arrows (apical localization) and arrowheads (internal endosomes) indicate the main pools where the protein is localized.

(E) Immunogold electron microscopy of *TgBAC*(*pllp-GFP*) fish posterior gut enterocyte. Pllp-GFP fusion protein was labeled using anti-GFP and protein-A bound to 15 nm gold particles. The majority of labeled protein (65%) resides in a

subapical endosomal compartment (SAC), whereas 15% of the label localized to microvilli (MVs) and 13% was labeling more basal localized tubulovesicles (E).

(F) Gavaging of zebrafish larvae. Dextran-Texas Red was force-fed by microinjection into anesthetized 6dpf larvae and allowed to endocytose from the apical plasma membrane for 2h.

(G) Dextran gavaged *TgBAC*(*pllp-GFP*) larvae. *TgBAC*(*pllp-GFP*) larvae were gavaged with Dextran-TR and analyzed by live confocal microscopy 2h post-gavaging. Notice the dextran was endocytosed only by Pllp^{high} cells in the posterior midgut (arrow) and not by Pllp^{low} cells. Pllp-GFP partially colocalized with Dextran-TR in endosomes.

(H) *TgBAC(pllp-GFP)*;*TgBAC(lamp2-spRFP)* 6dpf larval guts. Larvae were analyzed by live confocal microscopy. Expression of late/lysosomal marker Lamp2 was segregated to the PLLP^{high}) cells in the posterior midgut (arrows).

Figure 2. Pllp is required for epithelial morphogenesis and apical endocytosis in the zebrafish gut

(A) TALEN-generated *pllp^{pd1116}* mutant null allele. TALENs were generated to target the first exon of zebrafish *pllp* and injected into 1-cell embryos. After raising the founders, we cloned an allele, *pd1116* that harbors a null mutation. We confirmed RNA nonsense mediated decay of the *pllp* mRNA in the homozygous mutant embryos (see supplementary figure 1).

(B) Endocytosis of dextran in *pllp^{pd1116}* mutants. Posterior midgut sections (right panels) of WT and *pllp^{pd1116}* mutant dextran-gavaged 6dpf larvae were labeled with F-actin (green), Dextran-TR (red) and DAPI (DNA). Arrows indicate a few remaining cells that are able to endocytose dextran in the mutant.

(C) Toluidin-stained EM sections of *pllp^{pd1116}* mutant fish (400x magnification). Yellow arrows indicate enlarged immature endocytic compartments. Red bars are shown to compare the difference in cell height.

(D) Magnification of EM sections of *pllp^{pd1116}* mutant fish gavaged with dextran and BSA-gold(15nm). The BSA-positive compartments were analyzed and colored in red. Other mature (>200 nm) endocytic compartments were labeled in green. Recycling tubules on green endosomes are marked with magenta arrowheads.

(E) Quantification of endocytic cells in *pllp*^{pd1116} mutants. Posterior gut sections of 10 DextranTR-gavaged WT and *pllp*^{pd1116} 7dpf larvae were stained with phalloidin and DAPI and analyzed to quantify apical endocytosis. Data are expressed as mean±SD percentage of endocytic cells. WT, 63.9±8.2%; *pllp* ^{pd1116} 32±9,3%; >20 cells per section; ***p<0.005.

(F) Quantification of cell-height in *pllp*^{pd1116} mutants. Posterior midgut sections of 10 different WT vs. *pllp* 7dpf larvae were stained with phalloidin and analyzed to quantify cell height. Data are expressed as mean±SD cell height in μm; WT, 19.7±1.8 μm; *pllp*^{pd1116}, 11.7±1.7 μm; >20 cells per section; ***p<0.005.

(G) Epithelial morphology of 16 dpf *pllp* larvae. 16dpf WT and *pllp*^{pd1116} larvae were fixed, sectioned and stained with the anti-E-cadherin antibody (green), F-actin (red) and DAPI (blue, DNA).

(H) Quantification of larvae survival in the first 18 dpf. WT and *pllp*^{pd1116} 5dpf larvae (n=25) were raised in 1L tanks with a restricted diet (1 feeding per day) and animal survival was assessed by observing heartbeat every day until 18 dpf. Solid lines indicate WT larvae. Dotted lines indicate *pllp*^{pd1116} larvae.

(I) Rescue of dextran endocytosis in *pllp*^{pd1116} larvae carrying the *TgBAC*(*pllp-GFP*)*pd1115* transgene. 6dpf larvae were gavaged with Dextran-TR, incubated for 2h, sectioned and stained with DAPI (blue, DNA).

(J) Quantification of phenotype rescue. 6dpf larvae from a cross of *TgBAC*(*pllp-GFP*) *pllp+/-* with *pllp-/-* fish were gavaged with Dextran-TR, incubated for 2h, sorted by transgenic GFP expression, and then the percentage of larvae with disrupted endocytosis (<50% endocytic cells) and disrupted cell height (<15μm) phenotypes were quantified in each case (GFP+, N=39; GFP-, N=85).

Figure 3. PLLP is expressed in MDCK cysts and is required for lumen formation and endosomal acidification

(A) Expression of PLLP in MDCK cysts at different time points. MDCK cells were grown to form cysts and fixed after 24, 48 and 72h. MDCK cysts were labeled with anti-PLLP antibody (green), anti-Podxl (red), and DNA (blue) and analyzed by confocal microscopy using DIC. Notice the subapical localization of PLLP signal in the magnification panel.

(B) Expression of PLLP in MDCK cysts and monolayers at different time points. MDCK cells were grown to form cysts and lysed after 24, 48, 72, and 120h. Westernblot analysis was performed to quantify PLLP protein levels at different time points (bottom graph).

(C) Silencing of PLLP expression in MDCK cysts. MDCK cells transfected with control or PLLP-specific siRNAs were grown to form cysts and lysed after 72h. Westernblot analysis was performed to quantify PLLP protein levels at different time points.

(D) Phenotype of PLLP-KD in MDCK cysts. MDCK cells transfected with control or PLLP-specific siRNAs were grown to form cysts and fixed after 72h. MDCK cysts were labeled with anti-PLLP antibody (green), anti-Podxl (red) DAPI (DNA, blue) and analyzed by confocal microscopy with DIC. Notice the disruption of PLLP antibody signal in PLLP-KD cysts.

(E) Quantification of lumen formation phenotype in PLLP-KD MDCK cysts. Measurements are expressed as mean±SD total percentage of single lumen-forming cysts in 5 different independent experiments. Control, 74.2±5.0%; PLLP-KD, 44.3±16.4%; ***$p<0.005$.

(F) Rescue of PLLP-KD phenotype by expression of siRNA-resistant PLLP-GFP(R). WT MDCK cells or MDCK cells stably expressing PLLP-GFP(R) protein were transfected with control or PLLP-specific siRNAs and grown to form cysts. MDCK cysts were fixed and labeled with anti-Podxl (red) anti-βcatenin (blue) and analyzed by confocal microscopy.

(G) Endosomal acidification defect in PLLP-KD cysts. MDCK cells transfected with control or PLLP-specific siRNAs were grown to form cysts for 72h, labeled with Lysotracker-Red for 2h, and then fixed. MDCK cysts were also labeled with Phalloidin (green) and ToPRO3 (DNA, blue) and analyzed by confocal microscopy.

Figure 4. PLLP ablation disrupts the apical recycling endosomes

(A) PLLP and Rab11a colocalization in zebrafish enterocytes. *TgBAC(pllp-GFP)* 6dpf larvae were fixed, sectioned and stained with the anti-Rab11 antibody (red), to label endogenous Rab11, and DAPI (blue, DNA). Notice goblet/secretory cells are both Rab11 and PLLP-negative (arrowheads). Arrows indicate colocalization of

PLLP and Rab11 at the subapical PM. Arrowheads indicate large PLLP-positive, Rab11-negative endosomes.

(B) PLLP and Rab11a colocalization in MDCK cysts. MDCK cells stably expressing PLLP-GFP were grown to form cysts and fixed after 72h. MDCK cysts were labeled with anti-Rab11 antibody (red), anti-βcatenin (blue) and analyzed by confocal microscopy. Arrow indicates apical recycling endosome.

(C) Rab11 localization in WT and *pllp*^{pd1116} 96hpf larval guts. 96dpf WT larvae were fixed, sectioned and stained with the anti-Rab11 antibody (green), Phalloidin (red) and DAPI (blue, DNA). Arrow indicates subapical compartment. Notice the dispersion of subapical Rab11 endosomes in *pllp*^{pd1116} mutants.

(D) Rab11 localization in PLLP-KD cysts. MDCK cells transfected with control or PLLP-specific siRNAs were grown to form cysts and fixed after 72h. MDCK cysts were labeled with anti-Rab11 antibody (red), anti-Podxl (green) DAPI (DNA, blue) and analyzed by confocal microscopy with DIC. Right panels show whole z-axis projection of the Rab11 signal surrounding a single lumen. Arrows indicates apical recycling endosome.

Figure 5. EpsR interacts with PLLP to form recycling tubulovesicles from late endosomes

(A) In vivo biotinylation (bioID) assay for identifying PLLP proximal proteins. A myc-tagged birA*-PLLP fusion protein or birA* (control) protein was expressed in MDCK cysts. Cysts were incubated with biotin for 16h and lysed with RIPA buffer. Biotinylated proteins were purified using Streptavidin magnetic beads and analyzed by MALDI-TOF/TOF peptide-mass fingerprinting.

(B) Functional classification of PLLP-interacting proteins. Gene ontology (GO) and bibliographic research was used to classify the interacting proteins into functional classes. A significant GO-term enrichment was observed for proteins with putative SNARE function (left). The top interacting partner was EpsR (right), which contains the cargo binding ENTH domain followed by a long non-globular C-terminal region. In the PLLP bioID, we identified 31 peptides and 4 biotinylated peptides (in red) from EpsR.

(C) Pull down of endogenous PLLP using GST-tagged Eps fragments. GST-N-EpsR and GST-C-EpsR fusion proteins were expressed and incubated with GSH-beads.

Lysates from MDCK cells were incubated with GST-N/C-EpsR beads, washed, and dried. Beads were eluted with LB and analyzed by Western blot.

(D) Coimmunoprecipitation of endogenous PLLP on EpsR-GFP stable cells. Lysates from MDCK cells stably expressing EpsR-GFP were incubated with control or GFP antibody beads, washed, and dried. Beads were eluted with LB and analyzed by Western blot.

(E) Coimmunopreciptation of endogenous EpsR on PLLP-GFP stable cells. Lysates from MDCK cells stably expressing PLLP-GFP were incubated with control or GFP antibody beads, washed, and dried. Beads were eluted with LB and analyzed by Western blot.

(F) Endogenous EpsR and PLLP localization in MDCK cysts. MDCK cells were grown to form cysts and fixed after 72h. MDCK cysts were labeled with anti-PLLP antibody (red), anti-EpsR (green) and DNA (blue) and analyzed by confocal microscopy. Arrows indicate PLLP and EpsR colocalizing in perinuclear endosomes.

(G) EpsR localization in PLLP-Cherry cells. MDCK cells stably expressing PLLP-Cherry were fixed after 72h, labeled with anti-EpsR antibody (green) and analyzed by confocal microscopy. An x-y section of the apical region of a single cell is shown. Arrows indicate colocalization of PLLP and EpsR.

(H) Rab7 localization in PLLP-KD MDCK cysts. MDCK cells stably expressing Rab7-GFP were transfected with control or PLLP-specific siRNAs, grown to form cysts and fixed after 72h. MDCK cysts were labeled with anti-PLLP antibody (red) and anti-EpsR antibody (blue) and analyzed by confocal microscopy. Arrows indicate dispersed EpsR and Rab7 staining in PLLP-KD cells.

(I) Suboptimal transfection of PLLP siRNA. MDCK cells stably expressing Rab7-GFP were transfected with control or PLLP-specific siRNAs at reduced concentrations, grown to form cysts, and fixed after 72h. MDCK cysts were labeled with anti-PLLP antibody (red) and Epsin-R (blue) and analyzed by confocal microscopy. Arrows indicate maintenance of EpsR and Rab7 staining in non-depleted cells.

(J) Silencing of EpsR expression using siRNA. MDCK cells were transfected with control or EpsR-specific siRNAs, grown to form cysts and lysed after 72h. Westernblot analysis was performed to quantify endogenous EpsR protein levels at different time points.

(K) Phenotype of EpsR-KD MDCK cysts. WT MDCK cells were transfected with control or EpsR-specific siRNAs (#1), grown to form cysts and fixed after 72h. MDCK cysts were labeled with anti-EpsR (green), anti-ZO1 (red) and βcatenin (blue) and analyzed by confocal microscopy. L, lumen. Arrows indicate multiple lumens.

(L) Quantification of lumen formation phenotype in EpsR-KD MDCK cysts. Measurements are expressed as mean±SD percentage of single lumen-forming cysts in 3 different independent experiments. Control, 78.7±4.7%; EpsR-KD, 45.7±11.4%; *** $p<0.005$.

(M) Rab11 localization in EpsR-KD cysts. MDCK cells were transfected with control or EpsR-specific siRNAs, grown to form cysts and fixed after 72h. MDCK cysts were labeled with anti-Rab11 antibody (red), E-cadherin (green) and DNA (blue) and analyzed by confocal microscopy. Arrows indicate dispersed Rab11 endosomes in EpsR-KD cysts.

Figure 6. Sorting of endosomal SNAREs requires PLLP and EpsR-mediated recycling

(A) Stx7 localization in MDCK cysts. MDCK cells stably expressing Stx7-GFP were grown to form cysts and fixed after 72h. MDCK cysts were labeled with anti-Podxl antibody (red) and βcatenin (blue) and analyzed by confocal microscopy. Magnification scale bars, 2 μm.

(B) Stx7 and PLLP fluorescence recovery after photobleaching (FRAP) assay. MDCK cells stably expressing PLLP-Cherry were transfected with Stx7-GFP and grown to form cysts for 72h. Photobleaching was performed with both 488nm and 564nm lasers inside the region outlined by the dotted cyan line, and cysts were imaged 1 frame every 4 seconds until fluorescence inside the bleached region recovered to a steady state.

(C) Quantification of FRAP assay. Six cells were measured as in (B). The measurements are expressed in the graph as mean±SD percentage of total fluorescence intensity inside the photobleached region. Green line, Stx7; Red line, PLLP.

(D) Stx7 localization in PLLP-KD and EpsR-KD MDCK cysts. MDCK cells stably expressing Stx7-GFP were transfected with control, PLLP, or EpsR-specific siRNAs,

grown to form cysts and fixed after 72h. MDCK cysts were labeled with anti-PLLP antibody (red) and E-cadherin (blue) and analyzed by confocal microscopy. Arrowheads indicate colocalizing PLLP/Stx7 signal in subapical endosomes. Arrows indicate PLLP/Stx7 colocalizing signal in perinuclear endosomes.

(E) Stx7 localization in 6dpf *pllp*^{pd1116} mutant larvae. 96dpf WT or *pllp*^{pd1116} mutant larvae were fixed with acetone, sectioned and stained with the anti-Stx7 antibody (green), and DAPI (red, DNA). Arrows indicate apical Stx7 localization. Notice the mislocalized dispersed Stx7 localization in *pllp*^{pd1116} larvae.

(F) Silencing of Stx7 expression using siRNA. WT MDCK cells or MDCK cells stably expressing Stx7-GFP were transfected with control or Stx7-specific siRNAs, grown to form cysts and lysed after 72h. Westernblot analysis was performed to quantify Stx7 protein levels. * Unspecific bands from the antibody.

(G) Phenotype of Stx7-KD MDCK cysts and phenotype rescue. WT MDCK cells or MDCK cells stably expressing Stx7-GFP were transfected with control or Stx7-specific siRNAs, grown to form cysts and fixed after 72h. MDCK cysts were labeled with anti-Podxl antibody (red) and βcatenin (blue) and analyzed by confocal microscopy.

(H) Quantification of lumen formation phenotypes in Stx7-KD MDCK cysts and phenotype rescue. Measurements are normalized to WT MDCK cells (control) and expressed as mean±SD percentage relative to control of single lumen-forming cysts in 3 different independent experiments. Control, 100±5.3%; Stx7-KD, 52.3±6.4%; Control GFP-Stx7, 97.0±0.2%; Stx7-KD GFP-Stx7, 98.4±5.0%; *** $p<0.005$.

(I) Rab11 localization in Stx7-KD cysts. MDCK cells were transfected with control or Stx7-specific siRNAs, grown to form cysts and fixed after 72h. MDCK cysts were labeled with anti-Rab11 antibody (red), Phalloidin (green) and E-cadherin (blue) and analyzed by confocal microscopy. Arrows indicate apical recycling endosomes.

Figure 7. PLLP modulates Crb endocytosis in MDCK cysts

(A) Localization of endogenous Crb3 in MDCK cysts. MDCK cysts grown for 72h were fixed and labeled with anti-Crb3 antibody (green), ZO-1 (blue) and E-cadherin (red). Bottom panels, Crb3 signal. Arrowhead indicates apical localization

of Crb3 after initial lumen formation at 24h. Arrows indicate suprajunctional Crb3 localization at 72h.

(B) Localization of endogenous Crb3 in PLLP-KD, EpsR-KD and Stx7-KD MDCK cysts. WT MDCK cells were transfected with control, PLLP, EpsR or Stx7-specific siRNAs, grown to form cysts and fixed after 72h. MDCK cysts were labeled with anti-Crb3 antibody (green), ZO-1 (red) and E-cadherin (blue) and analyzed by confocal microscopy. L, lumen. Arrowheads indicate apical localization of Crb3. Arrows indicate supra-junctional Crb3 localization in control cysts.

(C) Crb3 protein levels in PLLP-KD cysts. WT MDCK cells were transfected with control or PLLP specific siRNAs, grown to form cysts and lysed after 72h. Western blot analysis was performed to quantify Crb3 protein levels. Data are expressed as mean±SD fold-increase vs. control. Control, 1±0.35 fold; PLLP-KD, 2.31±0.13 fold.

(D) Crb3 localization in WT 6dpf larvae. WT larvae were fixed, sectioned and stained with the anti-panCrb antibody (red), Phalloidin (green) and DAPI (blue, DNA). Arrows indicate Crb3 localization at TJ.

(E) Crb3 localization in *pllp*^{pd1116} mutant 6dpf larvae. *pllp*^{pd1116} mutant larvae were fixed, sectioned and stained with the anti-panCrb antibody (red), Phalloidin (green) and DAPI (blue, DNA). Arrows indicate Crb3 apical plasma membrane localization.

(F) Videomicroscopy of RUSH-Crb3a cysts. MDCK cells stably expressing an ER-Streptavidin luminal hook fusion protein and GFP-SBP-Crb3a were transfected with control or PLLP-siRNA and grown to form cysts. At 72h, biotin was added to the culture medium and cysts were recorded taking one image every minute for 1 hour, or until protein localization was stable. For Endocytosis inhibitor experiments, cysts were treated with 100 μM Dynasore at 40 min after biotin addition, when most Crb3 protein had reached the apical surface. Arrowheads indicate apical membrane. Arrows indicate tight junctions. Dotted lines mark the basal contour of the cysts. L, lumen. Scale bars, 5 μm. See Videos 2-5 in supplementary information.

(G) Downmodulation of Crb3 in PLLP-GFP clones in 2D monolayers. PLLP-GFP transfected cells were grown as monolayers for 4 days mixed with control MDCK cells, fixed and labeled for endogenous Crb3 (red). Green dotted line indicates the PLLP-GFP expressing clone.

(H) Quantification of (G). Medial and junctional Crb3 staining was measured as integrated density in 3 independent transfection experiments. Measurements are mean fluorescence intensity±SD as % of control. GFP-neg, 100±8.3%; PLLP-GFP, 73.6±7.7%; **p<0.01.

(I) Pulse-chase endocytosis of GFP-Crb3a in PLLP expressing cells. MDCK cells stably expressing GFP-Crb3a were transfected with PLLP-Cherry. After 24h, the apical surface of the cells was incubated with anti-GFP to label Crb3 at 4ºC, washed, and then cells were returned at 37º for 90 minutes to follow endocytosis. Then, cells were fixed, stained with anti-rabbit-Alexa647 (green), and analyzed by confocal microscopy. The images show a maximum z-stack projection at the apical pole. Arrows indicate endocytosed apical GFP-Crb3a. Note that at this time point PLLP-negative cells still present an apical localization of Crb3a.

Figure 8. PLLP controls Notch signaling.

(A) Notch-activity in PLLP-KD cysts. WT MDCK cells were transfected with control or PLLP specific siRNAs, grown to form cysts and lysed after 72h. Western blot analysis was performed to quantify cleaved Notch (NICD) protein levels.

(B) Notch localization in PLLP-KD cells. PLLP-wt expressing cells were transfected with Notch1a-myc and PLLP siRNA, grown as monolayers for 4 days, fixed, and labeled for myc (red), PLLP (green) and ZO1 (blue). Arrows indicate PLLP-depleted cells with apical/junctional Notch1a-myc expression. Arrowheads indicate PLLP and Notch1a-myc endosomal colocalization in non-depleted cells.

(C) Intestinal morphology in adult *pllp*^{pd1116} posterior guts. WT and *pllp*^{pd1116} adult fish were fixed, paraffin-embed, sectioned and stained with PAS to label mucous-secreting goblet cells in purple. Arrows indicate goblet cells.

(D) Quantification of endocytic cells and goblet cells. HE and PAS-stained posterior gut sections from WT and *pllp*^{pd1116} fish were analyzed to quantify secretory goblet cells (% of PAS-positive/nuclei) and endocytic cells (measured as % of vacuoles/nuclei). Data are expressed as mean±SD percentage of total cells from 9 crypts per animal. Endocytic cells: WT, 67.3±15.5%; *pllp* ^{pd1116}, 35.3±12.4%; Goblet cells: WT, 2.7±1.8%; *pllp* ^{pd1116}, 9.0±1.3%; N=3, ***p<0.005.

(E) Notch-target gene expression in *pllp*^{pd1116} adult guts. Posterior guts from adult WT and *pllp*^{pd1116} fish were dissected and RNA purification and cDNA

polymerization was performed. The expression of the Notch-effector genes *her15.1, her6 and her9* were analyzed by qPCR using rRNA 18S as normalizer. Data are expressed as mean±SD percentage of control expression (N=3; ***p<0.005).

(F) Dextran endocytosis phenotypes in *mib1*^{ta52b} and DAPT-treated larvae. Posterior midgut sections (right panels) of Dextran-TR gavaged (red) 6dpf larvae from DMSO-treated fish (WT), 100 μM DAPT (Notch inhibitor) treated fish and *mib1*^{ta52b} mutants were labeled with Phalloidin (green) and DAPI (DNA). Arrows indicate remaining cells that are able to endocytose dextran.

(G) Model. In the posterior gut, Pllp expression controls epithelial morphogenesis and differentiation. Pllp regulates endocytosis of apical membrane receptors such as Crb. During endocytosis PLLP is co-transported together with apical receptors and apical endosomal SNAREs as they traffic into late endosomes. There, Pllp recruits EpsR, which binds endosomal SNAREs to generate tubulovesicles that transport endosomal SNAREs such as Stx7 to the apical PM, recycling them to maintain and/or enhance the apical endosomal fusion process. Disruption of Pllp results in abnormal Notch signaling and reduced differentiation of absorptive endocytic cells in the posterior gut in favor of mucous secretory cell fates.

VIDEO1. Stx7/PLLP FRAP experiment. MDCK cells stably expressing PLLP-Cherry were transfected with Stx7-GFP and imaged using confocal microscopy every 4 s. The outlined region of interest was photobleached using the 488nm and 564nm lasers for 12 rounds after the 4th frame. Frame rate, 4 s^{-1}.

VIDEO2. Crb3 RUSH in MDCK cysts. MDCK cells stably expressing Streptavidin-KDEL and EGFP-SBP-Crb3a were cultured to grow cysts for 72h. Biotin was added at t=0 and cysts were imaged using confocal microscopy (pinhole = 1 μm) every 1 minute. Frame rate, 3 s^{-1}.

VIDEO3. Crb3 RUSH in control cells. MDCK cells stably expressing Streptavidin-KDEL and EGFP-SBP-Crb3a were transfected with control siRNA and cultured to grow cysts for 72h. Biotin was added at t=0 and cysts were imaged using confocal microscopy (pinhole = 1 μm) every 1 minute. Frame rate, 3 s^{-1}.

VIDEO4. Crb3 RUSH in PLLP-KD cells. MDCK cells stably expressing Streptavidin-KDEL and EGFP-SBP-Crb3a were transfected with PLLP-specific siRNA and cultured to grow cysts for 72h. Biotin was added at t=0 and cysts were

imaged using confocal microscopy (pinhole = 1 μm) every 1 minute. Frame rate, 3 s^{-1}.

VIDEO5. Crb3 RUSH in Dynasore-treated cells. MDCK cells stably expressing Streptavidin-KDEL and EGFP-SBP-Crb3a were cultured to grow cysts for 72h. Biotin was added at t=0 and cysts were imaged using confocal microscopy (pinhole = 1 μm) every 1 minute. Dynasore was added at 50 μM after 40 min. Frame rate, 3 s^{-1}.

Supplementary figure 1. RT-PCR and wholemount phenotype of *pllp*^{pd1116} mutant fish.

(A) *pllp* mRNA levels in *pllp*^{pd1116} mutant larvae. RNA was extracted from 20 larvae at 5dpf, and RT-qPCR was performed to analyze endogenous *pllp* expression. Results are mean+/-SD % expression relative to control and normalized with rRNA 18S expression.

(B) Live whole-mount images of WT and *pllp*^{pd1116} larvae at 6dpf.

(C) Quantification of total number of intestinal cells per section of 7dpf *pllp* ^{pd1116} larvae. WT and *pllp* ^{pd1116} larvae at 6dpf were fixed, sectioned and stained with DAPI and F-actin to quantify the total number of intestinal cells per section. Results are represented as mean+/-SD total number of nuclei in a 2 μm-thick cross-sections.

(D) Silencing of *TgBAC(pllp-GFP)* in morpholino-injected 4dpf larvae. *TgBAC(pllp-GFP)* embryos were injected with MO1 and MO2 morpholinos at one-cell stage and allowed to grow until 4dpf. Whole animal lysates from 20 larvae were analyzed by Western blot, using anti-GFP antibodies.

(E) Quantification of % of morpholino-injected larvae presenting disrupted epithelial columnar organization. *, $p<0.05$ in three independent experiments. WT embryos were injected with MO1 and MO2 morpholinos at one-cell stage and grown until 4dpf. Posterior gut sections were stained with Phalloidin (green) and DAPI (red) and analyzed by confocal microscopy.

(F) Phenotype of morpholino-injected larvae quantified in (E). L, lumen

Supplementary figure 2. Localization of endogenous PLLP in mouse intestine and kidney, and additional description of PLLP-KD phenotype.

(A) Localization of endogenous PLLP in mouse intestinal cells. Agarose-embedded sections of 1 month-old BL6 mice small intestines were stained with the PLLP antibody (green), Phalloidin (red) and DAPI (blue, DNA). A magnification of cells from a villar tip is shown.

(B) Localization of endogenous PLLP in mouse kidney cells. Agarose-embedded sections of 1 month-old BL6 mice kidneys were stained with the PLLP antibody (green), Phalloidin (red) and DAPI (blue, DNA). Magnifications of a medular and a cortical kidney tubule are shown.

(C) Quantification of mean particle size in Lysotracker-treated PLLP-KD cysts. 72h MDCK cysts were stained with Lysotracker-Red and analyzed by confocal microscopy. Resulting images were segmented to quantify the mean particle size. Data are represented as mean+/-SD particle size in square-pixels; N=50 cells per condition; ** $p<0.01$.

(D) Western-blot of PLLP rescue experiments. MDCK or PLLP-GFP(R) expressing cells were transfected with PLLP siRNA and grown into cysts for 72h. Whole cell lysates were prepared and analyzed by Western blot using anti-PLLP antibody and anti-p36 as a loading control.

(E) Quantification of PLLP-KD rescue by siRNA-resistant PLLP-GFP(R). Measurements are normalized to WT MDCK cells (control) and expressed as mean±SD percentage relative to control of single lumen-forming cysts in 3 different independent experiments. *** $p<0.005$; n.s, not significant.

Supplementary figure 3. Gain of function phenotypes of PLLP expression.

(A) Rescue of Rab11 subapical localization in *pllp*^{pd1116} larvae carrying the *TgBAC(pllp-GFP*) transgene. 6dpf WT larvae were fixed, sectioned and stained with the anti-Rab11 antibody (red) and DAPI (blue, DNA).

(B) Overexpression of PLLP-GFP in MDCK monolayers. MDCK cells cultured in monolayers were transiently transfected to overexpress PLLP-GFP and fixed after 48h. Cells were stained to detect Rab11, EEA1, Clathrin or Lysotracker.

(C) Subcellular EM localization of PLLP-GFP aggregates in overexpressing cells. PLLP-GFP overexpressing cells were FACS-sorted at 48h, pelleted, seeded into monolayers, and fixed after 24h. Then, cell pellets were processed for immunogold-EM using anti-GFP and 15nm protein-A gold beads.

(D) *In vivo* overexpression of Pllp-GFP in *TgBAC(pllp-GFP)pd1114* at 5dpf. Posterior gut sections of 5dpf larvae carrying a *TgBAC(pllp-GFP)pd1114* overexpessing allele were fixed and stained with Phalloidin (red) and DAPI (blue, DNA).

(E) Requirement for EpsR in PLLP-GFP overexpression phenotype. PLLP-GFP overexpressing cells were co-transfected with EpsR or control siRNA, grown for 48h, fixed and stained to detect Rab11.

Supplementary figure 4. Localization of Stx7 in mouse intestine, and PLLP/Stx7 probe ligation interaction assay.

(A) Endogenous subapical Stx7 localization in mouse small intestine villi. Agarose-embedded sections of 1 month-old BL6 mice small intestines were stained with the Stx7 antibody (green), Phalloidin (red) and DAPI (blue, DNA). A magnification of cells from a villar tip is shown.

(B) Stx7 and PLLP probe ligation assay (PLA). MDCK cells stably expressing WT untagged PLLP were transiently transfected with GFP mock, Rab11-GFP or Stx7-GFP plasmids. PLA was performed with mouse anti-GFP (green) and rabbit anti-PLLP antibodies and whole-cell maximum z-stack projections of the PLA signal (red) were analyzed by confocal microscopy (n>10 cells per condition; N=2). Arrow indicates colocalization of PLA signal and Stx7-GFP.

(C) Quantification of PLLP PLA. Integrated density of the PLA fluorescent signal was quantified in 16-bit images of maximum z-stack projections and represented as fold-increase over GFP background signal for GFP-Rab11 and GFP-Stx7. Mean results of three independent experiments are shown as base-2 log of signal-to-background ratio.

Supplementary figure 5. Additional data on PLLP regulation of intestinal differentiation.

(A) Effect of transient PLLP-GFP expression on Notch1a-myc localization. MDCK cells stably expressing full length Notch1a-myc were transfected with PLLP-GFP, grown for 48h and fixed to detect myc (red) and ZO1 (blue). Arrows indicate PLLP-GFP expressing cells next to non-expressing cells. Arrowheads indicate the internalized compartment with Notch1a-myc in PLLP-GFP expressing cells.

(B) Colocalization of PLLP-GFP and Notch1a-myc in endosomes. The images show basal (top panels) and apical (bottom panels) sections and magnifications of MDCK cells treated as in (A). Arrows indicate colocalization of Notch1a-myc in PLLP-GFP positive endosomes.

(C) HE and PAS staining of posterior guts of WT and *pllp*^{pd1116} zebrafish. WT and *pllp*^{pd1116} adult fish guts were dissected, formalin-fixed, paraffin-embed, sectioned and stained with Hematoxylin/Eosin (HE), or Periodic Acid Schiff (PAS).

Table S1. In vivo biotinylation of EpsR by PLLP (bioID).

List of purified peptides from EpsR protein isolated during PLLP-bioID. PLLP-bioID was performed in 3D-MDCK cultures and analyzed by LC-MS/MS peptide mass fingerprinting considering lysine biotinylation as a possible modification. The top-scoring identified protein was EpsR (Uniprot: Q14677), which showed 4 different biotinylated peptides and 31 total different peptides.

REFERENCES

Alvers, A.L., Ryan, S., Scherz, P.J., Huisken, J., and Bagnat, M. (2014). Single continuous lumen formation in the zebrafish gut is mediated by smoothened-dependent tissue remodeling. Development *141*, 1110-1119.

Apodaca, G., Gallo, L.I., and Bryant, D.M. (2012). Role of membrane traffic in the generation of epithelial cell asymmetry. Nature cell biology *14*, 1235-1243.

Bagnat, M., Cheung, I.D., Mostov, K.E., and Stainier, D.Y. (2007). Genetic control of single lumen formation in the zebrafish gut. Nature cell biology *9*, 954-960.

Bokel, C., and Brand, M. (2014). Endocytosis and Signaling during Development. Cold Spring Harbor perspectives in biology *6*.

Boncompain, G., Divoux, S., Gareil, N., de Forges, H., Lescure, A., Latreche, L., Mercanti, V., Jollivet, F., Raposo, G., and Perez, F. (2012). Synchronization of secretory protein traffic in populations of cells. Nature methods *9*, 493-498.

Bosse, F., Hasse, B., Pippirs, U., Greiner-Petter, R., and Muller, H.W. (2003). Proteolipid plasmolipin: localization in polarized cells, regulated expression and lipid raft association in CNS and PNS myelin. Journal of neurochemistry *86*, 508-518.

Bryant, D.M., Datta, A., Rodriguez-Fraticelli, A.E., Peranen, J., Martin-Belmonte, F., and Mostov, K.E. (2010). A molecular network for de novo generation of the apical surface and lumen. Nature cell biology *12*, 1035-1045.

Cermak, T., Doyle, E.L., Christian, M., Wang, L., Zhang, Y., Schmidt, C., Baller, J.A., Somia, N.V., Bogdanove, A.J., and Voytas, D.F. (2011). Efficient design and assembly

of custom TALEN and other TAL effector-based constructs for DNA targeting. Nucleic acids research *39*, e82.

Chidambaram, S., Mullers, N., Wiederhold, K., Haucke, V., and von Mollard, G.F. (2004). Specific interaction between SNAREs and epsin N-terminal homology (ENTH) domains of epsin-related proteins in trans-Golgi network to endosome transport. The Journal of biological chemistry *279*, 4175-4179.

Chidambaram, S., Zimmermann, J., and von Mollard, G.F. (2008). ENTH domain proteins are cargo adaptors for multiple SNARE proteins at the TGN endosome. Journal of cell science *121*, 329-338.

Cocchiaro, J.L., and Rawls, J.F. (2013). Microgavage of zebrafish larvae. Journal of visualized experiments : JoVE, e4434.

Crosnier, C., Vargesson, N., Gschmeissner, S., Ariza-McNaughton, L., Morrison, A., and Lewis, J. (2005). Delta-Notch signalling controls commitment to a secretory fate in the zebrafish intestine. Development *132*, 1093-1104.

Doyle, E.L., Booher, N.J., Standage, D.S., Voytas, D.F., Brendel, V.P., Vandyk, J.K., and Bogdanove, A.J. (2012). TAL Effector-Nucleotide Targeter (TALE-NT) 2.0: tools for TAL effector design and target prediction. Nucleic acids research *40*, W117-122.

Eaton, S., and Martin-Belmonte, F. (2014). Cargo Sorting in the Endocytic Pathway: A Key Regulator of Cell Polarity and Tissue Dynamics. Cold Spring Harbor perspectives in biology.

Fabrowski, P., Necakov, A.S., Mumbauer, S., Loeser, E., Reversi, A., Streichan, S., Briggs, J.A., and De Renzis, S. (2013). Tubular endocytosis drives remodelling of the apical surface during epithelial morphogenesis in Drosophila. Nature communications *4*, 2244.

Fre, S., Bardin, A., Robine, S., and Louvard, D. (2011). Notch signaling in intestinal homeostasis across species: the cases of Drosophila, Zebrafish and the mouse. Experimental cell research *317*, 2740-2747.

Golachowska, M.R., Hoekstra, D., and van, I.S.C. (2010). Recycling endosomes in apical plasma membrane domain formation and epithelial cell polarity. Trends in cell biology *20*, 618-626.

Herranz, H., Stamataki, E., Feiguin, F., and Milan, M. (2006). Self-refinement of Notch activity through the transmembrane protein Crumbs: modulation of gamma-secretase activity. EMBO reports *7*, 297-302.

Hirst, J., Motley, A., Harasaki, K., Peak Chew, S.Y., and Robinson, M.S. (2003). EpsinR: an ENTH domain-containing protein that interacts with AP-1. Molecular biology of the cell *14*, 625-641.

Horne-Badovinac, S., Rebagliati, M., and Stainier, D.Y. (2003). A cellular framework for gut-looping morphogenesis in zebrafish. Science *302*, 662-665.

Lee, J.H., Overstreet, E., Fitch, E., Fleenor, S., and Fischer, J.A. (2009). Drosophila liquid facets-Related encodes Golgi epsin and is an essential gene required for cell proliferation, growth, and patterning. Developmental biology *331*, 1-13.

Leuchowius, K.J., Weibrecht, I., and Soderberg, O. (2011). In situ proximity ligation assay for microscopy and flow cytometry. Current protocols in cytometry / editorial board, J Paul Robinson, managing editor [et al] *Chapter 9*, Unit 9 36.

Leventis, P.A., Da Sylva, T.R., Rajwans, N., Wasiak, S., McPherson, P.S., and Boulianne, G.L. (2011). Liquid facets-related (lqfR) is required for egg chamber morphogenesis during Drosophila oogenesis. PloS one *6*, e25466.

Liu, Y., Pathak, N., Kramer-Zucker, A., and Drummond, I.A. (2007). Notch signaling controls the differentiation of transporting epithelia and multiciliated cells in the zebrafish pronephros. Development *134*, 1111-1122.

Lu, H., and Bilder, D. (2005). Endocytic control of epithelial polarity and proliferation in Drosophila. Nature cell biology *7*, 1232-1239.

Martin-Belmonte, F., and Perez-Moreno, M. (2012). Epithelial cell polarity, stem cells and cancer. Nature reviews Cancer *12*, 23-38.

Miller, S.E., Collins, B.M., McCoy, A.J., Robinson, M.S., and Owen, D.J. (2007). A SNARE-adaptor interaction is a new mode of cargo recognition in clathrin-coated vesicles. Nature *450*, 570-574.

Mills, I.G., Praefcke, G.J., Vallis, Y., Peter, B.J., Olesen, L.E., Gallop, J.L., Butler, P.J., Evans, P.R., and McMahon, H.T. (2003). EpsinR: an AP1/clathrin interacting protein involved in vesicle trafficking. The Journal of cell biology *160*, 213-222.

Mummery-Widmer, J.L., Yamazaki, M., Stoeger, T., Novatchkova, M., Bhalerao, S., Chen, D., Dietzl, G., Dickson, B.J., and Knoblich, J.A. (2009). Genome-wide analysis of Notch signalling in Drosophila by transgenic RNAi. Nature *458*, 987-992.

Navis, A., Marjoram, L., and Bagnat, M. (2013). Cftr controls lumen expansion and function of Kupffer's vesicle in zebrafish. Development *140*, 1703-1712.

Ohata, S., Aoki, R., Kinoshita, S., Yamaguchi, M., Tsuruoka-Kinoshita, S., Tanaka, H., Wada, H., Watabe, S., Tsuboi, T., Masai, I.*, et al.* (2011). Dual roles of Notch in regulation of apically restricted mitosis and apicobasal polarity of neuroepithelial cells. Neuron *69*, 215-230.

Ohlstein, B., and Spradling, A. (2007). Multipotent Drosophila intestinal stem cells specify daughter cell fates by differential notch signaling. Science *315*, 988-992.

Richardson, E.C., and Pichaud, F. (2010). Crumbs is required to achieve proper organ size control during Drosophila head development. Development *137*, 641-650.

Rodriguez-Boulan, E., and Macara, I.G. (2014). Organization and execution of the epithelial polarity programme. Nature reviews Molecular cell biology *15*, 225-242.

Rodriguez-Fraticelli, A.E., Vergarajauregui, S., Eastburn, D.J., Datta, A., Alonso, M.A., Mostov, K., and Martin-Belmonte, F. (2010). The Cdc42 GEF Intersectin 2 controls mitotic spindle orientation to form the lumen during epithelial morphogenesis. The Journal of cell biology *189*, 725-738.

Roux, K.J., Kim, D.I., Raida, M., and Burke, B. (2012). A promiscuous biotin ligase fusion protein identifies proximal and interacting proteins in mammalian cells. The Journal of cell biology *196*, 801-810.

Saint-Pol, A., Yelamos, B., Amessou, M., Mills, I.G., Dugast, M., Tenza, D., Schu, P., Antony, C., McMahon, H.T., Lamaze, C.*, et al.* (2004). Clathrin adaptor epsinR is required for retrograde sorting on early endosomal membranes. Developmental cell *6*, 525-538.

Sanchez-Pulido, L., Martin-Belmonte, F., Valencia, A., and Alonso, M.A. (2002). MARVEL: a conserved domain involved in membrane apposition events. Trends in biochemical sciences *27*, 599-601.

Schier, A.F., Neuhauss, S.C., Harvey, M., Malicki, J., Solnica-Krezel, L., Stainier, D.Y., Zwartkruis, F., Abdelilah, S., Stemple, D.L., Rangini, Z.*, et al.* (1996). Mutations affecting the development of the embryonic zebrafish brain. Development *123*, 165-178.

Sudhof, T.C., and Rizo, J. (2011). Synaptic vesicle exocytosis. Cold Spring Harbor perspectives in biology *3*.

Upadhyay, A., Kandachar, V., Zitserman, D., Tong, X., and Roegiers, F. (2013). Sanpodo controls sensory organ precursor fate by directing Notch trafficking and binding gamma-secretase. The Journal of cell biology *201*, 439-448.

Vaccari, T., Lu, H., Kanwar, R., Fortini, M.E., and Bilder, D. (2008). Endosomal entry regulates Notch receptor activation in Drosophila melanogaster. The Journal of cell biology *180*, 755-762.

van Es, J.H., van Gijn, M.E., Riccio, O., van den Born, M., Vooijs, M., Begthel, H., Cozijnsen, M., Robine, S., Winton, D.J., Radtke, F.*, et al.* (2005). Notch/gamma-secretase inhibition turns proliferative cells in intestinal crypts and adenomas into goblet cells. Nature *435*, 959-963.

VanDussen, K.L., Carulli, A.J., Keeley, T.M., Patel, S.R., Puthoff, B.J., Magness, S.T., Tran, I.T., Maillard, I., Siebel, C., Kolterud, A.*, et al.* (2012). Notch signaling modulates proliferation and differentiation of intestinal crypt base columnar stem cells. Development *139*, 488-497.

Wibowo, I., Pinto-Teixeira, F., Satou, C., Higashijima, S., and Lopez-Schier, H. (2011). Compartmentalized Notch signaling sustains epithelial mirror symmetry. Development *138*, 1143-1152.

Williams, S.E., Beronja, S., Pasolli, H.A., and Fuchs, E. (2011). Asymmetric cell divisions promote Notch-dependent epidermal differentiation. Nature *470*, 353-358.

Yamamoto, M., Morita, R., Mizoguchi, T., Matsuo, H., Isoda, M., Ishitani, T., Chitnis, A.B., Matsumoto, K., Crump, J.G., Hozumi, K.*, et al.* (2010). Mib-Jag1-Notch signalling regulates patterning and structural roles of the notochord by controlling cell-fate decisions. Development *137*, 2527-2537.

Yan, Y., Denef, N., and Schupbach, T. (2009). The vacuolar proton pump, V-ATPase, is required for notch signaling and endosomal trafficking in Drosophila. Developmental cell *17*, 387-402.

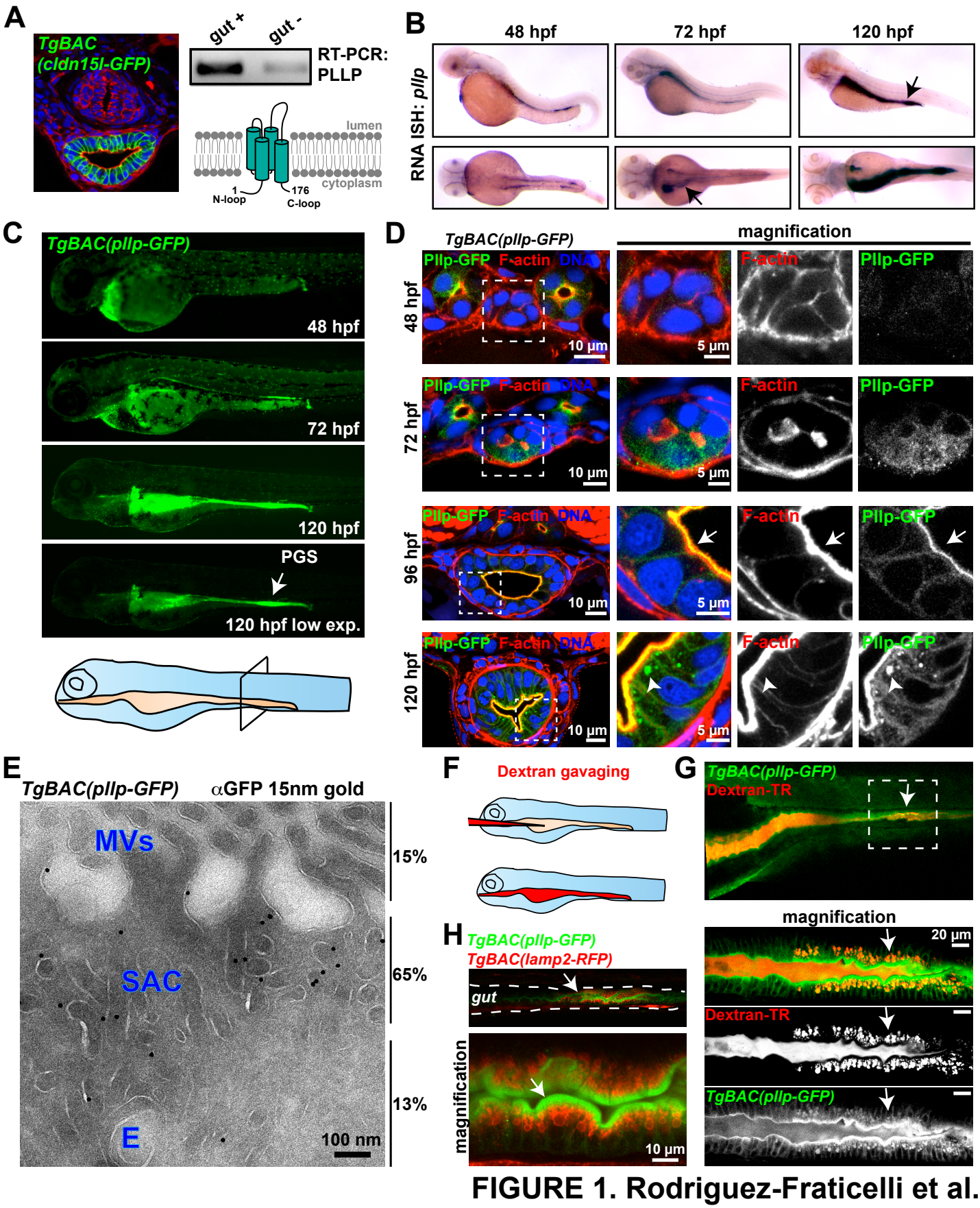

FIGURE 1. Rodriguez-Fraticelli et al.

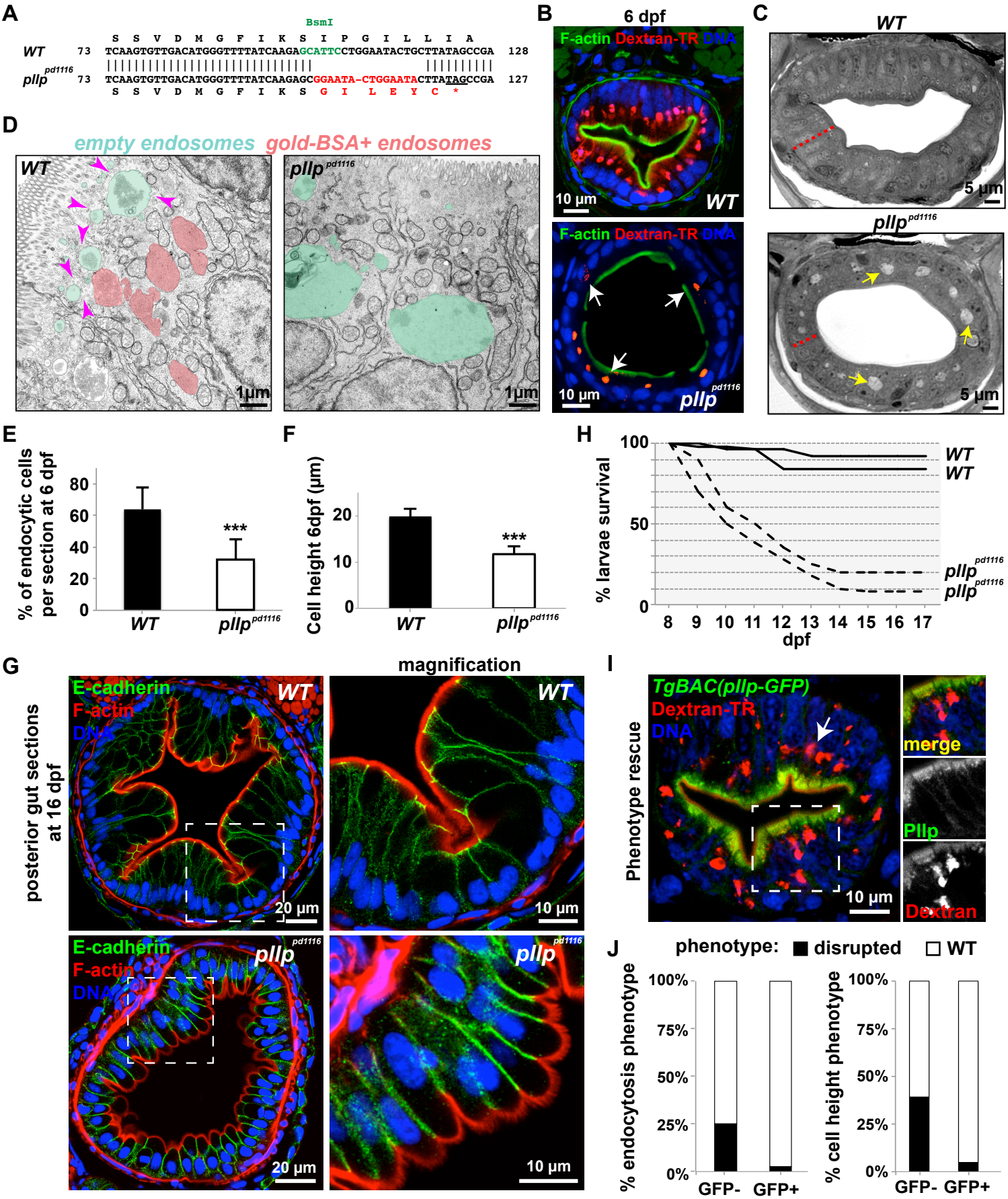

FIGURE 2. Rodriguez-Fraticelli et al.

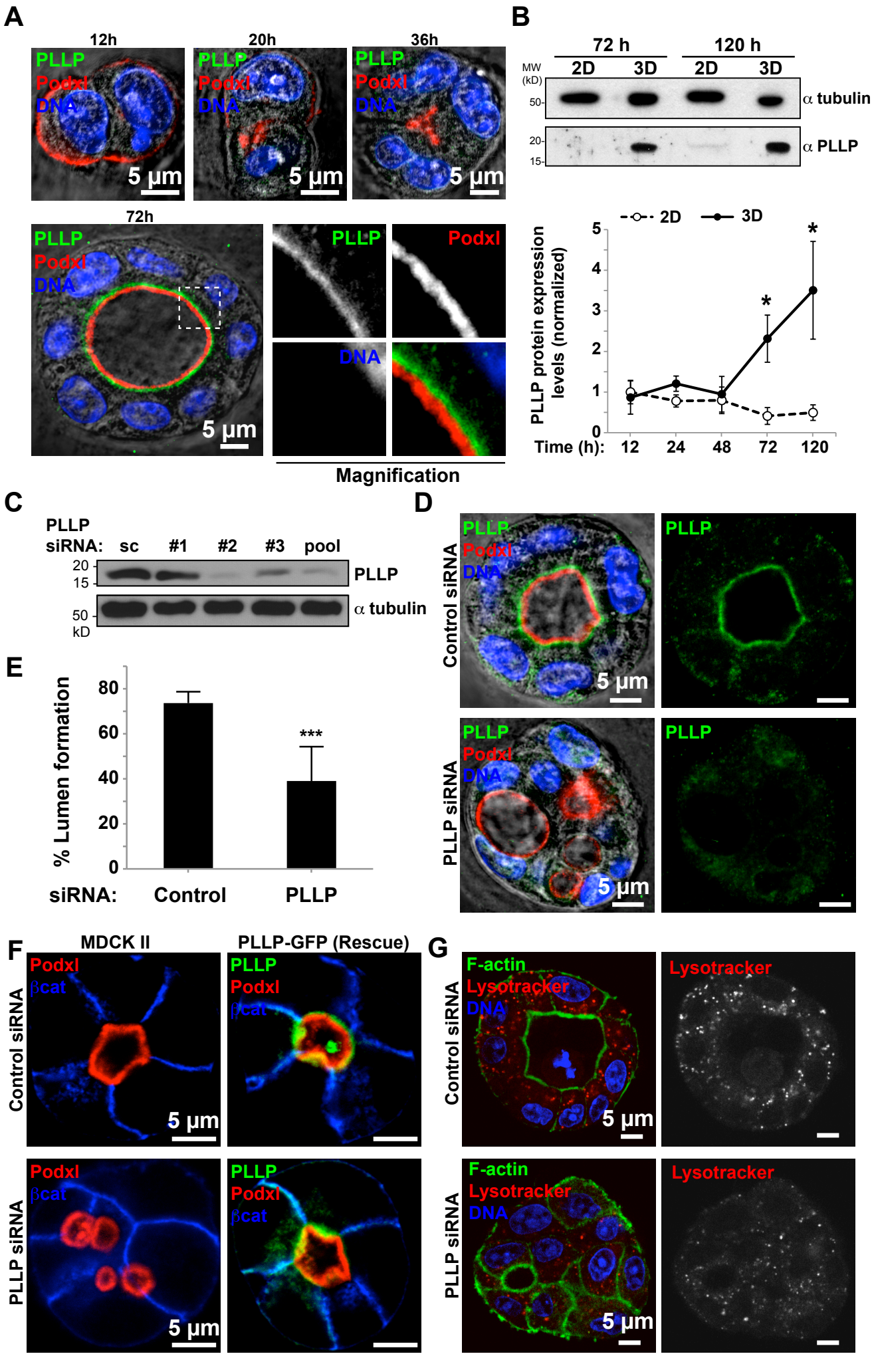

FIGURE 3. Rodriguez-Fraticelli et al.

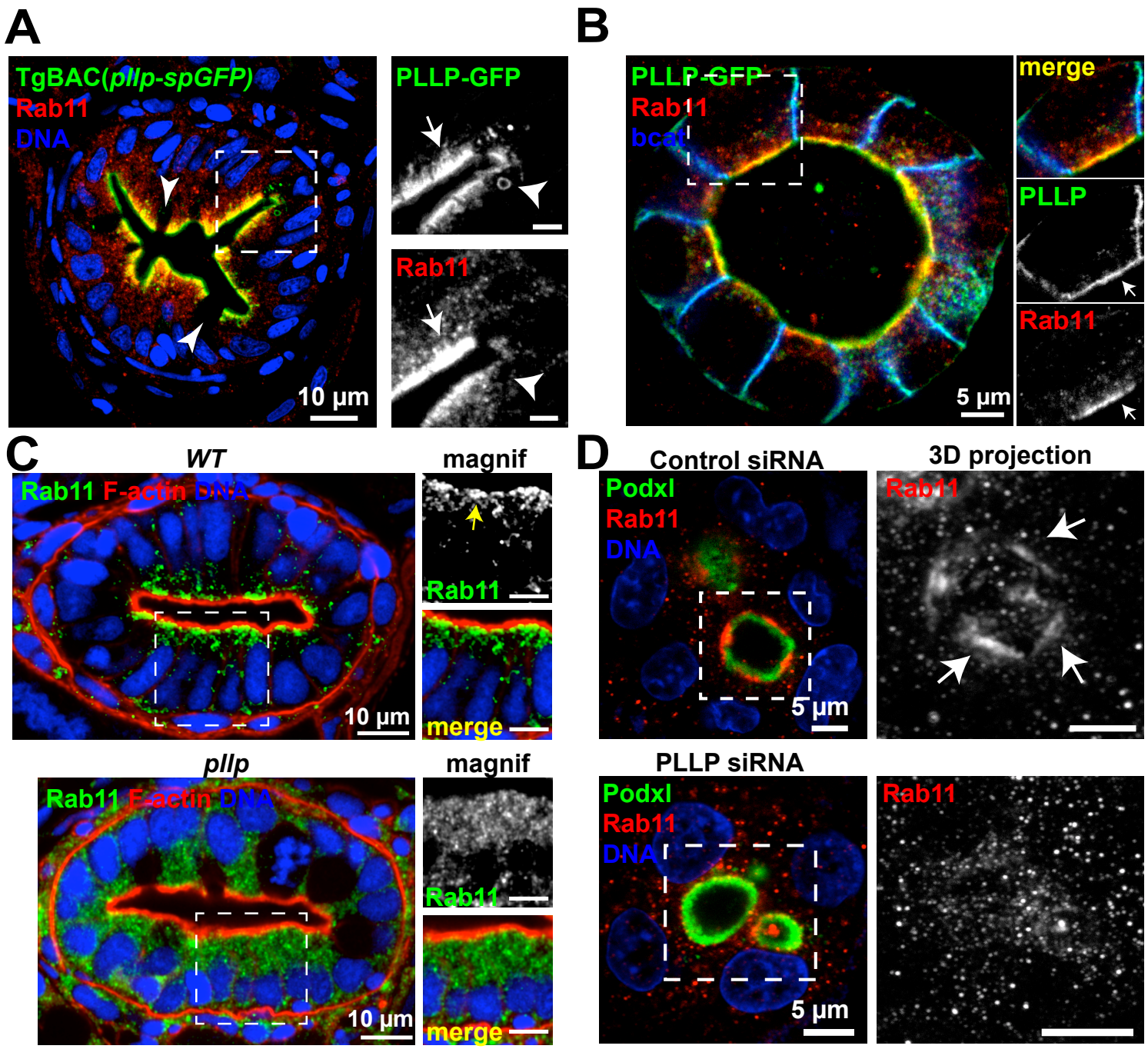

Figure 4. Rodriguez-Fraticelli et al.

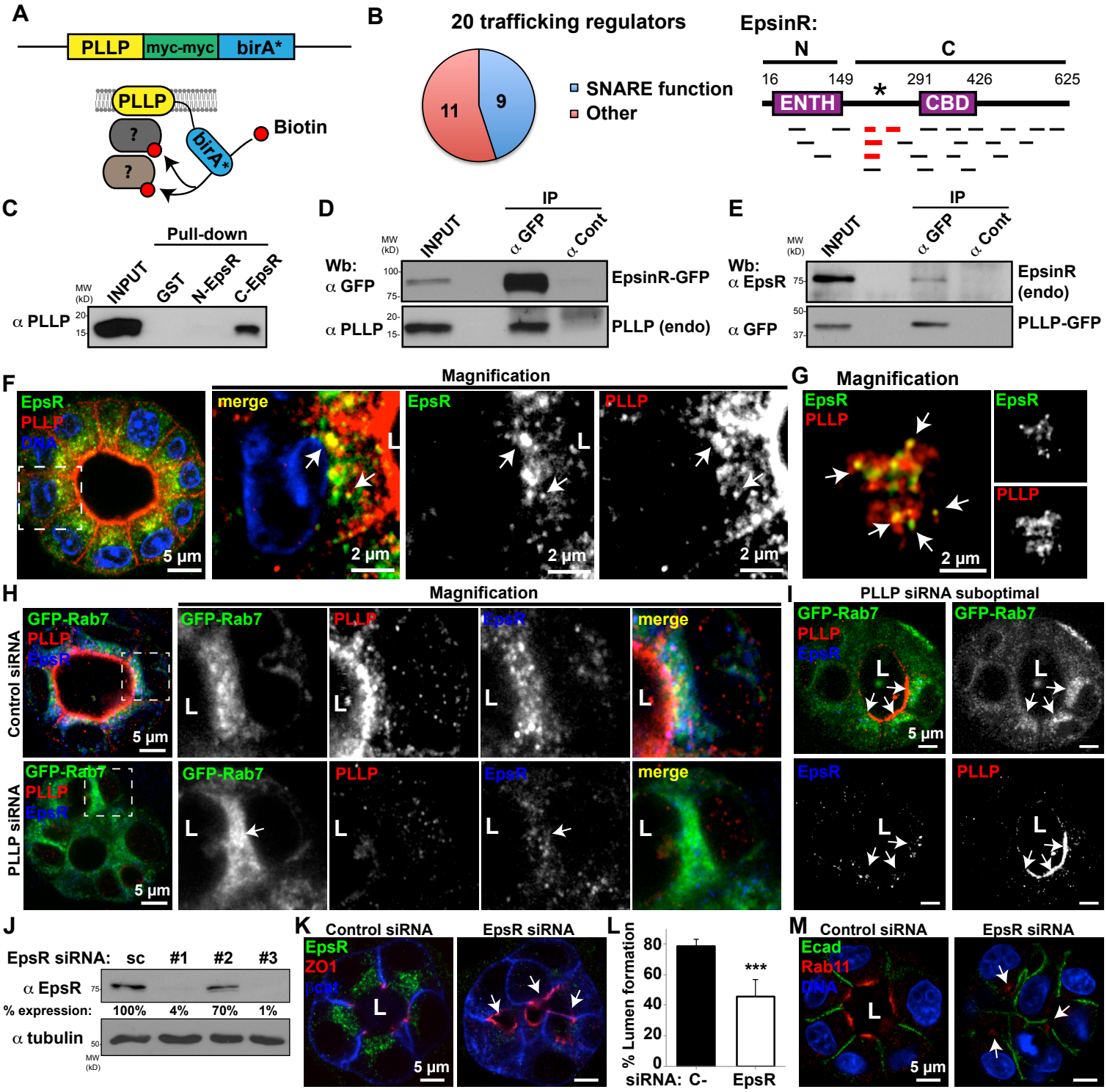

FIGURE 5. Rodriguez-Fraticelli et al.

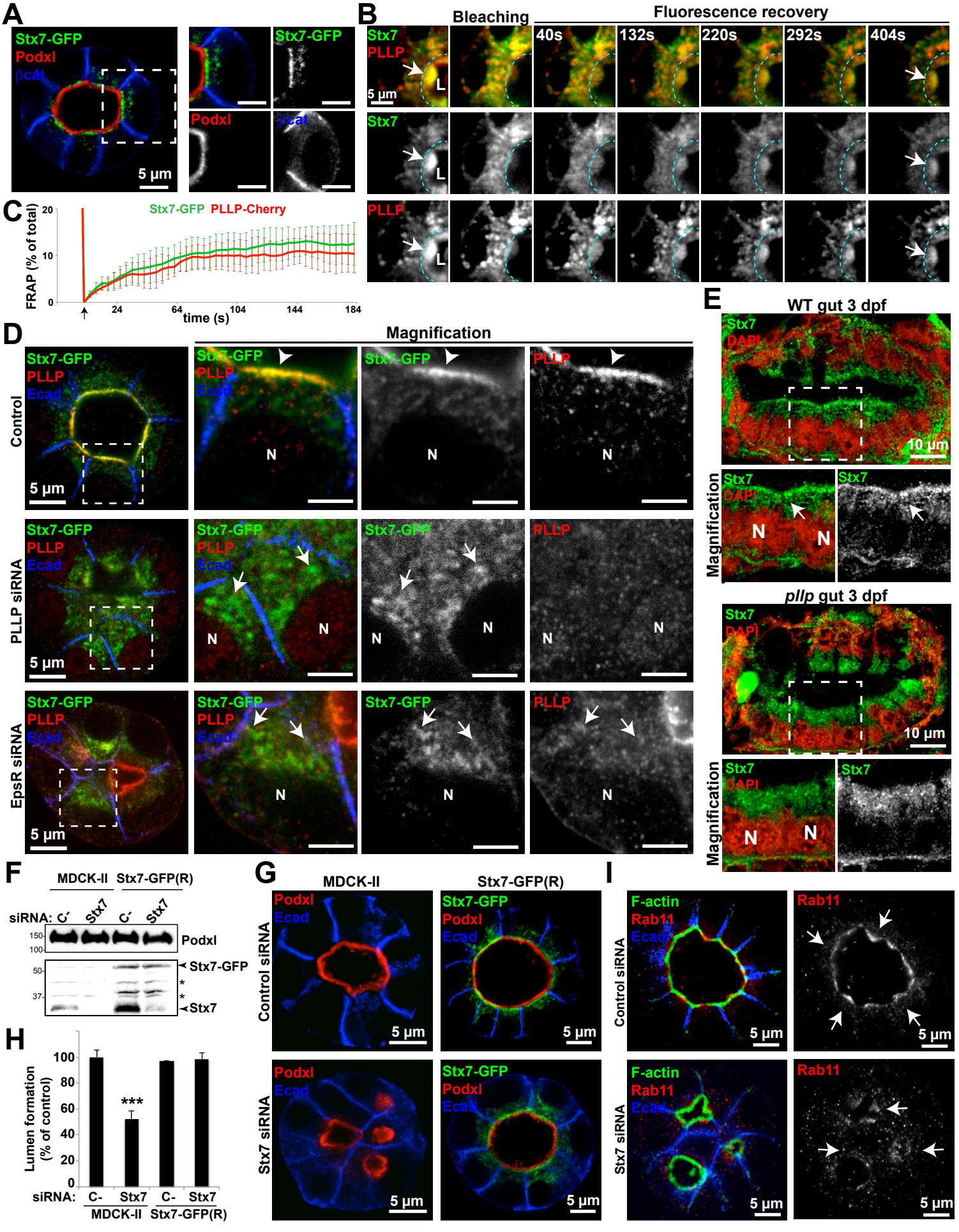

FIGURE 6. Rodriguez-Fraticelli et al.

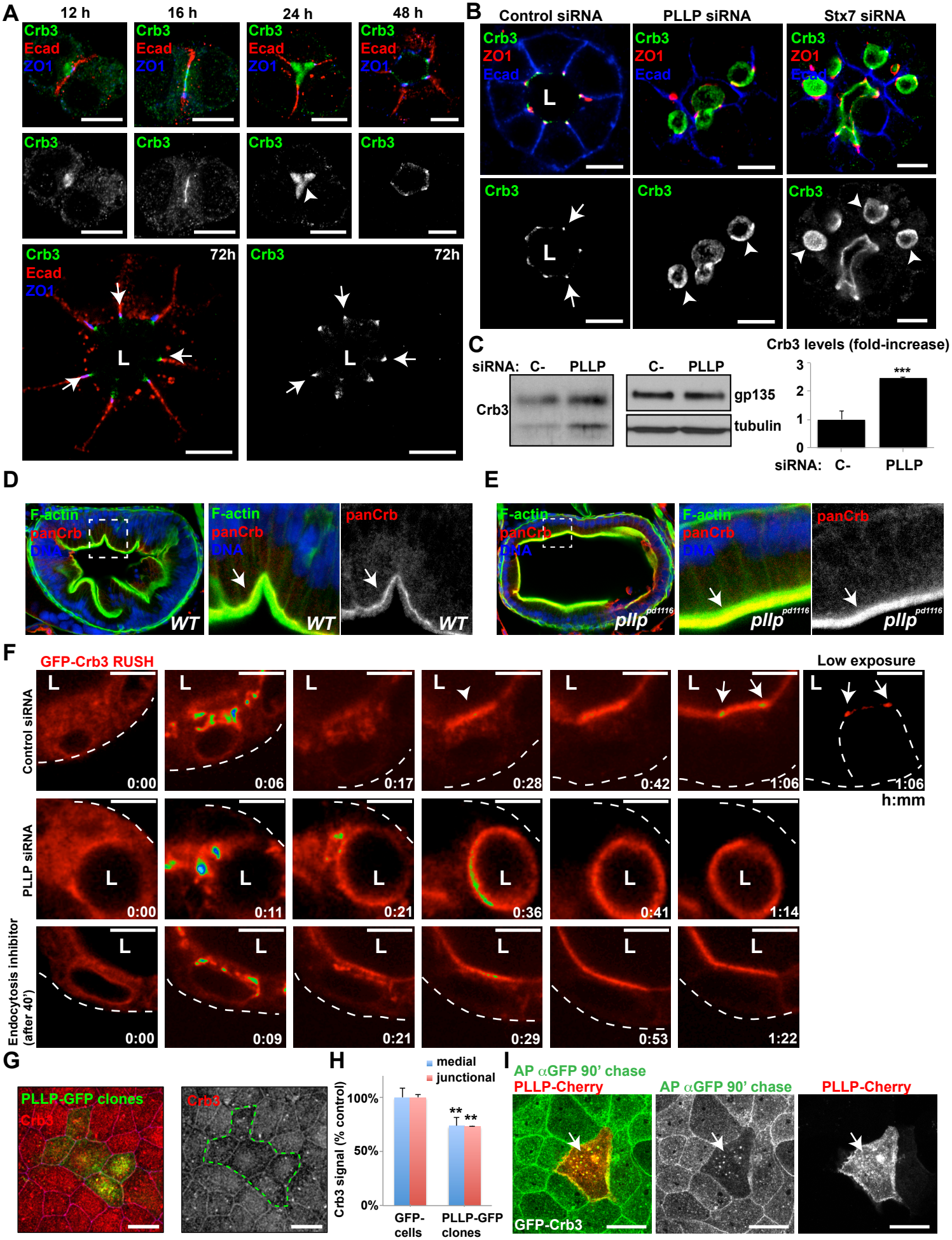

FIGURE 7. Rodriguez-Fraticelli et al.

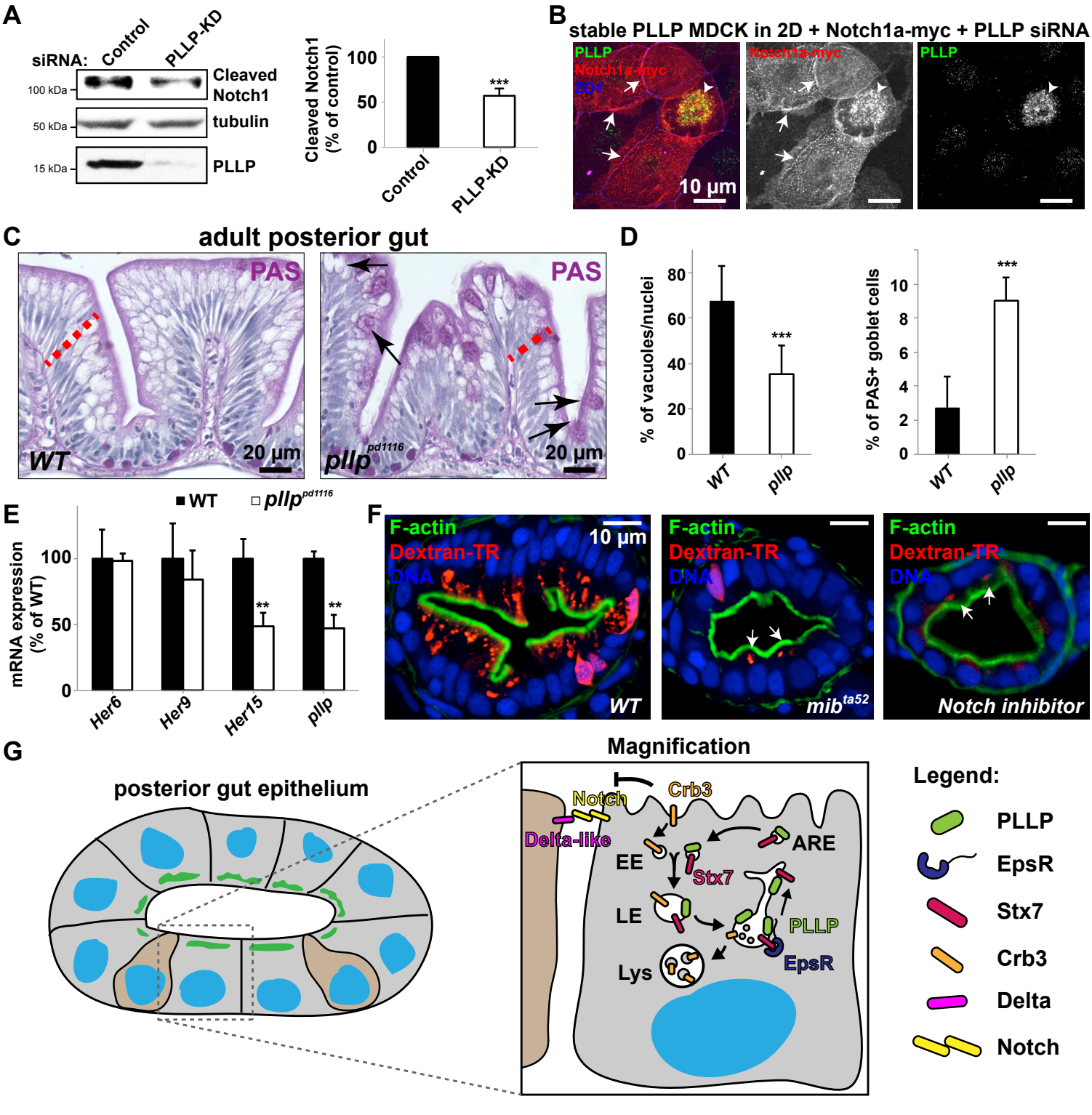

FIGURE 8. Rodriguez-Fraticelli et al.

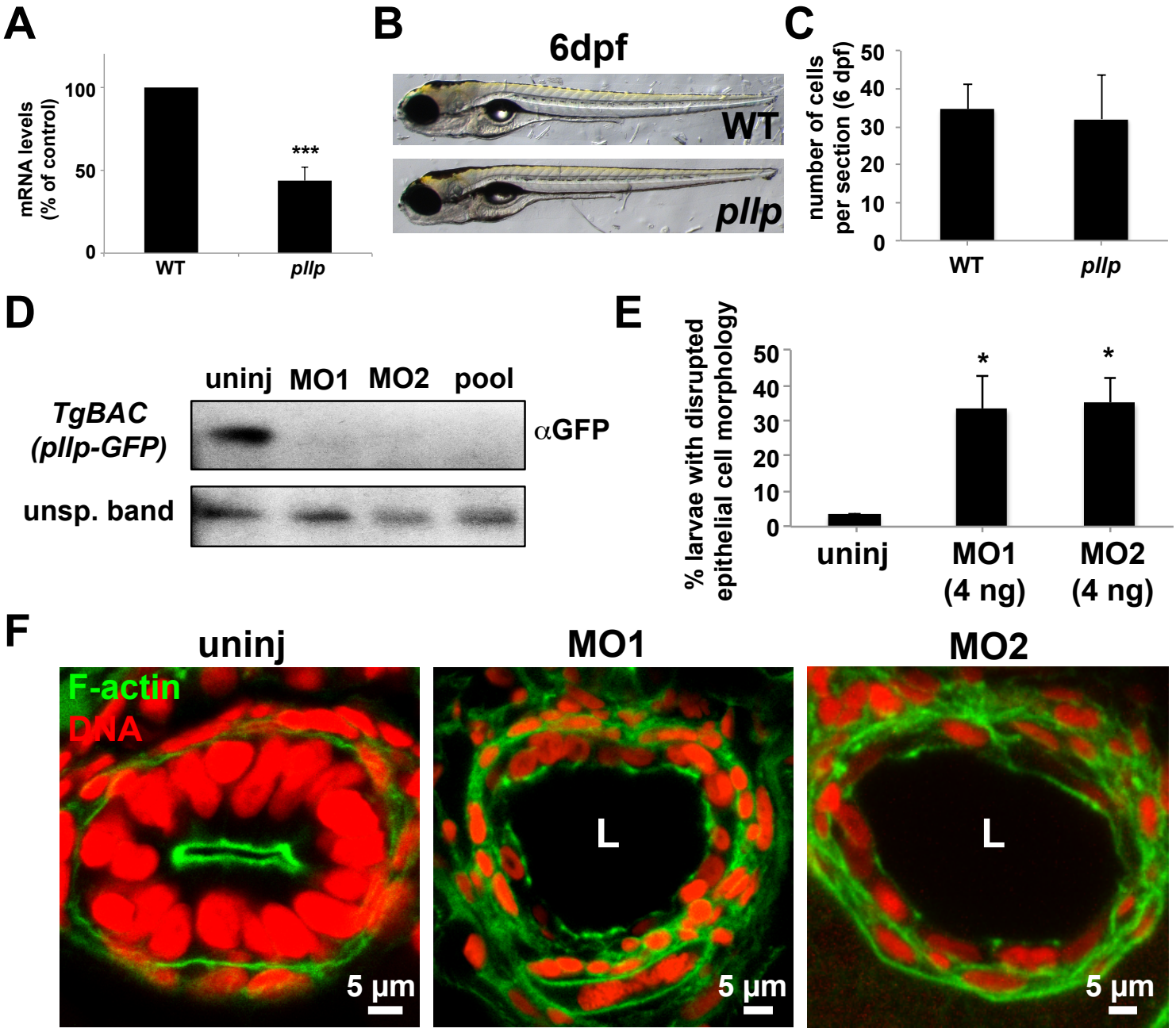

FIGURE S1. Rodriguez-Fraticelli et al.

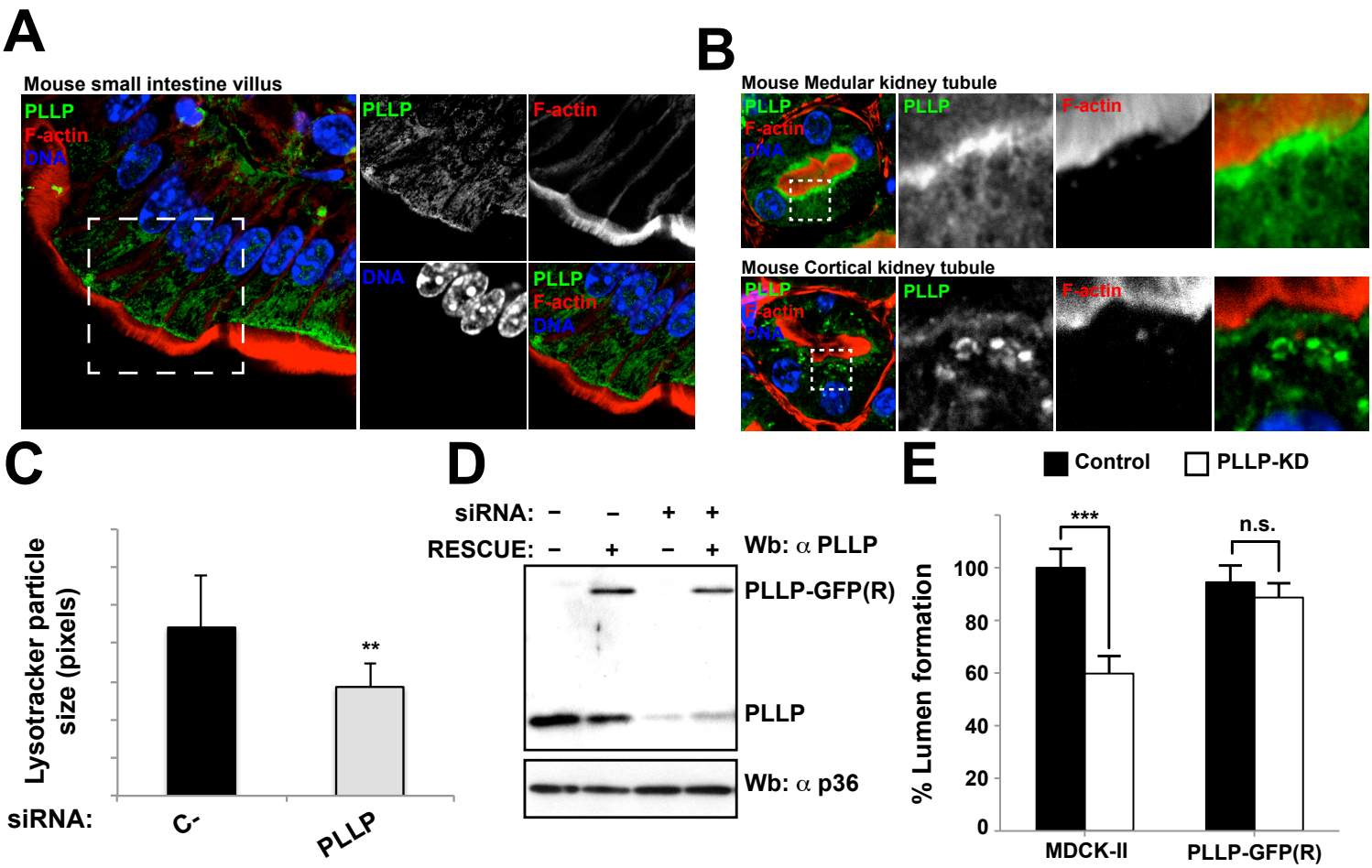

FIGURE S2. Rodriguez-Fraticelli et al.

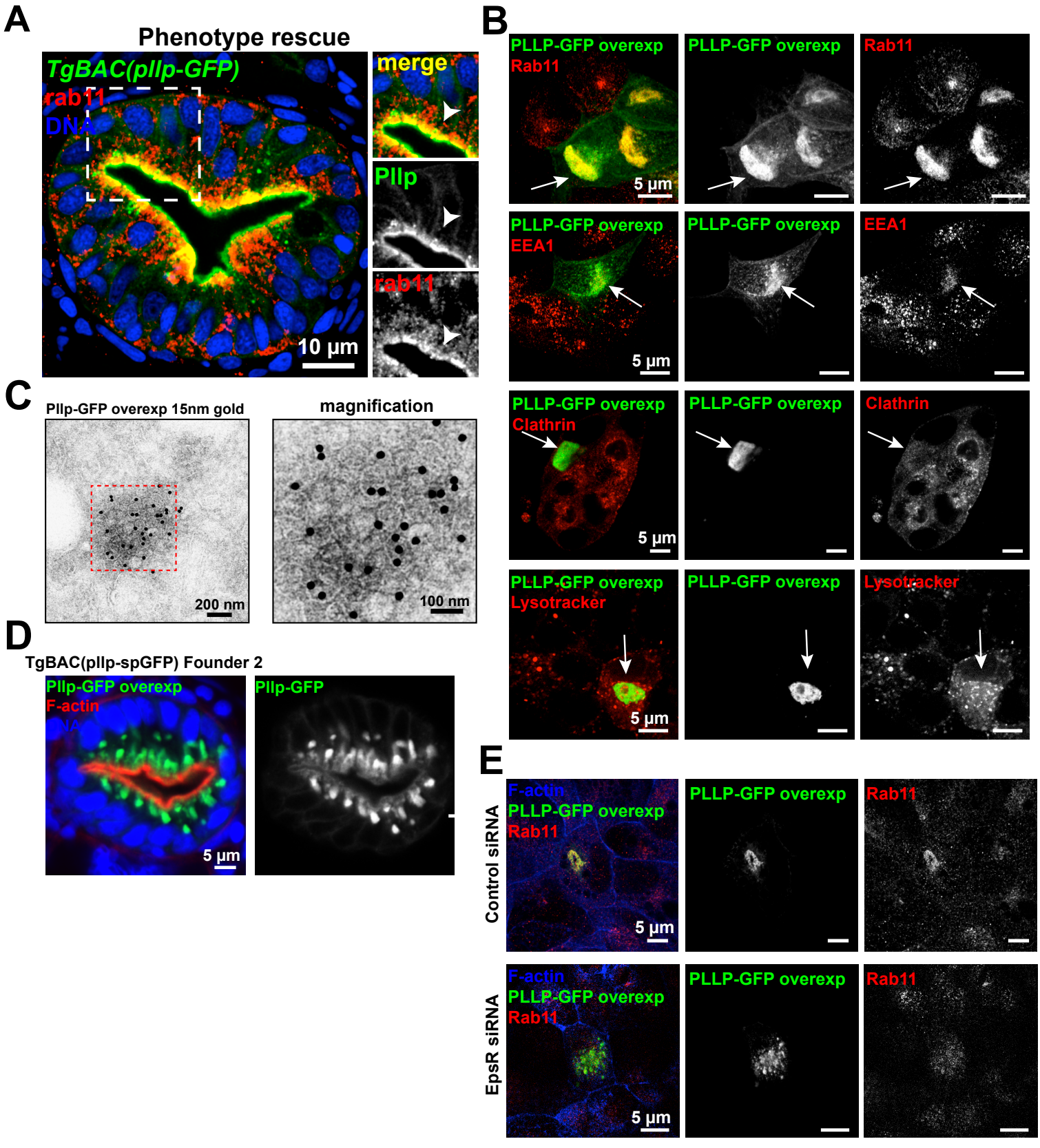

FIGURE S3. Rodriguez-Fraticelli et al.

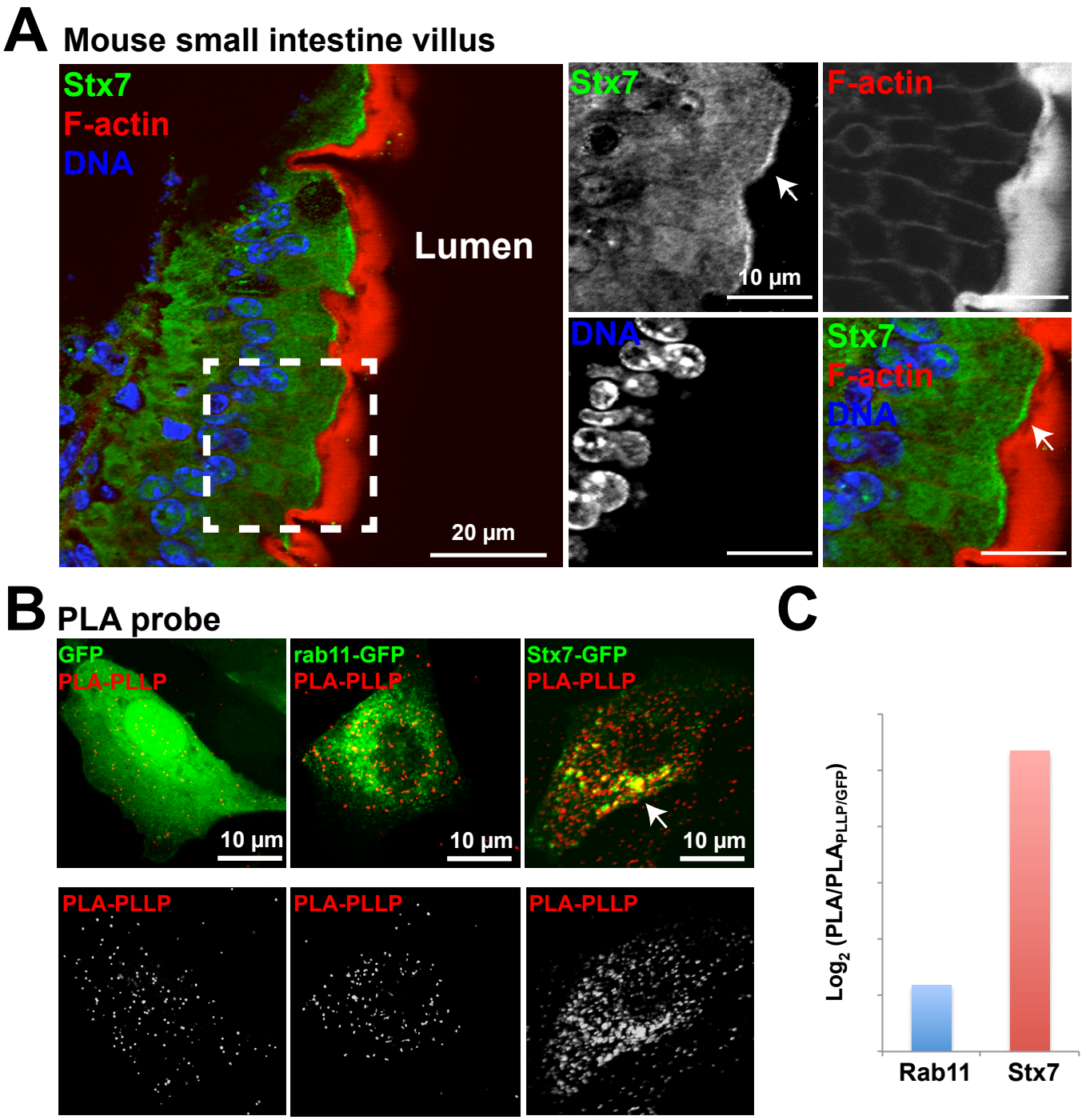

FIGURE S4. Rodriguez-Fraticelli et al.

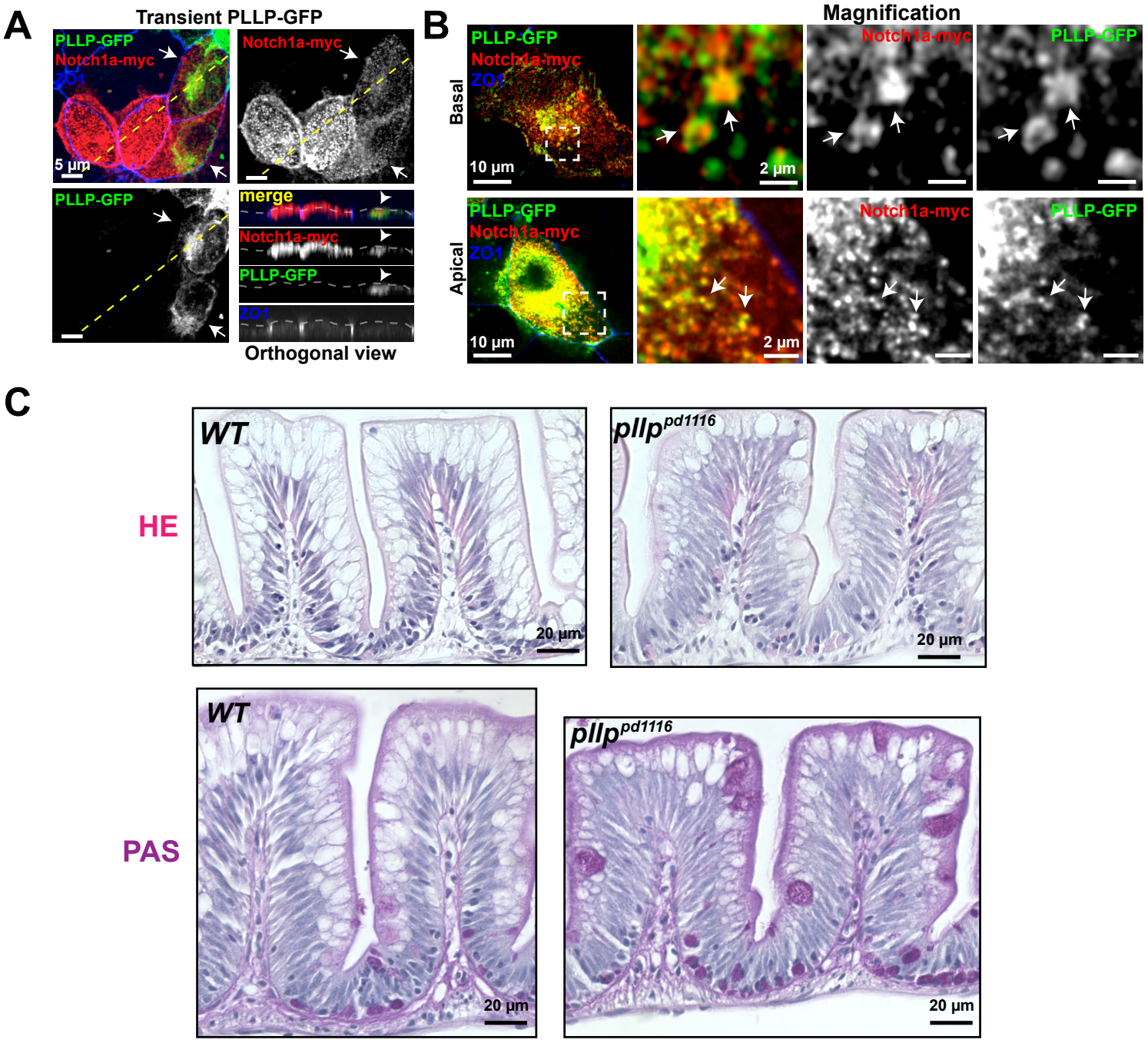

FIGURE S5. Rodriguez-Fraticelli et al.

V.
DISCUSSION

1. Mechanic control of epithelial morphogenesis

The effects of mechanical stress on morphogenesis have been thoroughly analyzed in developmental biology (Ingber, 1993). Early work using *in vitro* models established that different types of cells, including epithelial cells, could modify their behavior depending on the mechanical properties of the underlying matrix, through a complex mechanism requiring the cytoskeletal contractility machinery. To underpin the mechanical basis of morphogenesis, numerous tools have been developed, including the use of chips and micropatterns to control the adhesive properties of the cell environment (Huh et al., 2011). Using these tools, a recent study has revealed that ciliogenesis, a hallmark of differentiated epithelia, is controlled by the capacity of the cell to sense spatial confinement through changes in actin-mediated contractility (Pitaval et al., 2010). In this work, Pitaval et al. used micropatterned adhesive surfaces to modify cell confinement and analyzed ciliogenesis in a variety of different micropattern surface sizes. Cells in low confinement did not polarize or initiate ciliogenesis properly, and formed fewer and shorter ventral cilia. In contrast, cells in high confinement, using a smaller micropattern size per cell, formed longer and more physiological apical primary cilia. Cells in low confinement exhibited a highly contractile phenotype, with mature focal adhesions and abundant stress fiber formations. Consistently, inhibition of myosin-II-mediated contractility with blebbistatin or depolymerization of actin with cytochalasin D was sufficient to prevent stress fiber formation and restored primary cilia formation in the apical part of the cell. These results indicate that cell contractility and primary cilia formation are mutually exclusive processes in cell physiology.

Since some of the pathways involved in ciliogenesis and lumen formation appear to share common machinery (Datta et al., 2011), we decided to analyze whether contractility can affect lumen initiation in a model of MDCK cyst formation (Rodriguez-Fraticelli et al., 2012). For this purpose, we took advantage of a specific feature of this model, which is the formation of the initial lumen after the first cell division, at the two-cell stage, as this lumen is clearly visible by staining the apical marker podocalyxin/gp135. We repeated the same experiments as Pitaval and colleagues, and seeded MDCK cells on a substrate were they can stretch (collagen-I) and then modified the physical properties of the adhesive surface by using micropatterns of different sizes. In low confinement, MDCK cells produced numerous stress fibers and mature focal adhesions, and these cells did not form an initial lumen

after the first cell division (**Figure 8**). In contrast, high confinement was sufficient to induce correct lumen initiation. Similar to effects previously observed in ciliogenesis, lumen initiation was rescued in low confinement by myosin-II inhibition. Furthermore,

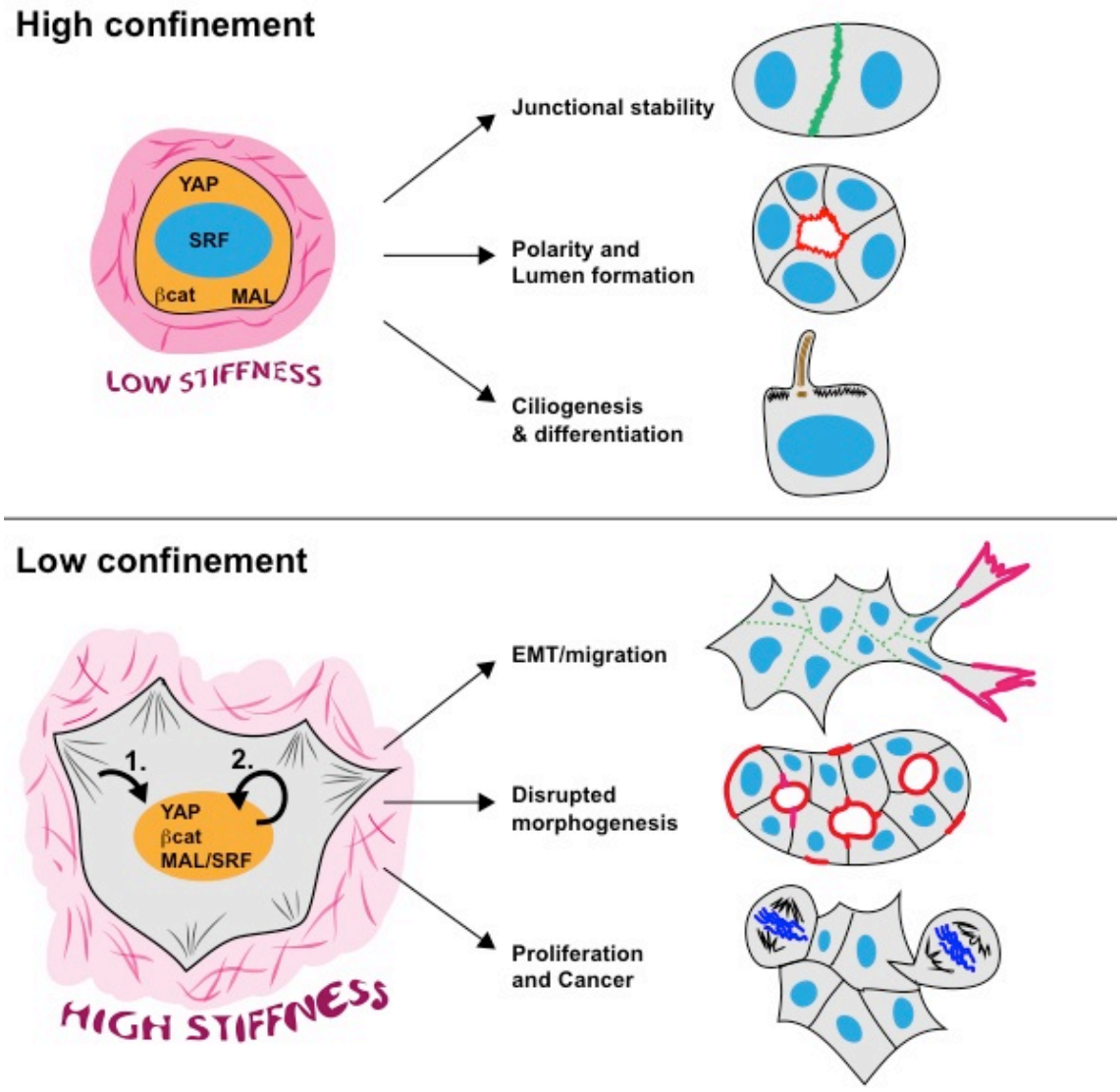

Figure 8. Cell confinement control of epithelial morphogenesis. In low stiffness or high confinement, the actin cytoskeleton is relaxed, YAP, MAL and bcatenin are excluded from the nucleus. In these conditions, junction stabilization, ciliogenesis and epithelial polarity and differentiation are promoted. In high stiffness or low confinement, the actin cytoskeleton is stressed, YAP, MAL and bcatenin are imported to the nucleus, and this induces an EMT-like program, which disrupts morphogenesis and polarity, and induces proliferation and migration.

forced contractility by overexpression of a constitutively active myosin-II regulatory chain showed that stress fiber formation was sufficient to prevent correct centrosomal positioning and lumen formation in high confinement. This demonstrates that cell-cell junctions and the increased confinement produced by cell-confluency were not sufficient to form the initial lumen in conditions that promote high cellular contractility. Then, we observed that RhoA and ROCK activity regulate contractility in

3D-MDCK cultures, and consistently, inhibition of Rho activity rescued lumen formation, resembling other mechanosensing pathways described during embryonic endothelial tubulogenesis (Xu et al., 2011). Furthermore, we found that liver kinase B1 (LKB1) activity was required for maintaining RhoA activation in this model, suggesting that this oncosuppressor is activated in highly contractile cells and its function prevents apical membrane reorganization. A recent report has elucidated that p114-GEF lies downstream of LKB1 independently of its kinase function (Xu et al., 2013). It remains to be described which RhoGEFs are activated by LKB1 in the 3D-MDCK model, and how broad these mechanisms are in other epithelial tissues *in vivo*.

Taken together, our results indicate that lumen initiation can only occur in conditions of low contractility, and that high confinement provides a mechanophysical cue that induces proper initial epithelial polarization. Interestingly, we found that laminin signaling is sufficient to prevent proper spreading and inhibits contractility of MDCK cells even in conditions of low confinement. MDCK cells express laminin-binding receptors, such as α3-β1 integrin, which may be the receptors responsible for these effects (Myllymaki et al., 2011). Indeed, β1 blocking antibodies prevent proper laminin organization and result in loss of polarity (Yu et al., 2005). In addition, laminin-mediated integrin activation controls microtubule orientation through integrin-linked kinase (ILK) (Akhtar and Streuli, 2012). ILK, together with Parvin and PINCH, forms part of the IPP complex, which is able to suppress F-actin polymerization and contractility (Qin and Wu, 2012). Altogether, these data suggest a possible model in epithelial tubes. In this model, α3β1 integrin binds to laminin and recruits ILK to suppress basal actin contractility, and subsequently orients microtubules to organize apicobasal polarity. Future studies in these directions will test if ILK mediates the inhibition of F-actin contractility induced by laminin.

After polarity is orientated, lumen formation requires vesicular trafficking and *de novo* assembly of tight junctions at the site where the new apical membrane is going to be formed (Apodaca et al., 2012). Centrosome positioning and microtubule organization play a decisive role in this process. The vesicular trafficking required for lumen formation occurs through a complex molecular mechanism orchestrated by the small Rho GTPase Cdc42, and specific Rab GTPases, including Rab11, Rab8, and Rab27 (Bryant et al., 2010; Galvez-Santisteban et al., 2012; Martin-Belmonte et al., 2007). The specific GEFs for Rab8 and Cdc42, respectively Rabin8 and ITSN2, bind

the centrosome, suggesting that centrosome orientation may localize the activation of small GTPases required for *de novo* apical plasma membrane formation (Bryant et al., 2010; Schmidt et al., 2012; Westlake et al., 2011). Thus, we propose that laminin signaling and cell confinement can mediate the orientation of the nucleo-centrosomal polarity axis, which results in a polarized activation of Cdc42 and specific Rab GTPases specifically at the membrane domain that first tethers the centrosome after cell division. This, in turn, recruits the necessary effectors involved in the generation of polarized membrane trafficking to form the lumen and the primary cilium.

2. Mechanotransduction pathways are regulated by cell confinement

During the past decade, several studies have demonstrated that all cell types sense the mechanical properties of the ECM through activation of a specific cytoskeletal machinery, and that this signaling modulates nuclear transcriptional programs that elicit differentiation or proliferation responses (Discher et al., 2009). Several studies have characterized a set of transcription factors, including β-catenin, serum response factor (SRF) and Yes-activated protein (YAP), that are transported into or out of the nucleus depending on the levels of mechanical cell stress (Mammoto et al., 2012).

The role of YAP on mechanotransduction was uncovered by analyzing differential expression of genes in cells cultured in stiff versus soft matrices and using micropatterns of different confinement properties (Dupont et al., 2011; Halder et al., 2012). When cells are in low confinement, YAP accumulates in the nucleus where it activates genes required for cell proliferation (Dupont et al., 2011). On soft substrates, or in high confinement, YAP is phosphorylated and excluded from the nucleus. Both actin and myosin-II inhibitors induce YAP phosphorylation and exclusion from the nucleus, suggesting that contractility and stress fiber formation are involved in YAP regulation.

Cell spreading and contractility also regulates the SRF cofactor MAL through binding and detection of globular actin (G-actin) levels (Miralles et al., 2003; Vartiainen et al., 2007). In high confinement conditions, SRF activates specific targets in the nucleus and induces epidermal stem cell differentiation. In high-stress (low confinement) conditions, filamentous actin (F-actin) is polymerized actively in the cytoplasm to maintain cell shape and movement, and this prevents epidermal stem-cell

differentiation. Thus, the G-actin/F-actin ratio controls SRF binding to MAL and produces the activation of different MAL-dependent and independent SRF-target genes.

Even though some progresses have been made, so far it remains unclear how these and other transcription factors modulate epithelial cell morphogenesis. Recent data has shown that SRF is required for polarized, oriented cell divisions and morphogenesis in the epidermis (Luxenburg et al., 2011). In addition, YAP induces Myosin-II regulatory light chain expression and constitutes a feedforward loop where nuclear YAP reinforces of RhoA activity and cytoskeletal contractility. Finally, YAP expression can modulate the epithelial EMT program and YAP overexpression leads to defects in mammary acini formation (Cordenonsi et al., 2011). Thus, in addition to regulating microtubule polarity, contractility also controls the transcriptional state of epithelial polarity genes. Based on our data, we expect that MDCK cells in low confinement would present YAP localized to the nucleus in an "active state", and depletion of YAP could suffice to induce lumen formation. Further experiments in this direction will unravel whether YAP inhibition is a prerequisite for lumen initiation, and whether YAP overexpression suppresses the transcriptional program of genes required for lumen formation.

3. Spindle orientation regulation by Cdc42

Rho-family GTPase signaling instructs most of the machinery involved in the orientation of cell polarity (Iden and Collard, 2008). The most ubiquitously expressed Rho-family GTPases, RhoA, Cdc42 and Rac1, have been shown to play a role in epithelial morphogenesis (Van Aelst and Symons, 2002). Whereas RhoA and Rac1 control adherens junction formation and the orientation of apicobasal polarity respectively, the Cdc42 GTPase was reported to be required for vesicular trafficking during formation of the luminal plasma membrane (Datta et al., 2011). A study led by the lab of Alan Hall elucidated that Cdc42 was required for spindle orientation and positioning of the midbody during cyst formation using the Caco2 model (Jaffe et al., 2008). We reproduced these results in the 3D-MDCK model and then sought to identify the Cdc42 GEFs that mediated Cdc42 activation during epithelial morphogenesis using the 3D-MDCK model. To achieve this, we performed an shRNA screen to target different GEFs reported to regulate vesicle exocytosis in bibliography and we identified ITSN2 as a key regulator of Cdc42 activity during lumen formation (**Figure 9**).

Previous GTPase pulldown experiments suggested that MDCK cells present very high levels of active Cdc42 specifically when cultured in 3D (Martin-Belmonte et al., 2007). However, we did not identify differences in the expression levels of ITSN2, suggesting that ITSN2 activity is promoted in 3D through a still unknown mechanism. It has been reported that ITSNs are autoinhibited GEFs that become activated by binding of other proteins to the SH3 domains, although recent careful mapping of the

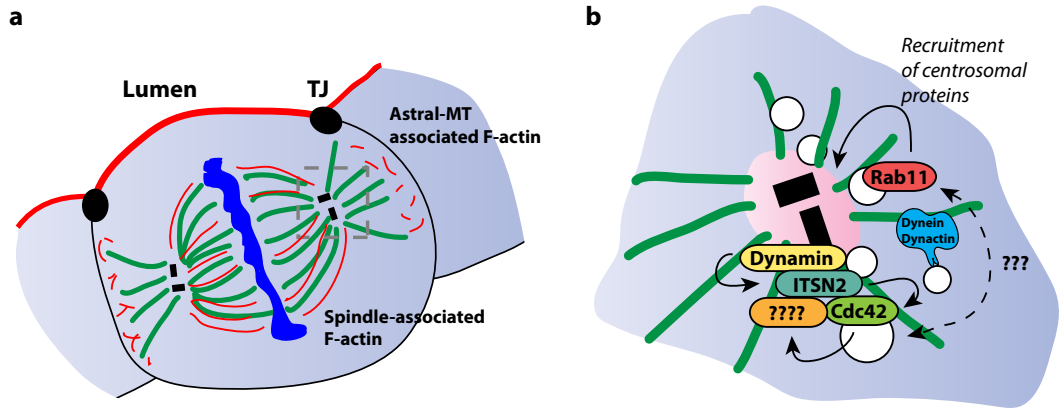

Figure 9. Moonlighting functions of endocytic proteins during mitotic spindle formation. a) The actin cytoskeleton is also associated to certain features of the mitotic spindle during cell division. Actomyosin bundles form parallel to the spindle microtubules, and astral-microtubules interact with the peripheral actin cortex. **b)** Several endosomal and endocytic proteins are recruited to the mitotic spindle pole during cell division. Rab11 recruits Dynein-dynactin, which in turn interacts with ITSN2. Dynamin also binds ITSN2, and together they activate Cdc42 at the spindle poles. The downstream effectors of Rab11, Cdc42 and ITSN2 have not yet been elucidated.

autoinhibitory domain suggests that SH3 domain binding is not required for its activity (Kintscher et al., 2010). Alternatively, GTPases can also be controlled by GTPase activating proteins (GAPs), and thus suppression of certain GAPs may also contribute to sustained Cdc42 activation during 3D morphogenesis.

Our report indicated that ITSN2 was responsible for about 40-50% of Cdc42 activity in 3D-MDCK, suggesting that other GEFs might be responsible for activating the remaining pool of Cdc42. In fact, a parallel study performing a screening for Cdc42 GEFs identified Tuba (and also ITSN2) to be required for lumen formation in 3D-MDCK (Yi Qin, 2010). The authors did not report a decrease in Cdc42 activity in Tuba-KD cysts but the results suggest that both ITSN2 and Tuba could account for the majority of Cdc42 activity in this model, perhaps performing specific functions. It remains to be seen whether other epithelial models in vertebrates also depend so highly on these two GEFs for lumen-formation functions of Cdc42.

Previous reports had identified ITSNs as clathrin coated-pit proteins involved in endocytosis (Pucharcos et al., 2000). Although we could not detect endogenous protein

levels with any antibodies, expression of ITSN2-GFP or HA at very low levels in our stable cell clones showed a prominent centrosomal localization. Interestingly, another GEF required for lumen formation, Rabin8, localizes to the centrosome (Westlake et al., 2011) and our results suggest that Cdc42 and Rab8 interact in the single lumen initiation pathway (Bryant et al., 2010). The current model proposes that Tuba is downstream of Rab8 in this model, but no localization data was shown in the aforementioned study. Since ITSN2 and Rabin8 both localize to the centrosome, it is possible that ITSN2 could also mediate this pathway. Moreover, Rab8-KD produces a much stronger phenotype than either ITSN2 or Tuba-KD, suggesting that both GEFs could be downstream of Rab8 during lumen formation.

The localization of ITSN2 to the centrosome sparked the investigation of what could regulate its localization to the centrosome. Although we found that ITSN2 could bind through the SH3 domains to Dynactin (p150-glued), part of the minus-end directed microtubule motor complex Dynein-dynactin, expression of the GFP-tagged SH3 domains is insufficient for centrosomal localization. Interestingly the EF-hands domain was sufficient to partially recapitulate the endogenous localization (although most of the protein was in fact localized to the cytoplasm). It is possible that domain-construct expression is insufficient, and that both the EF-hands and the SH3 domains are required for centrosomal localization.

The identification of ITSN2 in centrosomes follows a long list of endocytic proteins that have been found to localize to centrosomes (Royle, 2013). Most importantly, the main regulator of ITSN2, Dynamin, prominently localizes to the centrosome and is required to maintain proper spindle formation (Thompson et al., 2004). Although the studies were not performed in epithelial cells, it is possible that a partial Dynamin-KD could also affect spindle orientation through depletion of centrosomal ITSN2, and that dynamin at the centrosomes is a hub for endocytic protein function in spindle formation and orientation. However Dynamin-KD is highly toxic for cells, and did not allow analysis of lumen formation in our experiments. Alternatively, one possible experiment would be to rescue ITSN2-KD using ITSN2 mutants that specifically affect Dynamin interaction. The interaction between the SH3 domains of ITSN2 and Dynamin has been crystalized and imaged at high resolution, and certain aminoacids responsible for the interaction have been identified. Future study of a non-dynamin binding mutant of ITSN2 is paramount to understand the role of dynamin in ITSN2 regulation of the spindle.

GEFs are some of the most important molecules in the GTPase interactome not only because they mediate GTPase activation by GDP-GTP exchange, but also because they provide a layer of time-space regulation through their different scaffolding functions. What is the effector mechanism of Cdc42 downstream of ITSN2? Classical experiments showed that ITSN2 is activated by binding to its SH3 domains, and that this interaction releases an autoinhibitory loop, allowing ITSN2 to activate Cdc42. One of such molecules is the actin polymerizing factor, N-WASP. N-WASP is required for epithelial morphogenesis and carries important functions in the polymerization of apicojunctional actin. Different actin-based structures have been reported to interact with the spindle and control vertebrate cell division, including spindle orientation (Almonacid et al., 2014; Azoury et al., 2008; Cande et al., 1977; Gard et al., 1995; Gawadi, 1971; Holubcova et al., 2013; Karsenti and Nedelec, 2004; Kunda and Baum, 2009; Theesfeld et al., 1999; Verlhac, 2011; Xu and Saunders, 2008). Interestingly, Rab11-dependent vesicle trafficking has been shown to be responsible of the actin polymerization events during spindle positioning in mouse oocytes (Holubcova et al., 2013). Rab11/Rab8-dependent vesicle trafficking is required for recruitment of centrosomal components to the basal body and the spindle poles, and is necessary for proper spindle orientation (Hehnly and Doxsey, 2014). Finally at least one report suggests that Dynamin controls actin-based spindle movements in the mouse oocyte (Wang et al., 2014). Thus, during spindle formation and orientation, ITSN2 interaction with Dynamin and N-WASP could be responsible for the polymerization of the spindle-interacting actin matrix. In contrast to the more canonical NWASP regulation, the *Drosophila* homolog protein, Dap160, which does not present a Cdc42-GEF domain, is able to bind and regulate the Par6/aPKC complex in neuroblasts (Chabu and Doe, 2008). We did not detect an interaction of ITSN2 with either Par6 or aPKC, but this still does not rule out the possibility that they act as downstream effectors of Cdc42 in the spindle. An isoform of Par6 has been recently reported to localize partially to the centrosome where it recruits dynactin (p150-glued) for microtubule anchoring and stabilization (Dormoy et al., 2013). Although the authors report this function is independent of Par3 and aPKC, Cdc42 could still be required for this function of Par6. Our study showed that specific depletion of the long splicing form of ITSN2, which contains the GEF domain, is sufficient to cause multiple lumen formation. Thus, the binding of ITSN2 to NWASP, Dynamin, Dynactin, or its putative binding to Par6/aPKC

is not sufficient, and Cdc42 activation is necessary for ITSN2 function during lumen formation.

4. A genetic program for lumen formation

Differential gene expression drives most developmental processes, including morphogenesis. Our studies using 3D-MDCK cysts, together with those performed on *Drosophila* tracheal system and mouse pancreas, suggest the existence of master regulator signaling pathways that control epithelial tube formation. From our genetic screen of upregulated genes, one pathway was significantly represented: the Wnt-planar cell polarity (PCP) pathway. In particular, we found that Frzb, a modulator of Wnt signaling, and Fuzzy, an effector of the core PCP pathway, are induced during 3D morphogenesis and required for single lumen formation (Galvez-Santisteban et al., 2012). Wnt and PCP signaling have been shown to control epithelial differentiation in many different organs, including the kidney (Bernascone and Martin-Belmonte, 2013). Interestingly, recent data has elucidated that Wnt and PCP signaling can also read signals from mechanotransduction pathways, such as the Hippo-YAP pathway. Thus, Wnt signaling could lie at the intersection of the genetic pathways required for tube formation. Future analysis of the Wnt-PCP pathway will elucidate its role as a master regulator of the genetic programme of lumen initiation.

We performed the first profiling experiments using MDCK cells cultured in 3D and 2D. One interesting feature of this system is that it behaves as a single-cell organotypic model, and the genetic program to construct a single lumen is completely cell autonomous. However, the morphogenetic process *in vivo* is likely more complicated. For instance, the zebrafish gut cells form individual lumens in a cross section, but these lumens are formed separated along the length of the gut (Alvers et al., 2014). Final anterior-posterior coalescence of these lumens requires paracrine Hedgehog signaling to achieve a single continuous lumen from pharynx to cloaca. Interestingly, our profiling of MDCK cells observed a high induction of Indian Hedgehog (Ihh) expression, although experiments with siRNA showed it was not required for single lumen formation (Galvez-Santisteban et al., 2012). It has been described that Hedgehog and Wnt are secreted apically and then may undergo apical-to-basal transcytosis to be delivered to the underlying stroma in the form of exosomes, where they could provide a juxtacrine signal to other cell types (Greco et al., 2001;

Lakkaraju and Rodriguez-Boulan, 2008; McCarthy et al., 2002; Morales et al., 2006; Ortega et al., 2012). In the case of the *smoothened* zebrafish mutants, the guts present a strong defect in the organization of the smooth muscle layer that surrounds the gut epithelium. Future studies will elucidate the target of Hedgehog signaling in the 3D-MDCK model by using co-culture with stromal kidney cell types.

5. SNARE receptor recycling and intestinal physiology

To unravel genes that were controlling the single lumen formation process *in vivo*, we used the zebrafish gut model to perform gene profiling in collaboration with the lab of Michel Bagnat (unpublished data). Surprisingly, very few of the genes that we had found to be expressed in the 3D-MDCK model correlated with expression in the zebrafish gut microarrays, suggesting that although the basic lumen formation machinery may be common to all epithelial cells, the fine-tuning of organ morphogenesis is carried out by tissue-specific differential expression programmes. Nonetheless, we found one commonly expressed protein, PLLP, whose function was previously uncharacterized. We uncovered the molecular function of PLLP as a regulator of endosomal maturation during epithelial morphogenesis. PLLP localizes to recycling tubules of sorting and late endosomes where it promotes binding of clathrin adaptor EpsinR. EpsinR binds to clathrin-adaptors, such as AP1B, and regulates tubulation and formation of vesicular carriers containing SNARE proteins, such as Syntaxin 7, which are recycled for their continued use in the cell (**Figure 10a/b**). This regulated recycling is necessary for endosomal acidification, and endosomal maturation and its developmental regulation in time and space plays different functions during signaling and epithelial morphogenesis.

In our experiments, PLLP was highly expressed in a liquid-phase endocytic population of cells in the posterior segment of the midgut, and adult *pllp* mutants presented posterior guts that resembled more anterior segments, with reduced population of vacuolated (LAMP2+) cells and increased population of goblet cells. If PLLP is at least partially required for the morphogenesis of the posterior gut, one essential question that arises is how is the expression of PLLP in the posterior segment specified. Hox genes mediate developmental transcriptional programmes of segments and certain Hox genes have been shown to direct segment-specific epithelial morphogenesis such as in the spiracle organ in *Drosophila* (Lovegrove et al., 2006).

Also, Hox-related genes, such as Pdx1 direct the initial tubulogenesis of the pancreas (Kim and MacDonald, 2002; Wescott et al., 2009). In mouse, another Hox-related gene, Cdx2, has been shown to be the master regulator for morphogenesis and differentiation of the posterior gastrointestinal tract (Gao et al., 2009). Interestingly, a gradient like Cdx2 expression induces differentiation of the posterior gut identity. It is very likely that the posterior gut presents a similar mechanism of segmental morphogenesis, where Cdx2 gradients could control localization of PLLP expression.

Intriguinly, the posterior midgut was previously known to contain cells with supranuclear vacuoles in the adult zebrafish (**Figure 9c**). We demonstrated that these cells are PLLP and LAMP2-positive, and that they are highly endocytic cells, which differentiate 2 days after the onset of PLLP expression (at 5dpf), when PLLP starts to be upregulated in the posterior midgut. These posterior midgut enterocytes are constantly uptaking fluid-phase markers, such as dextran, and their differentiation and function requires PLLP expression. The only similar highly endocytic cell type that has been characterized in the mammalian intestine is the M cell, which lies over the Peyer patches and carries out a function in immune surveillance. It is unclear whether the vacuolated enterocytes perform a similar function. Interestingly, epithelial morphogenesis in the zebrafish is regulated by microbiotal homeostasis, and germ-free animals present defects in gut differentiation and proliferation (Cheesman et al., 2011). On the other hand, a large percentage of *pllp* larvae do not survive after 8 dpf, and die presenting characteristics of starvation, suggesting that the vacuolated gut compartment is required for some sort of specialized nutrition. Indeed, phenotypes of starvation and germ-free development also lead to defects in epithelial architecture, as it has recently been shown for the Par4/LKB1 mutant (Marshall et al., 2010; van der Velden et al., 2011). However, starvation is a highly unspecific phenotype, which could also appear secondary to defects in epithelial morphogenesis, if it results in malabsorption. Starvation-induced phenotypes are frequently observed after 10 dpf, and starved WT larvae can survive up to 14 dpf. However, in our experiments we observed failure to acquire columnar organization already 6-7 dpf *pllp* mutants. Also, the intestinal morphogenesis defects were still observed in feeding, germ-containing, swimming *pllp* mutants at 18dpf, suggesting that PLLP is not required for swim bladder inflation, feeding behaviour, or germ gut colonization. Nevertheless, our experiments at this point cannot completely rule out that partial nutritional defects are responsible for our observed defects in columnar morphogenesis, and future experiments will address these

questions to understand the role of PLLP in intestinal physiology.

To understand the molecular mechanism of PLLP, we turned to protein interactomic analysis (**Figure 10d**). For this purpose we chose the bioID technique,

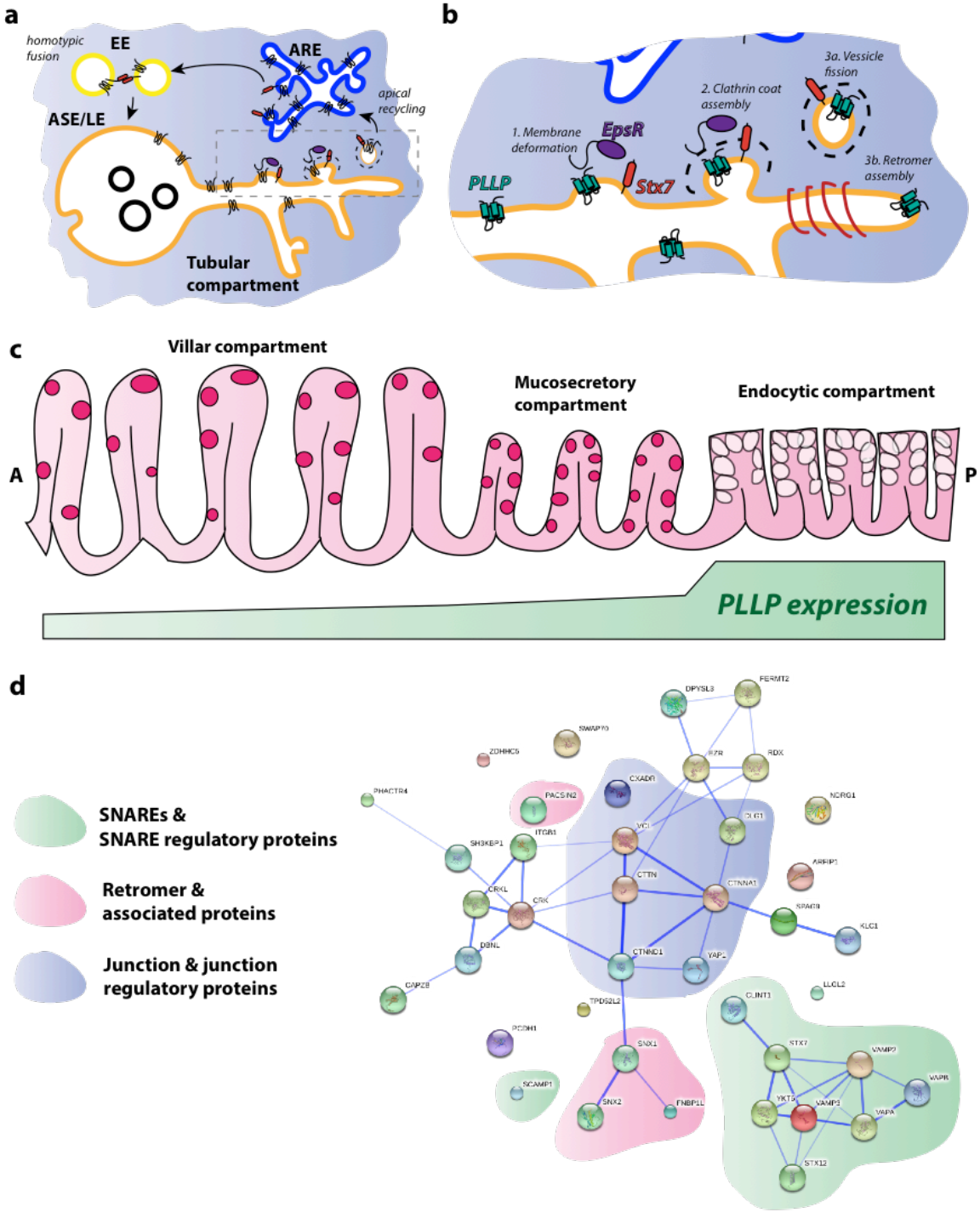

Figure 10. Molecular mechanism of PLLP expression. a) Early endosome fusion drives endosomal maturation. Mature endosomes recycle certain receptors through formation of sorting tubular domains. Proteins recycled from this tubular domains are delivered to recycling endosomes. **b)** PLLP in late endosomes recruits EpsinR to form clathrin-dependent sorting domains for SNARE receptors such as Stx7. **c)** In the midgut, PLLP is expressed highly in the posterior segment, which contains few mucosecretory cells, and highly endocytic enterocytes with supranuclear vacuoles. **d)** The PLLP bioID interactome suggests many possible interactions which could explain the pleiotropic phenotypes observed in the *pllp* mutants.

which has produced recent successful results in characterizing components of the centriole duplication machinery (Firat-Karalar et al., 2014; Roux et al., 2013; Roux et al., 2012). The majority of the proteins that interacted with PLLP could be grouped into 3 different hubs based on their known localization and function, using the STRING software. Proteins with SNARE motifs or SNARE-regulatory functions constituted the first hub (green colour, 9/42). The second hub belonged to cell-junction proteins (8/42). The third hub contained a second class of endosomal regulators, the retromer and accessory proteins (4/42). Most of the remaining proteins could be broadly grouped as regulators of actin or cytoskeleton, but failed to organize in a distinctive hub. The top interacting protein was EpsinR, which connected to the SNARE hub, through interaction with Syntaxin-7. The mechanism we propose in our manuscript provides a reasonable and elegant explanation for the interaction data of PLLP with SNAREs, retromer and EpsinR; SNAREs as cargo adaptors, and retromer and EpsR as part of the machinery involved in retrograde-pathway recycling. However, the role of PLLP interactions with junctional proteins is more elusive at this point, and further studies will be required to validate these interactions and establish their function.

Epithelial morphogenesis is a finely regulated process in which epithelial cells conduct a delicate balancing act between differentiation and proliferation, which becomes deregulated in many types of carcinomas (Martin-Belmonte and Perez-Moreno, 2012). Differentiation greatly depends on the establishment of junction and polarity complexes that serve to organize the physiology of the mature epithelial cell. These polarity complexes, such as the Crumbs complex, crosstalk with proliferation pathways, such as the Notch pathway, in order to prevent overgrowth and, at the same time, to provide a sufficient population of functional differentiated epithelial cells to carry out the role of the organ (Richardson and Pichaud, 2010). We have elucidated the role of PLLP in fine-tuning epithelial differentiation and architecture through the process of endosomal maturation, revealing that the role of developmental regulation of endocytosis modulators during these processes. These studies are particularly important since most Notch-dependent cancer cell lines are highly addicted to endocytosis for their tumorigenic ability (Kobia et al., 2014). Current-generation inhibitors of endocytosis target ubiquitously expressed and highly studied proteins and thus end up producing numerous deleterious side effects. Thus, characterization of tissue-specific control layers of endocytosis will provide more specific means to treat disease while minimizing undesired side effects.

VI. CONCLUSIONES/CONCLUSIONS

CONCLUSIONES

1. En el modelo *in vitro* de células MDCK cultivadas en tres dimensiones (3D-MDCK), el confinamiento celular regula la orientación de la polaridad celular y es necesario para el inicio de la formación del lumen.

2. En condiciones de bajo confinamiento, la tensión del citoesqueleto de actina se encuentra bajo el control de la quinasa LKB1 y la GTPasa monomérica RhoA, cuya actividad previene el inicio de la formación del lumen en 3D-MDCK.

3. Intersectin-2 (ITSN2) se localiza en el centrosoma y regula la actividad de Cdc42 para la formación de un único lumen.

4. La regulación de Cdc42 mediada por ITSN2 es necesaria para la orientación del huso mitótico en división celular, un proceso que es requisito para la formación de un único lumen central.

5. En el modelo 3D-MDCK, la expresión diferencial controla la inducción de 16 nuevos reguladores de la formación del lumen durante la morfogénesis epitelial.

6. Los expresión de los efectores de la GTPasa monomérica Rab27, Slp2 y Slp4 se induce durante la formación del lumen y controla la secreción apical polarizada de proteínas durante la morfogénesis

7. La expresión de Plasmolipin (PLLP) se induce durante la morfogénesis epitelial tanto *in vitro* en el modelo de 3D-MDCK como *in vivo* en el modelo de formación del intestino del pez cebra.

8. Plasmolipin se une a un adaptador de clatrina, Epsin-R, y dirige el transporte del receptor para fusión de membranas, la t-SNARE Syntaxin-7, hacia endosomas apicales para mantener el mecanismo de endocitosis apical.

9. Plasmolipin es necesario para la inhibición de Crumbs y la activación de Notch mediada por endocitosis, y regula la morfogénesis y diferenciación intestinal en el pez cebra.

1. Cell confinement regulates the orientation of cell polarity and is required for lumen initiation in the *in vitro* model of three-dimensional (3D) MDCK cells.

2. Under low confinement conditions, LKB1 and RhoA induce cytoskeletal actin stress and their activity prevents reorientation of polarity and lumen initiation in 3D-MDCK.

3. Intersectin-2 (ITSN2) is localized to the centrosome and regulates Cdc42 activity required for single lumen formation.

4. ITSN2 regulation of Cdc42 is required for spindle orientation during cell division, which is required for single lumen formation.

5. Differential gene expression controls the expression of at least 16 novel regulators that are required for lumen formation in 3D-MDCK.

6. Rab27-effectors, Slp2 and Slp4, are induced during 3D morphogenesis and control polarized apical protein secretion during morphogenesis.

7. Plasmolipin (PLLP) is differentially expressed during 3D morphogenesis both *in vivo* in the model of zebrafish intestine formation and *in vitro* in the model 3D-MDCK.

8. Plasmolipin binds clathrin adaptor Epsin-R and forms recycling tubulovesicles that help sort t-SNARE Syntaxin-7 into apical early endosomes to sustain the mechanism of apical endocytosis.

9. Plasmolipin is required for endocytic downmodulation of Crumbs and activation of Notch signaling to promote intestinal morphogenesis, patterning and differentiation.

VII.
REFERENCES

Affolter, M., and Caussinus, E. (2008). Tracheal branching morphogenesis in *Drosophila*: new insights into cell behaviour and organ architecture. Development *135*, 2055-2064.

Akhtar, N., and Streuli, C.H. (2012). An integrin-ILK-microtubule network orients cell polarity and lumen formation in glandular epithelium. Nature cell biology *15*, 17-27.

Alcaraz, J., Xu, R., Mori, H., Nelson, C.M., Mroue, R., Spencer, V.A., Brownfield, D., Radisky, D.C., Bustamante, C., and Bissell, M.J. (2008). Laminin and biomimetic extracellular elasticity enhance functional differentiation in mammary epithelia. The EMBO journal *27*, 2829-2838.

Almonacid, M., Terret, M.E., and Verlhac, M.H. (2014). Actin-based spindle positioning: new insights from female gametes. Journal of cell science *127*, 477-483.

Alonso, M.A., and Millan, J. (2001). The role of lipid rafts in signalling and membrane trafficking in T lymphocytes. Journal of cell science *114*, 3957-3965.

Alvers, A.L., Ryan, S., Scherz, P.J., Huisken, J., and Bagnat, M. (2014). Single continuous lumen formation in the zebrafish gut is mediated by smoothened-dependent tissue remodeling. Development *141*, 1110-1119.

Apodaca, G., Gallo, L.I., and Bryant, D.M. (2012). Role of membrane traffic in the generation of epithelial cell asymmetry. Nature cell biology *14*, 1235-1243.

Atwood, S.X., Chabu, C., Penkert, R.R., Doe, C.Q., and Prehoda, K.E. (2007). Cdc42 acts downstream of Bazooka to regulate neuroblast polarity through Par-6 aPKC. Journal of cell science *120*, 3200-3206.

Azoury, J., Lee, K.W., Georget, V., Rassinier, P., Leader, B., and Verlhac, M.H. (2008). Spindle positioning in mouse oocytes relies on a dynamic meshwork of actin filaments. Current biology *18*, 1514-1519.

Baas, A.F., Kuipers, J., van der Wel, N.N., Batlle, E., Koerten, H.K., Peters, P.J., and Clevers, H.C. (2004). Complete polarization of single intestinal epithelial cells upon activation of LKB1 by STRAD. Cell *116*, 457-466.

Bagnat, M., Cheung, I.D., Mostov, K.E., and Stainier, D.Y. (2007). Genetic control of single lumen formation in the zebrafish gut. Nature cell biology *9*, 954-960.

Benton, R., and St Johnston, D. (2003). *Drosophila* PAR-1 and 14-3-3 inhibit Bazooka/PAR-3 to establish complementary cortical domains in polarized cells. Cell *115*, 691-704.

Bernascone, I., and Martin-Belmonte, F. (2013). Crossroads of Wnt and Hippo in epithelial tissues. Trends in cell biology *23*, 380-389.

Beronja, S., Laprise, P., Papoulas, O., Pellikka, M., Sisson, J., and Tepass, U. (2005). Essential function of *Drosophila* Sec6 in apical exocytosis of epithelial photoreceptor cells. The Journal of cell biology *169*, 635-646.

Betschinger, J., Eisenhaber, F., and Knoblich, J.A. (2005). Phosphorylation-induced autoinhibition regulates the cytoskeletal protein Lethal (2) giant larvae. Current biology *15*, 276-282.

Bilder, D., Schober, M., and Perrimon, N. (2003). Integrated activity of PDZ protein complexes regulates epithelial polarity. Nature cell biology *5*, 53-58.

Blum, Y., Belting, H.G., Ellertsdottir, E., Herwig, L., Luders, F., and Affolter, M. (2008). Complex cell rearrangements during intersegmental vessel sprouting and vessel fusion in the zebrafish embryo. Developmental biology *316*, 312-322.

Blumer, J.B., Kuriyama, R., Gettys, T.W., and Lanier, S.M. (2006). The G-protein regulatory (GPR) motif-containing Leu-Gly-Asn-enriched protein (LGN) and Gialpha3 influence cortical positioning of the mitotic spindle poles at metaphase in symmetrically dividing mammalian cells. European journal of cell biology *85*, 1233-1240.

Brown, D.A., Crise, B., and Rose, J.K. (1989). Mechanism of membrane anchoring affects polarized expression of two proteins in MDCK cells. Science *245*, 1499-1501.

Bryant, D.M., Datta, A., Rodriguez-Fraticelli, A.E., Peranen, J., Martin-Belmonte, F., and Mostov, K.E. (2010). A molecular network for de novo generation of the apical surface and lumen. Nature cell biology *12*, 1035-1045.

Cai, Y., Yu, F., Lin, S., Chia, W., and Yang, X. (2003). Apical complex genes control mitotic spindle geometry and relative size of daughter cells in *Drosophila* neuroblast and pI asymmetric divisions. Cell *112*, 51-62.

Cande, W.Z., Lazarides, E., and McIntosh, J.R. (1977). A comparison of the distribution of actin and tubulin in the mammalian mitotic spindle as seen by indirect immunofluorescence. The Journal of cell biology *72*, 552-567.

Cao, J., Albertson, R., Riggs, B., Field, C.M., and Sullivan, W. (2008). Nuf, a Rab11 effector, maintains cytokinetic furrow integrity by promoting local actin polymerization. The Journal of cell biology *182*, 301-313.

Carracedo, A., and Pandolfi, P.P. (2008). The PTEN-PI3K pathway: of feedbacks and cross-talks. Oncogene *27*, 5527-5541.

Casanova, J.E., Apodaca, G., and Mostov, K.E. (1991). An autonomous signal for basolateral sorting in the cytoplasmic domain of the polymeric immunoglobulin receptor. Cell *66*, 65-75.

Chabu, C., and Doe, C.Q. (2008). Dap160/intersectin binds and activates aPKC to regulate cell polarity and cell cycle progression. Development *135*, 2739-2746.

Cheesman, S.E., Neal, J.T., Mittge, E., Seredick, B.M., and Guillemin, K. (2011). Epithelial cell proliferation in the developing zebrafish intestine is regulated by the Wnt pathway and microbial signaling via Myd88. Proceedings of the National Academy of Sciences of the United States of America *108 Suppl 1*, 4570-4577.

Chen, X., and Macara, I.G. (2005). Par-3 controls tight junction assembly through the Rac exchange factor Tiam1. Nature cell biology *7*, 262-269.

Cheong, K.H., Zacchetti, D., Schneeberger, E.E., and Simons, K. (1999). VIP17/MAL, a lipid raft-associated protein, is involved in apical transport in MDCK cells. Proceedings of the National Academy of Sciences of the United States of America *96*, 6241-6248.

Cohen, D., Rodriguez-Boulan, E., and Musch, A. (2004). Par-1 promotes a hepatic mode of apical protein trafficking in MDCK cells. Proceedings of the National Academy of Sciences of the United States of America *101*, 13792-13797.

Cohen, D., Tian, Y., and Musch, A. (2007). Par1b promotes hepatic-type lumen polarity in Madin Darby canine kidney cells via myosin II- and E-cadherin-dependent signaling. Molecular biology of the cell *18*, 2203-2215.

Cordenonsi, M., Zanconato, F., Azzolin, L., Forcato, M., Rosato, A., Frasson, C., Inui, M., Montagner, M., Parenti, A.R., Poletti, A.*, et al.* (2011). The Hippo transducer TAZ confers cancer stem cell-related traits on breast cancer cells. Cell *147*, 759-772.

Datta, A., Bryant, D.M., and Mostov, K.E. (2011). Molecular regulation of lumen morphogenesis. Current biology *21*, R126-136.

de Marco, M.C., Martin-Belmonte, F., Kremer, L., Albar, J.P., Correas, I., Vaerman, J.P., Marazuela, M., Byrne, J.A., and Alonso, M.A. (2002). MAL2, a novel raft protein of the MAL family, is an essential component of the machinery for transcytosis in hepatoma HepG2 cells. The Journal of cell biology *159*, 37-44.

Debnath, J., Mills, K.R., Collins, N.L., Reginato, M.J., Muthuswamy, S.K., and Brugge, J.S. (2002). The role of apoptosis in creating and maintaining luminal space within normal and oncogene-expressing mammary acini. Cell *111*, 29-40.

Deborde, S., Perret, E., Gravotta, D., Deora, A., Salvarezza, S., Schreiner, R., and Rodriguez-Boulan, E. (2008). Clathrin is a key regulator of basolateral polarity. Nature *452*, 719-723.

Delacour, D., Gouyer, V., Zanetta, J.P., Drobecq, H., Leteurtre, E., Grard, G., Moreau-Hannedouche, O., Maes, E., Pons, A., Andre, S.*, et al.* (2005). Galectin-4 and sulfatides in apical membrane trafficking in enterocyte-like cells. The Journal of cell biology *169*, 491-501.

Di Paolo, G., and De Camilli, P. (2006). Phosphoinositides in cell regulation and membrane dynamics. Nature *443*, 651-657.

Dickinson, D.J., Nelson, W.J., and Weis, W.I. (2011). A polarized epithelium organized by beta- and alpha-catenin predates cadherin and metazoan origins. Science *331*, 1336-1339.

Discher, D.E., Mooney, D.J., and Zandstra, P.W. (2009). Growth factors, matrices, and forces combine and control stem cells. Science *324*, 1673-1677.

Dormoy, V., Tormanen, K., and Sutterlin, C. (2013). Par6gamma is at the mother centriole and controls centrosomal protein composition through a Par6alpha-dependent pathway. Journal of cell science *126*, 860-870.

Du, Q., Stukenberg, P.T., and Macara, I.G. (2001). A mammalian Partner of inscuteable binds NuMA and regulates mitotic spindle organization. Nature cell biology *3*, 1069-1075.

DuFort, C.C., Paszek, M.J., and Weaver, V.M. (2011). Balancing forces: architectural control of mechanotransduction. Nature reviews Molecular cell biology *12*, 308-319.

Dupont, S., Morsut, L., Aragona, M., Enzo, E., Giulitti, S., Cordenonsi, M., Zanconato, F., Le Digabel, J., Forcato, M., Bicciato, S.*, et al.* (2011). Role of YAP/TAZ in mechanotransduction. Nature *474*, 179-183.

Elbert, M., Rossi, G., and Brennwald, P. (2005). The yeast par-1 homologs kin1 and kin2 show genetic and physical interactions with components of the exocytic machinery. Molecular biology of the cell *16*, 532-549.

Etienne-Manneville, S. (2004). Cdc42--the centre of polarity. Journal of cell science *117*, 1291-1300.

Fabrowski, P., Necakov, A.S., Mumbauer, S., Loeser, E., Reversi, A., Streichan, S., Briggs, J.A., and De Renzis, S. (2013). Tubular endocytosis drives remodelling of the

apical surface during epithelial morphogenesis in *Drosophila*. Nature communications *4*, 2244.

Feldman, J.L., and Priess, J.R. (2012). A role for the centrosome and PAR-3 in the hand-off of MTOC function during epithelial polarization. Current biology *22*, 575-582.

Fiedler, K., and Simons, K. (1995). The role of N-glycans in the secretory pathway. Cell *81*, 309-312.

Firat-Karalar, E.N., Rauniyar, N., Yates, J.R., 3rd, and Stearns, T. (2014). Proximity interactions among centrosome components identify regulators of centriole duplication. Current biology *24*, 664-670.

Fletcher, G.C., Lucas, E.P., Brain, R., Tournier, A., and Thompson, B.J. (2012). Positive feedback and mutual antagonism combine to polarize Crumbs in the *Drosophila* follicle cell epithelium. Current biology *22*, 1116-1122.

Folsch, H. (2008). Regulation of membrane trafficking in polarized epithelial cells. Current opinion in cell biology *20*, 208-213.

Folsch, H., Ohno, H., Bonifacino, J.S., and Mellman, I. (1999). A novel clathrin adaptor complex mediates basolateral targeting in polarized epithelial cells. Cell *99*, 189-198.

Folsch, H., Pypaert, M., Maday, S., Pelletier, L., and Mellman, I. (2003). The AP-1A and AP-1B clathrin adaptor complexes define biochemically and functionally distinct membrane domains. The Journal of cell biology *163*, 351-362.

Fortini, M.E., and Bilder, D. (2009). Endocytic regulation of Notch signaling. Current opinion in genetics & development *19*, 323-328.

Fujita, Y., Hogan, C., and Braga, V.M. (2006). Regulation of cell-cell adhesion by Rap1. Methods in enzymology *407*, 359-372.

Fukata, M., Nakagawa, M., and Kaibuchi, K. (2003). Roles of Rho-family GTPases in cell polarisation and directional migration. Current opinion in cell biology *15*, 590-597.

Galvez-Santisteban, M., Rodriguez-Fraticelli, A.E., Bryant, D.M., Vergarajauregui, S., Yasuda, T., Banon-Rodriguez, I., Bernascone, I., Datta, A., Spivak, N., Young, K.*, et al.* (2012). Synaptotagmin-like proteins control the formation of a single apical membrane domain in epithelial cells. Nature cell biology *14*, 838-849.

Gan, Y., McGraw, T.E., and Rodriguez-Boulan, E. (2002). The epithelial-specific adaptor AP1B mediates post-endocytic recycling to the basolateral membrane. Nature cell biology *4*, 605-609.

Gangar, A., Rossi, G., Andreeva, A., Hales, R., and Brennwald, P. (2005). Structurally conserved interaction of Lgl family with SNAREs is critical to their cellular function. Current biology *15*, 1136-1142.

Gao, N., White, P., and Kaestner, K.H. (2009). Establishment of intestinal identity and epithelial-mesenchymal signaling by Cdx2. Developmental cell *16*, 588-599.

Gard, D.L., Cha, B.J., and Roeder, A.D. (1995). F-actin is required for spindle anchoring and rotation in Xenopus oocytes: a re-examination of the effects of cytochalasin B on oocyte maturation. Zygote *3*, 17-26.

Gassama-Diagne, A., Yu, W., ter Beest, M., Martin-Belmonte, F., Kierbel, A., Engel, J., and Mostov, K. (2006). Phosphatidylinositol-3,4,5-trisphosphate regulates the formation of the basolateral plasma membrane in epithelial cells. Nature cell biology *8*, 963-970.

Gawadi, N. (1971). Actin in the mitotic spindle. Nature *234*, 410.

Ghabrial, A.S., Levi, B.P., and Krasnow, M.A. (2011). A systematic screen for tube morphogenesis and branching genes in the *Drosophila* tracheal system. PLoS genetics *7*, e1002087.

Golachowska, M.R., Hoekstra, D., and van, I.S.C. (2010). Recycling endosomes in apical plasma membrane domain formation and epithelial cell polarity. Trends in cell biology *20*, 618-626.

Goldstein, B., and Macara, I.G. (2007). The PAR proteins: fundamental players in animal cell polarization. Developmental cell *13*, 609-622.

Gonzalez, A., and Rodriguez-Boulan, E. (2009). Clathrin and AP1B: key roles in basolateral trafficking through trans-endosomal routes. FEBS letters *583*, 3784-3795.

Gravotta, D., Carvajal-Gonzalez, J.M., Mattera, R., Deborde, S., Banfelder, J.R., Bonifacino, J.S., and Rodriguez-Boulan, E. (2012). The clathrin adaptor AP-1A mediates basolateral polarity. Developmental cell *22*, 811-823.

Gravotta, D., Deora, A., Perret, E., Oyanadel, C., Soza, A., Schreiner, R., Gonzalez, A., and Rodriguez-Boulan, E. (2007). AP1B sorts basolateral proteins in recycling and biosynthetic routes of MDCK cells. Proceedings of the National Academy of Sciences of the United States of America *104*, 1564-1569.

Grawe, F., Wodarz, A., Lee, B., Knust, E., and Skaer, H. (1996). The *Drosophila* genes crumbs and stardust are involved in the biogenesis of adherens junctions. Development *122*, 951-959.

Greco, V., Hannus, M., and Eaton, S. (2001). Argosomes: a potential vehicle for the spread of morphogens through epithelia. Cell *106*, 633-645.

Grindstaff, K.K., Yeaman, C., Anandasabapathy, N., Hsu, S.C., Rodriguez-Boulan, E., Scheller, R.H., and Nelson, W.J. (1998). Sec6/8 complex is recruited to cell-cell contacts and specifies transport vesicle delivery to the basal-lateral membrane in epithelial cells. Cell *93*, 731-740.

Gumbiner, B.M. (2005). Regulation of cadherin-mediated adhesion in morphogenesis. Nature reviews Molecular cell biology *6*, 622-634.

Guruharsha, K.G., Kankel, M.W., and Artavanis-Tsakonas, S. (2012). The Notch signalling system: recent insights into the complexity of a conserved pathway. Nat Rev Genet *13*, 654-666.

Halder, G., Dupont, S., and Piccolo, S. (2012). Transduction of mechanical and cytoskeletal cues by YAP and TAZ. Nature reviews Molecular cell biology *13*, 591-600.

Hao, Y., Du, Q., Chen, X., Zheng, Z., Balsbaugh, J.L., Maitra, S., Shabanowitz, J., Hunt, D.F., and Macara, I.G. (2010). Par3 controls epithelial spindle orientation by aPKC-mediated phosphorylation of apical Pins. Current biology *20*, 1809-1818.

Harris, T.J., and Peifer, M. (2005). The positioning and segregation of apical cues during epithelial polarity establishment in *Drosophila*. The Journal of cell biology *170*, 813-823.

Hartsock, A., and Nelson, W.J. (2008). Adherens and tight junctions: structure, function and connections to the actin cytoskeleton. Biochim Biophys Acta *1778*, 660-669.

Hehnly, H., and Doxsey, S. (2014). Rab11 endosomes contribute to mitotic spindle organization and orientation. Developmental cell *28*, 497-507.

Hirose, T., Karasawa, M., Sugitani, Y., Fujisawa, M., Akimoto, K., Ohno, S., and Noda, T. (2006). PAR3 is essential for cyst-mediated epicardial development by establishing apical cortical domains. Development *133*, 1389-1398.

Holubcova, Z., Howard, G., and Schuh, M. (2013). Vesicles modulate an actin network for asymmetric spindle positioning. Nature cell biology *15*, 937-947.

Huh, D., Hamilton, G.A., and Ingber, D.E. (2011). From 3D cell culture to organs-on-chips. Trends in cell biology *21*, 745-754.

Hurd, T.W., Fan, S., Liu, C.J., Kweon, H.K., Hakansson, K., and Margolis, B. (2003a). Phosphorylation-dependent binding of 14-3-3 to the polarity protein Par3 regulates cell polarity in mammalian epithelia. Current biology *13*, 2082-2090.

Hurd, T.W., Gao, L., Roh, M.H., Macara, I.G., and Margolis, B. (2003b). Direct interaction of two polarity complexes implicated in epithelial tight junction assembly. Nature cell biology *5*, 137-142.

Hutterer, A., Betschinger, J., Petronczki, M., and Knoblich, J.A. (2004). Sequential roles of Cdc42, Par-6, aPKC, and Lgl in the establishment of epithelial polarity during *Drosophila* embryogenesis. Developmental cell *6*, 845-854.

Iden, S., and Collard, J.G. (2008). Crosstalk between small GTPases and polarity proteins in cell polarization. Nature reviews Molecular cell biology *9*, 846-859.

Ingber, D.E. (1993). The riddle of morphogenesis: a question of solution chemistry or molecular cell engineering? Cell *75*, 1249-1252.

Izumi, Y., Hirose, T., Tamai, Y., Hirai, S., Nagashima, Y., Fujimoto, T., Tabuse, Y., Kemphues, K.J., and Ohno, S. (1998). An atypical PKC directly associates and colocalizes at the epithelial tight junction with ASIP, a mammalian homologue of Caenorhabditis elegans polarity protein PAR-3. The Journal of cell biology *143*, 95-106.

Jacob, R., Heine, M., Eikemeyer, J., Frerker, N., Zimmer, K.P., Rescher, U., Gerke, V., and Naim, H.Y. (2004). Annexin II is required for apical transport in polarized epithelial cells. The Journal of biological chemistry *279*, 3680-3684.

Jaffe, A.B., Kaji, N., Durgan, J., and Hall, A. (2008). Cdc42 controls spindle orientation to position the apical surface during epithelial morphogenesis. The Journal of cell biology *183*, 625-633.

Johnson, J.M., Jin, M., and Lew, D.J. (2011). Symmetry breaking and the establishment of cell polarity in budding yeast. Current opinion in genetics & development *21*, 740-746.

Kamei, M., Saunders, W.B., Bayless, K.J., Dye, L., Davis, G.E., and Weinstein, B.M. (2006). Endothelial tubes assemble from intracellular vacuoles in vivo. Nature *442*, 453-456.

Karsenti, E., and Nedelec, F. (2004). The mitotic spindle and actin tails. Biology of the cell / under the auspices of the European Cell Biology Organization *96*, 237-240.

Kass, L., Erler, J.T., Dembo, M., and Weaver, V.M. (2007). Mammary epithelial cell: influence of extracellular matrix composition and organization during development and tumorigenesis. The international journal of biochemistry & cell biology *39*, 1987-1994.

Kerman, B.E., Cheshire, A.M., and Andrew, D.J. (2006). From fate to function: the *Drosophila* trachea and salivary gland as models for tubulogenesis. Differentiation; research in biological diversity *74*, 326-348.

Kim, S.K., and MacDonald, R.J. (2002). Signaling and transcriptional control of pancreatic organogenesis. Current opinion in genetics & development *12*, 540-547.

Kintscher, C., Wuertenberger, S., Eylenstein, R., Uhlendorf, T., and Groemping, Y. (2010). Autoinhibition of GEF activity in Intersectin 1 is mediated by the short SH3-DH domain linker. Protein science : a publication of the Protein Society *19*, 2164-2174.

Kobia, F., Duchi, S., Deflorian, G., and Vaccari, T. (2014). Pharmacologic inhibition of vacuolar H+ ATPase reduces physiologic and oncogenic Notch signaling. Molecular oncology *8*, 207-220.

Kohler, K., and Zahraoui, A. (2005). Tight junction: a co-ordinator of cell signalling and membrane trafficking. Biology of the cell / under the auspices of the European Cell Biology Organization *97*, 659-665.

Kovacs, E.M., Ali, R.G., McCormack, A.J., and Yap, A.S. (2002). E-cadherin homophilic ligation directly signals through Rac and phosphatidylinositol 3-kinase to regulate adhesive contacts. The Journal of biological chemistry *277*, 6708-6718.

Kunda, P., and Baum, B. (2009). The actin cytoskeleton in spindle assembly and positioning. Trends in cell biology *19*, 174-179.

Lakkaraju, A., and Rodriguez-Boulan, E. (2008). Itinerant exosomes: emerging roles in cell and tissue polarity. Trends in cell biology *18*, 199-209.

Lange, A., Wickstrom, S.A., Jakobson, M., Zent, R., Sainio, K., and Fassler, R. (2009). Integrin-linked kinase is an adaptor with essential functions during mouse development. Nature *461*, 1002-1006.

Laprise, P., Beronja, S., Silva-Gagliardi, N.F., Pellikka, M., Jensen, A.M., McGlade, C.J., and Tepass, U. (2006). The FERM protein Yurt is a negative regulatory component of the Crumbs complex that controls epithelial polarity and apical membrane size. Developmental cell *11*, 363-374.

Leight, J.L., Wozniak, M.A., Chen, S., Lynch, M.L., and Chen, C.S. (2012). Matrix rigidity regulates a switch between TGF-beta1-induced apoptosis and epithelial-mesenchymal transition. Molecular biology of the cell *23*, 781-791.

Lemmers, C., Michel, D., Lane-Guermonprez, L., Delgrossi, M.H., Medina, E., Arsanto, J.P., and Le Bivic, A. (2004). CRB3 binds directly to Par6 and regulates the morphogenesis of the tight junctions in mammalian epithelial cells. Molecular biology of the cell *15*, 1324-1333.

Leslie, N.R., Batty, I.H., Maccario, H., Davidson, L., and Downes, C.P. (2008). Understanding PTEN regulation: PIP2, polarity and protein stability. Oncogene *27*, 5464-5476.

Li, B.X., Satoh, A.K., and Ready, D.F. (2007). Myosin V, Rab11, and dRip11 direct apical secretion and cellular morphogenesis in developing *Drosophila* photoreceptors. The Journal of cell biology *177*, 659-669.

Li, S., Song, K.S., Koh, S.S., Kikuchi, A., and Lisanti, M.P. (1996). Baculovirus-based expression of mammalian caveolin in Sf21 insect cells. A model system for the

biochemical and morphological study of caveolae biogenesis. The Journal of biological chemistry *271*, 28647-28654.

Lingwood, D., and Simons, K. (2010). Lipid rafts as a membrane-organizing principle. Science *327*, 46-50.

Lisanti, M.P., Caras, I.W., Davitz, M.A., and Rodriguez-Boulan, E. (1989). A glycophospholipid membrane anchor acts as an apical targeting signal in polarized epithelial cells. The Journal of cell biology *109*, 2145-2156.

Lisanti, M.P., Sargiacomo, M., Graeve, L., Saltiel, A.R., and Rodriguez-Boulan, E. (1988). Polarized apical distribution of glycosyl-phosphatidylinositol-anchored proteins in a renal epithelial cell line. Proceedings of the National Academy of Sciences of the United States of America *85*, 9557-9561.

Lovegrove, B., Simoes, S., Rivas, M.L., Sotillos, S., Johnson, K., Knust, E., Jacinto, A., and Hombria, J.C. (2006). Coordinated control of cell adhesion, polarity, and cytoskeleton underlies Hox-induced organogenesis in *Drosophila*. Current biology *16*, 2206-2216.

Lu, H., and Bilder, D. (2005). Endocytic control of epithelial polarity and proliferation in *Drosophila*. Nature cell biology *7*, 1232-1239.

Lubarsky, B., and Krasnow, M.A. (2003). Tube morphogenesis: making and shaping biological tubes. Cell *112*, 19-28.

Luxenburg, C., Pasolli, H.A., Williams, S.E., and Fuchs, E. (2011). Developmental roles for Srf, cortical cytoskeleton and cell shape in epidermal spindle orientation. Nature cell biology *13*, 203-214.

Macara, I.G. (2004). Par proteins: partners in polarization. Current biology *14*, R160-162.

Madrid, R., Aranda, J.F., Rodriguez-Fraticelli, A.E., Ventimiglia, L., Andres-Delgado, L., Shehata, M., Fanayan, S., Shahheydari, H., Gomez, S., Jimenez, A.*, et al.* (2010). The formin INF2 regulates basolateral-to-apical transcytosis and lumen formation in association with Cdc42 and MAL2. Developmental cell *18*, 814-827.

Mammoto, A., Mammoto, T., and Ingber, D.E. (2012). Mechanosensitive mechanisms in transcriptional regulation. Journal of cell science *125*, 3061-3073.

Marshall, K.E., Tomasini, A.J., Makky, K., S, N.K., and Mayer, A.N. (2010). Dynamic Lkb1-TORC1 signaling as a possible mechanism for regulating the endoderm-intestine transition. Developmental dynamics : an official publication of the American Association of Anatomists *239*, 3000-3012.

Martin, S.G., and St Johnston, D. (2003). A role for *Drosophila* LKB1 in anterior-posterior axis formation and epithelial polarity. Nature *421*, 379-384.

Martin-Belmonte, F., Arvan, P., and Alonso, M.A. (2001). MAL mediates apical transport of secretory proteins in polarized epithelial Madin-Darby canine kidney cells. The Journal of biological chemistry *276*, 49337-49342.

Martin-Belmonte, F., Gassama, A., Datta, A., Yu, W., Rescher, U., Gerke, V., and Mostov, K. (2007). PTEN-mediated apical segregation of phosphoinositides controls epithelial morphogenesis through Cdc42. Cell *128*, 383-397.

Martin-Belmonte, F., Martinez-Menarguez, J.A., Aranda, J.F., Ballesta, J., de Marco, M.C., and Alonso, M.A. (2003). MAL regulates clathrin-mediated endocytosis at the

apical surface of Madin-Darby canine kidney cells. The Journal of cell biology *163*, 155-164.

Martin-Belmonte, F., and Mostov, K. (2007). Phosphoinositides control epithelial development. Cell Cycle *6*, 1957-1961.

Martin-Belmonte, F., and Mostov, K. (2008). Regulation of cell polarity during epithelial morphogenesis. Current opinion in cell biology.

Martin-Belmonte, F., and Perez-Moreno, M. (2012). Epithelial cell polarity, stem cells and cancer. Nature reviews Cancer *12*, 23-38.

Martin-Belmonte, F., Puertollano, R., Millan, J., and Alonso, M.A. (2000). The MAL proteolipid is necessary for the overall apical delivery of membrane proteins in the polarized epithelial Madin-Darby canine kidney and fischer rat thyroid cell lines. Molecular biology of the cell *11*, 2033-2045.

Marzolo, M.P., Yuseff, M.I., Retamal, C., Donoso, M., Ezquer, F., Farfan, P., Li, Y., and Bu, G. (2003). Differential distribution of low-density lipoprotein-receptor-related protein (LRP) and megalin in polarized epithelial cells is determined by their cytoplasmic domains. Traffic *4*, 273-288.

Massey-Harroche, D., Delgrossi, M.H., Lane-Guermonprez, L., Arsanto, J.P., Borg, J.P., Billaud, M., and Le Bivic, A. (2007). Evidence for a molecular link between the tuberous sclerosis complex and the Crumbs complex. Hum Mol Genet *16*, 529-536.

Matter, K., and Balda, M.S. (2003). Signalling to and from tight junctions. Nature reviews Molecular cell biology *4*, 225-236.

Matter, K., and Mellman, I. (1994). Mechanisms of cell polarity: sorting and transport in epithelial cells. Current opinion in cell biology *6*, 545-554.

McCarthy, R.A., Barth, J.L., Chintalapudi, M.R., Knaak, C., and Argraves, W.S. (2002). Megalin functions as an endocytic sonic hedgehog receptor. The Journal of biological chemistry *277*, 25660-25667.

Miralles, F., Posern, G., Zaromytidou, A.I., and Treisman, R. (2003). Actin dynamics control SRF activity by regulation of its coactivator MAL. Cell *113*, 329-342.

Montesano, R., Schaller, G., and Orci, L. (1991). Induction of epithelial tubular morphogenesis in vitro by fibroblast-derived soluble factors. Cell *66*, 697-711.

Morales, C.R., Zeng, J., El Alfy, M., Barth, J.L., Chintalapudi, M.R., McCarthy, R.A., Incardona, J.P., and Argraves, W.S. (2006). Epithelial trafficking of Sonic hedgehog by megalin. The journal of histochemistry and cytochemistry : official journal of the Histochemistry Society *54*, 1115-1127.

Morales, F.C., Takahashi, Y., Momin, S., Adams, H., Chen, X., and Georgescu, M.M. (2007). NHERF1/EBP50 head-to-tail intramolecular interaction masks association with PDZ domain ligands. Molecular and cellular biology *27*, 2527-2537.

Morin, X., Jaouen, F., and Durbec, P. (2007). Control of planar divisions by the G-protein regulator LGN maintains progenitors in the chick neuroepithelium. Nat Neurosci *10*, 1440-1448.

Morton, J.P., Jamieson, N.B., Karim, S.A., Athineos, D., Ridgway, R.A., Nixon, C., McKay, C.J., Carter, R., Brunton, V.G., Frame, M.C.*, et al.* (2010). LKB1 haploinsufficiency cooperates with Kras to promote pancreatic cancer through

suppression of p21-dependent growth arrest. Gastroenterology *139*, 586-597, 597 e581-586.

Moskalenko, S., Henry, D.O., Rosse, C., Mirey, G., Camonis, J.H., and White, M.A. (2002). The exocyst is a Ral effector complex. Nature cell biology *4*, 66-72.

Moskalenko, S., Tong, C., Rosse, C., Mirey, G., Formstecher, E., Daviet, L., Camonis, J., and White, M.A. (2003). Ral GTPases regulate exocyst assembly through dual subunit interactions. The Journal of biological chemistry *278*, 51743-51748.

Mostov, K., Su, T., and ter Beest, M. (2003). Polarized epithelial membrane traffic: conservation and plasticity. Nature cell biology *5*, 287-293.

Mostov, K.E., de Bruyn Kops, A., and Deitcher, D.L. (1986). Deletion of the cytoplasmic domain of the polymeric immunoglobulin receptor prevents basolateral localization and endocytosis. Cell *47*, 359-364.

Munro, E.M. (2006). PAR proteins and the cytoskeleton: a marriage of equals. Current opinion in cell biology *18*, 86-94.

Munson, C., Huisken, J., Bit-Avragim, N., Kuo, T., Dong, P.D., Ober, E.A., Verkade, H., Abdelilah-Seyfried, S., and Stainier, D.Y. (2008). Regulation of neurocoel morphogenesis by Pard6 gamma b. Developmental biology *324*, 41-54.

Muschler, J., Lochter, A., Roskelley, C.D., Yurchenco, P., and Bissell, M.J. (1999). Division of labor among the alpha6beta4 integrin, beta1 integrins, and an E3 laminin receptor to signal morphogenesis and beta-casein expression in mammary epithelial cells. Molecular biology of the cell *10*, 2817-2828.

Myat, M.M., and Andrew, D.J. (2002). Epithelial tube morphology is determined by the polarized growth and delivery of apical membrane. Cell *111*, 879-891.

Myllymaki, S.M., Teravainen, T.P., and Manninen, A. (2011). Two distinct integrin-mediated mechanisms contribute to apical lumen formation in epithelial cells. PloS one *6*, e19453.

Ng, A.N., de Jong-Curtain, T.A., Mawdsley, D.J., White, S.J., Shin, J., Appel, B., Dong, P.D., Stainier, D.Y., and Heath, J.K. (2005). Formation of the digestive system in zebrafish: III. Intestinal epithelium morphogenesis. Developmental biology *286*, 114-135.

O'Brien, L.E., Jou, T.S., Pollack, A.L., Zhang, Q., Hansen, S.H., Yurchenco, P., and Mostov, K.E. (2001). Rac1 orientates epithelial apical polarity through effects on basolateral laminin assembly. Nature cell biology *3*, 831-838.

O'Brien, L.E., Zegers, M.M., and Mostov, K.E. (2002). Opinion: Building epithelial architecture: insights from three-dimensional culture models. Nature reviews Molecular cell biology *3*, 531-537.

Ochoa-Espinosa, A., and Affolter, M. (2012). Branching morphogenesis: from cells to organs and back. Cold Spring Harbor perspectives in biology *4*.

Ortega, M.C., Cases, O., Merchan, P., Kozyraki, R., Clemente, D., and de Castro, F. (2012). Megalin mediates the influence of sonic hedgehog on oligodendrocyte precursor cell migration and proliferation during development. Glia *60*, 851-866.

Oztan, A., Silvis, M., Weisz, O.A., Bradbury, N.A., Hsu, S.C., Goldenring, J.R., Yeaman, C., and Apodaca, G. (2007). Exocyst requirement for endocytic traffic directed

toward the apical and basolateral poles of polarized MDCK cells. Molecular biology of the cell *18*, 3978-3992.

Pack, M., Solnica-Krezel, L., Malicki, J., Neuhauss, S.C., Schier, A.F., Stemple, D.L., Driever, W., and Fishman, M.C. (1996). Mutations affecting development of zebrafish digestive organs. Development *123*, 321-328.

Paladino, S., Sarnataro, D., Pillich, R., Tivodar, S., Nitsch, L., and Zurzolo, C. (2004). Protein oligomerization modulates raft partitioning and apical sorting of GPI-anchored proteins. The Journal of cell biology *167*, 699-709.

Paszek, M.J., Zahir, N., Johnson, K.R., Lakins, J.N., Rozenberg, G.I., Gefen, A., Reinhart-King, C.A., Margulies, S.S., Dembo, M., Boettiger, D*., et al.* (2005). Tensional homeostasis and the malignant phenotype. Cancer cell *8*, 241-254.

Perez Bay, A.E., Schreiner, R., Mazzoni, F., Carvajal-Gonzalez, J.M., Gravotta, D., Perret, E., Lehmann Mantaras, G., Zhu, Y.S., and Rodriguez-Boulan, E.J. (2013). The kinesin KIF16B mediates apical transcytosis of transferrin receptor in AP-1B-deficient epithelia. The EMBO journal.

Perez-Moreno, M., and Fuchs, E. (2006). Catenins: keeping cells from getting their signals crossed. Developmental cell *11*, 601-612.

Peyre, E., Jaouen, F., Saadaoui, M., Haren, L., Merdes, A., Durbec, P., and Morin, X. (2011). A lateral belt of cortical LGN and NuMA guides mitotic spindle movements and planar division in neuroepithelial cells. The Journal of cell biology *193*, 141-154.

Pitaval, A., Tseng, Q., Bornens, M., and Thery, M. (2010). Cell shape and contractility regulate ciliogenesis in cell cycle-arrested cells. The Journal of cell biology *191*, 303-312.

Pollarolo, G., Schulz, J.G., Munck, S., and Dotti, C.G. (2011). Cytokinesis remnants define first neuronal asymmetry in vivo. Nat Neurosci *14*, 1525-1533.

Price, L.S., Hajdo-Milasinovic, A., Zhao, J., Zwartkruis, F.J., Collard, J.G., and Bos, J.L. (2004). Rap1 regulates E-cadherin-mediated cell-cell adhesion. The Journal of biological chemistry *279*, 35127-35132.

Pucharcos, C., Estivill, X., and de la Luna, S. (2000). Intersectin 2, a new multimodular protein involved in clathrin-mediated endocytosis. FEBS letters *478*, 43-51.

Puertollano, R., Li, S., Lisanti, M.P., and Alonso, M.A. (1997). Recombinant expression of the MAL proteolipid, a component of glycolipid-enriched membrane microdomains, induces the formation of vesicular structures in insect cells. The Journal of biological chemistry *272*, 18311-18315.

Puertollano, R., Martin-Belmonte, F., Millan, J., de Marco, M.C., Albar, J.P., Kremer, L., and Alonso, M.A. (1999). The MAL proteolipid is necessary for normal apical transport and accurate sorting of the influenza virus hemagglutinin in Madin-Darby canine kidney cells. The Journal of cell biology *145*, 141-151.

Qin, J., and Wu, C. (2012). ILK: a pseudokinase in the center stage of cell-matrix adhesion and signaling. Current opinion in cell biology *24*, 607-613.

Rangarajan, S., Enserink, J.M., Kuiperij, H.B., de Rooij, J., Price, L.S., Schwede, F., and Bos, J.L. (2003). Cyclic AMP induces integrin-mediated cell adhesion through Epac and Rap1 upon stimulation of the beta 2-adrenergic receptor. The Journal of cell biology *160*, 487-493.

Rescher, U., and Gerke, V. (2004). Annexins--unique membrane binding proteins with diverse functions. Journal of cell science *117*, 2631-2639.

Rescher, U., Ruhe, D., Ludwig, C., Zobiack, N., and Gerke, V. (2004). Annexin 2 is a phosphatidylinositol (4,5)-bisphosphate binding protein recruited to actin assembly sites at cellular membranes. Journal of cell science *117*, 3473-3480.

Richardson, E.C., and Pichaud, F. (2010). Crumbs is required to achieve proper organ size control during *Drosophila* head development. Development *137*, 641-650.

Rodriguez-Boulan, E., Kreitzer, G., and Musch, A. (2005). Organization of vesicular trafficking in epithelia. Nature reviews Molecular cell biology *6*, 233-247.

Rodriguez-Boulan, E., and Macara, I.G. (2014). Organization and execution of the epithelial polarity programme. Nature reviews Molecular cell biology *15*, 225-242.

Rodriguez-Fraticelli, A.E., Auzan, M., Alonso, M.A., Bornens, M., and Martin-Belmonte, F. (2012). Cell confinement controls centrosome positioning and lumen initiation during epithelial morphogenesis. The Journal of cell biology *198*, 1011-1023.

Rodriguez-Fraticelli, A.E., Vergarajauregui, S., Eastburn, D.J., Datta, A., Alonso, M.A., Mostov, K., and Martin-Belmonte, F. (2010). The Cdc42 GEF Intersectin 2 controls mitotic spindle orientation to form the lumen during epithelial morphogenesis. The Journal of cell biology *189*, 725-738.

Roland, J.T., Bryant, D.M., Datta, A., Itzen, A., Mostov, K.E., and Goldenring, J.R. (2011). Rab GTPase-Myo5B complexes control membrane recycling and epithelial polarization. Proceedings of the National Academy of Sciences of the United States of America *108*, 2789-2794.

Roland, J.T., Kenworthy, A.K., Peranen, J., Caplan, S., and Goldenring, J.R. (2007). Myosin Vb interacts with Rab8a on a tubular network containing EHD1 and EHD3. Molecular biology of the cell *18*, 2828-2837.

Roux, K.J., Kim, D.I., and Burke, B. (2013). BioID: a screen for protein-protein interactions. Current protocols in protein science / editorial board, John E Coligan [et al] *74*, Unit 19 23.

Roux, K.J., Kim, D.I., Raida, M., and Burke, B. (2012). A promiscuous biotin ligase fusion protein identifies proximal and interacting proteins in mammalian cells. The Journal of cell biology *196*, 801-810.

Royle, S.J. (2013). Protein adaptation: mitotic functions for membrane trafficking proteins. Nature reviews Molecular cell biology *14*, 592-599.

Rubin, D.C. (2007). Intestinal morphogenesis. Current opinion in gastroenterology *23*, 111-114.

Sanchez-Pulido, L., Martin-Belmonte, F., Valencia, A., and Alonso, M.A. (2002). MARVEL: a conserved domain involved in membrane apposition events. Trends Biochem Sci *27*, 599-601.

Sang, T.K., and Ready, D.F. (2002). Eyes closed, a *Drosophila* p47 homolog, is essential for photoreceptor morphogenesis. Development *129*, 143-154.

Sato, T., Mushiake, S., Kato, Y., Sato, K., Sato, M., Takeda, N., Ozono, K., Miki, K., Kubo, Y., Tsuji, A.*, et al.* (2007). The Rab8 GTPase regulates apical protein localization in intestinal cells. Nature *448*, 366-369.

Schaefer, M., Shevchenko, A., Shevchenko, A., and Knoblich, J.A. (2000). A protein complex containing Inscuteable and the Galpha-binding protein Pins orients asymmetric cell divisions in *Drosophila*. Current biology *10*, 353-362.

Schluter, M.A., Pfarr, C.S., Pieczynski, J., Whiteman, E.L., Hurd, T.W., Fan, S., Liu, C.J., and Margolis, B. (2009). Trafficking of Crumbs3 during cytokinesis is crucial for lumen formation. Molecular biology of the cell *20*, 4652-4663.

Schmidt, K.N., Kuhns, S., Neuner, A., Hub, B., Zentgraf, H., and Pereira, G. (2012). Cep164 mediates vesicular docking to the mother centriole during early steps of ciliogenesis. The Journal of cell biology *199*, 1083-1101.

Seiler, C., Davuluri, G., Abrams, J., Byfield, F.J., Janmey, P.A., and Pack, M. (2012). Smooth muscle tension induces invasive remodeling of the zebrafish intestine. PLoS biology *10*, e1001386.

Shackelford, D.B., and Shaw, R.J. (2009). The LKB1-AMPK pathway: metabolism and growth control in tumour suppression. Nature reviews Cancer *9*, 563-575.

Shivas, J.M., Morrison, H.A., Bilder, D., and Skop, A.R. (2010). Polarity and endocytosis: reciprocal regulation. Trends in cell biology *20*, 445-452.

Siller, K.H., and Doe, C.Q. (2009). Spindle orientation during asymmetric cell division. Nature cell biology *11*, 365-374.

Spenle, C., Simon-Assmann, P., Orend, G., and Miner, J.H. (2013). Laminin alpha5 guides tissue patterning and organogenesis. Cell adhesion & migration *7*, 90-100.

St Johnston, D., and Sanson, B. (2011). Epithelial polarity and morphogenesis. Current opinion in cell biology *23*, 540-546.

Svensson, P., Williams, C., Lundeberg, J., Ryden, P., Bergqvist, I., and Edlund, H. (2007). Gene array identification of Ipf1/Pdx1-/- regulated genes in pancreatic progenitor cells. BMC developmental biology *7*, 129.

Takeda, T., Yamazaki, H., and Farquhar, M.G. (2003). Identification of an apical sorting determinant in the cytoplasmic tail of megalin. Am J Physiol Cell Physiol *284*, C1105-1113.

Tall, R.D., Alonso, M.A., and Roth, M.G. (2003). Features of influenza HA required for apical sorting differ from those required for association with DRMs or MAL. Traffic *4*, 838-849.

Tanentzapf, G., and Tepass, U. (2003). Interactions between the crumbs, lethal giant larvae and bazooka pathways in epithelial polarization. Nature cell biology *5*, 46-52.

Tepass, U. (1996). Crumbs, a component of the apical membrane, is required for zonula adherens formation in primary epithelia of *Drosophila*. Developmental biology *177*, 217-225.

Tepass, U., and Knust, E. (1993). Crumbs and stardust act in a genetic pathway that controls the organization of epithelia in *Drosophila melanogaster*. Developmental biology *159*, 311-326.

Tepass, U., Theres, C., and Knust, E. (1990). crumbs encodes an EGF-like protein expressed on apical membranes of *Drosophila* epithelial cells and required for organization of epithelia. Cell *61*, 787-799.

ter Beest, M.B., Chapin, S.J., Avrahami, D., and Mostov, K.E. (2005). The role of syntaxins in the specificity of vesicle targeting in polarized epithelial cells. Molecular biology of the cell *16*, 5784-5792.

Theesfeld, C.L., Irazoqui, J.E., Bloom, K., and Lew, D.J. (1999). The role of actin in spindle orientation changes during the Saccharomyces cerevisiae cell cycle. The Journal of cell biology *146*, 1019-1032.

Thery, M. (2010). Micropatterning as a tool to decipher cell morphogenesis and functions. Journal of cell science *123*, 4201-4213.

Thompson, H.M., Cao, H., Chen, J., Euteneuer, U., and McNiven, M.A. (2004). Dynamin 2 binds gamma-tubulin and participates in centrosome cohesion. Nature cell biology *6*, 335-342.

Torkko, J.M., Manninen, A., Schuck, S., and Simons, K. (2008). Depletion of apical transport proteins perturbs epithelial cyst formation and ciliogenesis. Journal of cell science *121*, 1193-1203.

Vaccari, T., Lu, H., Kanwar, R., Fortini, M.E., and Bilder, D. (2008). Endosomal entry regulates Notch receptor activation in *Drosophila* melanogaster. The Journal of cell biology *180*, 755-762.

Van Aelst, L., and Symons, M. (2002). Role of Rho family GTPases in epithelial morphogenesis. Genes & development *16*, 1032-1054.

van der Velden, Y.U., Wang, L., Zevenhoven, J., van Rooijen, E., van Lohuizen, M., Giles, R.H., Clevers, H., and Haramis, A.P. (2011). The serine-threonine kinase LKB1 is essential for survival under energetic stress in zebrafish. Proceedings of the National Academy of Sciences of the United States of America *108*, 4358-4363.

van Meer, G., and Simons, K. (1988). Lipid polarity and sorting in epithelial cells. Journal of cellular biochemistry *36*, 51-58.

Vartiainen, M.K., Guettler, S., Larijani, B., and Treisman, R. (2007). Nuclear actin regulates dynamic subcellular localization and activity of the SRF cofactor MAL. Science *316*, 1749-1752.

Vega-Salas, D.E., Salas, P.J., and Rodriguez-Boulan, E. (1987). Modulation of the expression of an apical plasma membrane protein of Madin-Darby canine kidney epithelial cells: cell-cell interactions control the appearance of a novel intracellular storage compartment. The Journal of cell biology *104*, 1249-1259.

Velling, T., Stefansson, A., and Johansson, S. (2008). EGFR and beta1 integrins utilize different signaling pathways to activate Akt. Experimental cell research *314*, 309-316.

Verlhac, M.H. (2011). Spindle positioning: going against the actin flow. Nature cell biology *13*, 1183-1185.

Vieira, O.V., Verkade, P., Manninen, A., and Simons, K. (2005). FAPP2 is involved in the transport of apical cargo in polarized MDCK cells. The Journal of cell biology *170*, 521-526.

von Stein, W., Ramrath, A., Grimm, A., Muller-Borg, M., and Wodarz, A. (2005). Direct association of Bazooka/PAR-3 with the lipid phosphatase PTEN reveals a link between the PAR/aPKC complex and phosphoinositide signaling. Development *132*, 1675-1686.

Wallace, K.N., Akhter, S., Smith, E.M., Lorent, K., and Pack, M. (2005). Intestinal growth and differentiation in zebrafish. Mech Dev *122*, 157-173.

Wang, Q., and Margolis, B. (2007). Apical junctional complexes and cell polarity. Kidney Int *72*, 1448-1458.

Wang, Q.C., Liu, J., Wang, Z.B., Zhang, Y., Duan, X., Cui, X.S., Kim, N.H., and Sun, S.C. (2014). Dynamin 2 regulates actin-mediated spindle migration in mouse oocytes. Biology of the cell / under the auspices of the European Cell Biology Organization.

Weisz, O.A., and Rodriguez-Boulan, E. (2009). Apical trafficking in epithelial cells: signals, clusters and motors. Journal of cell science *122*, 4253-4266.

Wescott, M.P., Rovira, M., Reichert, M., von Burstin, J., Means, A., Leach, S.D., and Rustgi, A.K. (2009). Pancreatic ductal morphogenesis and the Pdx1 homeodomain transcription factor. Molecular biology of the cell *20*, 4838-4844.

Westlake, C.J., Baye, L.M., Nachury, M.V., Wright, K.J., Ervin, K.E., Phu, L., Chalouni, C., Beck, J.S., Kirkpatrick, D.S., Slusarski, D.C*., et al.* (2011). Primary cilia membrane assembly is initiated by Rab11 and transport protein particle II (TRAPPII) complex-dependent trafficking of Rabin8 to the centrosome. Proceedings of the National Academy of Sciences of the United States of America *108*, 2759-2764.

Wickstrom, S.A., Lange, A., Montanez, E., and Fassler, R. (2010). The ILK/PINCH/parvin complex: the kinase is dead, long live the pseudokinase! The EMBO journal *29*, 281-291.

Windler, S.L., and Bilder, D. (2010). Endocytic internalization routes required for delta/notch signaling. Current biology *20*, 538-543.

Wodarz, A., Grawe, F., and Knust, E. (1993). CRUMBS is involved in the control of apical protein targeting during *Drosophila* epithelial development. Mech Dev *44*, 175-187.

Wu, H., Feng, W., Chen, J., Chan, L.N., Huang, S., and Zhang, M. (2007). PDZ domains of par-3 as potential phosphoinositide signaling integrators. Mol Cell *28*, 886-898.

Wu, H., Rossi, G., and Brennwald, P. (2008). The ghost in the machine: small GTPases as spatial regulators of exocytosis. Trends in cell biology.

Xu, F.L., and Saunders, W.S. (2008). Actin and microtubules: working together to control spindle polarity. Cancer cell *14*, 197-199.

Xu, K., Sacharidou, A., Fu, S., Chong, D.C., Skaug, B., Chen, Z.J., Davis, G.E., and Cleaver, O. (2011). Blood vessel tubulogenesis requires Rasip1 regulation of GTPase signaling. Developmental cell *20*, 526-539.

Xu, X., Jin, D., Durgan, J., and Hall, A. (2013). LKB1 controls human bronchial epithelial morphogenesis through p114RhoGEF-dependent RhoA activation. Molecular and cellular biology *33*, 2671-2682.

Yeaman, C., Grindstaff, K.K., and Nelson, W.J. (2004). Mechanism of recruiting Sec6/8 (exocyst) complex to the apical junctional complex during polarization of epithelial cells. Journal of cell science *117*, 559-570.

Yeaman, C., Grindstaff, K.K., Wright, J.R., and Nelson, W.J. (2001). Sec6/8 complexes on trans-Golgi network and plasma membrane regulate late stages of exocytosis in mammalian cells. The Journal of cell biology *155*, 593-604.

Yi Qin, W.H.M., Yi Hao, and Ian G. Macara (2010). Tuba, a Cdc42 GEF, is required for polarized spindle orientation during epithelial cyst formation. Journal of Cell Biology *189*, 10.

Yu, F., Morin, X., Cai, Y., Yang, X., and Chia, W. (2000). Analysis of partner of inscuteable, a novel player of *Drosophila* asymmetric divisions, reveals two distinct steps in inscuteable apical localization. Cell *100*, 399-409.

Yu, W., Datta, A., Leroy, P., O'Brien, L.E., Mak, G., Jou, T.S., Matlin, K.S., Mostov, K.E., and Zegers, M.M. (2005). Beta1-integrin orients epithelial polarity via Rac1 and laminin. Molecular biology of the cell *16*, 433-445.

Zegers, M.M., O'Brien, L.E., Yu, W., Datta, A., and Mostov, K.E. (2003). Epithelial polarity and tubulogenesis in vitro. Trends in cell biology *13*, 169-176.

Zheng, Z., Zhu, H., Wan, Q., Liu, J., Xiao, Z., Siderovski, D.P., and Du, Q. (2010). LGN regulates mitotic spindle orientation during epithelial morphogenesis. The Journal of cell biology *189*, 275-288.

Zhong, T.P. (2005). Zebrafish genetics and formation of embryonic vasculature. Current topics in developmental biology *71*, 53-81.